TECHNISCHE UNIVERSITÄT WIEN
Vienna University of Technology

DISSERTATION

Semiholographic Thermalization in Strongly Coupled Nonabelian Gauge Theories

ausgeführt zum Zwecke der Erlangung des akademischen Grades eines Doktors der Technischen Wissenschaften unter der Leitung von

Univ.-Prof. DI Dr. Anton Rebhan
Institut für Theoretische Physik,
Technische Universität Wien, Österreich

eingereicht an der Technischen Universität Wien,
Fakultät für Physik

von
Alexander Igor Soloviev, MSc
Matrikelnummer 1029195
Pilotengasse 98-2
1220 Wien

Wien, am 09.10.2019

Dr. Anton Rebhan
(Betreuer)

Dr. Edmond Iancu
(Gutachter)

Dr. Derek Teaney
(Gutachter)

Abstract

Semiholography is a theoretical framework, set up to provide a consistent effective description of the physical systems involving both weakly coupled and strongly coupled degrees of freedom, where the latter are modelled by gauge/gravity duality, also known as holography. In this thesis, we explore this framework in the context of strongly coupled plasmas in non-equilibrium settings, motivated in particular by the non-equilibrium evolution of the Quark Gluon Plasma. In the context of QGP, the model couples a weakly-coupled sector, describing hard partons, with a strongly-coupled soft holographic sector, representing the soft bath of gluons radiated by the hard partons, via gauge-invariant operators. Following a brief theoretical introduction, I will describe the semiholographic approach in general and using illustrative examples, focussing in particular on the phenomenological construction. A key element is that the semiholographic construction has a locally conserved total energy-momentum tensor.

After the general introduction, I discuss a hybrid two-fluid model coupled via their effective metrics. This coupling is dictated by the respective energy-momentum tensors. I explore the consequences of such a coupling in and near thermal equilibrium by investigating the rich phase structure and the collective modes.

Following this discussion, I will describe a semiholographic toy model for QGP thermalization in $2+1$ dimensions. This involves a classical Yang-Mills sector, describing the overoccupied gluon modes at the saturation scale, coupled to a strongly interacting holographic sector, representing the soft degrees of freedom. The toy model represents a proof of principle calculation, demonstrating for the first time the transfer of energy from the Yang-Mills sector at the boundary to a growing black hole in bulk anti-de Sitter (AdS) space including backreaction.

Finally, I will discuss a semiholographic model of trapped impurities in $0+1$-dimensions. Along the way, we will develop an algorithm to solve Jackiw-Teitelboim gravity coupled to non-conformal matter. The holographic sector, represented by an infrared anti-de Sitter spacetime with non-conformal matter, known as nearly-AdS_2, represents a confining potential for the trapped impurities. The impurities serve as a self-consistent boundary source for the holographic sector.

Zusammenfassung

Semiholographie ist eine theoretische Methode zur konsistenten, effektiven Beschreibung von physikalischen Systemen, die sowohl schwach wechselwirkende als auch stark wechselwirkende Freiheitsgrade aufweisen, wobei letztere mittels der Dualität von Eichtheorien und Gravitationstheorien (Holographie) modelliert werden. Diese Arbeit behandelt Semiholographie im Kontext stark gekoppelter Plasmen in Nichtgleichgewichtszuständen, die insbesondere durch die Nichtgleichgewichtsentwicklung des Quark-Gluon-Plasmas (QGP) motiviert sind. Zur Beschreibung des QGP verwendet man ein Model bestehend aus zwei Sektoren: einen schwach wechselwirkenden Sektor, der "harte" Partonen beschreibt, und einen stark wechselwirkenden, "weichen" holographischen Sektor, welcher das weiche Bad der von den harten Partonen ausgestrahlten Gluonen darstellt. Die Kopplung der beiden Sektoren erfolgt über eichinvariante Operatoren. Nach einer kurzen theoretischen Einführung beschreibe ich den semiholographischen Ansatz im Allgemeinen und verwende anschauliche Beispiele, wobei ich mich insbesondere auf die phänomenologische Konstruktion konzentriere. Ein Schlüsselelement ist, dass die semiholographische Konstruktion einen lokal erhaltenen Gesamt-Energie-Impuls-Tensor aufweist.

Nach der allgemeinen Einführung diskutiere ich ein hybrides Zweiflüssigkeitsmodell, das über effektive Metriken gekoppelt ist. Die Kopplung wird durch die jeweiligen Energie-Impuls-Tensoren vorgegeben. Ich untersuche die Konsequenzen einer solchen Kopplung im und in der Nähe des thermischen Gleichgewichts, indem ich die komplexe Phasenstruktur und die kollektiven Moden des Systems untersuche.

Im Anschluss an diese Diskussion beschreibe ich ein semiholographisches "Spielzeugmodell" für die Thermalisierung des QGP in $2+1$ Dimensionen. Das Modell besteht aus einem klassischen Yang-Mills-Sektor, der die hochbesetzten Gluon-Moden nahe der Sättigungsskala beschreibt, gekoppelt mit einem stark wechselwirkenden holographischen Sektor, der die weichen Freiheitsgrade darstellt. Das Spielzeugmodell dient als "proof of concept" der Berechnungsmethode und demonstriert zum ersten Mal die Übertragung von Energie aus dem Yang-Mills-Sektor am Rand zu einem wachsenden Schwarzen Loch im Anti-De-Sitter-Raum, unter der Berücksichtigung von Rückkopplung.

Abschließend diskutiere ich ein semiholographisches Modell von eingeschlossenen Verunreinigungen in $0+1$ Dimensionen. Ich entwickle einen Algorithmus, mit dem die Feldgleichungen der Gravitationstheorie von Jackiw und Teitelboim in Verbindung mit nicht-konformer Materie gelöst werden können. Der holographische Sektor, der durch eine infrarote Anti-De-Sitter-Raumzeit mit nicht konformer-Materie, $NAdS_2$, beschrieben wird, stellt einen Potentialtopf für die eingeschlossenen Verunreinigungen dar. Die Verunreinigungen dienen als selbstkonsistente Quellen am Rand der Raumzeit für den holographischen Sektor.

Preface

The main results and methods presented in this thesis are have been published in the following articles:

1. A. Kurkela, A. Mukhopadhyay, F. Preis, A. Rebhan and A. Soloviev.
   Hybrid Fluid Models from Mutual Effective Metric Couplings.
   Journal of High Energy Physics **08**, 054 (2018) [arXiv:1805.05213]

2. C. Ecker, A. Mukhopadhyay, F. Preis, A. Rebhan and A. Soloviev.
   Time evolution of a toy semiholographic glasma.
   Journal of High Energy Physics **08**, 074 (2018) [arXiv:1806.01850]

3. L. Joshi, A. Mukhopadhyay and A. Soloviev.
   Time-dependent $NAdS_2$ *holography with applications.*
   Submitted to the Journal of High Energy Physics [arXiv:1901.08877]

Acknowledgements

There are quite a few people that I would like to express my gratitude towards for their help during my journey.

First and foremost, I am grateful to my supervisor, Anton Rebhan, for giving me the opportunity to pursue my PhD studies. His guidance, support and good humor has made the experience memorable. I would also like to thank my co-supervisor, Ayan Mukhopadhyay, for his steadfast guidance, camaraderie and blue skies-thinking, as well as the warm hospitality I was showered with during my stay in IIT Madras. I also wish to warmly thank Aleksi Kurkela for his patience, support and hosting me in CERN.

I have had the pleasure of sharing an office with a delightful, determined and intelligent group, to whom I would like to give special thanks. Frederic Brünner, Christian Ecker, Alexander Haber and David Müller really made these past four years fun. It would be remiss of me to not thank the students that I met through the Doktoratskolleg Particles and Interactions (DKPI), with whom I spent a few great outings in the Austrian countryside, playing cards, hitting the sauna, skiing and finding time to discuss physics all the same: Elke Aeikens, Max Löschner, Moritz Preißer and Philipp Stanzer. I would like to thank Daniel Grumiller for introducing me to the delightful game of bridge and to the bridge gang for finding time to play.

Furthermore, I would like to thank Lata Joshi, Andrey Katz and Florian Preis for their collaboration during various times of my studies. I would like to thank Tanay Kibe, Toshali Mitra, Sukrut Mondkar, Sutapa Samanta and Hareram Swain, the group of bright students that I met at IIT Madras and had a fantastic time spending a few months getting to know. I would also like to thank Giuseppe Policastro and Alexandre Serantes for the interesting discussions and intense foosball games in Bangalore. I would also like to thank Kirill Boguslavski, Abhiram Kidambi and Josef Leutgeb for many stimulating discussions about and around physics.

Last, but certainly not least, I thank my lovely family: Igor and Irina; Anya, Will and Nina; Rosamaria, Arturo, Andrea and Ludo; and my fiancée Renata.

Units and conventions

For the metric signature, we take the mostly-plus convention, i.e. the Minkowski metric is

$$\eta_{\mu\nu} = \mathrm{Diag}(-1, 1, 1, 1).$$

We will use Greek indices to denote curved coordinates $\mu = 0, \ldots, d$. We will use Latin indices for spatial directions.

Our conventions for the Fourier transform are

$$f(k) = \int \frac{\mathrm{d}^d x}{(2\pi)^d} e^{ik\cdot x} f(x),$$

where $k \cdot x = -\omega t + k^i x_i$.

Unless stated otherwise, we will work in natural units, where the speed of light $c = 1$, Boltzmann's constant $k_b = 1$ and the reduced Planck constant $\hbar = 1$.

Contents

Chapter 1

Introduction

The study of matter produced by heavy ion collisions, performed at various major experimental facilities such as the Large Hadron Collider (LHC) at CERN and the Relativistic Heavy Ion Collider (RHIC) at Brookhaven National Laboratory, provides an enormous opportunity for understanding the fundamental nature of strong interactions. During these high energy ultra-relativistic collisions involving lead or gold ions, the quarks and gluons making up such ordinary nuclear matter *deconfine*. This fleeting, extremely hot and dense state of matter is known as the Quark Gluon Plasma (QGP). Studying such an exotic state of matter is key to exploring and understanding the phase diagram of quantum chromodynamics (QCD), the theory of strong interactions. Moreover, the QGP was a major component of the Universe for a few microseconds after the Big Bang [1].

A typical heavy ion collision begins with two ions approach one another at highly relativistic speeds. The ions appear as flattened disks or pancakes in the center of mass frame. The disks are made of partons, namely quarks and gluons. Due to the asymptotic freedom of QCD, it was thought that after the disks collide, the partons would be liberated and form a weakly coupled plasma [2, 3]. At such high energies, one could expect perturbation theory to apply as the strong coupling constant, α_s, would be small. Certain observables were computed at weak coupling, such as the ratio of the shear viscosity, η, to the entropic density, s, to be $\eta/s \sim 1/\alpha_s^2 \log \alpha_s \gg 1$ [4].

Surprisingly, this ratio was measured to be rather small, $\eta/s < 1$, in the wake of a heavy ion collision. As the remnants of the ions move away from the collision site, certain aspects of the "fireball" of the QGP matter left behind are better captured by a strongly coupled theory, in particular by an effective hydrodynamic description [5]. Intriguingly, a computation by Kovtun, Son and Starinets using holographic techniques [6] yields a ratio of the shear viscosity, η, to the entropy density, s, to be $\frac{\eta}{s} = \frac{1}{4\pi}$. It has been shown that this value is universal for a large class of large N theories in the limit of infinite coupling [7]. The estimated value of $\frac{\eta}{s}$ of the QGP produced at CERN and RHIC lies in the ballpark of this ratio.

At late times, as the "fireball" expands, the temperature of the system decreases to a point where it becomes more energetically favorable for the quarks and gluons to recombine and form a gas of hadrons. This is known as the freeze-out regime. This dilute gas of bound states flies towards the detectors, where the multiplicity and species of particles is measured.

While the final stage of the evolution is beyond a weak-coupling description, certain aspects of the dynamics at the earliest stage are better described by a weak-coupling approximation, suggesting the presence of both strongly and weakly coupled degrees of freedom simultaneously.

Currently, there is no theoretical framework which captures the complete evolution of heavy ion collisions in one framework. To date, most work has been done in a solely weak-coupling scenario or a solely strong-coupling scenario. Weak-coupling scenarios are usually based on perturbative QCD (pQCD) [9], where the strong coupling constant is treated as small, $\alpha_s \ll 1$. The weak-coupling scenario should indeed be suitable to describe, in particular, the early stages of heavy ion collisions, when the partons are highly energetic and thus, α_s can be taken small. However, for softer modes close to Λ_{QCD}, α_s increases sharply. The strong-coupling scenarios are usually encapsulated by the the Anti de Sitter/Conformal Field Theory (AdS/CFT) correspondence, providing a method to study collective effects which are difficult to describe perturbatively. Of course, the interplay between the weak and strong phenomena, for instance between the semi-hard partons and the soft gluonic bath, would not be captured in just a weakly or strongly coupled scenario.

Some qualitatitive and quantitative understanding has been achieved with a patchwork of theories. One particularly notable example of this is [10, 11], where the early post-collision stage, described via QCD kinetic theory, is matched to hydrodynamic evolution. This approach is remarkably successful in providing hydrodynamic simulations with realistic initial conditions arising from kinetic theory, which leads to more tractable predictions.

A proposal for a strong/weak hybrid approach in the QGP, addressing specifically jet quenching, is due to [12–15], where the energy loss of a jet is modeled via the AdS/CFT correspondence. The holographic aspect comes into play when modelling the soft interactions via trailing string solutions behind each parton. In particular, the energy loss of partons (light quarks and gluons) is computed from gauge/gravity duality, which then serves as an input into a hydrodynamic description of the evolution of the QGP. Note that backreaction was not taken into account.

Another approach to incorporating weak/strong dynamics is known as semiholography, the central topic of this thesis. The term semiholography was coined by Faulkner and Polchinski [16] in the context of non-Fermi liquids. As in [17–20], they proposed including gauge/gravity duality into the study of non-Fermi liquids, motivated by the observation that it can reproduce the low energy critical exponents of fermionic propagators on the Fermi surface, demonstrating particle-hole asymmetry from first principles that were previously proposed in [21] and [22] on phenomenological grounds. Including holography in the discussion of condensed matter system is by no means unique, [23–25]; the key insight was to realize that the non-Fermi liquids that were studied contain a Fermi surface, which can be tackled with conventional techniques, as well as an electron propagator with IR-singular behavior. They proposed a linear hybridization of the conventional electron with a fermionic operator in a quantum critical holographic theory represented by a freely propagating fermion in the $AdS_2 \times R^2$ geometry. Only the IR "half" of the physics was governed by holography; hence the name "semiholography". Later Mukhopadhyay and Policastro [26] studied a generalization of this model introducing arbitrary couplings within and between the two sectors with specific large N scalings, which demonstrated that semiholography can provide an effective description for a large class of non-Fermi liquids. The dynamical screening of Coulomb interactions reveals the possibility of a novel superconducting mechanism [27]. For other related works see [27–31].

The first application of semi-holography in heavy ion collisions was discussed by Iancu and Mukhopadhyay [32]. Namely, the semi-hard, weakly coupled overoccupied gluon modes are described by classical YM fields, which are minimally coupled to the soft, strongly coupled degrees of freedom, represented by gauge-invariant operators of the IR-CFT.

This was then modified and extended in [33, 34], where the self-consistency and numerical validity of the proposed model was tested. An additional demand of this approach was to have a well-defined action principle, allowing for the construction of a complete energy-momentum tensor for the total system in flat space. Although the YM system involves an effective metric, which is determined ultra-locally by the energy-momentum tensor of the holographic sector, this feature can be re-interpreted as a marginal deformation of the theory in flat space. Similarly the boundary metric of the holographic geometry representing the strongly interacting IR degrees of freedom is deformed by the energy-momentum tensor of the YM sector. The full energy-momentum tensor which is conserved in flat space is local and can be explicitly constructed. Furthermore, as a numerical test, the authors studied a homogeneous, isotropic model, with the added simplification that the YM gauge field was chosen to be color-spin-locked. An iterative procedure to solve the equations was outlined and it was demonstrated that the numerical procedure converges rapidly.

The semiholography approach was then further supplemented in [35] by a discussion of the derivation of semiholographic models. In particular it was argued that the perturbative physics should be able to determine nonperturbative effects, i.e. the strongly coupled holographic sector, as well as the hard-soft (perturbative-nonperturbative) coupling. This was explored in a simple model, where two holographic models are coupled semiholographically. The implications for QCD were also outlined, where the authors claimed that the renormalon Borel poles that are found in the perturbative series of QCD need to be cancelled against non-perturbative physics.

In this thesis, we study the properties and consequences of semiholographic couplings. In particular, we consider different aspects of applicability of semiholography. A particular innovation of the semiholographic approach is that one can work with effective descriptions, i.e. the microscopic detail of an action is not necessary. As a result, we can implement effective descriptions, such as hydrodynamics and kinetic theory, to make computations analytically accessible. To this end, we begin by considering two fluids coupled semiholographically, which we refer to as bi-hydrodynamics [36]. This is meant to model the interaction between the long wavelength excitations of the hard YM sector and the soft, holographic sector, which we expect to be present at intermediate times during the evolution of the QGP. We then move on to describe a toy model of glasma, where we demonstrate using numerical AdS/CFT techniques the first proof of principle transfer of energy from the hard YM sector to the holographic sector [37]. This would model the early times of the QGP.

The outline of this thesis is as follows: chapter 2 describes the relevant theoretical background to understand the various models considered later, in particular the AdS/CFT correspondence, hydrodynamics and an introduction to kinetic theory. In chapter 3, we describe the near equilibrium implications of a semiholographic model with metric coupling, i.e. bi-hydrodynamics. In chapter 4, we consider a scalar semiholographic coupling describing the early stages of QGP evolution, where energy is transferred from classical YM fields to a black hole. In chapter 5, a toy model describing the coupling between a scalar field and Jackiw-Teitelboim gravity coupled to non-conformal matter, known as nearly-AdS$_2$ ($NAdS_2$) is considered. Longer computations can be found in the appendices. For units and conventions, see page ix. For a list of abbreviations used, see Appendix F.

Chapter 2

Theoretical background

In this chapter, we aim to provide the relevant theoretical background and concepts that will prove useful in this thesis, however without reviewing the areas of general relativity and quantum field theory, for which we refer for example to [38–41].

We begin by describing the holographic principle as well as stating the AdS/CFT correspondence, which is necessary in motivating semiholography. We then shift our attention to effective descriptions that will be useful in chapter 4, first focussing on relativistic hydrodynamics and concluding with an introduction to kinetic theory.

2.1 Holography and the AdS/CFT correspondence

In this section we will provide a brief overview of holography, in particular as it will be used in this thesis. For a more complete treatment, see the following reviews [42–46] or the following textbooks: [47–49]. In particular, for a derivation of the AdS/CFT correspondence without recourse to string theory, it is worthwhile to read [44].

The holographic principle was originially formulated by ‘t Hooft [50] and then further refined by Susskind [51]. It states that in a theory of gravity, the number of degrees of freedom scale as the surface area A (instead of as volume V), like holograms, which store information from a higher dimensional setting (3D) to a lower dimensional film (2D). The argument describing this arises from considering the entropy of a black hole, known as the Bekenstein-Hawking entropy [52, 53]:

$$S_{BH} = \frac{A}{4G}, \tag{2.1}$$

where A is the surface area of the black hole and G is the Newton constant. The maximum amount of entropy stored in a given volume is given by S_{BH}.

One concrete example of holography is known as the AdS/CFT correspondence. The AdS/CFT correspondence, also known as the gauge/gravity correspondence, is one of the most celebrated recent results of theoretical physics, linking two seemingly distinct theories.

The original proposal of Maldacena [54] of the AdS/CFT correspondence can be stated as follows [48]:

$\mathcal{N} = 4$ Super Yang-Mills (SYM) theory with gauge group $SU(N)$ and coupling constant g_{YM} is dynamically equivalent to type IIB string theory with string length

l_s and coupling constant g_s on $AdS_5 \times S^5$ with radius of curvature L. The correspondence maps the free parameters on the field theory, g_{YM} and N, to the free parameters on the string theory side, g_s and L/l_s, via

$$g_{\mathrm{YM}}^2 = 2\pi g_s \qquad \text{and} \qquad 2g_{\mathrm{YM}}^2 N = L^4/l_s^4. \tag{2.2}$$

Note that the string length is often referred to in the literature as $l_s = \sqrt{\alpha'}$, where α' is known as the Regge slope and related to the string tension, T, via $2\pi T = 1/\alpha'$ [55].

The name of the correspondence arises from the fact that there is a conjectured correspondence between SYM, an example of a conformal field theory (CFT), and a theory of gravity, living in an Anti-de Sitter (AdS) background.

It is necessary to point out at this point that the AdS/CFT correspondence is exactly as the name suggests: a correspondence without a formal proof. However, there is a lot of non-trivial evidence supporting the conjecture. For instance, a check of the correspondence was undertaken in [56], where correlation functions were compared on both sides of the theory and found to agree.

The meaning of the correspondence is that the two theories, one a theory of gravity and the other a field theory, describe the same physics. The AdS/CFT correspondence provides a one-to-one map between these two theories. This map, commonly referred to as the *dictionary*, relates gauge-invariant operators on the field theory side to their respective dual fields on the gravity side. An explicit way to express this correspondence is by relating generating functionals to partition functions. Namely, the generating functional of CFT correlation functions is identified with the partition function of type IIB string theory [57], i.e.

$$\langle e^{\int \mathrm{d}^d x \mathcal{O}\phi_{(0)}} \rangle = Z_{string}[\phi], \tag{2.3}$$

where ϕ represents a bulk field dual to an operator $\mathcal{O}$ of dimension Δ and $\phi_{(0)}$ represents the asymptotic boundary value of ϕ, namely $\lim_{z\to 0} z^{\Delta-d}\phi(z,x) = \phi_{(0)}(x)$. This is how a theory of gravity in $d+1$ dimensions is related to a field theory in d dimensions.

The conjecture can be explored by considering various limits of its parameters. For instance, we will consider the weak coupling limit of string theory, where the coupling constant $g_s \ll 1$, while L/l_s is taken to be constant. Then on the field theory side, $g_{YM} \ll 1$, while $g_{YM}^2 N$ is fixed to be constant. This is only possible in the so-called large N limit or 't Hooft limit, $N \to \infty$.

As a result, in this limit, we have one free parameter on each side of the correspondence, namely the 't Hooft coupling $\lambda = g_{YM}^2 N$ on the CFT side and the radius of curvature L/l_s on the gravity side. Since these are to be kept finite, we can relate these parameters via

$$\frac{L^4}{l_s^4} = 2\lambda. \tag{2.4}$$

Thus, we only have one free parameter. If we take the string length to zero, then the strings become point-like. This represents the low-energy limit of string theory, which is described via a supergravity theory. Taking the string length to zero means that the 't Hooft coupling goes to infinity, i.e. the field theory becomes strongly coupled. More precisely, strongly coupled $\mathcal{N} = 4$ SYM is dual to type IIB supergravity on weakly curved $AdS_5 \times S^5$.

Hence, the AdS/CFT correspondence in this limit is an example of a *weak-strong* duality: a weakly coupled theory of gravity is related to a strongly coupled field theory. As weakly coupled gravity theories are accessible to study, the correspondence provides a tool to explore strongly coupled field theories. It should be pointed out that this argument can be reversed:

weakly coupled field theory can be used to probe strongly coupled, quantum gravity. As this thesis centers on studying strongly coupled plasmas, we will not pursue this aspect of the correspondence.

2.1.1 Applications of holography to the QGP

Holography is a promising tool for making progress in understanding the QGP whenever the coupling grows strong, i.e. $\alpha_s \sim 1$. In particular, this corresponds to the time a few fm/c after a heavy ion collision, when the QGP is undergoing hydrodynamical evolution. One can take the hydrodynamic limit of a given holographic model as in [60, 61].

Holography also can tell us about the real time evolution of the QGP by mapping the problem of colliding nuclei to colliding shock waves in a gravitational theory (the dual of which sheds insight into the properties of the QGP), see Fig. 2.1. Chesler and Yaffe [62, 63] laid the groundwork for studying far-from-equilibrium dynamics of gravitational shocks in an anisotropic, homogeneous system. There have since been many different applications of that approach: demonstrating that hydrodynamics is a valid description even with large anisotropies present [64], implementing radial flow [65] and studying collisions in non-conformal theories [66]. For a review of the current status of the field, see [67].

One of the more widely appreciated applications of the AdS/CFT correspondence is due to Policastro, Son and Starinets [68], where they compute in a holographic model the specific viscosity, i.e. the dimensionless ratio of the shear viscosity to the entropic density, to be

$$\frac{\eta}{s} = \frac{1}{4\pi} \tag{2.5}$$

for a strongly coupled plasma. Note that a larger shear viscosity corresponds to more momentum exchange between distant fluid cells [67]. In a subsequent work, Kovtun, Son and Starinets speculated that the low value of η/s could be interpreted as a lower bound for a wide range of physical models [6]. This is aptly summarized in Fig. 2.2.

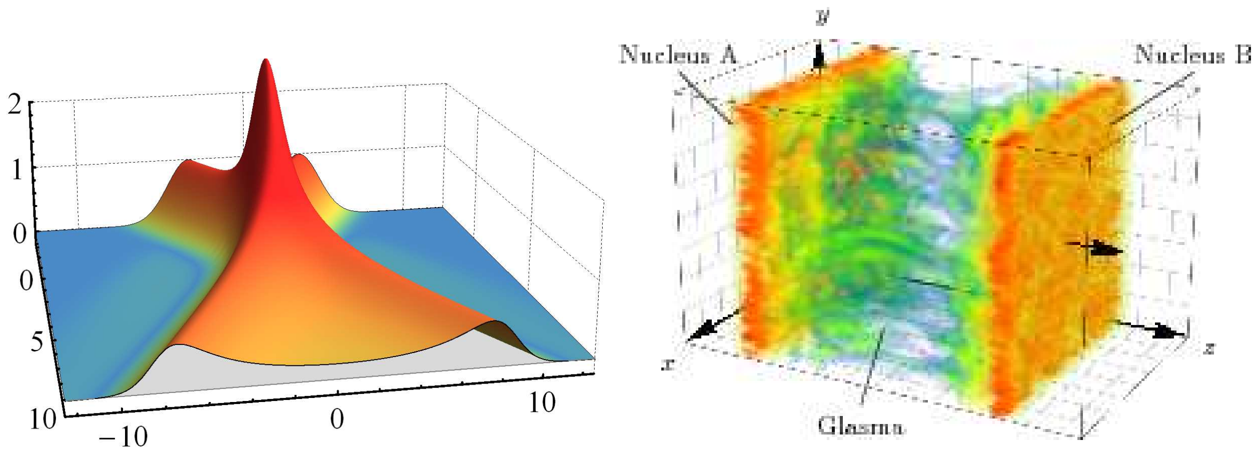

Figure 2.1: Left: Gravitational shocks simulation from [58]. The nuclei collide in the plane and move towards the bottom of the image, producing a wake. Right: CGC simulation after the collision of two nuclei. The glasma forms in the wake of the two nuclei passing through each other. Figure from [59].

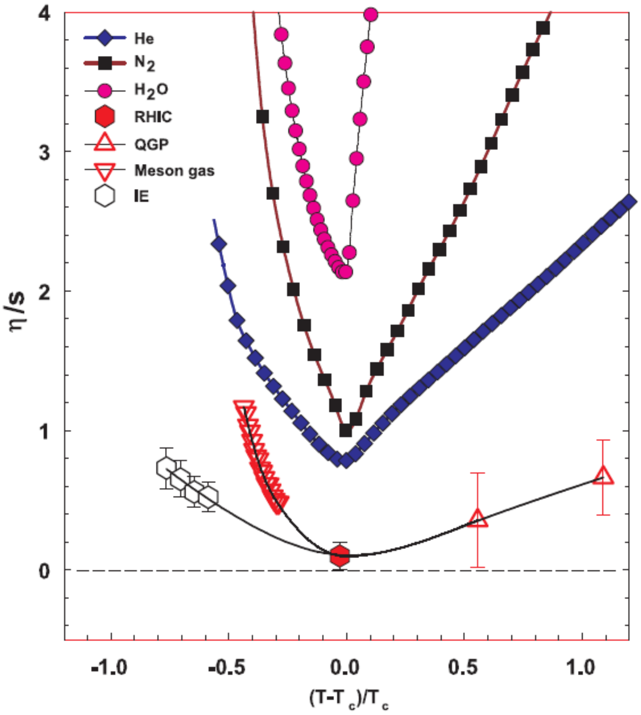

Figure 2.2: The ratio of the shear viscosity to the entropy density is plotted against the reduced temperature for various substances. Note that data from RHIC puts η/s at the lowest known value in nature, above what is predicted holographically. Plot from [69]

.

There are, of course, some limitations to employing the AdS/CFT correspondence to heavy ion collisions. One important difference is that the $\mathcal{N} = 4$ SYM theory is superconformal and does not exhibit confinement. Another is that in the AdS/CFT correspondence one tends to work in the limit of large number of colors, $N_c \to \infty$, whereas QCD has three colors. As such, the AdS/CFT correspondence should be treated as an effective tool to access strong coupling computations, when methods from first principles are not yet mature or the computation is perturbatively inaccessible.

2.2 Hydrodynamics

Hydrodynamics is an effective macroscopic description of some microscopic theory. It is an expression of the low energy, long wavelength of a theory and as such, represents an expansion in gradients. Here, we will follow the discussion of [70]. For a discussion on standard fluid dynamics, see [71]. A pertinent and useful review on relativistic hydrodynamics can be found in [72]. A more recent textbook on relativistic hydrodynamics can be found in [73]. Hydrodynamics has been an effective tool in describing collective behavior in the wake of heavy ion collisions. An incomplete list of results include: elliptic flow coefficient prediction matching with experiment at RHIC [74–77], evidence that the QCD shear viscosity is closer to the strong coupling value than to the weak coupling [5] and development of 3 + 1 dimensional anisotropic relativistic hydrodynamics [78]. For a more complete review of hydrodynamics in the QGP, see [79] and [80].

The equations of motion of hydrodynamics arise from considering the conservation of energy, momentum and other global charges. For this thesis, the hydrodynamical EOM will be just given by the conservation of the energy momentum tensor

$$\nabla_\mu T^{\mu\nu} = 0. \tag{2.6}$$

If one were to consider additional fields, e.g. heat current, then the equations above are supplemented by the conservation of the associated currents, e.g.

$$\nabla_\mu J_i^\mu = 0. \tag{2.7}$$

2.2.1 Perfect fluids

The perfect fluid energy momentum tensor is

$$T_0^{\mu\nu} = (\varepsilon + P)u^\mu u^\nu + P g^{\mu\nu}, \tag{2.8}$$
$$= \varepsilon u^u u^\nu + P\Delta^{\mu\nu}, \tag{2.9}$$

where ε is the energy density, P is the pressure and the spatial projection is defined as

$$\Delta^{\mu\nu} = u^\mu u^\nu + g^{\mu\nu}. \tag{2.10}$$

The combination $\varepsilon + P$ is known as the enthalpy. The fluid four-velocity u^μ is a timelike vector, which is normalized via

$$u^\mu u^\nu g_{\mu\nu} = -1. \tag{2.11}$$

As a warm-up exercise, let's consider the linearized equations of hydrodynamics in flat space, namely

$$\partial_\mu T_0^{\mu\nu} = 0. \tag{2.12}$$

First we should see if the system is solvable, i.e. the number of variables match the number of equations. The fluid velocity has four components, one of which is fixed by the normalization, such that we can choose in the rest frame of the fluid

$$u^\mu = \begin{pmatrix} 1 \\ 0 \\ 0 \\ 0 \end{pmatrix} + \begin{pmatrix} 0 \\ \delta u^x \\ \delta u^y \\ \delta u^z \end{pmatrix}. \tag{2.13}$$

As such, we have four equations in (2.6) with five variables: ε, P and δu^i. Thus, we need to provide another equation. Specifically, it is useful to relate the energy density with the pressure, which is known as the equation of state. For the moment, we will avoid precisely specifying the equation of state, merely referring to the pressure as a function of the energy density:

$$P = P(\varepsilon). \tag{2.14}$$

The linearized energy density is given by

$$\varepsilon = \varepsilon_0 + \delta\varepsilon. \tag{2.15}$$

Now the linearized equations are

$$\partial_0 \delta\epsilon + \partial_i \delta u^i = 0, \tag{2.16}$$
$$\partial_i P(\delta\varepsilon) + u^\mu \partial_\mu \delta u^i = 0. \tag{2.17}$$

Noting that the gradient of the pressure can be written as $\partial_i P = \frac{\partial P}{\partial \varepsilon} \partial_i \delta\varepsilon$ due to the chain rule and that $u^\mu \partial_\mu = \partial_0$ in the rest frame of the fluid, we can take the divergence of the last equation and solve for δu^i:

$$\partial_i \partial_0 \delta u^i = -\frac{\partial P}{\partial \varepsilon} \partial^2 \varepsilon. \tag{2.18}$$

We can now take the time derivative of (2.16) and insert (2.18) to arrive at

$$\left[\partial_0^2 - \frac{\partial P}{\partial \varepsilon} \partial_i \partial^i\right] \delta\varepsilon = 0, \tag{2.19}$$

which is just the wave equation. Likewise, a similar equation holds for δu^i. We can identify the speed of sound as

$$c_s^2 = \frac{\partial P}{\partial \varepsilon}. \tag{2.20}$$

Similarly, we can repeat the above exercise in Fourier space, such that (2.16) and (2.17) read

$$-i\omega\delta\varepsilon + ik_i \delta u^i = 0, \tag{2.21}$$
$$ik_i P(\varepsilon) - i\omega \delta u^i = 0, \tag{2.22}$$

which leads to the dispersion relation

$$\omega = \sqrt{\frac{\partial P}{\partial \varepsilon}} k. \tag{2.23}$$

Thus, the group velocity, $\mathrm{d}\omega/\mathrm{d}k$, is just the speed of sound given in (2.20).

2.2.2 Dissipative fluids

To add dissipation to the above discussion, it is necessary to supplement the energy momentum tensor with an extra term:

$$T^{\mu\nu} = T_0^{\mu\nu} + \Pi^{\mu\nu}. \tag{2.24}$$

Naturally, the question arises as to how to specify the form of $\Pi^{\mu\nu}$. First, we will need to specify a frame because u^μ and T have no microscopic definitions as of yet. We can define u^μ as the energy current, which means it must be the time-like eigenvector of the energy-momentum tensor with eigenvalue interpreted as the local energy density. We will work in the Landau frame, where the energy density is the eigenvalue of the following equation

$$T^\mu{}_\nu u^\nu = -\varepsilon u^\mu. \tag{2.25}$$

In this frame, the dissipative terms are thus orthogonal to the fluid velocity, i.e.

$$u_\mu \Pi^{\mu\nu} = 0. \tag{2.26}$$

As a side note, another common frame choice is the Eckart frame [81], where the number current is matched to the number density via $N^\mu = nu^\mu$.

It is useful to recall that the theory of hydrodynamics is given in terms of a derivative expansion. For the purpose of this thesis, we will restrict ourselves to first order hydrodynamics (for higher order corrections, see for example [82]). To proceed, one can write down all possible velocity gradients subject to the chosen frame; see [70] for more details. One finds that to first order in derivatives in the Landau frame, the dissipation term takes the following form

$$\Pi^{\mu\nu} = -2\eta\sigma^{\mu\nu} - \zeta\nabla_\alpha u^\alpha \Delta^{\mu\nu}, \tag{2.27}$$

$$\sigma^{\mu\nu} = (\nabla_\alpha u_\beta + \nabla_\beta u_\alpha)\Delta^{\alpha\mu}\Delta^{\beta\nu} - \frac{2}{3}\nabla_\alpha u^\alpha \Delta^{\mu\nu}, \tag{2.28}$$

where η is the shear viscosity and ζ is the bulk viscosity. Note that the shear tensor $\sigma^{\mu\nu}$ is symmetric and traceless. The shear viscosity is a measure of the shearing force. The bulk viscosity is a measure of the resistance of a fluid to deformations due to compression. These parameters can be computed from the underlying microscopic physics that one is modeling hydrodynamically or can be determined phenomenologically via experiment.

There is one outstanding issue in implementing first order hydrodynamics: the theory has acausal modes. An easy way to see this is to consider the linearized problem in one spatial dimension. Following [83], for the perturbation of the form

$$\varepsilon = \varepsilon_0 + \delta\varepsilon(t,x), \qquad u^\mu = (1,\vec{0}) + \delta u^\mu(t,x), \tag{2.29}$$

we see that (2.17) gets an extra viscous term

$$\partial_i P(\delta\varepsilon) + u^\mu \partial_\mu \delta u^i + \partial_j \Pi^{ij} = 0. \tag{2.30}$$

Keeping the lowest order terms in derivatives, the fluid velocity in, for example, the y-direction obeys the following diffusion equation:

$$\partial_t \delta u^y - \frac{\eta}{\varepsilon_0 + P_0}\partial_x^2 \delta u^y = \mathcal{O}(\delta^2). \tag{2.31}$$

Bringing the above equation to frequency-momentum space using a mixed Laplace-Fourier transform,

$$\delta u^y \to \delta u^y e^{-\omega t + ikx}, \tag{2.32}$$

one arrives at

$$\omega = \frac{\eta}{\varepsilon_0 + P_0}k^2, \tag{2.33}$$

which has a group velocity

$$v = \frac{\mathrm{d}\omega}{\mathrm{d}k} = \frac{2\eta}{\varepsilon_0 + P_0}k. \tag{2.34}$$

The speed of diffusion thus grows linearly with wavenumber, meaning that the diffusion speed will eventually surpass the speed of light and thus violate causality.

In order to cure this potential acausality, one can go to higher order in hydrodynamics. This is rather involved. A simpler fix is known as the Israel and Stewart method [84–86]. Essentially, one introduces an additional equation for the dissipative tensor $\Pi^{\mu\nu}$, such that it relaxes to the form in (2.27). In practical terms, one improves the dissipative term to include a relaxation time parameter, τ_π:

$$\Pi^{\mu\nu} = -2\eta\sigma^{\mu\nu} - \zeta\nabla_\alpha u^\alpha \Delta^{\mu\nu} - \tau_\pi u^\alpha \nabla_\alpha \Pi^{\mu\nu}. \tag{2.35}$$

The dissipative term relaxes to its true value in some finite time τ_π, limiting the acausality of the system.

2.2.3 Linear response and the Kubo formula

In this section, we introduce the Green-Kubo formula [87,88] (also sometimes referred to as just the Kubo formula). Although we will ground the discussion in hydrodynamics, it is important to remember that linear response theory proves useful for many theories and techniques outlined here can be implemented in other sectors, including holography and kinetic theory, see e.g. [60] and [89], respectively. We will follow the discussion in [90] and [48] for this section.

First, we will provide a quick overview of linear response theory. Consider a theory with a Hamiltonian, $\mathcal{H}_0$, which is perturbed by an external field $J(x^\mu)$. The external field is coupled to an operator $\mathcal{O}$. Then the change to $\mathcal{H}_0$ is given by

$$\delta\mathcal{H} = -\int d^d x J(x^\mu)\mathcal{O}(x^\mu). \tag{2.36}$$

Furthermore, the external fields provide a change to the expectation value of the operators themselves in a causal manner, which in Fourier space reads

$$\delta\langle O(k^\mu)\rangle = G_R(k^\mu)J(k^\mu), \tag{2.37}$$

where the retarded Green function is

$$G_R(x^\mu, y^\mu) = -i\theta(x^0 - y^0)\langle[\mathcal{O}(x^\mu), \mathcal{O}(y^\mu)]\rangle. \tag{2.38}$$

In other words, the external fields, J acts as a *source* for the change of the expectation value, i.e. the *response*.

The Kubo formula provides a method to compute transport coefficients in linear response theory. In particular, we will demonstrate here the computation of the shear viscosity. Consider perturbing the background metric of a viscous fluid in a homogeneous, time-dependent manner

$$g_{\mu\nu} = \eta_{\mu\nu} + h_{\mu\nu}(t), \tag{2.39}$$

with $h_{0i} = h_{ii} = h_{yz} = 0$. Note that this perturbation does not modify the equilibrium solution, so the four-velocity is still in the rest frame $u^\mu = (1, \mathbf{0})$ and the temperature is unchanged $T = T_0$. Furthermore, we are considering linear response, so we will drop all terms higher than linear order in the perturbation, $\mathcal{O}(h_{xy}^2)$. Fourier transforming, we can easily compute the shear tensor (2.28) to find that the only non-zero component is

$$\sigma_{xy} = -i\omega\eta h_{xy}. \tag{2.40}$$

The energy momentum tensor can be expanded in terms of perturbations [89] via

$$T^{\mu\nu} = T^{\mu\nu}_{(0)} - \frac{1}{2}G_R^{\mu\nu,\alpha\beta}h_{\alpha\beta} + \dots, \tag{2.41}$$

where $T^{\mu\nu}_{(0)}$ is the unperturbed energy momentum tensor and $G_R^{\mu\nu,\alpha\beta}$ is the retarded Green function. Varying the full energy momentum tensor w.r.t. the metric perturbation, we arrive at

$$\frac{\partial}{\partial h_{\alpha\beta}}(T^{\mu\nu} - T^{\mu\nu}_{(0)}) = -\frac{1}{2}G_R^{\mu\nu,\alpha\beta} \tag{2.42}$$

$$\Rightarrow G_R^{xy,xy} = -i\omega\eta. \tag{2.43}$$

Now if we want to read off the transport coefficient, we see that

$$\eta = -\lim_{\omega\to 0}\frac{1}{\omega}\mathrm{Im}G_R^{xy,xy}(\omega, k=0). \tag{2.44}$$

Remember that we are considering only a time-dependent perturbation. If we were to consider spatial dependence, then the hydrodynamic limit is given by first taking the wave number, k, to zero first, followed by the frequency, ω. This is important to point out, as these limits do not commute in general.

Similarly, we can compute the bulk viscosity via another Kubo relation. We choose another perturbation

$$g_{\mu\nu} = \eta_{\mu\nu} + h_{\mu\nu}(t), \tag{2.45}$$

with only $h_{ii} \neq 0$. The shear tensor is traceless, so we only need to consider the bulk term. We find that

$$\nabla_\alpha u^\alpha = \Gamma^\alpha{}_{\alpha 0} = -\frac{i\omega}{2}\delta^{ij}h_{ij}. \tag{2.46}$$

Then

$$\zeta = \lim_{\omega\to 0}\frac{1}{9\omega}\delta_{ij}\delta_{kl}G_R^{ij,kl}(\omega, k=0), \tag{2.47}$$

which agrees with [91] if one takes into account the differing definition of the retarded Green function (by a factor of 4).

2.3 Kinetic theory

Here we follow the discussion in [92]. For an introductory set of lecture notes, see [93]. Some textbooks on the topic are [94] and [95]. In the context of heavy ion collisions, kinetic theory has a range of applicability especially during the early stages of evolution of the QGP, when hard partons are in abundance. In particular, one can replace the complications of a first principles QCD treatment with a kinetic theory [11]. Another example is that one can study color mode instabilities in the QGP using kinetic theory [96].

Kinetic theory concerns itself with the microscopic detail of particles directly. For illustrative purposes, it is useful to keep the picture of a classical gas in $3+1$ dimensions of N distinct particles with various momenta in mind. We can then introduce a function which keeps track of the particles' positions and momenta. This is known as the N-particle distribution function, which we will call $f_N = f_N(x_1^\mu, ..., x_N^\mu, p_1^\mu, ..., p_N^\mu)$. As we are considering a closed system, the evolution of f_N in phase space is conserved due to Liouville's theorem [94]:

$$0 = \frac{\mathrm{d}f_N}{\mathrm{d}\tau} = \left[p^\mu\partial_\mu + F^\mu\partial_{p^\mu}\right]f_N, \tag{2.48}$$

where τ is an affine parameter, $p^\mu = \frac{\mathrm{d}u^\mu}{\mathrm{d}\tau}$ is the four momentum and $F^\mu = \frac{\mathrm{d}p^\mu}{\mathrm{d}\tau}$ is the four force.

Of course, keeping track of all particle positions and momenta is usually overkill – and oftentimes unfeasible, as systems of interest typically have a large number of particles. Instead, it is more practical to introduce the manifestly Lorentz invariant one-particle distribution function, $F = F(x^\mu, p^\mu)$, which labels a single on-shell particle with its position and momentum. The manifestly Lorentz invariant form of the one-particle distribution function is often reduced by putting it on-shell:

$$F(x^\mu, p^\mu) = \theta(p_0)\delta(p^\mu g_{\mu\nu} p^\nu + m^2) f(x^\mu, p^j), \tag{2.49}$$

where the Heaviside function, $\theta(p^0)$ chooses positive energies and the delta function enforces the mass-shell condition

$$p^2 = p^\mu p_\mu = -m^2, \tag{2.50}$$

where m is the mass. To make contact with literature, we will now refer to $f = f(x^\mu, p^j)$ as the one-particle distribution function, sometimes calling it just the distribution function. Note that the momentum is defined covariantly, with $p^\nu = g^{\mu\nu}(x)p_\mu$, (for alternate definitions, see [97, 98] for details).

To extract some more useful macroscopic information from the one-particle distribution function, it is helpful to integrate out the momentum dependence. The different moments of the distribution function correspond to physically interesting quantities:

$$\begin{aligned} n^\mu(x^\mu) &= -\sqrt{-g}\int \frac{\mathrm{d}^3 p}{(2\pi)^3}\frac{p^\mu}{p_0} f(x^\mu, p_i), \\ T^{\mu\nu}(x^\mu) &= -\sqrt{-g}\int \frac{\mathrm{d}^3 p}{(2\pi)^3}\frac{p^\mu p^\nu}{p_0} f(x^\mu, p_i), \end{aligned} \tag{2.51}$$

where $n \equiv n^0$ is the number density, n^μ is the number current and $T^{\mu\nu}$ is the energy momentum tensor [99]. Note that higher moments can also be considered, but for the purposes of this thesis these are less interesting.

As a simple example, we can compute the number density and the energy momentum tensor for a massless gas of particles in flat space. The mass-shell condition then reads

$$p_0 = \sqrt{p_i \eta^{ij} p_j}. \tag{2.52}$$

The distribution function for this system is the Maxwell-Jüttner distribution [100, 101]:

$$f = e^{p_\mu u^\mu / T}, \tag{2.53}$$

where T is the temperature. We then find

$$n = T^3/\pi^2, \tag{2.54}$$

$$T^{\mu\nu} = \mathrm{Diag}(\varepsilon, P, P, P), \tag{2.55}$$

where $\varepsilon = 3P = 3nT$.

The evolution of the distribution function will be described by an equation similar to (2.48), but with an extra term:

$$\frac{\mathrm{d}f}{\mathrm{d}\tau} = C[f_2]. \tag{2.56}$$

The term on the RHS is the so-called collision kernel. This will depend on higher order particle distribution functions, namely the two-particle distribution function, encoding higher order correlations between particles. The two-particle distribution function in turn depends on the three-particle distribution function and so on. This hierarchy of equations is known as the Bogoliubov–Born–Green–Kirkwood–Yvon (BBGKY) hierarchy [102–105].

Of course, if we wish to describe a physical system without resorting to the full N-particle information, we will need to truncate this hierarchy at some point, i.e. specify some form for the collision kernel. There is more than one way to truncate this theory. A widely used method developed by Maxwell [106] was to assume that the two particle distribution function is just the product of two independent one-particle distributions, i.e.

$$f_2(x_1^\mu, p_1^\mu; x_2^\mu, p_2^\mu) = f(x_1^\mu, p_1^\mu) f(x_2^\mu, p_2^\mu), \tag{2.57}$$

which is known as the molecular chaos hypothesis.

For the purposes of this thesis, we will be interested in another truncation, namely the relaxed time approximation (RTA), which is also known as and will be referred to in this thesis as the Bhatnagar-Gross-Krook (BGK) approximation [107]. This extremely convenient approximation can be used to facilitate analytical computation and probe near equilibrium systems. It amounts to identifying the collision kernel as follows

$$C[f] = \frac{p^\mu u_\mu}{\tau}(f - f_{eq}), \tag{2.58}$$

where τ is the relaxation time and f_{eq} is the equilibrium one-particle distribution function. Clearly, if the one-particle distribution function is in equilibrium, the collision kernel vanishes. The RTA effectively replaces the microscopic detail of the collision kernel with a tendency of the system to relax towards its equilibrium value on some characteristic time scale, τ.

Thus, we can write down the Boltzmann equation in the RTA, describing the evolution of the (one-particle) distribution function $f = f(x^\mu, p_i)$:

$$\Big[p^\mu \partial_\mu + F^\mu \frac{\partial}{\partial p_\mu}\Big] f = \frac{p^\mu u_\mu}{\tau}(f - f_{eq}). \tag{2.59}$$

We can easily see how the RTA is useful if we consider a one dimensional system, setting $F^\mu = 0$. Furthermore, since f_{eq} is a simple constant in this example, we can shift $f - f_{eq} \to f$ without loss of generality. Then (2.59) is given by

$$\partial_0 f = -\frac{1}{\tau} f, \tag{2.60}$$

which has solution

$$f \propto e^{-t/\tau}. \tag{2.61}$$

Shifting back, $f \to f + f_{eq}$, we have that $f = f_{eq} + e^{-t/\tau}$. Thus, the distribution relaxes to its equilibrium value exponentially quickly.

The force term, F^μ, is dependent on the relevant physics. For instance, for describing a system of electromagnetic particles, the force term will be given by the Lorentz force

$$F^\mu = -qF^{\mu\nu} u_\nu, \tag{2.62}$$

where q is the charge, $F^{\mu\nu} = \partial^\mu A^\nu - \partial^\nu A^\mu$ is the Faraday tensor and u_ν is the four velocity. The Boltzmann equation with this forcing term is known as the Maxwell-Vlasov-Boltzmann equation (see e.g. [108]). For particles in curved spacetime, which we will consider in Chapter 4 when we include effective metric couplings, we have

$$F^\mu = \Gamma^\mu{}_{\alpha\beta} p^\alpha p^\beta, \tag{2.63}$$

where $\Gamma^\mu{}_{\alpha\beta}$ is the Christoffel symbol. It is straightforward to see where this force term comes from. We will do this in the next section, by providing a short derivation of the Boltzmann equation from the point of view of a single particle.

2.3.1 Derivation of the Boltzmann equation in curved spacetimes

Here we present a derivation of the Boltzmann equation, following [92]. We begin by considering the action for a single particle:

$$S = -m \int \mathrm{d}s = -m \int \mathrm{d}s \sqrt{\left| g_{\mu\nu}(x) \frac{\mathrm{d}x^\mu}{\mathrm{d}s} \frac{\mathrm{d}x^\nu}{\mathrm{d}s} \right|}. \tag{2.64}$$

If we have a collection of N-free particles, the above action then generalizes to

$$S = -m \sum_{i=1}^{N} \int \mathrm{d}s_i \sqrt{\left| g_{\mu\nu}(x_i) \frac{\mathrm{d}x_i^\mu}{\mathrm{d}s_i} \frac{\mathrm{d}x_i^\nu}{\mathrm{d}s_i} \right|}. \tag{2.65}$$

It is straightforward to derive the equation of motion for the relativistic free particle, also known as the geodesic equation, which reads

$$\frac{\mathrm{d}^2 x_i^\mu}{\mathrm{d}s_i} + \Gamma^\mu{}_{\alpha\beta} \frac{\mathrm{d}x_i^\alpha}{\mathrm{d}s_i} \frac{\mathrm{d}x_i^\beta}{\mathrm{d}s_i} = 0. \tag{2.66}$$

Introducing the relativistic momentum as

$$p_i^\mu \equiv m \frac{\mathrm{d}x_i^\mu}{\mathrm{d}s_i}, \tag{2.67}$$

we can now rewrite the action by introducing an integration over x^μ and p_μ:

$$S = -m \int \mathrm{d}^4x \mathrm{d}^4p \sum_{i=1}^{N} \int \mathrm{d}s_i \; \delta(x - x_i(s_i)) \delta(p - p_i(s_i)). \tag{2.68}$$

We now define the explicitly covariant distribution function

$$F(x^\mu, p_\mu) = \left\langle \sum_{i=1}^{N} \int \mathrm{d}s_i \; \delta(x - x_i(s_i)) \delta(p - p_i(s_i)) \right\rangle. \tag{2.69}$$

Now to derive the Boltzmann equation, we make use of the following identity

$$0 = \sum_{i=1}^{N} \int \mathrm{d}s_i \frac{\mathrm{d}}{\mathrm{d}s_i} \Big(\delta(x - x_i(s_i)) \delta(p - p_i(s_i)) \Big), \tag{2.70}$$

which leads to

$$0 = \sum_{i=1}^{N} \int \mathrm{d}s_i \Big[\frac{\mathrm{d}x_i^\mu}{\mathrm{d}s_i} \frac{\partial}{\partial x_i^\mu} + \frac{\mathrm{d}p_{i\mu}}{\mathrm{d}s_i} \frac{\partial}{\partial p_{i\mu}} \Big] \Big(\delta(x - x_i(s_i)) \delta(p - p_i(s_i)) \Big),$$
$$= -\frac{1}{m} \sum_{i=1}^{N} \int \mathrm{d}s_i \Big[p_i^\mu \frac{\partial}{\partial x^\mu} + \Gamma^\alpha{}_{\mu\beta} p_{i\alpha} p_i^\beta \frac{\partial}{\partial p_\mu} \Big] \Big(\delta(x - x_i(s_i)) \delta(p - p_i(s_i)) \Big),$$
$$= -\frac{1}{m} \sum_{i=1}^{N} \int \mathrm{d}s_i \; \frac{\partial}{\partial x^\mu} \Big(p_i^\mu \delta(x - x_i(s_i)) \delta(p - p_i(s_i)) \Big)$$
$$+ \frac{\partial}{\partial p_\mu} \Big(\Gamma^\alpha{}_{\mu\beta} p_{i\alpha} p_i^\beta \delta(x - x_i(s_i)) \delta(p - p_i(s_i)) \Big), \tag{2.71}$$

where we used that (2.66) can be rewritten in terms of the momentum as follows

$$m \frac{\mathrm{d}p_{i\mu}}{\mathrm{d}s_i} = \Gamma^\alpha{}_{\mu\beta} p_{i\alpha} p_i^\beta. \tag{2.72}$$

Taking the ensemble average of (2.71), we arrive at the completely covariant Boltzmann equation

$$\partial_\mu (F p^\mu) + \partial_{p_\mu} (F \Gamma^\alpha{}_{\mu\beta} p_\alpha p^\beta) = 0. \tag{2.73}$$

Expanding (2.73), we have

$$0 = p^\mu \partial_\mu F + \Gamma^\alpha{}_{\mu\beta} p_\alpha p^\beta \partial_{p_\mu} F$$
$$+ F \partial_\mu p^\mu + F \partial_{p_\mu} (\Gamma^\alpha{}_{\mu\beta} p_\alpha p^\beta) \tag{2.74}$$

The last line vanishes due to metric compatibility

$$\partial_\mu p^\mu + \partial_{p_\mu} (\Gamma^\alpha{}_{\mu\beta} p_\alpha p^\beta) = p_\alpha (\partial_\beta g^{\alpha\beta} + \Gamma^\mu{}_{\mu\beta} g^{\alpha\beta} + \Gamma^\alpha{}_{\mu\beta} g^{\mu\beta})$$
$$= p_\alpha \nabla_\beta g^{\alpha\beta} = 0. \tag{2.75}$$

Of course, as we are interested in describing on-shell particles, the covariant distribution function is not specific enough. Thus, as mentioned previously, we can further specify

$$F(x^\mu, p^\mu) = \theta(p_0) \delta(p^\mu g_{\mu\nu} p^\nu + m^2) f(x^\mu, p^i). \tag{2.76}$$

Integrating over p_0, we have

$$0 = \int \mathrm{d}p_0 \; \theta(p_0) \delta(p_\mu g^{\mu\nu} p_\nu + m^2) \Big(p^\mu \partial_\mu + \Gamma^\alpha{}_{j\beta} p_\alpha p^\beta \partial_{p_j} \Big) f \tag{2.77}$$
$$+ \int \mathrm{d}p_0 \; \frac{\partial \theta(p_0)}{\partial p_0} \Gamma^\alpha{}_{0\beta} p_\alpha p^\beta \delta(p_\mu g^{\mu\nu} p_\nu + m^2) f \tag{2.78}$$
$$+ \int \mathrm{d}p_0 \; \theta(p_0) f \Big(p^\mu \partial_\mu + \Gamma^\alpha{}_{j\beta} p_\alpha p^\beta \partial_{p_\mu} \Big) \delta(p_\mu g^{\mu\nu} p_\nu + m^2). \tag{2.79}$$

If we examine (2.78), we see that the Heaviside step function is hit with a derivative, which is nothing more than the delta function, i.e.

$$\frac{\partial \theta(p_0)}{\partial p_0} = \delta(p_0). \tag{2.80}$$

Thus (2.78) vanishes for particles with non-zero energy.

Next, we examine (2.79) closer

$$\begin{aligned}\left(p^\mu\partial_\mu + \Gamma^\alpha{}_{j\beta}p_\alpha p^\beta\partial_{p_j}\right)\delta(p_\mu g^{\mu\nu}p_\nu + m^2) &\propto \frac{1}{2}p^\mu p_\alpha p_\beta\partial_\mu g^{\alpha\beta} + \Gamma^\alpha{}_{\mu\beta}p^\mu p_\alpha p^\beta,\\ &\propto p_\nu p_\alpha p_\beta g^{\mu\nu}\left(\partial_\mu g^{\alpha\beta} + \Gamma^\alpha{}_{\mu\gamma}g^{\gamma\beta} + \Gamma^\beta{}_{\mu\gamma}g^{\gamma\alpha}\right),\\ &= \nabla_\mu g^{\alpha\beta} = 0, \end{aligned} \tag{2.81}$$

due to metric compatability.

Thus we see that we are left with (2.77), which if we integrate over the energy, p_0, leaves us with the collisionless **Boltzmann equation** in a curved background:

$$\left[p^\mu\partial_\mu + \Gamma^\alpha{}_{i\beta}p_\alpha p^\beta\frac{\partial}{\partial p_i}\right]f = 0. \tag{2.82}$$

2.3.2 Linearized Boltzmann equation

Now we can proceed to linearize the curved Boltzmann equation, following [89]. For simplicity, we will linearize around a flat background, namely the Minkowski metric, as follows

$$g_{\mu\nu}(x^\mu) = \eta_{\mu\nu} + h_{\mu\nu}(x^\mu). \tag{2.83}$$

This perturbation will induce a change in the distribution function, as well as the equilibrium distribution function. The equilibrium in the curved background is different to the equlibrium in flat space. This will induce a fluctuation in the temperature and the fluid velocity

$$T(x^\mu) = T_0 + \delta T(x^\mu), \tag{2.84}$$
$$u^\mu(x^\mu) = u_0^\mu + \delta u^\mu(x^\mu), \tag{2.85}$$
$$u_0^\mu = (1,0,0,0). \tag{2.86}$$

Furthermore, we require that to linear order in perturbations the 4-velocity is properly normalized, i.e.

$$\begin{aligned} -1 = u^\mu u_\mu \Rightarrow -1 &= u_0^\mu u_0^\nu(\eta_{\mu\nu} + h_{\mu\nu}) + 2\delta u^\mu\eta_{\mu\nu}u^\nu,\\ \Rightarrow -1 &= -1 + h_{00} - 2\delta u^0,\\ \Rightarrow \delta u^0 &= \frac{1}{2}h_{00}. \end{aligned} \tag{2.87}$$

Thus the equilibrium distribution function is

$$f_{eq} = f_0 + \delta f_{eq}, \tag{2.88}$$
$$f_0 = e^{p^\mu u_\mu/T}, \tag{2.89}$$
$$\delta f_{eq} = f_0\frac{p^0}{T_0}\left(v^i\delta u^i + \frac{\delta T}{T_0}\right). \tag{2.90}$$

Finally, the distribution function will be given by

$$f(x^\mu) = f_0 + \delta f(x^\mu). \tag{2.91}$$

Then, Fourier transforming (2.59) and expanding to linear order in perturbations, we have

$$ip^{\mu}k_{\mu}\delta f + \Gamma^{\mu}{}_{\alpha\beta}p^{\alpha}p^{\beta}\frac{\partial f_0}{\partial p^{\mu}} = \frac{p^{\mu}u_0^{\nu}\eta_{\mu\nu}}{\tau}(\delta f - \delta f_{eq}), \tag{2.92}$$

which we can solve for δf to arrive at

$$\begin{aligned}\delta f &= \frac{1}{ip^{\mu}k_{\mu} + \frac{p^0}{\tau}}\Big(\frac{p^0}{\tau}\delta f_{eq} + \Gamma^{\mu}{}_{\alpha\beta}p^{\alpha}p^{\beta}\frac{\partial f_0}{\partial p^{\mu}}\Big),\\ &= \frac{1}{-i\omega + i\vec{v}\cdot\vec{k} + \frac{1}{\tau}}\Big(\frac{1}{\tau}\delta f_{eq} + \Gamma^{\mu}{}_{\alpha\beta}\frac{p^{\alpha}p^{\beta}}{p^0}\frac{\partial f_0}{\partial p^{\mu}}\Big),\end{aligned} \tag{2.93}$$

where $\vec{v} \equiv \vec{p}/|\vec{p}|$.

Now we can compute the correction to the energy momentum tensor due to the metric perturbation:

$$T^{\mu\nu} = T_0^{\mu\nu} + \delta T^{\mu\nu}, \tag{2.94}$$

which is just given by integrating δf in (2.51), i.e.

$$\delta T^{\mu\nu} = \int \frac{\mathrm{d}^3p}{(2\pi)^3p^0}p^{\mu}p^{\nu}\delta f. \tag{2.95}$$

An important step is to compute the fluctuations of the temperature and velocity as functions of the metric perturbations. We do this by identifying $\delta T^{00} = \delta\varepsilon$ and $\delta T^{0i} = (\varepsilon + P)\delta u^i$, where ε is the energy density and P is the pressure. Specifying the dependence of the energy density on temperature means that we can write $\delta\varepsilon = \delta\varepsilon(T)$, i.e. for a relativistic massless gas the energy density goes like

$$\varepsilon \sim T^4. \tag{2.96}$$

Thus, if we apply these four conditions, we can compute $\delta T(h_{\mu\nu})$ and $\delta u^i(h_{\mu\nu})$, eliminating these hydrodynamic variables.

2.3.3 Transport coefficients in kinetic theory

From here it is straightforward to compute retarded Greens functions, i.e.

$$G^{\mu\nu,\alpha\beta} = \frac{\delta T^{\mu\nu}}{\delta h_{\alpha\beta}}. \tag{2.97}$$

Following the discussion from Sec. 2.2.3, we can compute transport coefficients in kinetic theory. As a simple example, we consider the perturbation (2.83), but with h_{xy} as the only nonzero component.

We find that in this case the hydrodynamic variables vanish ($\delta T = 0 = \delta u^i$) and we are left with the energy momentum tensor proportional to h_{xy}. Computing (2.97) in the hydrodynamic limit $k \to 0, \omega \to 0$, we find comparing to (2.44)

$$\eta = \frac{(\varepsilon + P)\tau}{5}, \tag{2.98}$$

which if we use the thermodynamic identity $\varepsilon + P = Ts$, where s is the entropy density, means we can identify [82, 89] the ratio of the shear viscosity to the entropy density in the BGK approximation to be

$$\frac{\eta}{s} = \frac{T\tau}{5}. \tag{2.99}$$

2.3.4 Conservation of the energy momentum tensor

Here we show that the energy momentum tensor for a system described by a Boltzmann equation is indeed conserved in curved spacetime. For simplicity and elegance, we use the manifestly covariant expression for the energy momentum tensor. We have

$$\begin{aligned}\nabla_\mu T^{\mu\nu} &= \partial_\mu T^{\mu\nu} + \Gamma^\alpha{}_{\mu\alpha} T^{\mu\nu} + \Gamma^\nu{}_{\mu\alpha} T^{\mu\alpha} \\ &= \int \frac{\mathrm{d}^4 p}{m\sqrt{-g}} \partial_\mu (p^\mu p^\nu F) + \int \frac{\mathrm{d}^4 p}{m} p^\mu p^\nu F \partial_\mu \frac{1}{\sqrt{-g}} \\ &+ \Gamma^\alpha{}_{\mu\alpha} T^{\mu\nu} + \Gamma^\nu{}_{\mu\alpha} T^{\mu\alpha} \\ &= \int \frac{\mathrm{d}^4 p}{m\sqrt{-g}} \Big[\partial_\mu (p^\mu p^\nu F)\Big] + \Gamma^\nu{}_{\mu\alpha} T^{\mu\alpha},\end{aligned} \tag{2.100}$$

where we used that

$$\partial_\mu \frac{1}{\sqrt{-g}} = -\frac{1}{\sqrt{-g}} \Gamma^\alpha{}_{\mu\alpha}. \tag{2.101}$$

We can proceed by noting that the covariant derivative of the inverse metric vanishes due to metric compatibility:

$$\nabla_\mu g^{\alpha\nu} = \partial_\mu g^{\alpha\nu} + g^{\beta\nu} \Gamma^\alpha{}_{\mu\beta} + g^{\alpha\beta} \Gamma^\nu{}_{\mu\beta} = 0. \tag{2.102}$$

Then

$$\begin{aligned}\nabla_\mu T^{\mu\nu} &= \int \frac{\mathrm{d}^4 p}{m\sqrt{-g}} \Big[\partial_\mu (p^\mu p^\nu F) + p^\mu p^\alpha \Gamma^\nu{}_{\mu\alpha}\Big] \\ &= \int \frac{\mathrm{d}^4 p}{m\sqrt{-g}} \Big[p^\nu \partial_\mu (p^\mu F) + F p^\mu \partial_\mu p^\nu + F p^\mu p^\alpha \Gamma^\nu{}_{\mu\alpha}\Big] \\ &= \int \frac{\mathrm{d}^4 p}{m\sqrt{-g}} \Big[p^\nu \partial_\mu (p^\mu F) + F p^\mu p_\alpha (\partial_\mu g^{\alpha\nu} + g^{\alpha\beta} \Gamma^\nu{}_{\mu\beta})\Big] \\ &= \int \frac{\mathrm{d}^4 p}{m\sqrt{-g}} \Big[p^\nu \partial_\mu (p^\mu F) + F p^\mu p_\alpha (-g^{\beta\nu} \Gamma^\alpha{}_{\mu\beta})\Big]\end{aligned} \tag{2.103}$$

We can use the product rule to rewrite the last term and drop the boundary term, to arrive at

$$\nabla_\mu T^{\mu\nu} = \int \frac{\mathrm{d}^4 p}{m\sqrt{-g}} \Big[p^\nu \partial_\mu (p^\mu F) + p^\nu \frac{\partial}{\partial p_\mu} (F \Gamma^\alpha{}_{\mu\rho} p^\rho p_\alpha)\Big] = 0 \tag{2.104}$$

The last equality follows from (2.73).

Thus, we have shown that in the absence of collisions, the energy momentum tensor is conserved.

Chapter 3

Semiholographic couplings

In this chapter, we aim to provide an outline of the generic couplings between the two sectors of a semiholographic construction. First, we will discuss the effective description of semiholography, following [36]. We will then extend this by describing an action principle for semiholographic theories. Finally, we will present a few illustrative examples, demonstrating the semiholographic philosophy and approach in the simplest possible systems: coupled pendula and a QFT with simple harmonic oscillation.

3.1 Semiholographic couplings and effective descriptions

The main advantage of our method in the context of phenomenology is that it works even when we cannot invoke action principles for the effective descriptions of one or both subsystems. The full dynamics is obtained by solving the subsystems in a mutually self-consistent way as has been illustrated in the case of the vacuum state in a toy example [35].

We consider a dynamical system $\mathfrak{S}$ in a fixed background metric $g^{(\mathrm{B})}_{\mu\nu}$ (to be set to the Minkowski metric $\eta_{\mu\nu}$ in most of Chapters 4 and 5 and set to the Bjorken background in Sec. 4.2), which consists of two subsystems $\mathfrak{S}_1$ and $\mathfrak{S}_2$. The notation that we will use is that relevant quantities of the subsystems will be distinguished either with a label of $1, 2$ or by having (or not) a tilde for quantities in $\mathfrak{S}_2$.

The coupling between the two subsystems will be chosen in a *democratic* fashion, motivated by the discussion in [35]. In this context, democratic coupling denotes that both subsystems are deformed in the same way. The semiholographic coupling between the two sectors works by promoting the background metric and the couplings of each subsystem to functionals of the operators of the other one. The individual subsystems will exhibit covariant dynamics involving the conservation of their respective energy momentum tensors, $t^{\mu\nu}$ and $\tilde{t}^{\mu\nu}$, in their respective effective background metrics while the full system, $\mathfrak{S}$, will have a local energy momentum tensor that will be conserved in the *actual* background metric, which for most of this thesis, will be the flat Minkowski metric. The two subsystems are assumed to share the same topological space so that we can use the same coordinates for both of them (and thus the total system). Coordinate transformations would thus affect the background metric of the complete system and the effective metrics of the subsystems simultaneously.

To see this in action, we can begin by focussing on the case of scalar operators, O and $\tilde{O}$. We can consider two subsytems with couplings λ and $\tilde{\lambda}$. We can deform the coupling democratically via

$$\lambda(x^\mu) = \lambda^0 + \alpha\tilde{O}(x^\mu), \quad \tilde{\lambda}(x^\mu) = \tilde{\lambda}^0 + \alpha O(x^\mu), \tag{3.1}$$

where we introduce the dimensionful semiholographic coupling, α, and λ^0 and $\tilde{\lambda}^0$ are constants. It is worthwhile to point out that the coupling equations, (3.1), are a non-dynamic set of equations, i.e. these are algebraic or auxiliary equations, so that no new degrees of freedom are added by the coupling. In the present example, the Ward identities for each subsystem are simply

$$\partial_\mu t^\mu{}_\nu = O\partial_\nu\lambda, \quad \partial_\mu\tilde{t}^\mu{}_\nu = \tilde{O}\partial_\nu\tilde{\lambda}. \tag{3.2}$$

We can then construct an energy-momentum tensor, $T^\mu{}_\nu$, for the full system

$$T^\mu{}_\nu = t^\mu{}_\nu + \tilde{t}^\mu{}_\nu - \alpha O\tilde{O}\delta^\mu_\nu, \tag{3.3}$$

which is easily shown to be conserved using the coupling equations (3.1) and the Ward identities (3.2),

$$\begin{aligned}\partial_\mu T^\mu{}_\nu &= \partial_\mu t^\mu{}_\nu + \partial_\mu\tilde{t}^\mu{}_\nu - \alpha\partial_\mu(O\tilde{O}\delta^\mu_\nu),\\ &= \alpha O\partial_\nu\tilde{O} + \alpha(\partial_\nu O)\tilde{O} - \alpha\partial_\nu(O\tilde{O}) = 0.\end{aligned} \tag{3.4}$$

Next, we will describe the tensorial effective metric coupling. In this case, the two subsystems have covariant dynamics w.r.t. their individual effective metrics $g_{\mu\nu}$ and $\tilde{g}_{\mu\nu}$. These effective metrics are locally determined by the subsystem energy-momentum tensors, i.e.

$$g_{\mu\nu} = g_{\mu\nu}[\tilde{t}^{\alpha\beta}, \ldots], \qquad \tilde{g}_{\mu\nu} = \tilde{g}_{\mu\nu}[t^{\alpha\beta}, \ldots]. \tag{3.5}$$

The two subsystems are closed w.r.t. to their effective metrics, but they can exchange energy and momentum from the point of view of the physical background metric $g^{(\mathrm{B})}_{\mu\nu}$ (which will be later set to be $\eta_{\mu\nu}$). The diffeomorphism invariance of the two subsystems imply the Ward identities

$$\nabla_\mu t^{\mu\nu} = 0, \quad \tilde{\nabla}_\mu\tilde{t}^{\mu\nu} = 0, \tag{3.6}$$

where ∇ and $\tilde{\nabla}$ refer to the covariant derivatives with respect to the different effective metrics with the Levi-Civita connections

$$\begin{aligned}\Gamma^\mu{}_{\nu\rho} &= \frac{1}{2}g^{\mu\sigma}(\partial_\nu g_{\sigma\rho} + \partial_\rho g_{\sigma\nu} - \partial_\sigma g_{\nu\rho}) = \Gamma^{\mu(\mathrm{B})}_{\nu\rho} + \frac{1}{2}g^{\mu\sigma}(\nabla^{(\mathrm{B})}_\nu g_{\sigma\rho} + \nabla^{(\mathrm{B})}_\rho g_{\sigma\nu} - \nabla^{(\mathrm{B})}_\sigma g_{\nu\rho}),\\ \tilde{\Gamma}^\mu{}_{\nu\rho} &= \frac{1}{2}\tilde{g}^{\mu\sigma}(\partial_\nu\tilde{g}_{\sigma\rho} + \partial_\rho\tilde{g}_{\sigma\nu} - \partial_\sigma\tilde{g}_{\nu\rho}) = \Gamma^{\mu(\mathrm{B})}_{\nu\rho} + \frac{1}{2}\tilde{g}^{\mu\sigma}(\tilde{\nabla}^{(\mathrm{B})}_\nu\tilde{g}_{\sigma\rho} + \tilde{\nabla}^{(\mathrm{B})}_\rho\tilde{g}_{\sigma\nu} - \tilde{\nabla}^{(\mathrm{B})}_\sigma\tilde{g}_{\nu\rho}).\end{aligned} \tag{3.7}$$

Above, $\nabla^{(\mathrm{B})}$ is the covariant derivative with respect to $g^{(\mathrm{B})}_{\mu\nu}$ and $\Gamma^{\mu(\mathrm{B})}_{\nu\rho}$ is the corresponding Levi-Civita connection. Note that these relations indicate that from the point of view of the actual physical background metric $g^{(\mathrm{B})}_{\mu\nu}$, the identities (3.6) imply that work is done on the respective subsystems by external forces. The second equalities in each of the above equations can be readily verified. Expanding the term in brackets on the RHS

$$\begin{aligned}\frac{1}{2}g^{\mu\sigma}(\nabla^{(\mathrm{B})}_\nu g_{\sigma\rho} + \nabla^{(\mathrm{B})}_\rho g_{\sigma\nu} - \nabla^{(\mathrm{B})}_\sigma g_{\nu\rho}) = {}&\frac{1}{2}g^{\mu\sigma}(\partial_\nu g_{\sigma\rho} + \partial_\rho g_{\sigma\nu} - \partial_\sigma g_{\nu\rho})\\ &- \frac{1}{2}g^{\mu\sigma}\Big[\underline{\Gamma^{\alpha(\mathrm{B})}_{\nu\sigma}g_{\alpha\rho}} + \Gamma^{\alpha(\mathrm{B})}_{\nu\rho}g_{\alpha\sigma}\\ &+ \underline{\underline{\Gamma^{\alpha(\mathrm{B})}_{\sigma\rho}g_{\alpha\nu}}} + \Gamma^{\alpha(\mathrm{B})}_{\rho\nu}g_{\alpha\sigma}\\ &- \underline{\underline{\Gamma^{\alpha(\mathrm{B})}_{\sigma\rho}g_{\alpha\nu}}} - \underline{\Gamma^{\alpha(\mathrm{B})}_{\sigma\nu}g_{\alpha\rho}}\Big].\end{aligned} \tag{3.8}$$

The first term is just the Christoffel symbol $\Gamma^{\mu}{}_{\nu\rho}$. The underlined terms cancel out and we are left with

$$\begin{aligned}\frac{1}{2}g^{\mu\sigma}(\nabla^{(\mathrm{B})}_{\nu}g_{\sigma\rho}+\nabla^{(\mathrm{B})}_{\rho}g_{\sigma\nu}-\nabla^{(\mathrm{B})}_{\sigma}g_{\nu\rho}) &= \Gamma^{\mu}{}_{\nu\rho}-\frac{1}{2}g^{\mu\sigma}\Big[\Gamma^{\alpha(\mathrm{B})}_{\nu\rho}g_{\alpha\sigma}+\Gamma^{\alpha(\mathrm{B})}_{\rho\nu}g_{\alpha\sigma}\Big],\\ &= \Gamma^{\mu}{}_{\nu\rho}-\Gamma^{\mu(\mathrm{B})}_{\nu\rho},\end{aligned}\tag{3.9}$$

as required.

Finally, we require that the forms of the effective metrics $g_{\mu\nu}$ and $\tilde{g}_{\mu\nu}$ are chosen in such a way that there exists an energy momentum tensor $T^{\mu\nu}$ for the full system, which is locally conserved in the physical background metric $g^{(\mathrm{B})}_{\mu\nu}$:

$$\nabla^{(\mathrm{B})}_{\mu}T^{\mu\nu}=0.\tag{3.10}$$

Since the effective metrics will be described by a non-dynamical equation, we anticipate that the full energy-momentum tensor will only depend on the energy-momentum tensors of the individual sectors and the background metric:

$$T^{\mu\nu}=T^{\mu\nu}[g^{(\mathrm{B})}_{\mu\nu},t^{\mu\nu},\tilde{t}^{\mu\nu}].\tag{3.11}$$

Hence one can readily construct effective descriptions of the full dynamics from the effective descriptions of the subsectors.

3.1.1 Determining effetive metric coupling rules

In this subsection, we determine the precise form of the coupling (3.5). We start the construction of the coupling rules between two subsystems by demanding that the total system $\mathfrak{S}$ has a conserved energy-momentum tensor $T^{\mu\nu}$ in the physical background metric $g^{(\mathrm{B})}_{\mu\nu}$. Setting $g^{(\mathrm{B})}_{\mu\nu}=\eta_{\mu\nu}$, we should have

$$\partial_{\mu}T^{\mu\nu}=0,\tag{3.12}$$

while simultaneously satisfying the Ward identities of the two subsystems (3.6) in their respective curved metrics.

For the rest of this section, unless indicated otherwise, all lowering and raising of indices is done by the effective metric of the respective theory, i.e. by t^{μ}_{ν} we will mean $t^{\mu\rho}g_{\rho\nu}$ and $t_{\mu\nu}=g_{\mu\rho}t^{\rho\sigma}g_{\sigma\nu}$, etc. The Ward identity of subsystem $\mathfrak{S}_1$ implies that

$$0=\nabla_{\mu}t^{\mu}{}_{\nu}=\partial_{\mu}t^{\mu}{}_{\nu}+\Gamma^{\mu}_{\mu\rho}t^{\rho}{}_{\nu}-\Gamma^{\mu}_{\nu\rho}t^{\rho}{}_{\mu},\tag{3.13}$$

$$\Rightarrow 0=\partial_{\mu}(t^{\mu}{}_{\nu}\sqrt{-g})-\frac{1}{2}t^{\mu\sigma}\sqrt{-g}\partial_{\nu}g_{\mu\sigma}.\tag{3.14}$$

To arrive at the second line, we multiplied both sides of (3.13) with $\sqrt{-g}$ and used

$$\Gamma^{\mu}_{\mu\nu}=\partial_{\nu}(\ln\sqrt{-g}),\quad \Gamma^{\mu}_{\nu\rho}t^{\rho}{}_{\mu}=\frac{1}{2}t^{\mu\rho}\partial_{\nu}g_{\mu\rho}.\tag{3.15}$$

Similarly, the Ward identity for subsystem $\mathfrak{S}_2$ implies that

$$\partial_{\mu}(\tilde{t}^{\mu}{}_{\nu}\sqrt{-\tilde{g}})=\frac{1}{2}\tilde{t}^{\mu\sigma}\sqrt{-\tilde{g}}\partial_{\nu}\tilde{g}_{\mu\sigma}.\tag{3.16}$$

Using these Ward identities, it is straightforward to verify that the following local relations for the effective metrics

$$\begin{aligned} g_{\mu\nu} &= \eta_{\mu\nu} + \gamma\, \eta_{\mu\alpha}\tilde{t}^{\alpha\beta}\eta_{\beta\nu}\sqrt{-\tilde{g}} + \gamma'\, \eta_{\mu\nu}\eta_{\alpha\beta}\tilde{t}^{\alpha\beta}\sqrt{-\tilde{g}}, \\ \tilde{g}_{\mu\nu} &= \eta_{\mu\nu} + \gamma\, \eta_{\mu\alpha}t^{\alpha\beta}\eta_{\beta\nu}\sqrt{-g} + \gamma'\, \eta_{\mu\nu}\eta_{\alpha\beta}t^{\alpha\beta}\sqrt{-g}, \end{aligned} \tag{3.17}$$

where γ and γ' are coupling constants (with mass dimension $-D$, where D is the dimension of spacetime), allow us to construct a symmetric conserved tensor for the full system in flat space.

We can now construct

$$K^{\mu}{}_{\nu} = t^{\mu}{}_{\nu}\sqrt{-g} + \tilde{t}^{\mu}{}_{\nu}\sqrt{-\tilde{g}} + \Delta K \delta^{\mu}{}_{\nu}, \tag{3.18}$$

with

$$\Delta K = -\frac{1}{2}\left[\gamma\,(t^{\rho\alpha}\sqrt{-g})\eta_{\alpha\beta}(\tilde{t}^{\beta\sigma}\sqrt{-\tilde{g}})\eta_{\sigma\rho} + \gamma'\,(t^{\alpha\beta}\sqrt{-g})\eta_{\alpha\beta}(\tilde{t}^{\sigma\rho}\sqrt{-\tilde{g}})\eta_{\sigma\rho}\right] \tag{3.19}$$

that is subject to the conservation equation

$$\begin{aligned} \partial_\mu K^{\mu}{}_{\nu} &= \partial_\mu\left[t^{\mu}{}_{\nu}\sqrt{-g} + \tilde{t}^{\mu}{}_{\nu}\sqrt{-\tilde{g}} + \Delta K \delta^{\mu}{}_{\nu}\right], \\ &= \partial_\mu(t^{\mu}{}_{\nu}\sqrt{-g}) + \partial_\mu(\tilde{t}^{\mu}{}_{\nu}\sqrt{-\tilde{g}}) + \partial_\nu \Delta K \\ &= \frac{1}{2}t^{\mu\sigma}\sqrt{-g}\partial_\nu g_{\mu\sigma} + \frac{1}{2}\tilde{t}^{\mu\sigma}\sqrt{-\tilde{g}}\partial_\nu \tilde{g}_{\mu\sigma} \\ &\quad - \frac{1}{2}\partial_\nu[\gamma\,(t^{\rho\alpha}\sqrt{-g})\eta_{\alpha\beta}(\tilde{t}^{\beta\sigma}\sqrt{-\tilde{g}})\eta_{\sigma\rho} + \gamma'\,(t^{\alpha\beta}\sqrt{-g})\eta_{\alpha\beta}(\tilde{t}^{\sigma\rho}\sqrt{-\tilde{g}})\eta_{\sigma\rho}] && (3.20) \\ &= \frac{1}{2}t^{\mu\sigma}\sqrt{-g}\partial_\nu\left[g_{\mu\sigma} - \sqrt{-\tilde{g}}(\gamma\,\eta_{\mu\alpha}\tilde{t}^{\alpha\beta}\eta_{\beta\sigma} + \gamma'\,\eta_{\mu\sigma}\eta_{\alpha\beta}\tilde{t}^{\alpha\beta})\right] \\ &\quad + \frac{1}{2}\tilde{t}^{\mu\sigma}\sqrt{-\tilde{g}}\partial_\nu\left[\tilde{g}_{\mu\sigma} - \sqrt{-g}(\gamma\,\eta_{\mu\alpha}t^{\alpha\beta}\eta_{\beta\sigma} + \gamma'\,\eta_{\mu\sigma}\eta_{\alpha\beta}t^{\alpha\beta})\right] && (3.21) \\ &= 0. && (3.22) \end{aligned}$$

To get to (3.20), we have used the two Ward identities, (3.14) and (3.16). The final equality holds due to the coupling equations (3.17).

Similarly, it is straightforward to see that

$$L_{\mu}{}^{\nu} = t_{\mu}{}^{\nu}\sqrt{-g} + \tilde{t}_{\mu}{}^{\nu}\sqrt{-\tilde{g}} + \Delta K \delta_{\mu}{}^{\nu} \tag{3.23}$$

satisfies

$$\partial_\nu L_{\mu}{}^{\nu} = 0. \tag{3.24}$$

Putting (3.18) and (3.24) together, we can define a symmetric and conserved total energy-momentum tensor $T^{\mu\nu} = \eta^{\mu\rho}T_{\rho}{}^{\nu} = T^{\mu}{}_{\rho}\eta^{\rho\nu}$ with $\partial_\mu T^{\mu\nu} = 0 = \partial_\mu T^{\mu}{}_{\nu}$ by

$$T^{\mu}{}_{\nu} = \frac{1}{2}(K^{\mu}{}_{\nu} + L_{\nu}{}^{\mu}). \tag{3.25}$$

We can easily generalize the above construction for a curved background metric $g^{(\mathrm{B})}_{\mu\nu}$ instead of the Minkowski metric using the identities in (3.7) which imply

$$\begin{aligned} \Gamma^{\mu}_{\nu\mu} - \Gamma^{(\mathrm{B})\mu}{}_{\nu\mu} &= \partial_\nu(\ln\sqrt{-g}) - \partial_\nu(\ln\sqrt{-g^{(\mathrm{B})}}) = \partial_\nu\left(\ln\frac{\sqrt{-g}}{\sqrt{-g^{(\mathrm{B})}}}\right) \\ &= \frac{\sqrt{-g^{(\mathrm{B})}}}{\sqrt{-g}}\partial_\nu\left(\frac{\sqrt{-g}}{\sqrt{-g^{(\mathrm{B})}}}\right) = \frac{\sqrt{-g^{(\mathrm{B})}}}{\sqrt{-g}}\nabla^{(\mathrm{B})}_\nu\left(\frac{\sqrt{-g}}{\sqrt{-g^{(\mathrm{B})}}}\right), \end{aligned} \tag{3.26}$$

where we have used that $\sqrt{-g}/\sqrt{-g^{(\mathrm{B})}}$ is a scalar under general coordinate transformations.

With the help of these relations, one can readily see that the consistent coupling rules have the following general covariant forms

$$\begin{aligned} g_{\mu\nu} &= g^{(\mathrm{B})}_{\mu\nu} + \left(\gamma\, g^{(\mathrm{B})}_{\mu\alpha}\tilde{t}^{\alpha\beta}g^{(\mathrm{B})}_{\beta\nu} + \gamma'\, g^{(\mathrm{B})}_{\mu\nu}\tilde{t}^{\alpha\beta}g^{(\mathrm{B})}_{\alpha\beta}\right)\frac{\sqrt{-\tilde{g}}}{\sqrt{-g^{(\mathrm{B})}}}, \\ \tilde{g}_{\mu\nu} &= g^{(\mathrm{B})}_{\mu\nu} + \left(\gamma\, g^{(\mathrm{B})}_{\mu\alpha}t^{\alpha\beta}g^{(\mathrm{B})}_{\beta\nu} + \gamma'\, g^{(\mathrm{B})}_{\mu\nu}t^{\alpha\beta}g^{(\mathrm{B})}_{\alpha\beta}\right)\frac{\sqrt{-g}}{\sqrt{-g^{(\mathrm{B})}}}. \end{aligned} \tag{3.27}$$

Then with

$$\begin{aligned} \Delta K &= -\frac{\gamma}{2}\left(t^{\rho\alpha}\frac{\sqrt{-g}}{\sqrt{-g^{(\mathrm{B})}}}\right)g^{(\mathrm{B})}_{\alpha\beta}\left(\tilde{t}^{\beta\sigma}\frac{\sqrt{-\tilde{g}}}{\sqrt{-g^{(\mathrm{B})}}}\right)g^{(\mathrm{B})}_{\sigma\rho} \\ &\quad -\frac{\gamma'}{2}\left(t^{\alpha\beta}\frac{\sqrt{-g}}{\sqrt{-g^{(\mathrm{B})}}}\right)g^{(\mathrm{B})}_{\alpha\beta}\left(\tilde{t}^{\sigma\rho}\frac{\sqrt{-\tilde{g}}}{\sqrt{-g^{(\mathrm{B})}}}\right)g^{(\mathrm{B})}_{\sigma\rho}, \end{aligned} \tag{3.28}$$

the full conserved energy-momentum tensor is again given by (3.25), and it satisfies $\nabla^{(\mathrm{B})}_{\mu}T^{\mu}{}_{\nu} = 0$ in the actual background where all degrees of freedom live. (Note $T^{\mu\nu} = T^{\mu}{}_{\rho}g^{(\mathrm{B})\rho\nu}$).

It is interesting to note that more general consistent couplings can be constructed. The case of the most general scalar couplings was studied in [35]. The case of general tensorial coupling is explored in Appendix A of [36] (correcting and generalizing Ref. [35] in this respect). Note that in both of these cases, we would be permitting higher powers of operators with new coupling constants carrying correspondingly higher inverse mass dimension. In Chapter 4 and 5 we will restrict ourselves to the lowest order coupling rules (3.17) and (3.1), respectively.

An observant reader would have noticed that the dimensionful coupling constants seem arbitrary. It is interesting to note that we will find that physical requirements restrict the range of these parameters. For example, as we will see in the equilibrium and near-equilibrium systems considered in Chapter 4, requiring that the system is causal leads to the condition that $\gamma > 0$.

Note that this discussion can be generalized in a straightforward manner to n subsystems. This would mean that there would be n coupling equations. For example, in the case of the tensor coupling, the effective metrics would be each deformed by the $n-1$ other energy-momentum tensors in a democratic way, each with a pair of coupling constants exactly as in (3.27).

3.1.2 Thermodynamic consistency of the phenomenological construction

An important test that the formalism laid out in the previous section is sound is to determine whether it is thermodynamically consistent. Practically, thermodynamic consistency means that for any consistent effective metric coupling rule with a total conserved energy-momentum tensor (3.25) with a globally defined temperature, $\mathcal{T}$, we will have a total entropy $\mathcal{S}(\mathcal{T})$. Note that this discussion is general, covering not only the simplest metric coupling rules (3.17), but also the most general ansatz for ΔK found in Appendix A of [36].

We proceed by considering a system with a static gravitational potential, such that the background metric is:

$$g^{(\mathrm{B})}_{\mu\nu} = \mathrm{diag}\left(-e^{-2\phi(\mathbf{x})}, 1, 1, 1\right), \tag{3.29}$$

where $\phi(\mathbf{x})$ is static. We will assume that we can obtain flat-space solutions by smoothly taking $\phi(\mathbf{x}) \to 0$. Then, we can make static ansätze for the effective metrics of the individual sectors, i.e.

$$g_{\mu\nu} = \mathrm{diag}(-a(\mathbf{x})^2, b(\mathbf{x})^2, b(\mathbf{x})^2, b(\mathbf{x})^2), \quad \tilde{g}_{\mu\nu} = \mathrm{diag}(-\tilde{a}(\mathbf{x})^2, \tilde{b}(\mathbf{x})^2, \tilde{b}(\mathbf{x})^2, \tilde{b}(\mathbf{x})^2). \tag{3.30}$$

The individual energy-momentum tensors will be in thermodynamic equilibrium w.r.t. to their respective temperatures, T_1 and T_2,

$$\begin{aligned} t^{\mu\nu} &= \mathrm{diag}\left(\frac{\epsilon_1(T_1(\mathbf{x}))}{a(\mathbf{x})^2}, \frac{P_1(T_1(\mathbf{x}))}{b(\mathbf{x})^2}, \frac{P_1(T_1(\mathbf{x}))}{b(\mathbf{x})^2}, \frac{P_1(T_1(\mathbf{x}))}{b(\mathbf{x})^2}\right), \\ \tilde{t}^{\mu\nu} &= \mathrm{diag}\left(\frac{\epsilon_2(T_2(\mathbf{x}))}{\tilde{a}(\mathbf{x})^2}, \frac{P_2(T_2(\mathbf{x}))}{\tilde{b}(\mathbf{x})^2}, \frac{P_2(T_2(\mathbf{x}))}{\tilde{b}(\mathbf{x})^2}, \frac{P_2(T_2(\mathbf{x}))}{\tilde{b}(\mathbf{x})^2}\right). \end{aligned} \tag{3.31}$$

The metric coupling equations will involve no derivatives of the metric and as such, will still be algebraic. However, the coupling equations need to be taken in their generalized form with nontrivial background metric, $g^{(\mathrm{B})}_{\mu\nu}$.

Now, there are multiple temperatures at play for the moment. Since we are assuming that the full system is in thermal equilibrium, the system or physical temperature, $\mathcal{T}$, of the full system $\mathfrak{S}$ is given simply by the inverse length of the thermal circle, i.e.

$$\mathcal{T}^{-1} = \int_0^\beta \sqrt{-g^{(\mathrm{B})}_{00}}\,\mathrm{d}\tau, \tag{3.32}$$

where β is the inverse temperature and τ is the imaginary time. The temperature for each subsystem is defined similarly as

$$T_1^{-1} = \int_0^\beta \sqrt{-g_{00}}\,\mathrm{d}\tau, \tag{3.33}$$

$$T_2^{-1} = \int_0^\beta \sqrt{-\tilde{g}_{00}}\,\mathrm{d}\tau, \tag{3.34}$$

so that the two subsystem temperatures are related to the temperature of the physical system in flat space $g^{(\mathrm{B})}_{\mu\nu} = \eta_{\mu\nu}$ via

$$T_1(\mathbf{x})a(\mathbf{x}) = T_2(\mathbf{x})\tilde{a}(\mathbf{x}) = \mathcal{T}(\mathbf{x})e^{-\phi(\mathbf{x})} = \mathcal{T}_0, \tag{3.35}$$

where $\mathcal{T}_0$ is a constant, parametrizing the global thermal equilibrium of the full system in the background metric (3.29).

Now, we demonstrate that the above assumption of a global equilbrium temperature is compatible with the Ward identities. Using (3.14), we can check that the conservation of the individual thermal energy-momentum tensors (3.31) in the respective effective metrics (3.30) imply that

$$\frac{\partial_i P_1}{\epsilon_1 + P_1} + \frac{\partial_i a}{a} = 0, \quad \frac{\partial_i P_2}{\epsilon_2 + P_2} + \frac{\partial_i \tilde{a}}{\tilde{a}} = 0, \tag{3.36}$$

respectively. Note that $b(\mathbf{x})$ and $\tilde{b}(\mathbf{x})$ do not feature directly in the above equations. Since $\mathrm{d}P_1 = s_1 \mathrm{d}T_1$, $\epsilon_1 + P_1 = T_1 s_1$, $\mathrm{d}P_2 = s_2 \mathrm{d}T_2$, $\epsilon_2 + P_2 = T_2 s_2$, we can show with a little algebra that the conservation equations (3.36) are equivalent to

$$\partial_i(\ln(T_1 a)) = 0, \quad \partial_i(\ln(T_2 \tilde{a})) = 0, \tag{3.37}$$

and thus implied by the global equilibrium condition (3.35).

By construction, the effective metric couplings ensure that the total energy-momentum tensor, which can be parameterized as

$$T^{\mu\nu} = \mathrm{diag}\left(\mathcal{E}(\mathcal{T}(\mathbf{x}))e^{2\phi(\mathbf{x})}, \mathcal{P}(\mathcal{T}(\mathbf{x})), \mathcal{P}(\mathcal{T}(\mathbf{x})), \mathcal{P}(\mathcal{T}(\mathbf{x}))\right), \tag{3.38}$$

will be conserved in the background metric (3.29), since the individual thermal energy-momentum tensors are conserved with respect to the respective effective metrics. We therefore have

$$\frac{\partial_i \mathcal{P}}{\mathcal{E}+\mathcal{P}} - \partial_i \phi = 0. \tag{3.39}$$

Equations (3.35) and (3.37) together imply that

$$\frac{\partial_i \mathcal{T}}{\mathcal{T}} - \partial_i \phi = 0, \tag{3.40}$$

and therefore

$$\frac{\partial_i \mathcal{T}}{\mathcal{T}} = \frac{\partial_i \mathcal{P}}{\mathcal{E}+\mathcal{P}}. \tag{3.41}$$

Identifying $\mathcal{E}+\mathcal{P} = \mathcal{T}\mathcal{S}$ leads to

$$\partial_i \mathcal{P} = \mathcal{S}\partial_i \mathcal{T}. \tag{3.42}$$

Since the above should hold for arbitrary smooth $\phi(\mathbf{x})$, we conclude that

$$\mathrm{d}\mathcal{P} = \mathcal{S}\mathrm{d}\mathcal{T}, \tag{3.43}$$

where the variation is taken by changing the constant parameter $\mathcal{T}_0$. Together with $\mathcal{E}+\mathcal{P} = \mathcal{T}\mathcal{S}$ the above implies

$$\mathrm{d}\mathcal{E} = \mathcal{T}\mathrm{d}\mathcal{S}. \tag{3.44}$$

This shows that thermodynamic consistency follows from the conservation of the full energy-momentum tensor as ensured by our effective metric coupling. In particular, assuming $\mathcal{E}+\mathcal{P} = \mathcal{T}\mathcal{S}$ and the global equilibrium condition (3.35), we obtain $\mathrm{d}\mathcal{E} = \mathcal{T}\mathrm{d}\mathcal{S}$ from the conservation of the full energy-momentum tensor. Clearly, we can take the limit $\phi(\mathbf{x}) \to 0$ limit to obtain the proof of thermodynamic consistency in flat space.

We can now deduce the form that $\mathcal{S}$ takes. Since the form of the full energy-momentum tensor with one contravariant and one covariant index is such that the explicit interaction terms involving ΔK are always diagonal, they come with opposite signs for $\mathcal{E}$ and $\mathcal{P}$. Therefore,

$$(\epsilon_1 + P_1)ab^3 + (\epsilon_2 + P_2)\tilde{a}\tilde{b}^3 = (\mathcal{E}+\mathcal{P})e^{-\phi(\mathbf{x})}. \tag{3.45}$$

Thus from $(\mathcal{E}+\mathcal{P}) = \mathcal{T}\mathcal{S}$ we get

$$T_1 s_1 ab^3 + T_2 s_2 \tilde{a}\tilde{b}^3 = \mathcal{T}\mathcal{S}e^{-\phi(\mathbf{x})}. \tag{3.46}$$

The relation between the temperatures (3.35) reduces this to

$$\mathcal{S} = s_1 b^3 + s_2 \tilde{b}^3. \tag{3.47}$$

Furthermore, the above form holds for the general consistent effective metric coupling discussed in Appendix A of [36]. Thus, we obtain a general proof of thermodynamic consistency with (3.35) and the above form of the full entropy.

3.2 Semiholographic couplings through an action principle

Although the orginal formulation of semiholography [32] stressed that only an effective description of each sector was needed for a complete formulation, making it useful for phenomenology, it became clear that one can reformulate the semiholographic picture from the point of view of an action. This makes the formulation cleaner when a microscopic description is available, while functionally equivalent to the previous method.

3.2.1 Scalar coupling

The scalar coupling action will be the subject of Chapter 5 and 6. We will provide a slightly more general construction here. The scalar action in (3.3) is given by

$$S[\phi, \tilde{\phi}, O, \tilde{O}] = S[\phi, O] + S[\tilde{\phi}, \tilde{O}] - \frac{1}{\alpha} O\tilde{O}, \tag{3.48}$$

where ϕ and $\tilde{\phi}$ represent matter fields, and O and $\tilde{O}$ represent the auxiliary scalar sources. The final term has the interpretation of the scalar coupling due to semiholography where α represents the coupling.

3.2.2 Tensor coupling

Here we provide the full action of the semiholographic model with democratic tensorial couplings. Thusfar, the method employed builds the complete energy momentum tensor of the full system subject to the Ward identities of each subsector being satisfied. Here we turn the argument on its head: given an energy momentum tensor, would it be possible to construct an action which satisfies the semiholographic constuction? From (3.25), the full energy-momentum tensor is explicitly

$$\begin{aligned} T^{\mu}{}_{\nu}\sqrt{-g^{(B)}} &= \frac{1}{2}\sqrt{-g}\left(t^{\mu}{}_{\nu} + t_{\nu}{}^{\mu}\right) + \frac{1}{2}\sqrt{-\tilde{g}}\left(\tilde{t}^{\mu}{}_{\nu} + \tilde{t}_{\nu}{}^{\mu}\right) \\ &\quad - \delta^{\mu}_{\nu}\frac{\sqrt{-g}\sqrt{-\tilde{g}}}{\sqrt{-g^{(B)}}}\left(\frac{\gamma}{2} t\cdot\tilde{t} + \frac{\gamma'}{2} t^{\rho\sigma} g^{(B)}_{\rho\sigma}\tilde{t}^{\gamma\delta} g^{(B)}_{\gamma\delta}\right), \end{aligned} \tag{3.49}$$

$$t\cdot\tilde{t} \equiv t^{\rho\alpha} g^{(B)}_{\alpha\beta}\tilde{t}^{\beta\sigma} g^{(B)}_{\sigma\rho}, \tag{3.50}$$

and the corresponding coupling equations (3.27) given by

$$\begin{aligned} g_{\mu\nu} &= g^{(B)}_{\mu\nu} + \gamma\frac{\sqrt{-\tilde{g}}}{\sqrt{-g^{(B)}}} g^{(B)}_{\mu\gamma}\tilde{t}^{\gamma\delta} g^{(B)}_{\delta\nu} + \gamma'\frac{\sqrt{-\tilde{g}}}{\sqrt{-g^{(B)}}} g^{(B)}_{\mu\nu}\tilde{t}\cdot g^{(B)}, \\ \tilde{g}_{\mu\nu} &= g^{(B)}_{\mu\nu} + \gamma\frac{\sqrt{-g}}{\sqrt{-g^{(B)}}} g^{(B)}_{\mu\gamma} t^{\gamma\delta} g^{(B)}_{\delta\nu} + \gamma'\frac{\sqrt{-g}}{\sqrt{-g^{(B)}}} g^{(B)}_{\mu\nu} t\cdot g^{(B)}. \end{aligned} \tag{3.51}$$

The complete action reads

$$\begin{aligned} S_{full}[\phi, \tilde{\phi}, g_{\mu\nu}, \tilde{g}_{\mu\nu}, g^{(B)}_{\mu\nu}] = \int \mathrm{d}^D x \Big[&\sqrt{-g}\mathcal{L}[\phi, g_{\mu\nu}] + \sqrt{-\tilde{g}}\tilde{\mathcal{L}}[\tilde{\phi}, \tilde{g}_{\mu\nu}] \\ &+ \frac{1}{2\gamma}\sqrt{-g^{(B)}}\left(g - g^{(B)}\right)\cdot\left(\tilde{g} - g^{(B)}\right) \\ &- \frac{\gamma'}{2\gamma}\sqrt{-g^{(B)}}\frac{(g\cdot g^{(B)} - D)(\tilde{g}\cdot g^{(B)} - D)}{\gamma + \gamma' D}\Big], \end{aligned} \tag{3.52}$$

where $D = d + 1$ is the number of spacetime dimensions. The variation of this action with respect to the:

- matter fields, ϕ and $\tilde{\phi}$, gives the usual equations of motion for each subsystem,
- effective metrics, $g_{\mu\nu}$ and $\tilde{g}_{\mu\nu}$, yields the coupling equations (3.27),
- background metric, $g^{(B)}_{\mu\nu}$, gives the full energy-momentum tensor (3.25).

Furthermore, the individual sectors satisfy their respective Ward identities (3.6). For more details, see Appendix A.

Remember that the effective metrics, $g_{\mu\nu}$ and $\tilde{g}_{\mu\nu}$, are auxiliary fields. As such, they are not dynamical. The full system has only *one dynamical metric*, i.e. the background metric, $g^{(\mathrm{B})}_{\mu\nu}$. In this thesis, we take the background metric to be flat (either a Minkowski or Bjorken background). In principle, one could be interested in the situation where the background metric is evolving dynamically. One could then supplement the action (3.52) with an Einstein-Hilbert term:

$$S = S_{full}[\phi, \tilde{\phi}, g_{\mu\nu}, \tilde{g}_{\mu\nu}, g^{(B)}_{\mu\nu}] + \frac{1}{16\pi G}\int d^D x\sqrt{-g^{(\mathrm{B})}}R^{(\mathrm{B})}. \tag{3.53}$$

We will have an extra equation of motion in this case, arising from the variation w.r.t. the background metric:

$$R^{(B)}_{\mu\nu} - \frac{1}{2}g^{(B)}_{\mu\nu}R^{(B)} = 8\pi G T_{\mu\nu}, \tag{3.54}$$

with the energy-momentum tensor on the RHS given by (3.25) and (3.49). We can remark that this equation can be supplemented to the phenomenological discussion.

3.3 An illustrative example of scalar coupling

In this section, we will discuss an illustrative example of the scalar semiholographic coupling. We will not consider a holographic sector here, as holographic computations add technical complications.

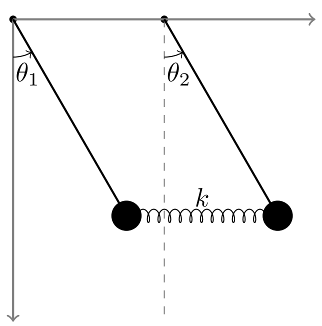

Figure 3.1: A system of pendula coupled with a spring serves as an example of dynamical sourcing.

In fact, we will reinterpret a well-known system of two pendula coupled by a spring, as shown in Fig. 3.1. The philosophy will be to consider each pendulum as its own subsystem, with the spring acting as some "external" force. Of course, as the system is particularly simple, it is clear how the spring will effect the behavior of the pendula.

The action of this system in the small angle approximation is given by

$$S = \int \mathrm{d}t \left[\frac{1}{2}\Big(\dot{\theta}_1^2 - \omega^2\theta_1^2 + \dot{\theta}_2^2 - \omega^2\theta_2^2\Big) + \theta_1 J_1 + \theta_2 J_2 - \frac{1}{k} J_1 J_2\Big], \tag{3.55}$$

Omitting the last term, the action has the interpretation of two uncoupled scalar $0+1$ dimensional harmonic oscillators, driven by external sources J_i with $i = 1, 2$.

The last term acts as the semiholographic coupling. Essentially, we are supplying the system with an additional coupling constraint equation with coupling constant k. Using the Euler-Lagrange equations

$$\frac{\partial S}{\partial \theta_i} - \partial_t \frac{\partial S}{\partial \dot{\theta}_i} = 0, \tag{3.56}$$

$$\frac{\partial S}{\partial J_i} - \partial_t \frac{\partial S}{\partial \dot{J}_i} = 0, \tag{3.57}$$

we see that the EOM of the system is given by

$$\ddot{\theta}_1 + \omega^2\theta_1 = J_1, \tag{3.58}$$

$$\ddot{\theta}_2 + \omega^2\theta_1 = J_2, \tag{3.59}$$

$$\theta_1 = \frac{1}{k} J_2, \tag{3.60}$$

$$\theta_2 = \frac{1}{k} J_1. \tag{3.61}$$

Of course, the last two equations are not dynamical and so we can eliminate the "external" sources J_i to arrive at

$$\ddot{\theta}_1 + \omega^2\theta_1 = k\theta_2, \tag{3.62}$$

$$\ddot{\theta}_2 + \omega^2\theta_2 = k\theta_1. \tag{3.63}$$

The conserved energy can be computed from (3.55). The total energy momentum tensor is just $T^{\mu\nu} = T^{00} \equiv E$. Anticipating the later chapters, we divide the total energy into three contributions: the energies of the two pendula, E_1 and E_2, and the interaction energy, E_{int}:

$$E = E_1 + E_2 + E_{int}, \tag{3.64}$$

$$E_1 = \frac{1}{2}(\dot{\theta}_1^2 + \omega^2\theta_1^2), \tag{3.65}$$

$$E_2 = \frac{1}{2}(\dot{\theta}_2^2 + \omega^2\theta_2^2), \tag{3.66}$$

$$E_{int} = -k\theta_1\theta_2. \tag{3.67}$$

The split of the energies is summarized in the right panel of Fig. 3.2 for a particular choice of parameters and initial conditions.

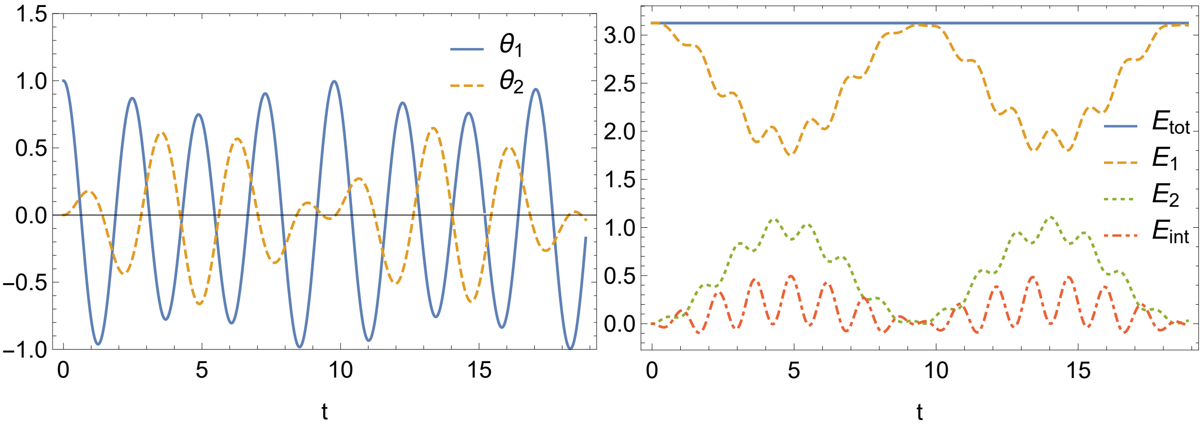

Figure 3.2: Example solution for two coupled pendula with frequencies $\omega_1 = 2.5$ and $\omega_1 = 2$, initial conditions $\theta_1(0) = 1$, $\theta_1'(0) = \theta_2(0) = \theta_2'(0) = 0$ and spring constant (semiholographic coupling) $k = 1$. Left: the motion of the the two pendula. Right: the total energy is conserved, while the energies of the two subsystems and the interaction energy are oscillatory.

3.4 Semiholographic harmonic oscillator

Here we consider an example of the tensorial coupling, i.e. one which induces a change in the effective metric of each theory. The model will rest on a field theoretic description of a classical simple harmonic oscillator in a curved background, i.e. the massive scalar field.

3.4.1 The $0 + 1D$ case

We can now consider a slightly more involved example, one which, however, doesn't provide a meaningful coupling. This negative example still provides the simplest example of a metric coupling (as opposed to the scalar coupling in the previous section).

We begin with the action of a harmonic oscillator, $x(t)$, in a curved background

$$S[x(t), g_{tt}] = \frac{1}{2}\int \mathrm{d}t\sqrt{-g}(-g^{tt}\dot{x}^2 - m^2x^2) \equiv \frac{1}{2}\int \mathrm{d}t\; e\,\mathcal{L}, \tag{3.68}$$

where we introduce the einbein

$$\begin{aligned} g_{\mu\nu} &= \eta_{\alpha\beta}e^\alpha_\mu e^\beta_\nu, \\ \Rightarrow g_{tt} &= -e^2. \end{aligned} \tag{3.69}$$

The equation of motion is

$$\partial_t(e^{-1}\dot{x}) + em^2x = 0. \tag{3.70}$$

The energy momentum tensor is simply

$$t_{tt} = \frac{2}{\sqrt{-g}}\frac{\partial S}{\partial g^{tt}} = \dot{x}^2 - e^2\mathcal{L}. \tag{3.71}$$

The conservation equation is given by

$$\begin{aligned} 0 &= \partial_t t^{tt} + 2\Gamma^t{}_{tt}t^{tt} \\ \Rightarrow 0 &= e^2\partial_t t^{tt} + t^{tt}\partial_t e^2 = \partial_t(e^2 t^{tt}) \end{aligned} \tag{3.72}$$

So the combination $e^2 t^{tt}$ is a constant of motion.

We now couple this oscillator to another via the semiholographic metric coupling rules. We embed the two subsystems in the same flat topological space, i.e. $g^{(B)}_{\mu\nu} = \eta_{\mu\nu}$. Say the second system is described by the action $\tilde{S}[y(t), \tilde{g}_{tt}]$. The two systems are coupled via the following coupling equations:

$$\begin{aligned} g_{tt} &= \eta_{tt} + \gamma \eta_{tt} \tilde{t}^{tt} \eta_{tt} \sqrt{-\tilde{g}}, \\ \tilde{g}_{tt} &= \eta_{tt} + \gamma \eta_{tt} t^{tt} \eta_{tt} \sqrt{-g}, \end{aligned} \tag{3.73}$$

which have the following form

$$\begin{aligned} -e^2 &= -1 + \gamma \tilde{t}_{tt} \tilde{e}, \\ -\tilde{e}^2 &= -1 + \gamma t_{tt} e. \end{aligned} \tag{3.74}$$

Note that in higher dimensions, we have a tensorial term (e.g. $\propto g^{(\mathrm{B})}_{\mu\alpha} t^{\alpha\beta} g^{(\mathrm{B})}_{\beta\nu}$) and a trace term (e.g. $\propto t^{\alpha\beta} g^{(\mathrm{B})}_{\alpha\beta} g^{(\mathrm{B})}_{\mu\nu}$) in the coupling equations. Clearly in 0+1 dimensions, there is no distinction between these two terms.

To simplify notation, say that $e^2 t^{tt} = a$ and $\tilde{e}^2 \tilde{t}^{tt} = \tilde{a}$, as these are constants of motion from (3.72). Then the coupling equations are solvable:

$$\begin{aligned} 1 - \tilde{e}^2 &= \gamma t^{tt} e = \gamma \frac{a}{e} \\ \Rightarrow e &= \frac{\gamma a}{1 - \tilde{e}^2}. \end{aligned} \tag{3.75}$$

Substituting this into the other coupling equation leads to

$$0 = \tilde{e}^5 - \tilde{a}\gamma \tilde{e}^4 - 2\tilde{e}^3 + 2\tilde{a}\gamma \tilde{e}^2 + (1 - a^2\gamma^2)\tilde{e} - \tilde{a}\gamma \tag{3.76}$$

which is a quintic equation for the metric $\tilde{e}$. A similar equation holds for e. This means that once the initial conditions are specified, the metric coupling remains non-dynamical, as does the energy-momentum tensor of each sector.

The total energy momentum tensor is then

$$\mathcal{T}^{tt} = e t^{tt} + \tilde{e} \tilde{t}^{tt} - \frac{1}{2} \gamma e \tilde{e} t^{tt} \tilde{t}^{tt}, \tag{3.77}$$

which is conserved due to the previous discussion.

Thus, we conclude by remarking that the $0 + 1D$ dimensional case is too simplistic to have an interesting metric coupling.

3.4.2 The $1 + 1D$ case

We now turn our attention to one dimension higher than the previous case. The action that we consider is for a massive time-dependent scalar field, $\phi = \phi(t)$:

$$S[\phi(t), g_{\mu\nu}] = \int \mathrm{d}^2 x \sqrt{-g} \mathcal{L} = -\frac{1}{2} \int \mathrm{d}^2 x \sqrt{-g} (\partial_\mu \phi g^{\mu\nu} \partial_\nu \phi + m^2 \phi^2), \tag{3.78}$$

which leads to the following EOM:

$$0 = \frac{1}{\sqrt{-g}} \partial_\mu \left(g^{\mu\nu} \sqrt{-g} \partial_\nu \phi \right) - m^2 \phi. \tag{3.79}$$

We can parametrize the effective metric via

$$g_{\mu\nu} = \begin{pmatrix} -a^2 & 0 \\ 0 & b^2 \end{pmatrix} = b^2 \begin{pmatrix} -v^2 & 0 \\ 0 & 1 \end{pmatrix}, \tag{3.80}$$

where we introduce the effective light-cone velocity $1 > v = x/y > 0$, a useful parameterization which tells us about the causal structure of the solution. We discuss effective light-cones in detail in Chapter 4. The EOM now reads

$$\begin{aligned} 0 &= \partial_t\Big(\frac{\dot\phi}{v}\Big) + m^2 v b^2 \phi \\ \Rightarrow 0 &= \ddot\phi - \partial_t \log(v)\dot\phi + m^2 v^2 b^2 \phi, \end{aligned} \tag{3.81}$$

where $\dot\phi = \partial_t \phi$. Note that the time derivative of the logarithm of the light-cone velocity enters as the coefficient of $\dot\phi$, which would tempt us to identify it as a time dependent damping coefficient.

The energy momentum tensor of this sector is diagonal and reads

$$\begin{aligned} t^{\mu\nu} &= \frac{2}{\sqrt{-g}}\frac{\partial S}{\partial g_{\mu\nu}}, \\ \Rightarrow t^{\mu\nu} &= \partial^\mu\phi\partial^\nu\phi + g^{\mu\nu}\mathcal{L}. \end{aligned} \tag{3.82}$$

Remember that $\partial^\mu\phi = g^{\mu\nu}\partial_\nu\phi$. Explicitly, we have the following non-zero components

$$t^{tt} = a^{-4}\dot\phi^2 - a^{-2}\mathcal{L}, \qquad \text{and} \qquad t^{xx} = b^{-2}\mathcal{L}. \tag{3.83}$$

We now introduce a second subsystem, which is also described as a free massive scalar field, with mass $\tilde m$, in a curved background with action $\tilde S[\tilde\phi, \tilde g_{\mu\nu}]$ of the same form as (3.78). The equation of motion for this sector is

$$0 = \ddot{\tilde\phi} - \partial_t \log(\tilde v)\dot{\tilde\phi} + \tilde m^2 \tilde v^2 \tilde b^2 \tilde\phi. \tag{3.84}$$

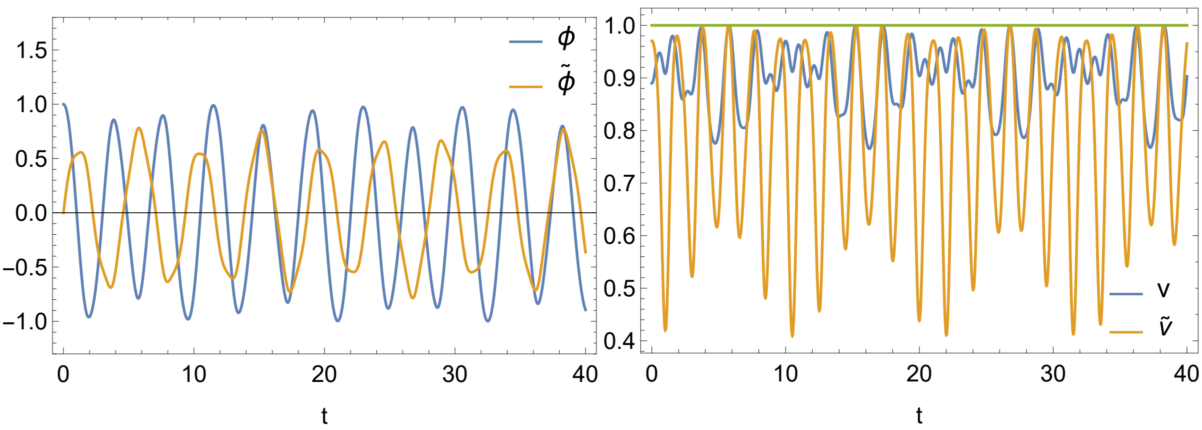

Figure 3.3: Left panel: numerical solution for two massive scalar fields with masses $m = 1.5$ and $\tilde m = 1$, initial conditions $\phi(0) = 1, \partial_t\phi|_{t=0} = 0$, $\tilde\phi(0) = 0, \partial_t\tilde\phi|_{t=0} = 1$ and couplings $\gamma = 1$ and $r = 2$. Right panel: the effective light-cone velocities of both sectors. The green line denotes the light-cone velocity of the Minkowski background, i.e. the speed of light $c = 1$.

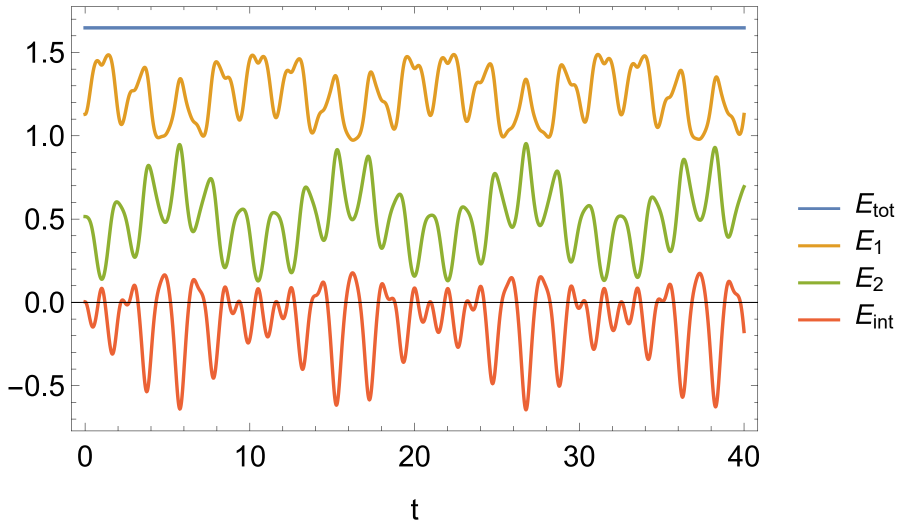

Figure 3.4: Total energy, individual subsystem energies and interaction energy for the choice of parameters and initial conditions described in Fig. 3.3. Note that E_1 refers to the energy of the first subsystem and E_2 of the other subsystem.

We embed these two subsystems, S and $\tilde{S}$, in a Minkowski background metric $g^{(\mathrm{B})}_{\mu\nu} = \eta_{\mu\nu}$. The two systems are then coupled via the coupling equations (3.27), which for completeness we reproduce for this specific case:

$$
\begin{aligned}
-v^2 b^2 &= -1 + \gamma\Big(\frac{(\partial_t\tilde{\phi})^2}{\tilde{v}^3\tilde{b}^2} - \frac{\tilde{\mathcal{L}}}{\tilde{v}} + r\tilde{v}\tilde{b}^2\tilde{t}\cdot\eta\Big),\\
-\tilde{v}^2\tilde{b}^2 &= -1 + \gamma\Big(\frac{\dot{\phi}^2}{v^3 y^2} - \frac{\mathcal{L}}{v} + rvb^2 t\cdot\eta\Big),\\
b^2 &= 1 + \gamma\tilde{v}(\tilde{\mathcal{L}} - r\tilde{b}^2\tilde{t}\cdot\eta),\\
\tilde{b}^2 &= 1 + \gamma v(L - rb^2 t\cdot\eta),
\end{aligned}
\tag{3.85}
$$

where to make connection with Chapter 4 we introduce the dimensionless constant $r \equiv -\gamma'/\gamma$ and the shorthand notation $t\cdot\eta \equiv t_{\mu\nu}\eta^{\mu\nu} = -t_{tt} + t_{xx}$.

Now the setup is complete. The system of equations that we need to solve involve the EOM of each subsystem, (3.81) and (3.84), and the set of coupling equations, (3.85). Even in this example, the equations are high degree and do not permit an analytic solution, but are otherwise numerically solvable.

The result of a particular computation can be found in Fig. 3.3 and 3.4. Note that the effective light-cone velocities in the right panel of Fig. 3.3 are bounded by the speed of light. The energies can be divided as in the previous section. From (3.49), we read off

$$
E_1 = \frac{1}{2}\sqrt{-g}\Big({t^0}_0 + {t_0}^0\Big), \tag{3.86}
$$

$$
E_2 = \frac{1}{2}\sqrt{-\tilde{g}}\Big({\tilde{t}^0}_0 + {\tilde{t}_0}^0\Big), \tag{3.87}
$$

$$
E_{int} = -\frac{\gamma}{2}\frac{\sqrt{-g}\sqrt{-\tilde{g}}}{\sqrt{-g^{(B)}}}\Big(t\cdot\tilde{t} - rt^{\rho\sigma}g^{(B)}_{\rho\sigma}\tilde{t}^{\gamma\delta}g^{(B)}_{\gamma\delta}\Big), \tag{3.88}
$$

There is no dissipation in the subsystems as can be seen in Fig. 3.4, so although (3.81) looks to contain a dissipative term, this is illusory.

Chapter 4

Hybrid metric model

In the present chapter, we build on the semiholographic metric coupling, introduced in Chapter 3. Since working with holography is technically involved, we will instead focus on a particularly interesting limit in the QGP dynamics. The physical picture to keep in mind is that we are a few fm/c after the collision and the soft sector has had time to gain energy. We will assume that both sectors are in thermal equilibrium and study the implications of the semiholographic coupling in this case.

First, we will be considering the coupling between two perfect conformal fluids in a Minkowski background in Sec. 4.1. We can characterize this equilibrium state by a set of parameters, which we can restrict by requiring causality and ultraviolet completeness. Furthermore, we find that the complete system exhibits a rich phase structure, which takes the system from a sum of two individual subsystems at low temperatures to a new emergent conformal system at high temperatures. The transition is either a cross-over or a first-order transition, and the two are separated by second-order critical endpoint with specific heat critical exponent $\alpha = 2/3$. Next in Sec. 4.2, we briefly consider the case of two coupled inviscid Bjorken subsystems. In Sec. 4.3, we will consider two fluids described by relativistic hydrodynamics, in particular working in first order hydrodynamics with viscous corrections. In the shear sector, we find that the overall viscosity interpolates between the viscosities of the individual subsystems and decreases with the coupling between the subsystems. In the sound sector, we have two modes where only one is propagating with the thermodynamic speed of sound at large coupling. However both have attenuation vanishing with the square of momentum, implying that spatially homogeneous density perturbations of the individual subsystems are not attenuated. This means that more dynamics is required for the thermal equilibrium to be reached between the two sectors. Finally, in Sec. 4.4, we describe the perturbative sector by an effective kinetic theory and the non-perturbative sector by a strongly coupled fluid to ascertain to what extent non-hydrodynamic modes in one subsystem are attenuated due to the other dissipative subsystem.

This chapter is largely based on work published in [36], with the exception of Sec. 4.2.

4.1 Perfect fluids

We now will outline the $3+1$ dimensional case of two coupled perfect fluids. For a discussion in general $d+1$ dimensions, see Appendix B.

4.1.1 General equilibrium solution

We now will assume that we have a full system, $\mathfrak{S}$, in a flat background $g_{\mu\nu}^{(\mathrm{B})} = \eta_{\mu\nu}$, composed of two subsystems, $\mathfrak{S}_1$ and $\mathfrak{S}_2$. These subsystems will be described as perfect fluids, which will be interacting via the coupling equations (3.17) that deform their respective effective metrics. Furthermore, let's assume that the subsystems are thermalized with respect to their static, homogeneous and isotropic effective metrics, for which we make the ansätze:

$$g_{\mu\nu} = \mathrm{diag}(-a^2, b^2, b^2, b^2), \quad \tilde{g}_{\mu\nu} = \mathrm{diag}(-\tilde{a}^2, \tilde{b}^2, \tilde{b}^2, \tilde{b}^2), \tag{4.1}$$

where the constants $a, b, \tilde{a}, \tilde{b}$ are to be determined self-consistently. It is useful to keep in mind that if one of the systems is to be described by gauge/gravity duality, the simple metric ansatz above does not pertain to the bulk, but rather to the boundary of the gravity dual.

The energy-momentum tensors of the subsystems are then of the form

$$\begin{aligned} t^{\mu\nu} &= (\epsilon_1(T_1) + P_1(T_1))u^\mu u^\nu + P_1(T_1)g^{\mu\nu}, \quad \text{with} \quad u^\mu = (1/a, 0, 0, 0), \\ \tilde{t}^{\mu\nu} &= (\epsilon_2(T_2) + P_2(T_2))\tilde{u}^\mu \tilde{u}^\nu + P_2(T_2)\tilde{g}^{\mu\nu}, \quad \text{with} \quad \tilde{u}^\mu = (1/\tilde{a}, 0, 0, 0), \end{aligned} \tag{4.2}$$

i.e.

$$\begin{aligned} t^{\mu\nu} &= \mathrm{diag}\left(\frac{\epsilon_1(T_1)}{a^2}, \frac{P_1(T_1)}{b^2}, \frac{P_1(T_1)}{b^2}, \frac{P_1(T_1)}{b^2}\right), \\ \tilde{t}^{\mu\nu} &= \mathrm{diag}\left(\frac{\epsilon_2(T_2)}{\tilde{a}^2}, \frac{P_2(T_2)}{\tilde{b}^2}, \frac{P_2(T_2)}{\tilde{b}^2}, \frac{P_2(T_2)}{\tilde{b}^2}\right), \end{aligned} \tag{4.3}$$

with individual temperatures T_1 and T_2. Recall from the previous chapter that the temperatures of both systems are related via (3.35), which in the present case reads:

$$\mathcal{T} = T_1 a = T_2 \tilde{a}. \tag{4.4}$$

So although there are two temperatures, these are related in a simple manner and the system temperature, $\mathcal{T}$, parameterizes the space of equilibrium solutions.

The simplest coupling rules (3.17) now read

$$\begin{aligned} 1 - a^2 &= \left(\gamma \frac{\epsilon_2(T_2)}{\tilde{a}^2} - \gamma' \left(-\frac{\epsilon_2(T_2)}{\tilde{a}^2} + \frac{3P_2(T_2)}{\tilde{b}^2}\right)\right)\tilde{a}\tilde{b}^3, \\ b^2 - 1 &= \left(\gamma \frac{P_2(T_2)}{\tilde{b}^2} + \gamma' \left(-\frac{\epsilon_2(T_2)}{\tilde{a}^2} + \frac{3P_2(T_2)}{\tilde{b}^2}\right)\right)\tilde{a}\tilde{b}^3, \\ 1 - \tilde{a}^2 &= \left(\gamma \frac{\epsilon_1(T_1)}{a^2} - \gamma' \left(-\frac{\epsilon_1(T_1)}{a^2} + \frac{3P_1(T_1)}{b^2}\right)\right)ab^3, \\ \tilde{b}^2 - 1 &= \left(\gamma \frac{P_1(T_1)}{b^2} + \gamma' \left(-\frac{\epsilon_1(T_1)}{a^2} + \frac{3P_1(T_1)}{y^2}\right)\right)ab^3, \end{aligned} \tag{4.5}$$

which along with (4.4) determine a, b, $\tilde{a}$ and $\tilde{b}$ as functions of $\mathcal{T}$ and the coupling constants γ and γ'.

Finally, we can assume that the total energy-momentum tensor is given by

$$T^{\mu\nu} = (\mathcal{E} + \mathcal{P})U^\mu U^\nu + \mathcal{P}\eta^{\mu\nu}, \quad U^\mu = (1, 0, 0, 0), \tag{4.6}$$

where we can compute the full energy-density and pressure from (3.25) to find

$$\begin{aligned}
\mathcal{E} &= \epsilon_1(T_1)ab^3 + \epsilon_2(T_2)\tilde{a}\tilde{b}^3 \\
&+\frac{\gamma}{2}\left(\frac{\epsilon_1(T_1)\epsilon_2(T_2)}{a^2\tilde{a}^2} + \frac{3P_1(T_1)P_2(T_2)}{b^2\tilde{b}^2}\right)\tilde{a}\tilde{b}^3 ab^3 \\
&+\frac{\gamma'}{2}\left(-\frac{\epsilon_1(T_1)}{a^2} + \frac{3P_1(T_1)}{b^2}\right)\left(-\frac{\epsilon_2(T_2)}{\tilde{a}^2} + \frac{3P_2(T_2)}{\tilde{b}^2}\right)\tilde{a}\tilde{b}^3 ab^3, \\
\mathcal{P} &= P_1(T_1)ab^3 + P_2(T_2)\tilde{a}\tilde{b}^3 \\
&-\frac{\gamma}{2}\left(\frac{\epsilon_1(T_1)\epsilon_2(T_2)}{a^2\tilde{a}^2} + \frac{3P_1(T_1)P_2(T_2)}{b^2\tilde{b}^2}\right)\tilde{a}\tilde{b}^3 ab^3 \\
&-\frac{\gamma'}{2}\left(-\frac{\epsilon_1(T_1)}{a^2} + \frac{3P_1(T_1)}{b^2}\right)\left(-\frac{\epsilon_2(T_2)}{\tilde{a}^2} + \frac{3P_2(T_2)}{\tilde{b}^2}\right)\tilde{a}\tilde{b}^3 ab^3.
\end{aligned} \tag{4.7}$$

4.1.2 A consistency check on thermodynamics of the full system

Using the thermodynamic identities

$$\epsilon_{1,2} + P_{1,2} = T_{1,2}s_{1,2}, \quad \mathcal{E} + \mathcal{P} = \mathcal{T}\mathcal{S}, \tag{4.8}$$

and taking (4.7) into account, we can determine the total entropy density,

$$\mathcal{T}\mathcal{S} = T_1 s_1(T_1)ab^3 + T_2 s_2(T_2)\tilde{a}\tilde{b}^3 = \mathcal{T}\left[s_1(T_1)b^3 + s_2(T_2)\tilde{b}^3\right], \tag{4.9}$$

showing that the total entropy density is the sum of the two entropy densities. Therefore, we identify the total entropy current as

$$\mathcal{S}^\mu = \sqrt{-g}s_1^\mu + \sqrt{-\tilde{g}}s_2^\mu \tag{4.10}$$

for $s_1^\mu = s_1(T_1)u^\mu$, $s_2^\mu = s_2(T_2)\tilde{u}^\mu$, and $\mathcal{S}^\mu = \mathcal{S}U^\mu$.

This indeed makes perfect sense in a general non-equilibrium situation. When each sector has an entropy current $s_{1,2}^\mu$ satisfying

$$\nabla_\mu s_1^\mu \geq 0, \quad \tilde{\nabla}_\mu s_2^\mu \geq 0, \tag{4.11}$$

this implies

$$\partial_\mu(\sqrt{-g}s_1^\mu) \geq 0, \quad \partial_\mu(\sqrt{-\tilde{g}}s_2^\mu) \geq 0, \tag{4.12}$$

such that

$$\partial_\mu(\sqrt{-g}s_1^\mu + \sqrt{-\tilde{g}}s_2^\mu) = \partial_\mu\mathcal{S}^\mu \geq 0. \tag{4.13}$$

In thermal equilibrium, we also need to have

$$\mathrm{d}\mathcal{E} = \mathcal{T}\mathrm{d}\mathcal{S}, \tag{4.14}$$

or, equivalently, $\mathrm{d}\mathcal{P}/\mathrm{d}\mathcal{T} = \mathcal{S}$, for thermodynamic consistency, which we have shown in Sec. 3.1.2.

We will now show the consistency of (4.4), (4.9) and (4.14) for the coupling discussed here as well as for the coupling rules that generalize (3.17). The mutual compatibility of the thermodynamic identities (4.8) and (4.14) of the full system with the global equilibrium condition (4.4), along with the additivity of the total entropies that can be expected from the fact that each subsystem is closed in an effective point of view, provides a strong low-energy consistency check of our approach.

With the results (4.7), the thermodynamic relation $\mathcal{E}+\mathcal{P}=\mathcal{T}\mathcal{S}$ is evidently fulfilled with $\mathcal{T}=T_1 a = T_2\tilde{a}$ and $\mathcal{S}=s_1 b^3+s_2\tilde{b}^3$, when $\epsilon_{1,2}+P_{1,2}=T_{1,2}s_{1,2}$. Here we shall check that then also

$$\mathcal{S}=\frac{d\mathcal{P}}{d\mathcal{T}}, \tag{4.15}$$

holds provided the two subsystems satisfy

$$s_1=\frac{\epsilon_1+P_1}{T_1}=\frac{dP_1}{dT_1}, \quad s_2=\frac{\epsilon_2+P_2}{T_2}=\frac{dP_2}{dT_2}. \tag{4.16}$$

We need to evaluate

$$\begin{aligned}\frac{d\mathcal{P}}{d\mathcal{T}} &= \frac{d}{d\mathcal{T}}\left[P_1 ab^3+P_2\tilde{a}\tilde{b}^3\right]-\frac{\gamma}{2}\frac{d}{d\mathcal{T}}\left[\left\{\epsilon_1 a^{-1}b^3\right\}\left\{\epsilon_2\tilde{a}^{-1}\tilde{b}^3\right\}+3\left\{P_1 ab\right\}\left\{P_2\tilde{a}\tilde{b}\right\}\right]\\ &\quad -\frac{\gamma'}{2}\frac{d}{d\mathcal{T}}\left[\left(-\epsilon_1 a^{-2}+3P_1 b^{-2}\right)ab^3\left(-\epsilon_2\tilde{a}^{-2}+3P_2\tilde{b}^{-2}\right)\tilde{a}\tilde{b}^3\right]. \end{aligned} \tag{4.17}$$

Differentiating the equations for the metric factors allows us to substitute the derivatives of the parts written within curly brackets as follows:

$$\gamma\frac{d}{d\mathcal{T}}\left\{\epsilon_1 a^{-1}b^3\right\}=\gamma'\frac{d}{d\mathcal{T}}\left[\left(-\epsilon_1 a^{-2}+3P_1 b^{-2}\right)ab^3\right]-2\tilde{a}\frac{d\tilde{a}}{d\mathcal{T}}, \tag{4.18}$$

$$\gamma\frac{d}{d\mathcal{T}}\left\{P_1 ab\right\}=-\gamma'\frac{d}{d\mathcal{T}}\left[\left(-\epsilon_1 a^{-2}+3P_1 b^{-2}\right)ab^3\right]+2\tilde{b}\frac{d\tilde{b}}{d\mathcal{T}}, \tag{4.19}$$

$$\gamma\frac{d}{d\mathcal{T}}\left\{\epsilon_2\tilde{a}^{-1}\tilde{b}^3\right\}=\gamma'\frac{d}{d\mathcal{T}}\left[\left(-\epsilon_2\tilde{a}^{-2}+3P_2\tilde{b}^{-2}\right)\tilde{a}\tilde{b}^3\right]-2a\frac{da}{d\mathcal{T}}, \tag{4.20}$$

$$\gamma\frac{d}{d\mathcal{T}}\left\{P_2\tilde{a}\tilde{b}\right\}=-\gamma'\frac{d}{d\mathcal{T}}\left[\left(-\epsilon_2\tilde{a}^{-2}+3P_2\tilde{b}^{-2}\right)\tilde{a}\tilde{b}^3\right]+2b\frac{db}{d\mathcal{T}}, \tag{4.21}$$

This leads to

$$\begin{aligned}\frac{d\mathcal{P}}{d\mathcal{T}} &= \frac{d}{d\mathcal{T}}\left[P_1 ab^3+P_2\tilde{a}\tilde{b}^3\right]+\epsilon_1 b^3\frac{da}{d\mathcal{T}}+\epsilon_2\tilde{b}^3\frac{d\tilde{a}}{d\mathcal{T}}-3P_1 ab^2\frac{db}{d\mathcal{T}}-3P_2\tilde{a}\tilde{b}^2\frac{d\tilde{b}}{d\mathcal{T}},\\ &= \frac{dP_1}{d\mathcal{T}}ab^3+(\epsilon_1+P_1)\frac{da}{d\mathcal{T}}b^3+\frac{dP_2}{d\mathcal{T}}\tilde{a}\tilde{b}^3+(\epsilon_2+P_2)\frac{d\tilde{a}}{d\mathcal{T}}\tilde{b}^3,\\ &= \frac{dP_1}{dT_1}\frac{dT_1}{d\mathcal{T}}ab^3+T_1\frac{dP_1}{dT_1}\frac{da}{d\mathcal{T}}b^3+\frac{dP_2}{dT_2}\frac{dT_2}{d\mathcal{T}}\tilde{a}\tilde{b}^3+T_2\frac{dP_2}{dT_2}\frac{d\tilde{a}}{d\mathcal{T}}\tilde{b}^3,\\ &= s_1 b^3\left(\frac{dT_1}{d\mathcal{T}}a+T_1\frac{da}{d\mathcal{T}}\right)+s_2\tilde{b}^3\left(\frac{dT_2}{d\mathcal{T}}\tilde{a}+T_2\frac{d\tilde{a}}{d\mathcal{T}}\right),\\ &= \mathcal{S}. \end{aligned} \tag{4.22}$$

The two expressions within parentheses in the last step are both $d\mathcal{T}/d\mathcal{T}=1$, which completes the proof: $d\mathcal{P}/d\mathcal{T}=\mathcal{S}$.

4.1.3 Causal structure of equilibrium solution

Causality is a powerful, necessary requirement for physical systems. The dynamics of each subsystem are bound causally by their respective effective metrics only. As a result, causality in the full system (which we have assumed here to be Minkowski) is not guaranteed a priori. Since the causal structure of the dynamics taking place in the subsystems is dictated by the respective effective metrics only, causality in the full system, which is living in Minkowski space, is not

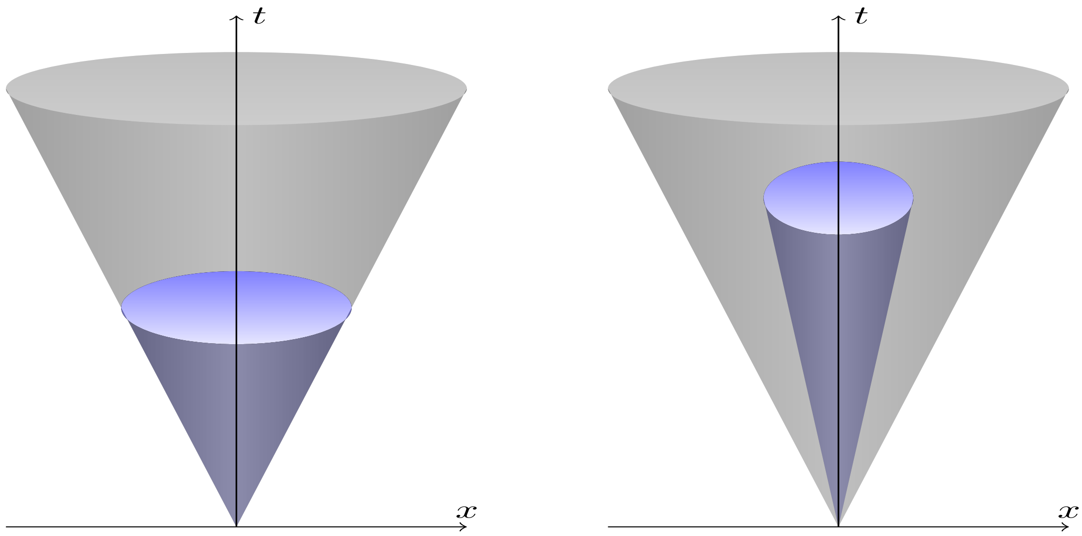

Figure 4.1: The gray light cone is the background Minkowski metric $\eta_{\mu\nu}$. The blue light cone is the effective metric $g_{\mu\nu}$. For clarity, only one of the effective metrics is shown. Note that the Minkowski light cone always needs to encompass the effective light cone for all values of the coupling, $\gamma > 0$. Left: Low $\gamma^{1/4}T$. Right: High $\gamma^{1/4}T$. Note that massless excitations w.r.t. the effective metric are perceived as massive excitations in the Minkowski background.

guaranteed. For instance, massless excitations in Minkowski space travel at $c = 1$, whereas in e.g. massless excitations in subsystem $\mathfrak{S}_1$ would propagate at a velocity $v = a/b$. There is no requirement thusfar for $c > v$.

As such, we can eliminate solutions of (3.17) that have superluminal propagation. To see this in action, take the sum of the first and second as well as of the third and fourth equation in (4.5), leading to

$$\begin{aligned} b^2 - a^2 &= \gamma \left(\frac{\epsilon_2(T_2)}{\tilde{a}^2} + \frac{P_2(T_2)}{\tilde{b}^2} \right) \tilde{a}\tilde{b}^3 \geq 0, \\ \tilde{b}^2 - \tilde{a}^2 &= \gamma \left(\frac{\epsilon_1(T_1)}{a^2} + \frac{P_1(T_1)}{b^2} \right) ab^3 \geq 0, \end{aligned} \tag{4.23}$$

independent of γ'. The inequality follows by requiring that the individual light cones remain below c:

$$b^2 - a^2 = b^2(1 - v^2) \geq 0. \tag{4.24}$$

Thus, we require that the coupling constant $\gamma \geq 0$, the individual subsystem energy densities are not negative $\epsilon_{1,2} \geq 0$ and we allow for a small range of negative pressures $v^2 P_{1,2} \geq -\varepsilon$. The change in the light cone can be aptly summed up in Fig. 4.1. Note that the (blue) effective light cone defined by the metric $g_{\mu\nu}$ is contained entirely within the light cone defined by the background Minkowski metric.

4.1.4 Conformal subsystems

It is clear that (3.17) is not yet a closed system of equations. We need to further specify equations of state to relate the energy densities to the pressures. For simplicity, we will consider the case of conformal subsystems. The equations of state of the two subsystems are then simply

$$\begin{aligned}\epsilon_1(T_1) = 3P_1(T_1) = 3n_1T_1^4,\\ \epsilon_2(T_2) = 3P_2(T_2) = 3n_2T_2^4,\end{aligned} \tag{4.25}$$

with constant prefactors n_1 and n_2. Then the energy-momentum tensors $t^{\mu\nu}$ and $\tilde{t}^{\mu\nu}$ are traceless with respect to the effective metrics $g_{\mu\nu}$ and $\tilde{g}_{\mu\nu}$, which can be seen easily by taking the trace of (4.2) and (4.3).

It becomes useful to parameterize our coupling equations in terms of the effective light cone velocities, where

$$v := \frac{a}{b}, \quad \tilde{v} := \frac{\tilde{a}}{\tilde{b}}, \tag{4.26}$$

which are associated with the effective metrics $g_{\mu\nu}$ and $\tilde{g}_{\mu\nu}$, respectively. In this case, the total entropy of the system (4.10) is

$$\mathcal{S} = 4\mathcal{T}^3\left(\frac{n_1}{v^3} + \frac{n_2}{\tilde{v}^3}\right), \tag{4.27}$$

where we used that the entropy of each subsystem is just

$$s_{1,2} = \frac{\epsilon_{1,2} + P_{1,2}}{T_{1,2}} = 4n_{1,2}T_{1,2}^3. \tag{4.28}$$

The coupling equations, together with the assumption of conformality and the temperature condition (4.4), leads to

$$\begin{aligned}1 - v^2b^2 &= 3\gamma\mathcal{T}^4 n_2\frac{1 - r(1-\tilde{v}^2)}{\tilde{v}^5\tilde{b}^2},\\ b^2 - 1 &= \gamma\mathcal{T}^4 n_2\frac{\tilde{v}^2 + 3r(1-\tilde{v}^2)}{\tilde{v}^5\tilde{b}^2},\\ 1 - \tilde{v}^2\tilde{b}^2 &= 3\gamma\mathcal{T}^4 n_1\frac{1 - r(1-v^2)}{v^5b^2},\\ \tilde{b}^2 - 1 &= \gamma\mathcal{T}^4 n_1\frac{v^2 + 3r(1-v^2)}{v^5b^2},\end{aligned} \tag{4.29}$$

where

$$r := -\frac{\gamma'}{\gamma}, \tag{4.30}$$

is a dimensionless coupling constant that we shall use from now on in exchange for γ'. Eliminating b and $\tilde{b}$ yields the two equations

$$n_1\gamma\mathcal{T}^4 = \frac{v^5(1-\tilde{v}^2)(3+\tilde{v}^2)}{[3 + v^2\tilde{v}^2 - 3r(1-v^2)(1-\tilde{v}^2)]^2}, \tag{4.31}$$

$$n_2\gamma\mathcal{T}^4 = \frac{\tilde{v}^5(1-v^2)(3+v^2)}{[3 + v^2\tilde{v}^2 - 3r(1-v^2)(1-\tilde{v}^2)]^2}. \tag{4.32}$$

Since causality implies $0 < v, \tilde{v} < 1$, we see that solutions exist for arbitrary $\mathcal{T}$ only when the denominator on the right-hand side of (4.31) is able to reach a zero. This leads to

$$0 = 3 + v^2\tilde{v}^2 - 3r(1-v^2)(1-\tilde{v}^2),$$
$$\Rightarrow r = \frac{3 + v^2\tilde{v}^2}{3(1-v^2)(1-\tilde{v}^2)} \tag{4.33}$$

Clearly, the range of r is between $\infty > r > 1$. Thus for ultraviolet completeness for the simplest coupling rules (3.17), we require that $r > 1$. Otherwise this model would exist only up to some finite value of $\mathcal{T}$.

Now we present some general observations that we can make analytically.

Although the subsystems are conformal, when the two sectors interact, the full system in general is no longer conformally invariant. We find the trace, using the expression for the full energy density and pressure (4.7), to be

$$-T^{\mu\nu}\eta_{\mu\nu} = \mathcal{E} - 3\mathcal{P} = \frac{6\gamma n_1 n_2 \mathcal{T}^8}{v^3\tilde{v}^3 a^2\tilde{a}^2}\left[3 + v^2\tilde{v}^2 - 3r(1-v^2)(1-\tilde{v}^2)\right]. \tag{4.34}$$

Note that in [36] there is a typo in the coefficient of this expression.

The term in square brackets in (4.34) is the square root of the denominator in (4.32). It is positive in the small γ case (where $v = \tilde{v} = 1$). Due to the previous discussion, it cannot change sign for any finite value of $\gamma\mathcal{T}^4$. Therefore, the conditions for causality $\gamma > 0$ and condition for ultraviolet completeness, $r > 1$, imply that the interaction measure $\mathcal{E} - 3P = -T^{\mu}{}_{\mu}$ is positive, which is also a feature of (lattice) Yang-Mills theories at finite temperature [109, 110]. Furthermore, since large $\mathcal{T}^4$ in (4.31) corresponds to a small value of the square root of the denominator in (4.32), we see that the interaction measure goes to zero for large temperatures and the full system thus approaches conformality for large $\mathcal{T}$.

Also, one can derive perturbative expansions for all quantities (for more details, see Appendix C). When writing down perturbative results, we shall assume that $\gamma\mathcal{T}^4$ and $\gamma'\mathcal{T}^4$ are of the same order, i.e. r is of order 1. For small couplings or for small temperature, $|\gamma|, |\gamma'| \ll \mathcal{T}^{-4}$, the resulting a, $\tilde{a}$, v, and $\tilde{v}$ are all close to unity, and thus $\mathcal{E} - 3\mathcal{P} \approx 24\gamma n_1 n_2 \mathcal{T}^8$, i.e., the full system approaches conformality at small temperature as expected. This corresponds to the decoupling limit of the system.

The emerging conformality at large temperatures can also be seen in the speed of sound (squared) of the full system, defined thermodynamically by

$$c_s^2 = \frac{d\mathcal{P}}{d\mathcal{E}} = \left(\frac{d\ln\mathcal{S}}{d\ln\mathcal{T}}\right)^{-1}, \tag{4.35}$$

which expanded up to third order in $\gamma\mathcal{T}^4$ reads

$$c_s(\mathcal{T}) = \frac{1}{\sqrt{3}} - \frac{8}{\sqrt{3}}\gamma\mathcal{T}^4\frac{n_1 n_2}{n_1+n_2} - 32\sqrt{3}\gamma^2\mathcal{T}^8\frac{n_1 n_2(n_1^2+n_2^2)}{(n_1+n_2)^2} + \mathcal{O}((\gamma\mathcal{T}^4)^3). \tag{4.36}$$

With conformal subsystems the dependence on $r = -\gamma'/\gamma$ appears only at third order. In quantities which only depend on v and $\tilde{v}$, as is the case for the entropy, also the third-order term is still independent of r.

As shown in Appendix C, the high-temperature behavior of the total system is governed by the fact that the metric factors $a, \tilde{a}, b, \tilde{b}$ asymptote to linear functions of the physical temperature $\mathcal{T}$. Since the effective temperatures of the subsystems are given by $T_1 = \mathcal{T}/a$ and $T_2 = \mathcal{T}/\tilde{a}$, they stop growing together with $\mathcal{T}$ and instead saturate at finite values proportional to $\gamma^{-1/4}$. For $r = 2$ Fig. 4.2 displays this behavior for equal and unequal subsystems, i.e., $n_1 = n_2$ and $n_1 \neq n_2$, respectively.

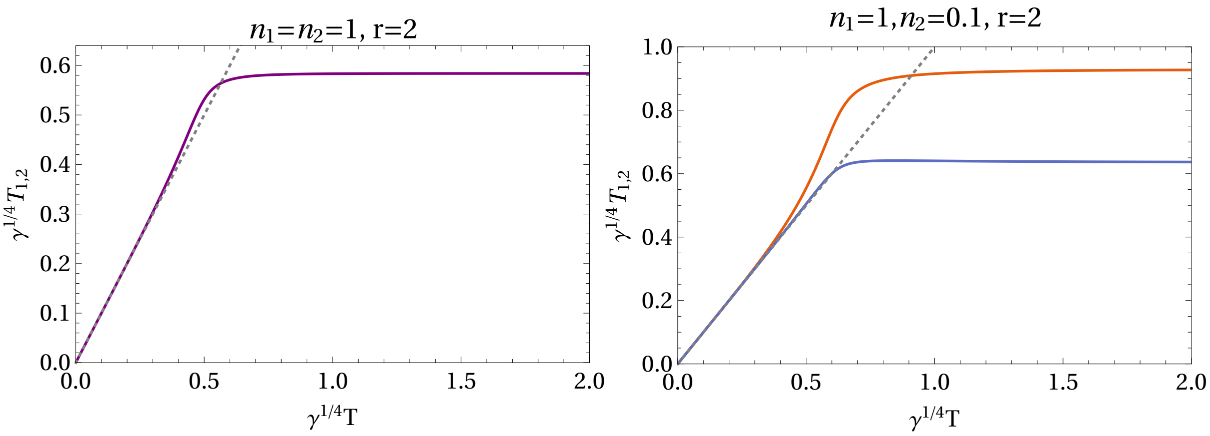

Figure 4.2: Effective temperatures of the subsystems as a function of the physical temperature with $r = 2$ for equal subsystems in the left panel and unequal ($n_2 = n_1/10$) subsystems in the right panel. As the physical temperature increases, the effective temperature of the subsystems first increases in line with the former (the dotted line marks equality), but when $\mathcal{T}$ becomes larger than $\gamma^{-1/4}$, the effective temperatures asymptote to a limiting value. This limiting value is larger for the subsystem with fewer degrees of freedom.

Equal subsystems

For the special case where the number of degrees of freedom are equal, i.e. $n_1 = n_2$, it is clear that $v = \tilde{v}$. The numerical solution of (4.31) is displayed in Fig. 4.3 for various values of $r > 1$.

It turns out that for

$$1 < r < r_c = \frac{1}{540}(195 + 43\sqrt{15} + \sqrt{30(4082 - 557\sqrt{15})}) \approx 1.1145$$

more than one solution exists. This corresponds to a phase transition that will be discussed in Sec. 4.1.4. For details on how we analytically determined the critical value of r, see Appendix B.

Concentrating first on the case $r > r_c$, the behavior of the pressure and the interaction measure is shown in the left panel of Fig. 4.5 for a typical case, when the coupling $r = 2$. Intriguingly, $\mathcal{P}/\mathcal{T}^4$ shows an increase somewhat reminiscent of the deconfinement crossover transition in QCD.

Since $\mathcal{S}/\mathcal{T}^3 \propto v^{-3}$, the entropy increases from the decoupling limit value at $\gamma^{1/4}\mathcal{T} = 0$, where $v = 1$, in parallel to the drop in v displayed in Fig. 4.3.

The speed of sound squared (4.35) is shown in the right panel of Fig. 4.5. At $\gamma^{1/4}\mathcal{T} = 0$, c_s^2 unsurpisingly takes the conformal value, $c_s^2 = \frac{1}{3}$, as both subsystems are conformal and this is the decoupling limit. For intermediate values, the speed of sound squared drops from the conformal limit, indicating a crossover as opposed to a phase transition. Finally, for $\gamma^{1/4}\mathcal{T} \to \infty$, the speed of sound squared asymptotes to conformal behavior from below.

In the case of two identical conformal subsystems, the relation between the effective light cone velocity v and $\gamma\mathcal{T}^4$ is given by the roots of a polynomial equation of 9th degree (given in (4.31) for $v = \tilde{v}$), which has no general closed form solution. However, it is simple to determine

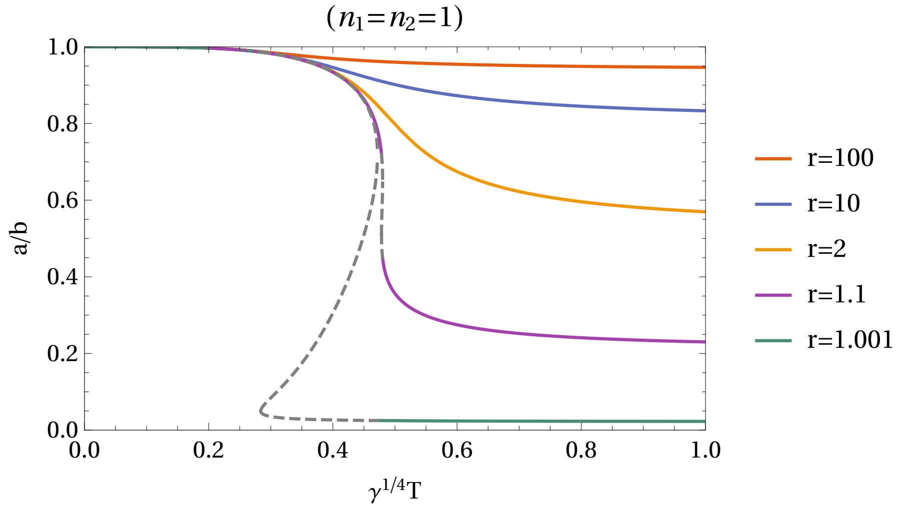

Figure 4.3: Effective light-cone speeds of the two subsystems with $n_1 = n_2 = 1$ for different values of $r = -\gamma'/\gamma$. Above $r = r_c \approx 1.1145$ there is a unique solution for all values of $\gamma^{1/4}\mathcal{T}$ (full lines), while below r_c there are ranges of $\gamma^{1/4}\mathcal{T}$ with three solutions (dashed lines).

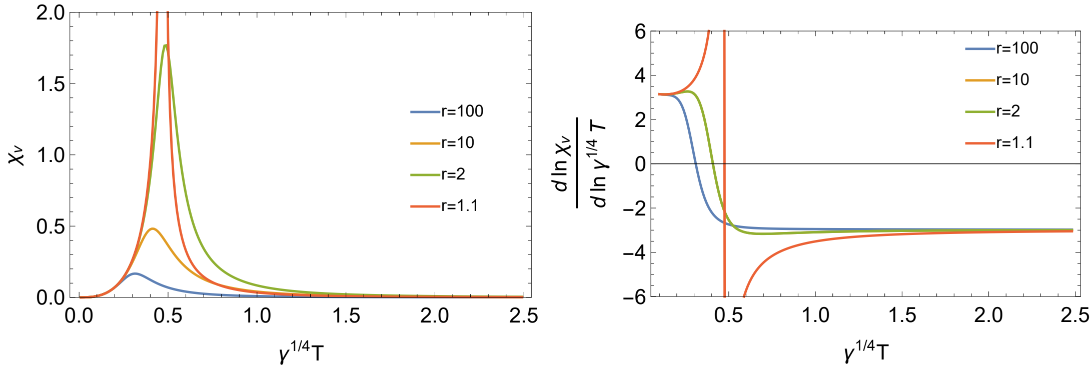

Figure 4.4: Left panel: light-cone susceptibility, χ_v for equal subsystems $n_1 = n_2 = 1$, fixed γ and varying r. Right panel: the logarithmic derivative of the logarithm of the susceptibility.

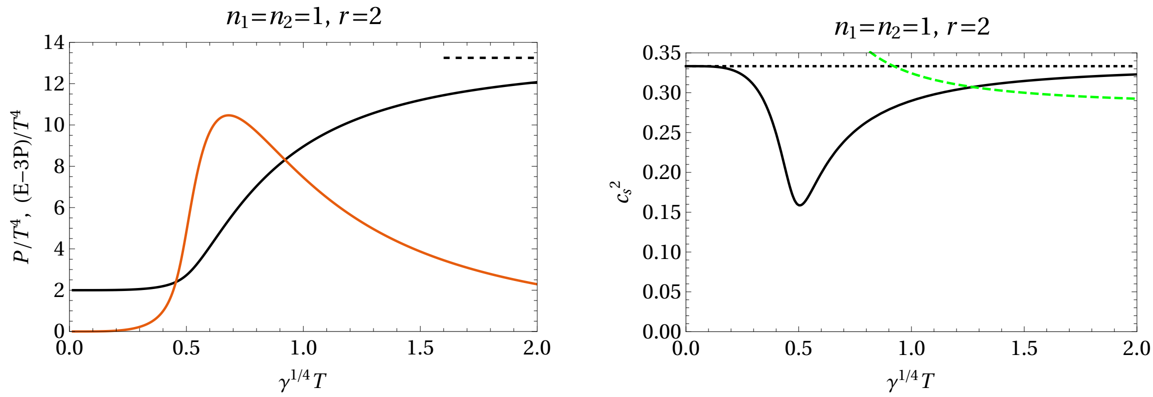

Figure 4.5: Left panel: Pressure (black line) and trace of the energy-momentum tensor (red) divided by $\mathcal{T}^4$, with the asymptotic value of the pressure indicated by the short dashed line. Right panel: speed of sound squared (full black line) – both for $n_1 = n_2 = 1$ and $r = 2$. As $\gamma^{1/4}\mathcal{T}$ increases from small to large values, a crossover between regimes with different values of $\mathcal{P}/\mathcal{T}^4$ takes place that is accompanied by a dip in the speed of sound which takes on a conformal value in both asymptotic regimes. At large $\gamma^{1/4}\mathcal{T}$ and for sufficiently low values of r (including the case $r = 2$ at hand), the speed of sound in the full system turns out to be larger than the effective light cone speed v of the subsystems (green dashed line: v^2).

the asymptotic value of v:

$$v_\infty^2 := \lim_{\gamma\mathcal{T}^4\to\infty} v^2 = \frac{3r - \sqrt{3}\sqrt{4r-1}}{3r-1}. \tag{4.37}$$

Evidently, the entire physical range $0 < v_\infty < 1$ is covered as $1 < r < \infty$.

It is important to point out something which might be counterintuitive. We note that for certain values of r, the asymptotic light cone velocity can be smaller than the conformal speed of sound, $1/\sqrt{3}$. From (4.37) and knowing that for large $\gamma^{1/4}\mathcal{T}$ the speed of sound asymptotes to the conformal value, we see that this is the generic case for $r < 7/3$. In the right panel of Fig. 4.5, we have plotted this for $r = 2$, where the green dotted line is the light cone velocity. There is no contradiction to causality, since this occurs within the light cone of the physical system, $\eta_{\mu\nu}$. The dynamics of the individual subsystems are being superseded by the collective dynamics between them. This idea will be developed further in Section 4.3.2.

Unequal subsystems

For unequal systems one can show (using formulae (4.31) and (4.32)) that there exist solutions for v and $\tilde{v}$ in the limit $\gamma\mathcal{T}^4 \to \infty$ for any value of n_2/n_1 and $r > 1$. They are given by the (sextic) equations

$$\frac{3[r(1-v_\infty^2)-1]^{5/2}}{(4r-1)v_\infty^5[r(1-v_\infty^2)+v_\infty^2/3]^{1/2}} = \frac{n_2}{n_1} = \frac{(4r-1)\tilde{v}_\infty^5[r(1-\tilde{v}_\infty^2)+\tilde{v}_\infty^2/3]^{1/2}}{3[r(1-\tilde{v}_\infty^2)-1]^{5/2}}, \tag{4.38}$$

which have a unique solution in the domain $0 < v_\infty, \tilde{v}_\infty < 1$ when $r > 1$. In the extreme limit that one of the systems completely dominates, say $n_2/n_1 \to 0$, the asymptotic effective light-cone velocity of the smaller system approaches zero, $\tilde{v}_\infty \sim O((n_2/n_1)^{1/5})$, while the dominant system has the limit $v_\infty \to \sqrt{1-r^{-1}}$. This case of one dominant system is described further in Appendix B.2.

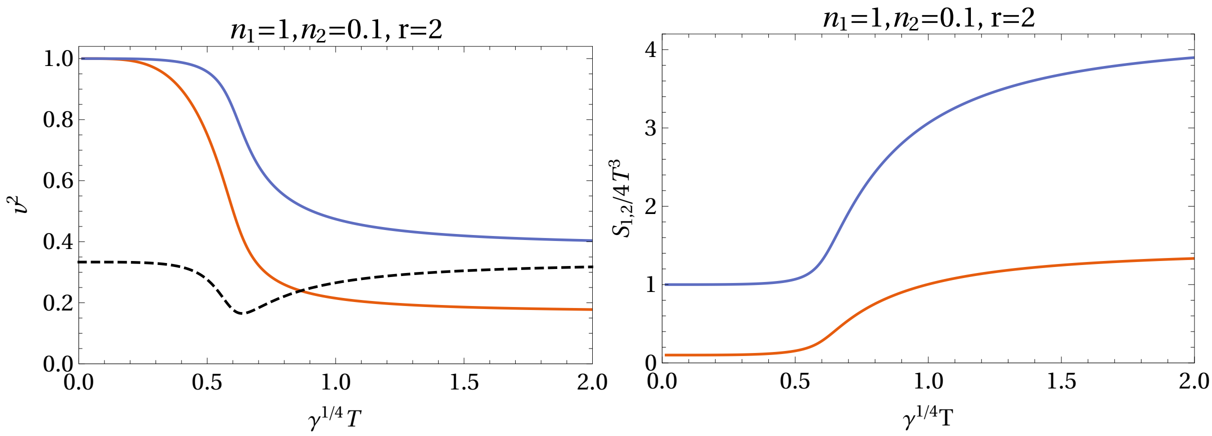

Figure 4.6: Unequal systems with $n_1 = 1, n_2 = 0.1$ and $r = 2$. Left panel: light-cone velocities squared in the two subsystems (v^2: upper, blue line, $\tilde{v}^2$: lower, red line) compared to c_s^2 (dashed black line). Right panel: entropies of the two subsystems ($\mathcal{S}_1$: upper, blue line, $\mathcal{S}_2$: lower, red line).

In Fig. 4.6, the full numerical solution of the effective light-cone velocities is displayed for $n_2/n_1 = 1/10$ and $r = 2$ as well as the entropies of the two subsystems. The blue line is the dominant system. While the smaller subsystem has a much larger relative growth of S/T^3 than the larger subsystem, the latter remains dominant. Considering again the extreme limit $n_2/n_1 \to 0$, S_2/S_1 changes from being of order n_2/n_1 at low $\gamma\mathcal{T}^4$ to $(n_2/n_1)^{2/5}$ at high $\gamma\mathcal{T}^4$.

At the value $r = 2$ used in Fig. 4.6, the behavior of the speed of sound is similar to the case shown in Fig. 4.5. Again, there is a dip at the crossover between the regimes of small and large $\gamma^{1/4}\mathcal{T}$, where c_s asymptotes to the conformal value $1/\sqrt{3}$. In the case displayed in Fig. 4.6, now only one of the effective light-cone velocities, namely the smaller subsystem light-cone velocity $\tilde{v}$, falls below the conformal value of the speed of sound at large $\gamma^{1/4}\mathcal{T}$.

Phase transition

Here we discuss the nature of the phase transition of the two coupled perfect fluids. For $1 < r < r_c$, perturbative expansions have to break down for $1 < r < r_c$, where the light-cone velocity is multivalued at finite values of $\gamma\mathcal{T}^4$, as shown in Fig. 4.3 for $n_1 = n_2$. For $1 < r < r_c \approx 1.1145$ in the case $n_1 = n_2$ and $1 < r < r_c \approx 1.25$ for $n_1 \neq n_2$, this corresponds to a first-order phase transition that turns into a second-order phase transition at r_c.

We can characterize the phase transition by introducing the light-cone susceptibility:

$$\chi_v := \frac{\partial v}{\partial(\gamma^{1/4}\mathcal{T})}, \tag{4.39}$$

which we have plotted in Fig. 4.4 for equal subsystems, $n_1 = n_2 = 1$, and various r. Note that χ_v diverges near the critical temperature as we approach r_c. In the right panel, we plot the logarithmic derivative of the logarithm of χ_v and find that if we approach the phase transition from above T_c, then the light cone susceptibility scales like

$$\chi_v \sim (\gamma^{1/4}\mathcal{T})^{-3}. \tag{4.40}$$

In Fig. 4.7 pressure and entropy are plotted in the region around the first-order phase transition for equal subsystems, $n_1 = n_2 = 1$, and $r = 1.1$. The range in $\gamma^{1/4}\mathcal{T}$ where the

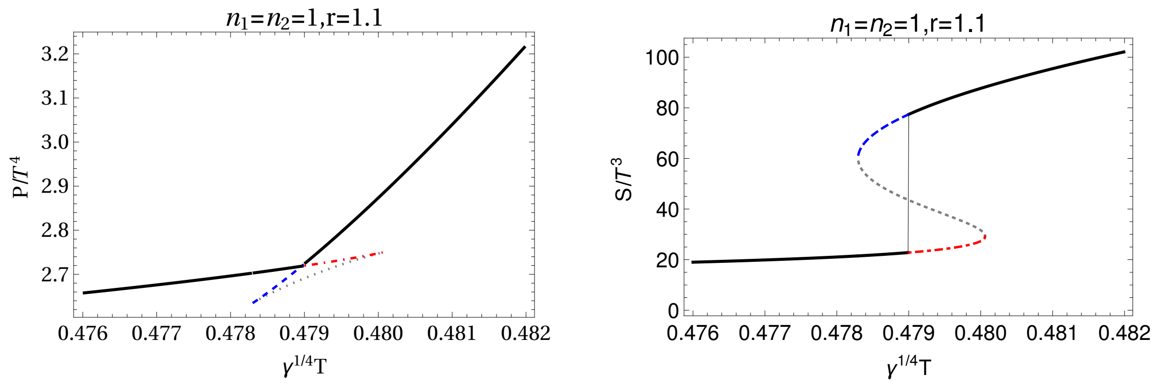

Figure 4.7: Pressure (left panel) and entropy (right panel) around the first-order phase transition with $n_1 = n_2 = 1$ and $r = 1.1$. The pressure of the ground state is given by the maximal value at each temperature. At the critical temperature the slope changes discontinuously. The lines which extend smoothly beyond this point when coming from lower or higher temperatures correspond to superheating or supercooling phases, respectively. (The lower line connecting the endpoints of supercooling and superheating corresponds to the entropy curve with negative slope and thus cannot be accessed physically.) The dotted line in the entropy curve indicates the jump in the entropy that occurs when there is no supercooling or superheating.

pressure has three solutions corresponds to the possibility of superheating or supercooling, indicated by red and blue lines, respectively. This happens if one does not immediately switch to the thermodynamically preferred phase with higher pressure (lower free energy). The third solution, denoted by a gray line, which directly connects the endpoints of superheating and supercooling, is always thermodynamically disfavored and cannot be accessed physically, as it comes with negative specific heat (corresponding to the part of the curve for the entropy with negative slope).

In Fig. 4.8 the effective temperature of the subsystems is shown for the same set of parameters as above. At the phase transition the effective temperature jumps and approaches the asymptotic value from above as the physical temperature goes to infinity. In fact, although hardly visible in the left plot in Fig. 4.2, the effective temperature also approaches the asymptotic value from above for $r = 2$ in the crossover region; only for $r \gtrsim 2.048$ (in the case of $n_1 = n_2$) the effective temperature eventually shows monotonic behavior.

At $r = r_c$ the phase transition becomes second-order with continuous pressure and entropy. In Appendix B and D, the parameters of the second-order phase transition are obtained in closed form for $n_1 = n_2$ in arbitrary dimension. We can determine the critical exponent α, which characterizes the specific heat, in $3 + 1$ dimensions to find

$$\mathcal{C}_V \sim |\mathcal{T} - \mathcal{T}_c|^{-\alpha}, \quad \alpha = \frac{2}{3}, \tag{4.41}$$

which is independent of n_2/n_1. It is different from any mean-field result, as well as larger than the value in the Ising model ($\alpha \approx 0.11$) or in the polymer models ($\alpha \approx 0.236$), which are the largest values occurring in N vector models (for $N = 1$ and $N = 0$, respectively) [111]. The comparatively large value of α in (4.41) is within the same ballpark as in the matrix model for deconfinement in [112], which yields $\alpha = 3/5$. Curiously, this value of α is precisely the same as in the four-state Potts or Ashkin-Teller model, which describes a regular lattice with two Ising spins per site [113, 114].

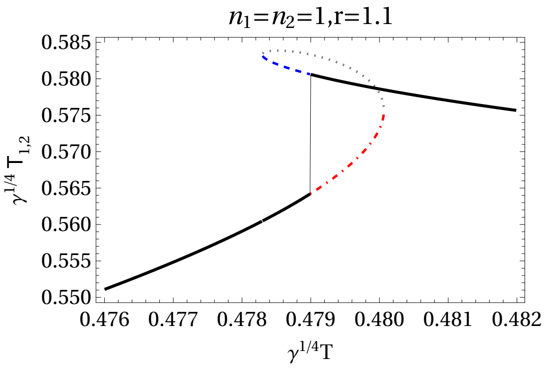

Figure 4.8: The behavior of the effective temperature of the subsystems during the first-order phase transition with $n_1 = n_2 = 1$ and $r = 1.1$. The dotted line in the entropy curve indicates the jump in the effective temperature when there is no supercooling or superheating.

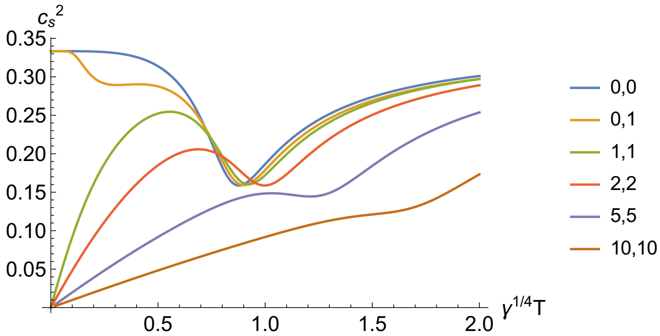

Figure 4.9: Speed of sound (squared) in two systems where one or both are replaced by a gas of free massive bosons at $r = 2$. If both systems are massive, the speed of sound starts from zero at zero temperature; if one is still conformal, the lower end point remains at $1/3$. The values given in the plot legend refer to the two masses in units of $\gamma^{-1/4}$. (The massless case corresponds to $n_{1,2} = \pi^2/90$ in (4.25).)

The qualitative features of the phase transition are the same for unequal conformal subsystems. For $1 < r < r_c$, the transition is first order, at $r = r_c$ the phase transition is second order, and for $r > r_c$ it is a crossover. Furthermore, the critical value r_c shows a rather weak dependence on n_2/n_1, it lies in the narrow interval $1.119\ldots < r_c < 1.25$, and the critical exponent α at the second-order phase transition point $r = r_c$ is always $2/3$ (for more details see Appendix D).

4.1.5 Massive subsystems

The simplest coupling rules, (3.17) and specifically (4.5) with $r > 1$ and $\gamma > 0$, also make sense for a more general choice of equations of state of the subsystems. In this subsection, we consider two free Bose gases with various masses, described by the on-shell distribution function:

$$f_1 = \frac{1}{e^{-\sqrt{p^2+m_1^2}/T_1} - 1}, \tag{4.42}$$

and similarly for the other subsystem. The energy density and pressure can be computed via (2.51), which after the integration over angles gives:

$$\varepsilon_1 = \frac{n_1}{2\pi^2} \int_0^\infty \mathrm{d}p \, \sqrt{p^2 + m_1^2} p^2 f_1, \tag{4.43}$$

$$P_1 = \frac{n_1}{2\pi^2} \int_0^\infty \mathrm{d}p \, \frac{p^4}{\sqrt{p^2 + m_1^2}} f_1, \tag{4.44}$$

and similarly for the other subsystem.

We can then proceed to compute the total energy density $\mathcal{E}$ and $\mathcal{P}$ via (4.7) and find the speed of sound for the full system via (4.35). In Fig. 4.9, we display the results for the speed of sound (squared) for $r = 2$ and a variety of masses, where there is only a crossover. We see that generically, when both subsystems have massive particles, the speed of sound starts from zero at $\gamma\mathcal{T}^4 = 0$ and non-monotonically approaches the conformal value at large $\gamma\mathcal{T}^4$. When one or both components contain massless particles, c_s^2 starts from the conformal value of 1/3.

The way approximate conformality is approached at high $\mathcal{T}$ is again similar to the conformal case discussed above, although we cannot demonstrate this analytically as in Appendix C. The high-temperature behavior for $r > 1$ is governed again by an asymptotically linear behavior of the metric coefficients $a, \tilde{a}, b, \tilde{b} \sim \mathcal{T}$. Such a behavior is at least consistent with the (simplest) coupling rules (3.17): Once $a, \tilde{a}, b, \tilde{b}$ have grown sufficiently large, these equations are homogeneous of degree two in the metric coefficients, provided the effective temperatures T_1, T_2 become constant, which is the case when $a, \tilde{a} \sim \mathcal{T}$.

However, an important difference to the conformal case is that the trace-term $\Delta K \delta^\mu_\nu$ in the full energy-momentum tensor is no longer subdominant, but in fact needed to cancel the contributions to the trace of the full energy-momentum tensor at order $\mathcal{T}^4$. This is a consequence of the form (4.9) of the full entropy, $\mathcal{S} = s_1(T_1)b^3 + s_2(T_2)\tilde{b}^3 \sim \mathcal{T}^3$, together with thermodynamic consistency, $\mathcal{S} = d\mathcal{P}/d\mathcal{T}$ (which is proved in Section 3.1.2 for arbitrary equations of state of the subsystems).

We expect that it is equally possible to couple more involved equations of state than gases of free massive particles with the simplest coupling rule and to obtain a UV-complete setup.

4.2 Bjorken fluids

We now briefly turn our attention to Bjorken fluids, following [115]. Bjorken flow describes a simple model for heavy ion collisions. We assume that the collision axis is along the z-axis and the system is otherwise homogeneous. Essentially, the nuclei are modelled as infinite flat sheets in the transverse (x, y) directions. Furthermore, the matter produced in the forward light cone is boost invariant. The background metric is given in Milne coordinates as

$$g^{(\mathrm{B})}_{\mu\nu} = \mathrm{diag}(-1, 1, 1, \tau^2), \tag{4.45}$$

where $\tau = \sqrt{t^2 - z^2}$ is the proper time. Note that the Bjorken background is flat, but expanding. A perfect fluid in this background has the following form:

$$T^{\mu\nu} = \mathrm{diag}(\mathcal{E}, \mathcal{P}_\perp, \mathcal{P}_\perp, \frac{\mathcal{P}_L}{\tau^2}) \tag{4.46}$$

The uncoupled inviscid Bjorken equation leads to the Ward identity of the following form:

$$\nabla_\mu t^{\mu\nu} = 0 \Rightarrow \partial_\tau \mathcal{E} + \frac{\mathcal{E} + \mathcal{P}_L}{\tau} = 0, \tag{4.47}$$

where $\mathcal{P}_L$ is the longitudinal pressure (in the z-direction). There are two important cases to consider. First, in the case of a conformal isotropic fluid, i.e. $\mathcal{P}_L = \mathcal{P}_\perp = \mathcal{P}$ and $\mathcal{E} = c_s^2 \mathcal{P}$, where $c_s^2 = 1/3$ is the speed of sound, we find the solution of (4.47) is

$$\mathcal{E} \sim \tau^{-4/3}. \tag{4.48}$$

In the case of extreme anisotropy, when $\mathcal{P}_L \ll \mathcal{P}_\perp$, we find find from (4.47)

$$\mathcal{E} \sim \tau^{-1}. \tag{4.49}$$

Thus, we are motivated to choose the following ansatz for the effective metrics

$$g_{\mu\nu} = \mathrm{diag}(-a^2, b^2, b^2, c^2), \tag{4.50}$$
$$\tilde{g}_{\mu\nu} = \mathrm{diag}(-\tilde{a}^2, \tilde{b}^2, \tilde{b}^2, \tilde{c}^2). \tag{4.51}$$

The energy-momentum tensors are given by

$$t^{\mu\nu} = \mathrm{diag}\Big(\frac{\varepsilon}{a^2}, \frac{P_\perp}{b^2}, \frac{P_\perp}{b^2}, \frac{P_L}{c^2}\Big), \tag{4.52}$$
$$\tilde{t}^{\mu\nu} = \mathrm{diag}\Big(\frac{\tilde{\varepsilon}}{\tilde{a}^2}, \frac{\tilde{P}_\perp}{\tilde{b}^2}, \frac{\tilde{P}_\perp}{\tilde{b}^2}, \frac{\tilde{P}_L}{\tilde{c}^2}\Big), \tag{4.53}$$

which we choose to be conformal, with equations of state $\varepsilon = 2P_\perp + P_L$ and $\tilde{\varepsilon} = 2\tilde{P}_\perp + \tilde{P}_L$.

The evolution of both subsystems is determined by the conservation of the energy-momentum tensors:

$$0 = \partial_\tau \varepsilon + \varepsilon \partial_\tau \log(bc) + 2P_\perp \partial_\tau \log b + P_L \partial_\tau \log c, \tag{4.54}$$
$$0 = \partial_\tau \tilde{\varepsilon} + \tilde{\varepsilon} \partial_\tau \log(\tilde{b}\tilde{c}) + 2\tilde{P}_\perp \partial_\tau \log \tilde{b} + \tilde{P}_L \partial_\tau \log \tilde{c}, \tag{4.55}$$

As a check, it is instructive to see that we recover the EOM in the Bjorken background. In this case, $b = 1$ and $c = \tau$ and we see that we indeed recover (4.47).

The coupling equations (3.27) in this case are given by

$$1 - a^2 = \gamma \frac{\tilde{a}\tilde{b}^2\tilde{c}}{\tau}\Big[\frac{\tilde{\varepsilon}}{\tilde{a}^2} + r\Big(\frac{2\tilde{P}_\perp}{\tilde{b}^2} + \frac{\tau^2 \tilde{P}_L}{\tilde{c}^2} - \frac{\tilde{\varepsilon}}{\tilde{a}^2}\Big)\Big], \tag{4.56}$$
$$b^2 - 1 = \gamma \frac{\tilde{a}\tilde{b}^2\tilde{c}}{\tau}\Big[\frac{\tilde{P}_\perp}{\tilde{b}^2} - r\Big(\frac{2\tilde{P}_\perp}{\tilde{b}^2} + \frac{\tau^2 \tilde{P}_L}{\tilde{c}^2} - \frac{\tilde{\varepsilon}}{\tilde{a}^2}\Big)\Big], \tag{4.57}$$
$$c^2 - \tau^2 = \gamma \frac{\tilde{a}\tilde{b}^2\tilde{c}}{\tau}\Big[\frac{\tau^4 \tilde{P}_L}{\tilde{c}^2} - r\tau^2\Big(\frac{2\tilde{P}_\perp}{\tilde{b}^2} + \frac{\tau^2 \tilde{P}_L}{\tilde{c}^2} - \frac{\tilde{\varepsilon}}{\tilde{a}^2}\Big)\Big], \tag{4.58}$$
$$1 - \tilde{a}^2 = \gamma \frac{ab^2c}{\tau}\Big[\frac{\varepsilon}{a^2} + r\left(\frac{2P_\perp}{b^2} + \frac{\tau^2 P_L}{c^2} - \frac{\varepsilon}{a^2}\right)\Big], \tag{4.59}$$
$$\tilde{b}^2 - 1 = \gamma \frac{ab^2c}{\tau}\Big[\frac{P_\perp}{b^2} - r\Big(\frac{2P_\perp}{b^2} + \frac{\tau^2 P_L}{c^2} - \frac{\varepsilon}{a^2}\Big)\Big], \tag{4.60}$$
$$\tilde{c}^2 - \tau^2 = \gamma \frac{ab^2c}{\tau}\Big[\frac{\tau^4 P_L}{c^2} - r\tau^2\Big(\frac{2P_\perp}{b^2} + \frac{\tau^2 P_L}{c^2} - \frac{\varepsilon}{a^2}\Big)\Big]. \tag{4.61}$$

From the discussion in the previous section, we can add (4.56) to (4.57) and (4.59) to (4.60), which cancels the terms proportional to r to leave us with

$$b^2 - a^2 = \gamma \frac{\tilde{a}\tilde{b}^2\tilde{c}}{\tau}\Big[\frac{\tilde{P}_\perp}{\tilde{b}^2} + \frac{\tilde{\varepsilon}}{\tilde{a}^2}\Big] > 0, \tag{4.62}$$
$$\tilde{b}^2 - \tilde{a}^2 = \gamma \frac{ab^2c}{\tau}\Big[\frac{P_\perp}{b^2} + \frac{\varepsilon}{a^2}\Big] > 0, \tag{4.63}$$
$$\frac{c^2}{\tau^2} - a^2 = \gamma \frac{\tilde{a}\tilde{b}^2\tilde{c}}{\tau}\Big[\frac{\tau^2\tilde{P}_L}{\tilde{c}^2} + \frac{\tilde{\varepsilon}}{\tilde{a}^2}\Big] > 0, \tag{4.64}$$
$$\frac{\tilde{c}^2}{\tau^2} - \tilde{a}^2 = \gamma \frac{ab^2c}{\tau}\Big[\frac{\tau^2 P_L}{c^2} + \frac{\varepsilon}{a^2}\Big] > 0. \tag{4.65}$$

This set of inequalities arises from considering that the effective light-cone velocity in the perpendicular direction, i.e. $1 > v_\perp = \frac{a}{b} > 0$, as well as the light-cone velocity in the longitudinal direction, i.e. $1 > v_L = \frac{a}{(c/\tau)} > 0$, needs to remain within the Minkowski light cone. We can conclude that we need to choose $\gamma > 0$, as in the previous case. Notice that we can permit negative pressures, so long as $v^2_{\perp,L}P_{\perp,L} > -\varepsilon$ and likewise for the other subsystem.

The total energy-momentum tensor, $T^{\mu\nu}$, is computed from (3.25) and we find

$$T^0{}_0 \equiv -\mathcal{E} = -\frac{ab^2c}{\tau}\varepsilon - \frac{\tilde{a}\tilde{b}^2\tilde{c}}{\tau}\tilde{\varepsilon} - \frac{ab^2c\tilde{a}\tilde{b}^2\tilde{c}}{\tau^2}\Delta K, \tag{4.66}$$
$$T^\perp{}_\perp \equiv \mathcal{P}_\perp = \frac{ab^2c}{\tau}P_\perp + \frac{\tilde{a}\tilde{b}^2\tilde{c}}{\tau}\tilde{P}_\perp - \frac{ab^2c\tilde{a}\tilde{b}^2\tilde{c}}{\tau^2}\Delta K, \tag{4.67}$$
$$T^L{}_L \equiv \mathcal{P}_L = \frac{ab^2c}{\tau}P_L + \frac{\tilde{a}\tilde{b}^2\tilde{c}}{\tau}\tilde{P}_L - \frac{ab^2c\tilde{a}\tilde{b}^2\tilde{c}}{\tau^2}\Delta K, \tag{4.68}$$
$$\Delta K = \frac{1}{2}\gamma\Big[\frac{\varepsilon\tilde{\varepsilon}}{a^2\tilde{a}^2} + \frac{2P_\perp\tilde{P}_\perp}{b^2\tilde{b}^2} + \frac{\tau^4\tilde{P}_LP_L}{c^2\tilde{c}^2}\Big] \tag{4.69}$$
$$+\gamma r\Big[\frac{\varepsilon\tilde{\varepsilon}}{2a^2\tilde{a}^2} - \frac{P_\perp\tilde{\varepsilon}}{\tilde{a}^2b^2} - \frac{\tilde{P}_\perp\varepsilon}{a^2\tilde{b}^2} + \frac{2P_\perp\tilde{P}_\perp}{b^2\tilde{b}^2} + \tau^2\Big(\frac{P_\perp\tilde{P}_L}{b^2\tilde{c}^2} + \frac{\tilde{P}_\perp P_L}{\tilde{b}^2c^2} - \frac{\tilde{P}_L\varepsilon}{2a^2\tilde{c}^2} - \frac{P_L\tilde{\varepsilon}}{2\tilde{a}^2c^2}\Big) + \frac{\tau^4\tilde{P}_LP_L}{2c^2\tilde{c}^2}\Big].$$

The energy-momentum tensor is conserved in the Bjorken expanding background, $\nabla^{(\mathrm{B})}_\mu T^\mu{}_\nu = 0$. Note that if we compute the total (partial) enthalpy, we find that it is simply the sum of the subsystem partial enthalpies:

$$\mathcal{E} + \mathcal{P}_\perp = \sqrt{-g}(\varepsilon + P_\perp) + \sqrt{-\tilde{g}}(\tilde{\varepsilon} + \tilde{P}_\perp), \tag{4.70}$$
$$\mathcal{E} + \mathcal{P}_L = \sqrt{-g}(\varepsilon + P_L) + \sqrt{-\tilde{g}}(\tilde{\varepsilon} + \tilde{P}_L), \tag{4.71}$$

We can now proceed to simplify the coupling equations by using the light-cone velocities, $v_L, v_\perp, \tilde{v}$ and $\tilde{v}_L$, to replace $b, \tilde{b}, c$ and $\tilde{c}$. Eliminating a and $\tilde{a}$ and using the conformal equations of state, we are left with

$$\sqrt{-g}P_\perp = \frac{v_\perp^2 v_L^2}{\gamma N^2}\Big(\tilde{v}_\perp^2 + (\tilde{v}_\perp^2+2)\tilde{v}_L^2\Big)\Big(\tilde{v}_L^2 - \tilde{v}_\perp^2 + (1-\tilde{v}_\perp^2)\tilde{v}_L^2 v_L^2\Big), \tag{4.72}$$

$$\sqrt{-\tilde{g}}\tilde{P}_\perp = \frac{\tilde{v}_\perp^2 \tilde{v}_L^2}{\gamma N^2}\Big(v_\perp^2 + (v_\perp^2+2)v_L^2\Big)\Big(v_L^2 - v_\perp^2 + (1-v_\perp^2)\tilde{v}_L^2 v_L^2\Big), \tag{4.73}$$

$$\sqrt{-g}P_L = \frac{v_\perp^2 v_L^2}{\gamma N^2}\Big(\tilde{v}_\perp^2 + (\tilde{v}_\perp^2+2)\tilde{v}_L^2\Big)\Big(2\tilde{v}_\perp^2 - 2\tilde{v}_L^2 + (1-\tilde{v}_L^2)\tilde{v}_\perp^2 v_\perp^2\Big), \tag{4.74}$$

$$\sqrt{-\tilde{g}}\tilde{P}_L = \frac{\tilde{v}_\perp^2 \tilde{v}_L^2}{\gamma N^2}\Big(v_\perp^2 + (v_\perp^2+2)v_L^2\Big)\Big(2v_\perp^2 - 2v_L^2 + v_\perp^2\tilde{v}_\perp^2(1-v_L^2)\Big), \tag{4.75}$$

$$\begin{aligned} N \equiv\, & v_\perp^2(\tilde{v}_\perp^2(r(\tilde{v}_L^2(3v_L^2-1) - v_L^2+3) - \tilde{v}_L^2 v_L^2 - 1) - 2r\tilde{v}_L^2(v_L^2+1)) \\ & - 2v_L^2(r\tilde{v}_\perp^2(\tilde{v}_L^2+1) - 2r\tilde{v}_L^2 + \tilde{v}_L^2). \end{aligned} \tag{4.76}$$

If we have solutions for arbitrary large pressures, we need the denominator of the RHS to vanish. This provides a condition for the asymptotic values of velocities, which reads

$$N = 0 \Rightarrow r = \frac{v_\perp^2\tilde{v}_\perp^2(1+\tilde{v}_L^2 v_L^2) + 2\tilde{v}_L^2 v_L^2}{v_\perp^2\Big(\tilde{v}_\perp^2(\tilde{v}_L^2(3v_L^2-1) - v_L^2+3) - 2\tilde{v}_L^2(v_L^2+1)\Big) - 2v_L^2\Big(\tilde{v}_\perp^2(\tilde{v}_L^2+1) - 2\tilde{v}_L^2\Big)}. \tag{4.77}$$

Note that if we take the isotropic limit, $v_L \to v_\perp$ and similarly for the other sector, we recover (4.33).

A notable difference to the previous discussion is that now the effective metrics have a non-trivial Ricci scalar, which is given by

$$\begin{aligned} R = \frac{1}{a^2}\Big(& 2\left[\partial_\tau \log(b)\right]^2 - 4\partial_\tau \log(a)\partial_\tau \log(b) - 2\partial_\tau \log(a)\partial_\tau \log(c) \\ & + 4\partial_\tau \log(b)\partial_\tau \log(c) + \frac{4b''}{b} + \frac{2c''}{c}\Big), \end{aligned} \tag{4.78}$$

(and similarly for the other sector). Clearly, when we are in the Bjorken background with $a = b = 1$ and $c = \tau$, the Ricci scalar vanishes and we are again in flat space, $R = 0$. When we turn on the metric coupling, we see that the Ricci scalar is non-vanishing. This is demonstrated numerically in the left plot of Fig. 4.10.

4.2.1 A few interesting cases

In the following, we will consider a variety of numerical solutions. We will take the view that the tilded sector will be always represented by an isotropic conformal fluid $\tilde{P}_\perp = \tilde{P}_L = \tilde{P}$ and $\tilde{\varepsilon} = 3\tilde{P}$, whereas the untilded sector will also be conformal with $\varepsilon = 2P_\perp + P_L$ and the different relationship between the pressures will be the distinguishing feature of the numerical explorations. The interpretation of this setup is that the tilded subsystem represents the soft degrees of freedom, a conformal fluid, whereas the untilded subsystem represents the hard sector.

It is also important to remember that at this level of discussion, the individual subsystems do not have a mechanism with which to evolve their pressures. Thus, when we set the relationship between the untilded subsystem's longitudinal and transverse pressure, this is kept fixed. We are then watching the evolution of the full system's energy density and pressure.

To somewhat standardize the discussion, we will set $\gamma = 1$ and $r = 2$. Furthermore, we begin the simulation at $\tau_0 = 0.3$ and set our initial conditions as $\varepsilon(\tau_0) = 0.25$ and $\tilde{\varepsilon}(\tau_0) = 0.1$.

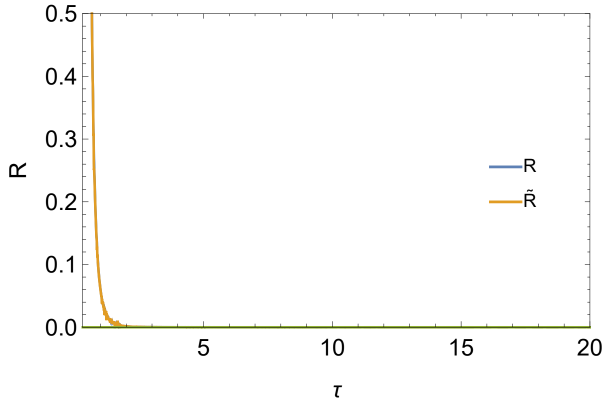

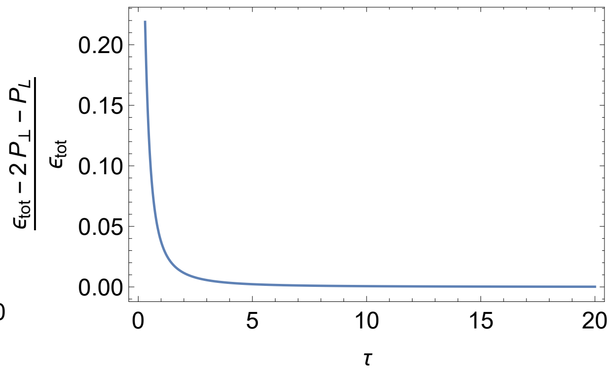

Figure 4.10: Left: Ricci scalar for the Bjorken flow, with choice of parameters as in the text and $P_L = \varepsilon$, $P_\perp = 0$. Right: Trace of the full system for the same parameters. The figures would look qualitatitively similar with the other parameters, so we have not included it here.

An interesting observation is that the anisotropic sector induces an anisotropic light cone (i.e. $v_\perp \neq v_L$) in the other subsystem, while the isotropic sector tends to induce an isotropic light cone.

We also note that the trace of the total system acts in a similar way for the cases that we consider, namely the trace vanishes for late times as can be seen in Fig. 4.10.

Isotropic inviscid fluids

Here we consider the case of two coupled conformal isotropic inviscid fluids. In this case, the perpendicular and the longitudinal light cones coincide for both fluids $v_L = v_\perp$, which are plotted in Fig. 4.11. We also see that the energy of both subsystems drops with time, as we would expect in a Bjorken expanding system. Furthermore, the anisotropy parameter, $\mathcal{P}_L/\mathcal{P}_\perp$, is exactly 1, i.e. the total pressures are isotropic. We can see in Fig. 4.12 for late times that the total energy density tends to the isotropic value, as does the total pressure.

Transverse particle (TP) distribution

We set $P_L = 0$, which implies $\varepsilon = 2P_\perp$. This corresponds to free particles with only transverse momentum. In Fig. 4.13, we plot the light-cone velocities for both subsystems. The generic behavior of the light-cone velocities is to asymptote to 1. This is not surprising, as we expect for large τ for the system to fly apart and for interactions to decrease. When we plot the ratio of the light-cone velocities, it becomes clear that the light cones in the isotropic system are deformed by the anisotropic system and become anisotropic. In the bottom right plot, we also plot the ratio of the energy densities, which falls off in the same way as the previous case.

In Fig. 4.14, we plot the ratio of the longitudinal pressure to the transverse pressure of the full system, which is known as the anisotropy parameter. It is curious to note that this parameter increases at early times, indicating that the system is tending to isotropize, before falling away.

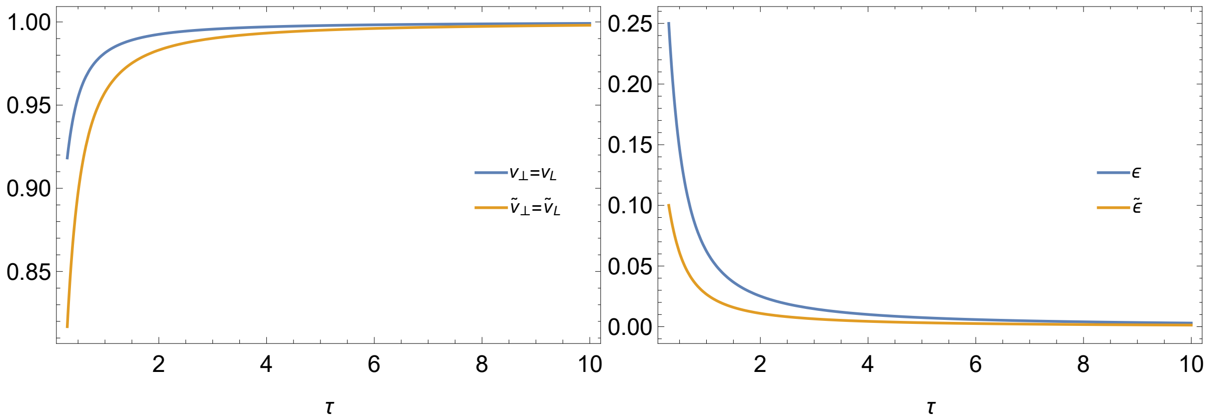

Figure 4.11: Light-cone velocities and energy densities in the case of two isotropic fluids. Left: light-cone velocities are degenerate in each subsystem. Right: energy densities in each subsystem.

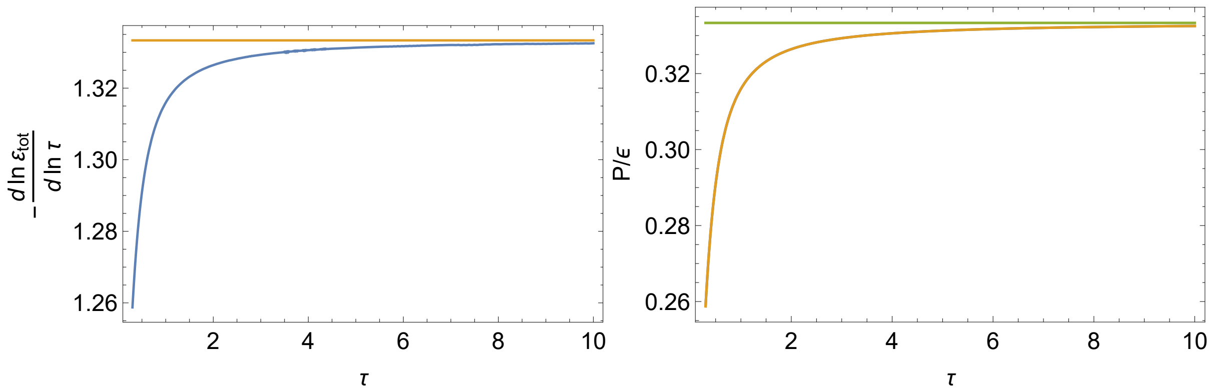

Figure 4.12: Anisotropy in the isotropic fluid case. For late times the full system seems to isotropize. Left: The anisotropy parameter for the total pressures. The orange line represents full isotropy, $\mathcal{P}_L/\mathcal{P}_\perp = 1$. Right: The power law fall-off of the total energy density. The fully isotropic value is in orange, $\mathcal{E} \sim \tau^{-4/3}$. Bottom: The total pressures, $\mathcal{P}_\perp$ and $\mathcal{P}_L$. The green line is the isotropic value 1/3.

Longitudinal particle (LP) distribution

Here, we set $P_L = \varepsilon$, $P_\perp = 0$. The anisotropy of this choice is apparent in Fig. 4.15. The light cones develop anisotropically, but tellingly, the light cone of the anisotropic subsystem (induced by the isotropic fluid subsystem), is approximately isotropic, whereas the isotropic fluid feels an anisotropic light cone. This is summarized in the bottom left plot. As before, the energy densities drop with increasing time.

In Fig. 4.16, the anisotropy parameter approaches the isotropic value from a maximal anisotropic value. In the bottom plot, the two pressures approach the conformal value from two different directions, while the total energy density approaches the isotropic fall-off (4.48).

Dark energy-like configuration

We now set $P_L = -\varepsilon = -P_\perp$, which is dark energy-like w.r.t. the longitudinal direction. In Fig. 4.17, we see that the behavior of the untilded subsystem's light cone is similar to the

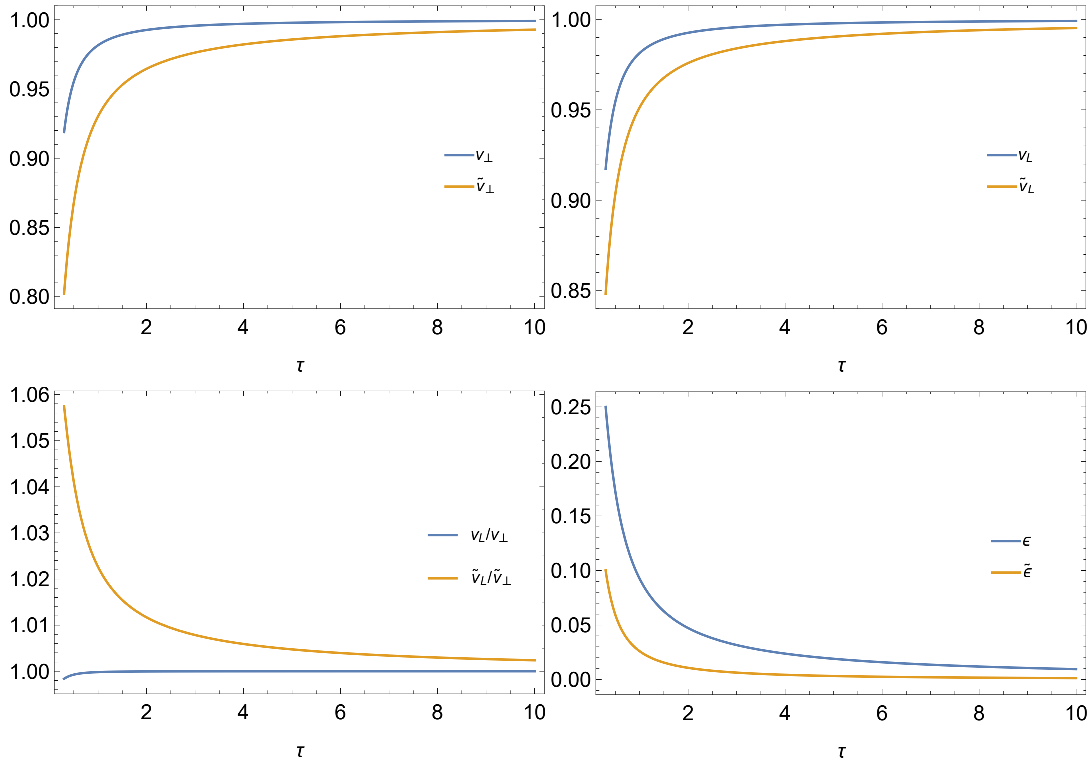

Figure 4.13: Light-cone velocities and energy densities for TP. Top left: light-cone velocity in the perpendicular directions. Top right: light-cone velocities in the longitudinal direction. Bottom left: ratio of the longitudinal light-cone velocities to the perpendicular light-cone velocities. Note that the system with the isotropic equation of state has the more anisotropic behavior of light cones. Bottom right: energy densities of the two subsystems.

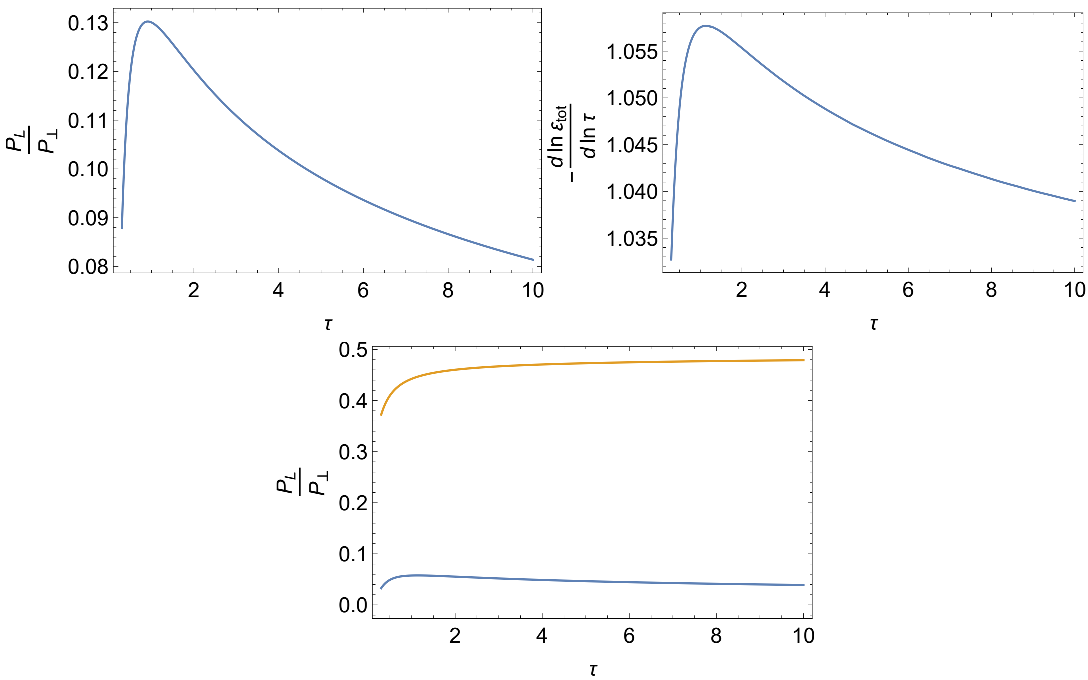

Figure 4.14: Characterizing TP anisotropy. Left: The anisotropy parameter for the total pressures. Right: The power law fall-off of the total energy density. Bottom: The total pressures, $\mathcal{P}_\perp$ and $\mathcal{P}_L$.

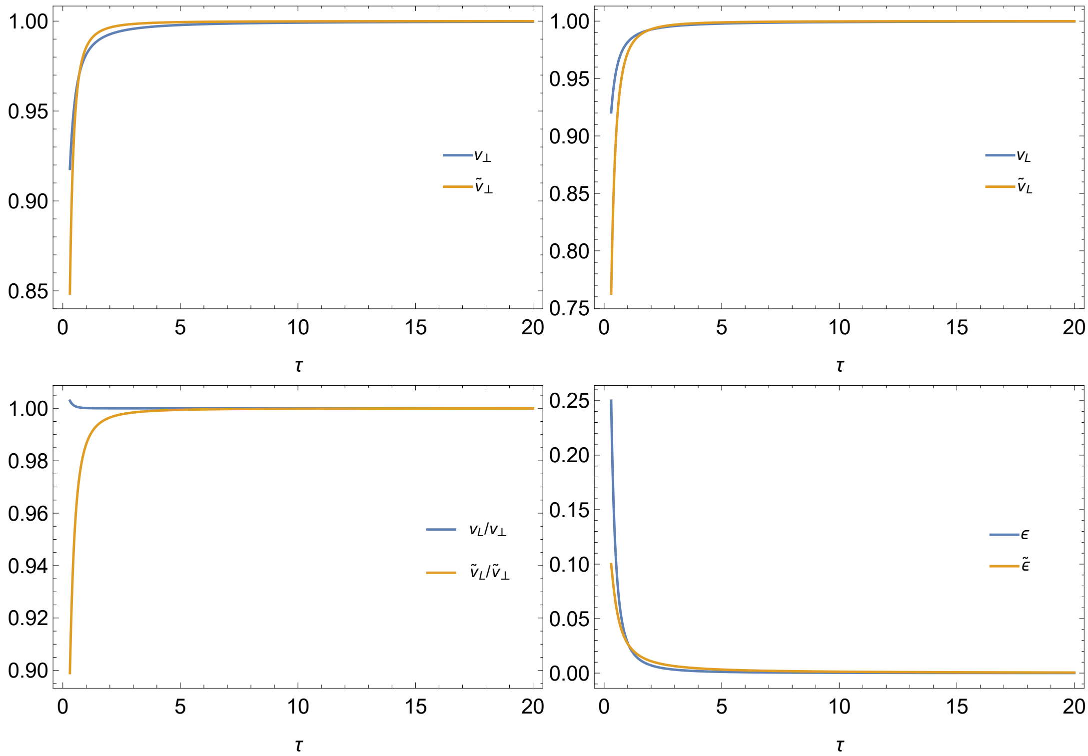

Figure 4.15: Light-cone velocities and energy densities in the LP case. Top left: light-cone velocity in the perpendicular directions. Top right: light-cone velocities in the longitudinal direction. Bottom left: ratio of the longitudinal light-cone velocities to the perpendicular light-cone velocities. Bottom right: energy densities of the two subsystems.

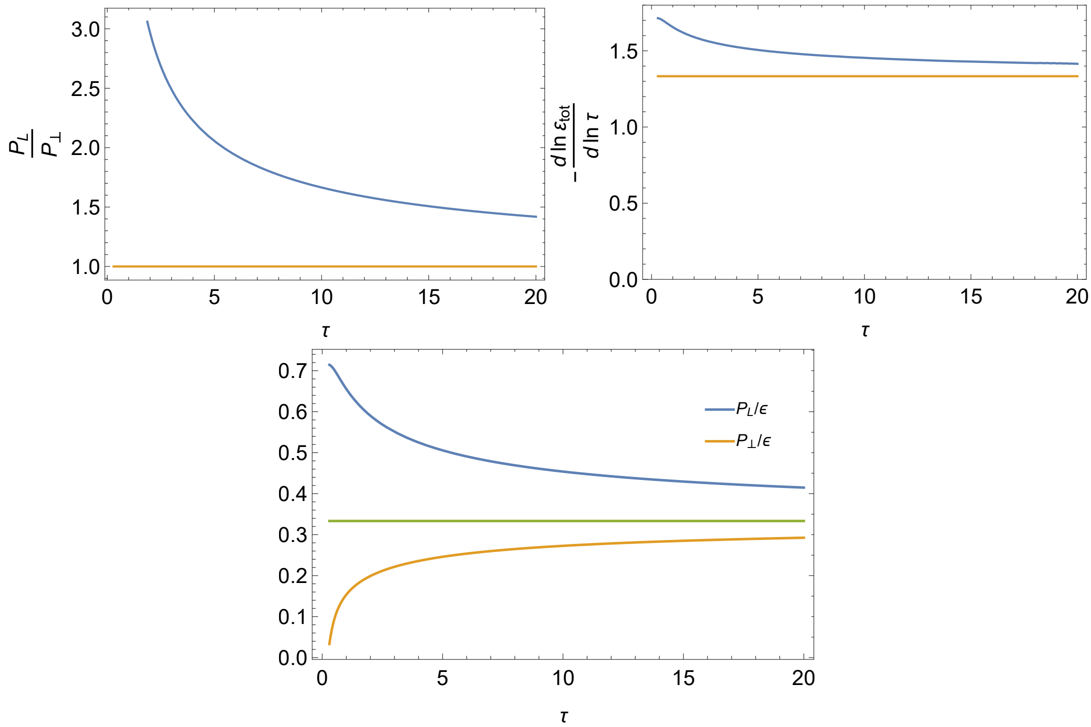

Figure 4.16: LP anisotropy. Left: The anisotropy parameter for the total pressures. The orange line represents full isotropy, $\mathcal{P}_L/\mathcal{P}_\perp = 1$. Right: The power law fall-off of the total energy density. The fully isotropic value is in orange, $\mathcal{E} \sim \tau^{-4/3}$. Bottom: The total pressures, $\mathcal{P}_\perp$ and $\mathcal{P}_L$. The green line is the isotropic value $1/3$.

previous case. Interestingly, the transverse light-cone velocity of the fluid subsystem freezes to a smaller value than the speed of light. Furthermore, the behavior of the energy density is distinct from the previous discussion: the fluid energy density decreases as before, but the hard subsystem has its energy density *increase* to some finite value. Since the isotropic fluid is drained, it is logical to conclude that the anisotropy of the system increases.

In Fig. 4.18, we see more evidence that the full system becomes more anisotropic. The longitudinal pressure becomes more negative, while the transverse pressure becomes as positive. Finally, from the plot on the top right, we see that the total system energy density at late times behaves like

$$\mathcal{E} \sim \tau^0, \tag{4.79}$$

as opposed to the usual fall-off behavior of the energy density in a Bjorken background, (4.48) and (4.49). Essentially, the negative longitudinal pressure is compensating the effects of the expansion, such that the energy density of the system remains constant.

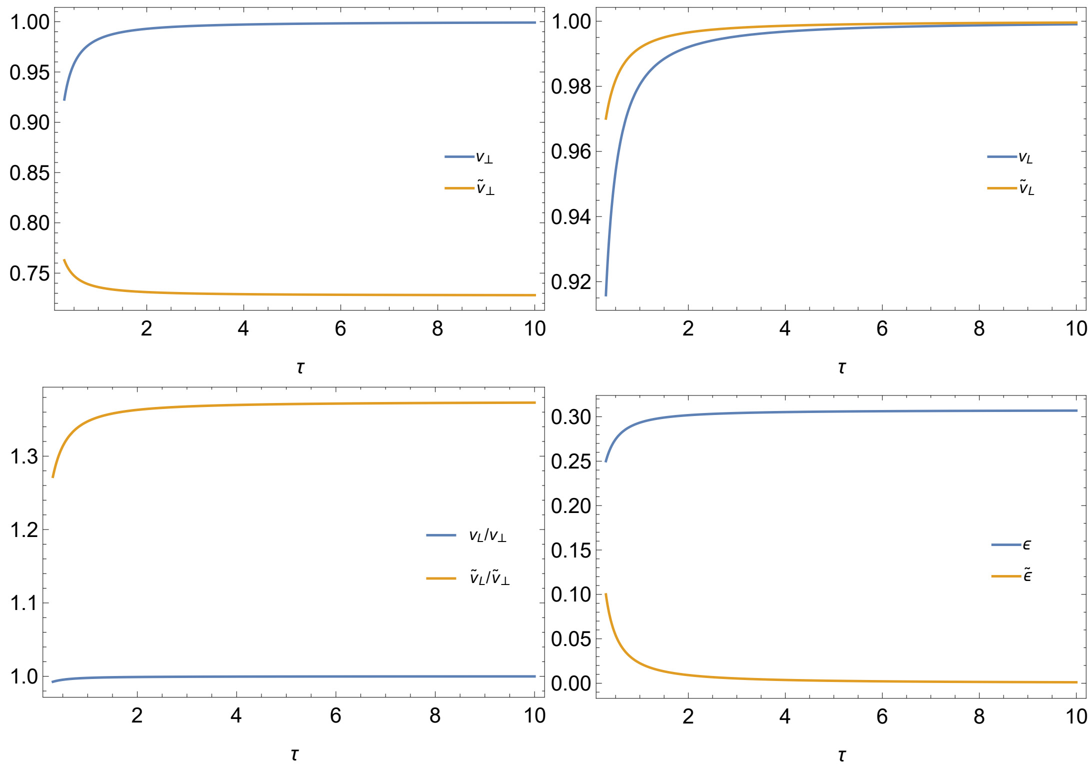

Figure 4.17: Light-cone velocities and energy densities in the dark energy-like case. Top left: light-cone velocities in the perpendicular direction. Top right: light-cone velocities in the longitudinal direction. Bottom left: ratio of the longitudinal light-cone velocities to the perpendicular light-cone velocities. Bottom right: energy densities of the two subsystems.

4.3 Bi-hydrodynamics

In the following we investigate the linearized perturbations of the full hybrid system about thermal equilibrium. We consider two subsystems, whose energy-momentum tensors are param-

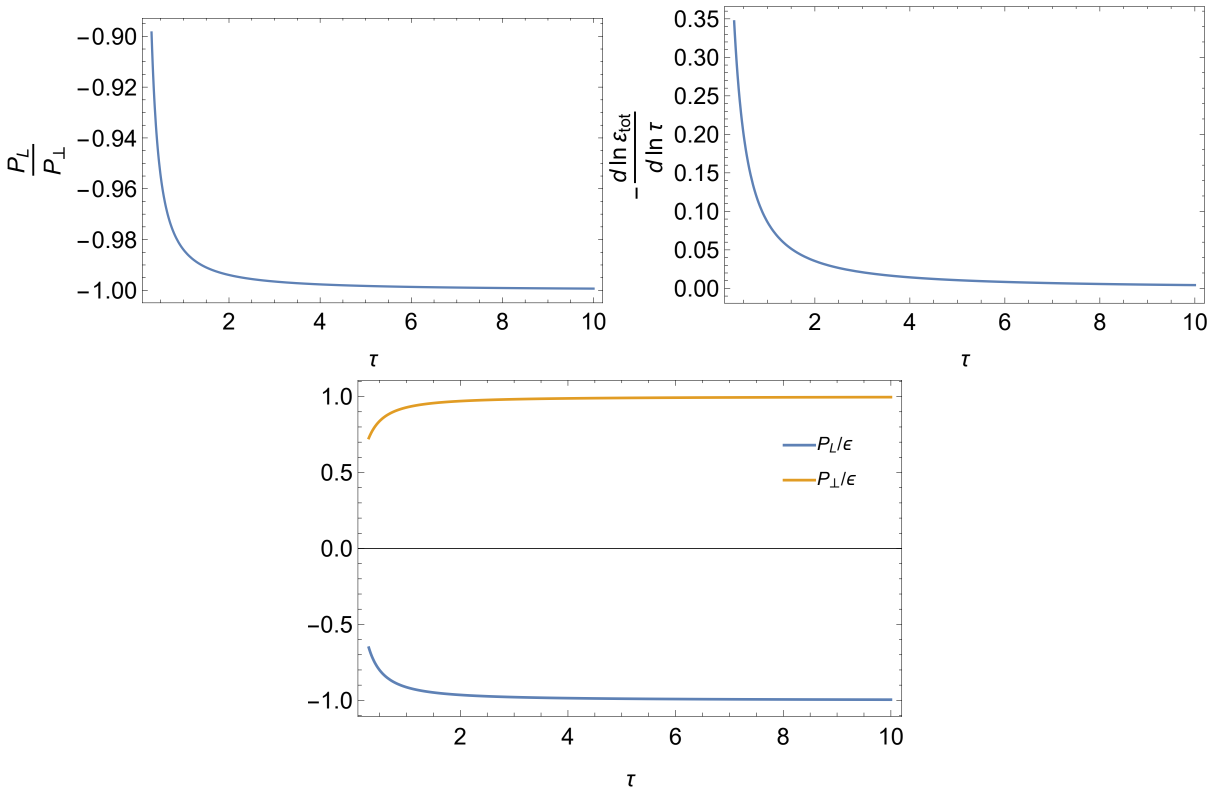

Figure 4.18: Anisotropy in the dark energy-like case. Left: The anisotropy parameter for the total pressures. Right: The power law fall-off of the total energy density. Bottom: The total pressures, $\mathcal{P}_\perp$ and $\mathcal{P}_L$.

eterized up to first order in the gradient expansion according to (2.24), which is given explicitly as

$$
\begin{aligned}
t^{\mu\nu} &= (\epsilon_1 + P_1)u^\mu u^\nu + P_1 g^{\mu\nu} - 2\eta_1\sigma^{\mu\nu}, \\
\tilde{t}^{\mu\nu} &= (\epsilon_2 + P_2)\tilde{u}^\mu\tilde{u}^\nu + P_2\tilde{g}^{\mu\nu} - 2\eta_2\tilde{\sigma}^{\mu\nu}.
\end{aligned} \tag{4.80}
$$

For simplicity we will continue to analyze the case of conformal subsystems, and therefore we will set the bulk viscosities in each subsystem, $\zeta_1 = \zeta_2 = 0$, with equations of state given by (4.25).

Since the thermal equilibrium is homogeneous and rotationally symmetric, we can classify the perturbations into three distinct sectors, which are called the shear, sound and tensor channels. Each channel has distinct low energy characteristics. If we take the hydrodynamic limit in both sectors, only the shear and sound channels yield dynamic propagating modes with distinct forms of dispersion relations. The tensor channel in the bi-hydrodynamic limit does not have a pole, but is useful for computing the shear viscosity of the full hybrid system using the Kubo formula.

4.3.1 Bi-hydrodynamic shear mode

In the shear sector, the velocity fields of both sectors point in the same direction, but are orthogonal to the momentum of a perturbation, i.e. the direction of its propagation. Without loss of generality, we will assume that the momentum $\mathbf{k}$ is in the z-direction and the velocity fields are in the x-direction. We can thus consistently assume that the effective metrics are parametrized via

$$g_{\mu\nu} = \mathrm{diag}(-a^2, b^2, b^2, b^2) + \delta g_{\mu\nu}, \quad \tilde{g}_{\mu\nu} = \mathrm{diag}(-\tilde{a}^2, \tilde{b}^2, \tilde{b}^2, \tilde{b}^2) + \delta\tilde{g}_{\mu\nu} \tag{4.81}$$

with the non-vanishing components of $\delta g_{\mu\nu}$ and $\delta\tilde{g}_{\mu\nu}$

$$\begin{aligned} \delta g_{01} &= \beta e^{i(kz-\omega t)}, \quad \delta g_{13} = \gamma_{13} e^{i(kz-\omega t)}, \\ \delta\tilde{g}_{01} &= \tilde{\beta} e^{i(kz-\omega t)}, \quad \delta\tilde{g}_{13} = \tilde{\gamma}_{13} e^{i(kz-\omega t)}. \end{aligned} \tag{4.82}$$

The perturbed velocity fields in both sectors including the infinitesimal linearized perturbations assume the form:

$$u^\mu = \left(\frac{1}{a}, \nu e^{i(kz-\omega t)}, 0, 0\right), \quad \tilde{u}^\mu = \left(\frac{1}{\tilde{a}}, \tilde{\nu} e^{i(kz-\omega t)}, 0, 0\right). \tag{4.83}$$

Note that the metric perturbations (4.82) preserve the norm of the velocity fields (4.83) at the linearized level. Furthermore, in the shear channel, there is no temperature perturbation, as this would enter at higher order.

Thus the perturbed hydrodynamic energy-momentum tensors of the individual sectors is given by

$$\begin{aligned} t^{\mu\nu} &= \mathrm{diag}\left(\frac{\epsilon_1(T_1)}{a^2}, \frac{P_1(T_1)}{b^2}, \frac{P_1(T_1)}{b^2}, \frac{P_1(T_1)}{b^2}\right) + \delta t^{\mu\nu}, \\ \tilde{t}^{\mu\nu} &= \mathrm{diag}\left(\frac{\epsilon_2(T_2)}{\tilde{a}^2}, \frac{P_2(T_2)}{\tilde{b}^2}, \frac{P_2(T_2)}{\tilde{b}^2}, \frac{P_2(T_2)}{\tilde{b}^2}\right) + \delta\tilde{t}^{\mu\nu}, \end{aligned} \tag{4.84}$$

with the non-zero components of $\delta t^{\mu\nu}$ and $\delta\tilde{t}^{\mu\nu}$ being

$$\begin{aligned} \delta t^{01} &= -\frac{P_1\beta + (P_1+\epsilon_1)\nu a b^2}{a^2 b^2} e^{i(kz-\omega t)}, \quad \delta t^{13} = \left(-\frac{P_1\gamma_{13}}{b^4} - ik\frac{\eta_1\nu}{b^2} + i\omega\frac{\eta_1\gamma_{13}}{ab^4}\right) e^{i(kz-\omega t)}, \\ \delta\tilde{t}^{01} &= -\frac{P_2\tilde{\beta} + (P_2+\epsilon_2)\tilde{\nu}\tilde{a}\tilde{b}^2}{\tilde{a}^2\tilde{b}^2} e^{i(kz-\omega t)}, \quad \delta\tilde{t}^{13} = \left(-\frac{P_2\tilde{\gamma}_{13}}{\tilde{b}^4} - ik\frac{\eta_2\tilde{\nu}}{\tilde{b}^2} + i\omega\frac{\eta_2\tilde{\gamma}_{13}}{\tilde{a}\tilde{b}^4}\right) e^{i(kz-\omega t)}. \end{aligned} \tag{4.85}$$

The hydrodynamic equations of the two sectors in the two effective metrics are

$$\nabla_\mu t^{\mu\nu} = 0, \qquad \nabla_\mu \tilde{t}^{\mu\nu} = 0, \tag{4.86}$$

which read explicitly in Fourier space as

$$\begin{aligned} \omega\frac{(\epsilon_1+P_1)(\beta+\nu a b^2)}{a^2b^2} &= -ik^2\frac{\eta_1\nu}{b^2} + i\omega k\frac{\eta_1\gamma_{13}}{ab^4}, \\ \omega\frac{(\epsilon_2+P_2)(\tilde{\beta}+\tilde{\nu}\tilde{a}\tilde{b}^2)}{\tilde{a}^2\tilde{b}^2} &= -ik^2\frac{\eta_2\tilde{\nu}}{\tilde{b}^2} + i\omega k\frac{\eta_2\tilde{\gamma}_{13}}{\tilde{a}\tilde{b}^4}. \end{aligned} \tag{4.87}$$

As discussed previously, the hydrodynamic equations automatically guarantee the conservation of the full energy-momentum tensor at the linearized level.

We will also introduce the dimensionless parameters κ_1, κ_2, which parameterize the shear

$$\eta_1 = \frac{\kappa_1}{\pi} n_1 T_1^3, \quad \eta_2 = \frac{\kappa_2}{\pi} n_2 T_2^3 \tag{4.88}$$

so that

$$\frac{4\pi\eta_1}{s_1} = \kappa_1, \quad \frac{4\pi\eta_2}{s_2} = \kappa_2. \tag{4.89}$$

With a Minkowski background metric, the linearized coupling equations determining β, $\tilde{\beta}$, γ_{13} and $\tilde{\gamma}_{13}$ are simply

$$\begin{aligned} \delta g_{01} &= -\gamma\delta\tilde{t}^{01}\tilde{a}\tilde{b}^3, \quad \delta g_{13} = \gamma\delta\tilde{t}^{13}\tilde{a}\tilde{b}^3, \\ \delta\tilde{g}_{01} &= -\gamma\delta t^{01}ab^3, \quad \delta\tilde{g}_{13} = \gamma\delta t^{13}ab^3. \end{aligned} \tag{4.90}$$

With (4.82) and (4.85) the solutions are:

$$\begin{aligned} \beta &= \frac{4\gamma n_2 T_2^4 a\tilde{b}\left(\tilde{a}\tilde{b}^2\tilde{\nu} - \gamma n_1 T_1^4 b^3\nu\right)}{-a\tilde{a} + \gamma^2 n_1 n_2 b\tilde{b} T_1^4 T_2^4}, \\ \gamma_{13} &= \frac{i\gamma k n_2 T_2^3 b\left(\pi\kappa_2\tilde{\nu}\tilde{a}\tilde{b}^2 - \gamma\kappa_1 n_1 T_1^3\nu ab(\pi T_2\tilde{a} - i\kappa_2\omega)\right)}{\pi^2\left(\gamma^2 n_1 n_2 T_1^4 T_2^4 a\tilde{a} - b\tilde{b}\right) + \gamma^2 n_1 n_2 T_1^3 T_2^3(\kappa_1\kappa_2\omega^2 - i\pi\omega(\kappa_2 T_1 a + \kappa_1 T_2\tilde{a}))}, \end{aligned} \tag{4.91}$$

and similarly for $\tilde{\beta}$ and $\tilde{\gamma}_{13}$.

Inserting these into the linearized hydrodynamic equations (4.87) yields equations for ν and $\tilde{\nu}$ of the form

$$Q_{AB}(\omega, k)\nu_B = 0, \tag{4.92}$$

where $\nu_A = (\nu, \tilde{\nu})$ and Q_{AB} is a 2×2 matrix. The eigenmodes have dispersion relations $\omega(k)$ for which the determinant of Q vanishes, i.e.

$$\det Q(\omega(k), k) = 0. \tag{4.93}$$

The corresponding eigenvectors involve a momentum dependent combination of ν and $\tilde{\nu}$. These modes are intrinsic to the full system, independent of external perturbations.

The shear-diffusion modes are modes with a dispersion relation of the characteristic form:

$$\omega_I = -iD_I k^2 + \mathcal{O}(k^3), \tag{4.94}$$

where the index I labels different solutions. Note that $D_I = D_I(\mathcal{T}, \gamma, \gamma')$ in general.

We find that the perturbative expansions of the shear diffusion constants D_I are given by:

$$\begin{aligned} D_a(\mathcal{T}) &= \frac{\kappa_1}{4\pi\mathcal{T}} - \frac{\gamma\kappa_1 n_2\mathcal{T}^3}{\pi} + \frac{\gamma^2\kappa_1 n_2\mathcal{T}^7[n_2(\kappa_1-\kappa_2) + n_1(9\kappa_2 - 5\kappa_1)]}{\pi(\kappa_1-\kappa_2)} + \mathcal{O}(\gamma^3), \\ D_b(\mathcal{T}) &= \frac{\kappa_2}{4\pi\mathcal{T}} - \frac{\gamma\kappa_2 n_1\mathcal{T}^3}{\pi} + \frac{\gamma^2\kappa_2 n_1\mathcal{T}^7[n_1(\kappa_1-\kappa_2) - n_2(9\kappa_1 - 5\kappa_2)]}{\pi(\kappa_1-\kappa_2)} + \mathcal{O}(\gamma^3). \end{aligned} \tag{4.95}$$

In the decoupling limit, $\gamma^{1/4}\mathcal{T} \to 0$ (with fixed r), we recover the usual shear diffusion modes of the individual subsystems.

The propagating mode corresponding to the first diffusion constant D_1 involves velocity amplitudes with[1]

$$\tilde{\nu} = \left(\frac{4n_1\kappa_1}{(\kappa_1-\kappa_2)}\gamma\mathcal{T}^4 + \mathcal{O}(\gamma^2\mathcal{T}^8)\right)\nu \tag{4.96}$$

[1]Note that the combination of ν and $\tilde{\nu}$ in the propagating mode is $k-$independent. This is so because each element in the matrix Q in (4.92) is $\mathcal{O}(k^2)$ at the leading order on-shell, i.e. when $\omega = -iD_{a,b}k^2 + \cdots$.

and therefore it is indeed localized mostly in the first subsystem when $\gamma\mathcal{T}^4$ is small. Similarly, the other propagating mode has

$$\nu = -\left(\frac{4n_2\kappa_2}{(\kappa_1-\kappa_2)}\gamma\mathcal{T}^4 + \mathcal{O}(\gamma^2\mathcal{T}^8)\right)\tilde{\nu} \tag{4.97}$$

and thus is localized mostly in the second subsystem for small $\gamma\mathcal{T}^4$. For finite $\gamma\mathcal{T}^4$, both these modes receive significant contributions from both subsystems (see Fig. 4.19).

The dependence on γ' of the perturbative expansions (4.95) start only at third order in the perturbative expansion – so this dependence is weak at small $\gamma\mathcal{T}^4$. We also note that the perturbation expansion in $\gamma\mathcal{T}^4$ evidently breaks down when $|\kappa_1-\kappa_2| \lesssim \gamma\mathcal{T}^4$, irrespective of the values of n_1 and n_2.

In the coincidence limit of $\kappa_1 = \kappa_2 = \kappa$, we instead obtain the following perturbative series

$$\begin{aligned} D_a(\mathcal{T}) &= \frac{\kappa}{4\pi\mathcal{T}}, \\ D_b(\mathcal{T}) &= \frac{\kappa}{4\pi\mathcal{T}} - \frac{\gamma\mathcal{T}^3\kappa(n_1+n_2)}{\pi} + \frac{\gamma^2\mathcal{T}^7\kappa\left(n_1^2-10n_1n_2+n_2^2\right)}{\pi} + \mathcal{O}(\gamma^3\mathcal{T}^{11}), \end{aligned} \tag{4.98}$$

where one of the diffusion modes turns out to be independent of $\gamma\mathcal{T}^4$. The propagating mode corresponding to this $\gamma\mathcal{T}^4$-independent diffusion constant has

$$\tilde{\nu} = \left(1 + \frac{3}{2}(n_1-n_2)\gamma\mathcal{T}^4 + \mathcal{O}(\gamma^2,\gamma'^2)\right)\nu. \tag{4.99}$$

When $n_1 = n_2$, i.e. when the two subsystems are identical, then the propagating mode is exactly given by $\tilde{\nu} = \nu$ (parallel and equal motion within the subsystems). In any case, this mode gets significant contributions from both subsystems *even in the decoupling limit* $\gamma, \gamma' \to 0$. The other propagating mode corresponding to the second diffusion constant D_b in (4.98) is the following combination of ν and $\tilde{\nu}$ where

$$\nu = -\frac{n_2}{n_1}\left(1 + \frac{9}{2}(n_1-n_2)\gamma\mathcal{T}^4 + \mathcal{O}(\gamma^2,\gamma'^2)\right)\tilde{\nu}. \tag{4.100}$$

When $n_1 = n_2$, this mode is exactly given by $\nu = -\tilde{\nu}$ (anti-parallel and equal motion within the subsystems). This mode evidently gets significant contributions from both subsystems even in the decoupling limit $\gamma^{1/4}\mathcal{T} \to 0$ (as long as $|\kappa_1-\kappa_2| \ll \gamma^{1/4}\mathcal{T}$). The nonperturbative dependence of $\tilde{\nu}/\nu$ on $\gamma^{1/4}\mathcal{T}$ is displayed in Fig. 4.19.

Kubo formula

We now turn our attention to defining the shear viscosity of the full system. We consider an extrinsic homogeneous time-dependent perturbation, such that the background metric is perturbed via

$$g_{\mu\nu} = \eta_{\mu\nu} + h_{\mu\nu}(t), \tag{4.101}$$

with only $h_{13}(t) \neq 0$. Now we are interested in only the external linear response, as in Sec. 2.2.3. First, we note that the velocity fields, ν and $\tilde{\nu}$, as well as the temperature perturbations in each sector, vanish at first order in the derivative expansion for homogeneous γ_{13} and $\tilde{\gamma}_{13}$, as can be

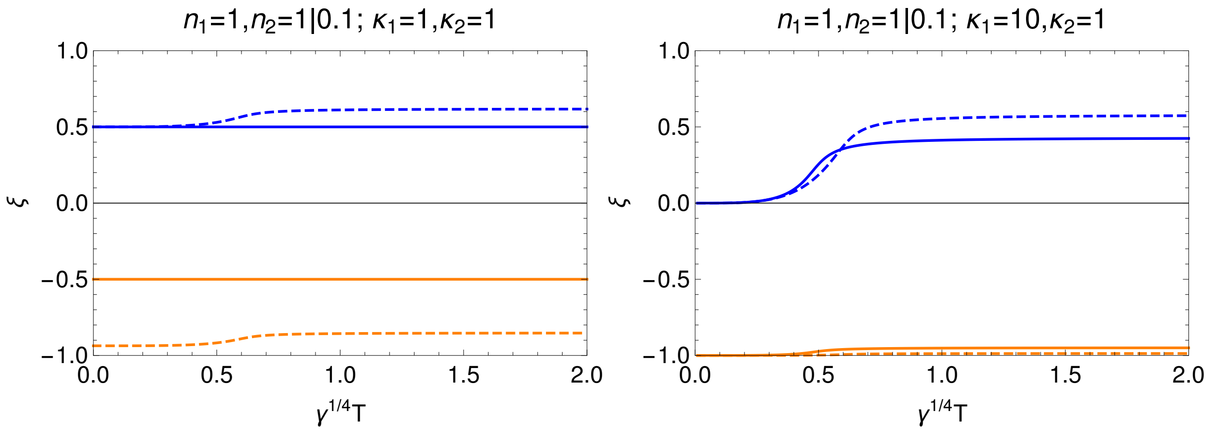

Figure 4.19: The relation between the velocity amplitudes ν and $\tilde{\nu}$ of the shear eigenmodes displayed in Fig. 4.20 in the form $\xi \equiv \frac{2}{\pi}\arctan(\tilde{\nu}/\nu)$. A value of $\xi = 0$ or $\xi = \pm 1$ (with these two latter values to be identified) means that the mode is carried only by subsystem 1 or 2, respectively; $\xi = 0.5$ or $\xi = -0.5$ corresponds to exactly equal amplitudes with equal or opposite phase.

deduced from e.g. (4.87). Thus, the linearized perturbations of the energy momentum tensors of the individual subsystems are

$$\begin{aligned} \delta t^{13} &= -\frac{P_1}{b^4}\gamma_{13} - \frac{\eta_1}{ab^4}\dot{\gamma}_{13} + \mathcal{O}(\partial_t^2), \\ \delta \tilde{t}^{13} &= -\frac{P_2}{\tilde{b}^4}\tilde{\gamma}_{13} - \frac{\eta_2}{\tilde{a}\tilde{b}^4}\dot{\tilde{\gamma}}_{13} + \mathcal{O}(\partial_t^2). \end{aligned} \tag{4.102}$$

The coupling equations (3.17) will only involve homogeneous perturbations of $\gamma_{13}(t)$ and $\tilde{\gamma}_{13}(t)$ and take the following form:

$$\begin{aligned} \gamma_{13} &= h_{13}\left(1 - 2\gamma P_2 \tilde{a}\tilde{b} + \gamma'\left(-\frac{\epsilon_2}{\tilde{a}^2} + 3\frac{P_2}{\tilde{b}^2}\right)\tilde{a}\tilde{b}^3\right) - \gamma P_2 \frac{\tilde{a}}{\tilde{b}}\tilde{\gamma}_{13} + \mathcal{O}(\partial_t), \\ \tilde{\gamma}_{13} &= h_{13}\left(1 - 2\gamma P_1 ab + \gamma'\left(-\frac{\epsilon_1}{a^2} + 3\frac{P_1}{b^2}\right)ab^3\right) - \gamma P_1 \frac{a}{b}\gamma_{13} + \mathcal{O}(\partial_t). \end{aligned} \tag{4.103}$$

Solving the above coupling equations, we obtain

$$\begin{aligned} \gamma_{13} &= \frac{\left(1 - 2\gamma P_2 \tilde{a}\tilde{b} + \gamma'\left(-\frac{\epsilon_2}{\tilde{a}^2} + 3\frac{P_2}{\tilde{b}^2}\right)\tilde{a}\tilde{b}^3\right) - \gamma P_2 \frac{\tilde{a}}{\tilde{b}}\left(1 - 2\gamma P_1 ab + \gamma'\left(-\frac{\epsilon_1}{a^2} + 3\frac{P_1}{b^2}\right)ab^3\right)}{1 - \gamma^2 P_1 P_2 \frac{a\tilde{a}}{b\tilde{b}}} h_{13} + \mathcal{O}(\partial_t), \\ \tilde{\gamma}_{13} &= \frac{\left(1 - 2\gamma P_1 ab + \gamma'\left(-\frac{\epsilon_1}{a^2} + 3\frac{P_1}{b^2}\right)ab^3\right) - \gamma P_1 \frac{a}{b}\left(1 - 2\gamma P_2 \tilde{a}\tilde{b} + \gamma'\left(-\frac{\epsilon_2}{\tilde{a}^2} + 3\frac{P_2}{\tilde{b}^2}\right)\tilde{a}\tilde{b}^3\right)}{1 - \gamma^2 P_1 P_2 \frac{a\tilde{a}}{b\tilde{b}}} h_{13} + \mathcal{O}(\partial_t). \end{aligned} \tag{4.104}$$

The energy-momentum tensor of the full system including the linearized perturbation is straightforward to compute from (3.25). We find that it assumes the standard hydrodynamic form with vanishing velocity and temperature perturbations. Note it is not a priori clear that even if the individual sector energy-momentum tensors are hydrodynamic, the full energy-momentum tensor also assumes a hydrodynamic form. This is particularly so because there are two independent entropy currents. Although in this specific example, the full energy-momentum tensor does indeed assume a hydrodynamic form, in the following subsection we

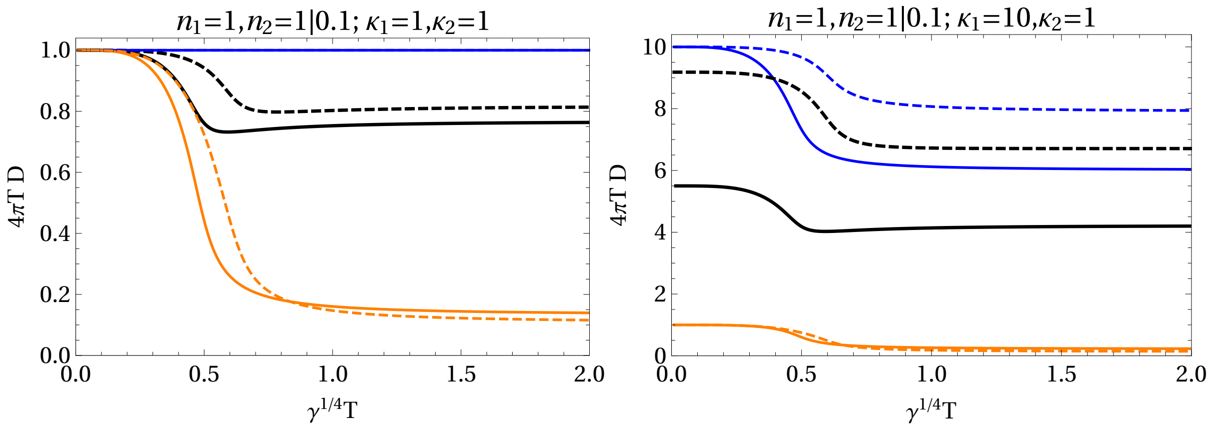

Figure 4.20: Shear diffusion constants $D_{a,b}$ (blue and orange lines) corresponding to shear eigenmodes in the hybrid fluid model for different parameters as a function of $\gamma^{1/4}\mathcal{T}$ compared to the overall (Kubo) shear diffusion constant $\mathcal{D}$ (red lines) corresponding to the total shear viscosity $\eta/\mathcal{S} \equiv T\mathcal{D}$. Full and dashed lines correspond to equal numbers of degrees of freedom, $n_1 = n_2 = 1$, and unequal ones, $n_1 = 1, n_2 = 1/10$, respectively. The left panel has equal values of individual shear viscosities $\kappa_i = 4\pi\eta_i/s_i = 1$, the right panel has $\kappa_1 = 10$ so that the first system corresponds to a more weakly coupled sector.

will find counterexamples. Explicitly,

$$\delta T^{13} = -\mathcal{P}h_{13} - \eta\dot{h}_{13} + \mathcal{O}(\partial_t^2) \tag{4.105}$$

where $\mathcal{P}$ is the equilibrium pressure of the full system given by (4.7). We can then read off the shear viscosity η of the full system:

$$\begin{aligned}\eta = \frac{1}{1-\gamma^2 P_1 P_2 \frac{a\tilde{a}}{b\tilde{b}}} \Bigg\{ &\eta_1 b\Bigg[\left(1 - 2\gamma P_2 \tilde{a}\tilde{b} + \gamma'\left(-\frac{\epsilon_2}{\tilde{a}^2} + 3\frac{P_2}{\tilde{b}^2}\right)\tilde{a}\tilde{b}^3\right) \\ &- \gamma P_2 \frac{\tilde{a}}{\tilde{b}}\left(1 - 2\gamma P_1 ab + \gamma'\left(-\frac{\epsilon_1}{a^2} + 3\frac{P_1}{b^2}\right)ab^3\right)\Bigg] \\ &+ \eta_2 \tilde{b}\Bigg[\left(1 - 2\gamma P_1 ab + \gamma'\left(-\frac{\epsilon_1}{a^2} + 3\frac{P_1}{b^2}\right)ab^3\right) \\ &- \gamma P_1 \frac{a}{b}\left(1 - 2\gamma P_2 \tilde{a}\tilde{b} + \gamma'\left(-\frac{\epsilon_2}{\tilde{a}^2} + 3\frac{P_2}{\tilde{b}^2}\right)\tilde{a}\tilde{b}^3\right)\Bigg]\Bigg\}.\end{aligned} \tag{4.106}$$

Note that the bulk viscosity would play no role in the shear sector or in the response to a homogeneous $h_{13}(t)$ perturbation of the background metric.

Given that $\mathcal{S}$ of the full system is given by (4.9) we readily obtain the full system $\eta/\mathcal{S}$. We may thus define the Kubo diffusion constant:

$$\mathcal{D} \equiv \frac{\eta}{\mathcal{T}\mathcal{S}} = \frac{\kappa_1 n_1 + \kappa_2 n_2}{4\pi\mathcal{T}(n_1+n_2)} + \mathcal{O}(\gamma). \tag{4.107}$$

In Fig. 4.20 the shear diffusion constants D_I in (4.95) corresponding to shear eigenmodes are compared with the overall diffusion constant $\mathcal{D}$ corresponding to the total shear viscosity $\eta/\mathcal{S} \equiv T\mathcal{D}$ for various parameters. The left panel shows the situation for two strongly coupled systems with $\eta_i/s_i = 1/4\pi$, whereas the right panel has one sector more weakly coupled. The dashed lines denote the case where one subsystem, namely $\mathfrak{S}_1$, contributes more to the pressure ($n_1 > n_2$). We find that $\mathcal{D}$ is always between the individual shear diffusion constants D_I.

The shear diffusion constants decrease when the effective coupling, $\gamma^{1/4}\mathcal{T}$, is dialed from zero. There is a slight nonmonotonic behavior in the crossover region between weak and strong coupling between the subsystems for the full viscosity. At large coupling all results appear to saturate at finite values.

Finally, it is worthwhile to note that when solving (4.93), one in fact obtains two additional eigenmodes which are spurious. These are non-hydrodynamic, i.e. ω is finite as we take k to zero. Furthermore, when k vanishes, these eigenmodes correspond to spontaneous fluctuations of the effective metric components γ_{13} and $\tilde{\gamma}_{13}$ without involving any fluctuation of the velocity fields or any external background metric fluctuation. This fluctuation is possible due to the presence of time-derivatives of the effective background metrics in (4.102): these make the coupling equations (4.90) dynamical in the sense that these are differential equations for γ_{13} and $\tilde{\gamma}_{13}$. These spurious modes are also acausal, having positive imaginary parts in the dispersion relation. This is related to the acausal behavior of first-order hydrodynamics. We can cure this bad behavior by embedding the first order hydrodynamics of each sector into an Israel-Stewart framework, kinetic theory or holographic gravity. This will be discussed in detail in the next section.

To summarize our findings for shear diffusion and specific viscosity:

1. The full system has two shear diffusion modes with diffusion constants $D_{a,b}$ such that $\mathcal{T}D_{a,b}$ decrease monotonically with increasing temperature $\mathcal{T}$ before saturating at finite values at large $\mathcal{T}$.

2. The overall specific viscosity $\eta/\mathcal{S}$ derived using the Kubo formula from the total conserved energy-momentum tensor is in between the values of $\mathcal{T}D_{a,b}$ with slight nonmonotonic behavior at the phase transition.

3. When one of the systems has a dominant contribution to the total energy/pressure and a different specific viscosity, the overall specific shear viscosity is closer to that of the dominant system.

4.3.2 Bi-hydrodynamic sound mode

We now turn our attention to the sound mode. Owing to the rotational symmetry of the thermal equilibrium state, we can consistently assume that the velocity fluctuations in both sectors are longitudinal, i.e., pointing in the same direction as the momentum $\mathbf{k}$. Without loss of generality, we will take ν, $\tilde{\nu}$ and $\mathbf{k}$ to be in the z-direction. The consistent forms of the effective metrics are (4.81) with the non-vanishing components of $\delta g_{\mu\nu}$ and $\delta\tilde{g}_{\mu\nu}$ are

$$\begin{aligned}
&\delta g_{03} = \beta e^{i(kz-\omega t)}, \quad \delta g_{00} = -2a\,\delta a\, e^{i(kz-\omega t)}, \\
&\qquad \delta g_{11} = \delta g_{22} = (2b\,\delta b + \chi)e^{i(kz-\omega t)}, \quad \delta g_{33} = (2b\,\delta b - 2\chi)e^{i(kz-\omega t)}, \\
&\delta\tilde{g}_{03} = \tilde{\beta} e^{i(kz-\omega t)}, \quad \delta\tilde{g}_{00} = -2\tilde{a}\,\delta\tilde{a}\, e^{i(kz-\omega t)}, \\
&\qquad \delta\tilde{g}_{11} = \delta\tilde{g}_{22} = (2\tilde{b}\,\delta\tilde{b} + \tilde{\chi})e^{i(kz-\omega t)}, \quad \delta\tilde{g}_{33} = (2\tilde{b}\,\delta\tilde{b} - 2\tilde{\chi})e^{i(kz-\omega t)}.
\end{aligned} \tag{4.108}$$

The normalized four-velocity fields are

$$\begin{aligned} u^\mu &= \left(\frac{1}{a} - \frac{1}{a^2}\delta a\, e^{i(kz-\omega t)}, 0, 0, \nu e^{i(kz-\omega t)}\right), \\ \tilde{u}^\mu &= \left(\frac{1}{\tilde{a}} - \frac{1}{\tilde{a}^2}\delta \tilde{a}\, e^{i(kz-\omega t)}, 0, 0, \tilde{\nu} e^{i(kz-\omega t)}\right). \end{aligned} \tag{4.109}$$

We may also anticipate that the temperatures also fluctuate from their equilibrium values so that we also have

$$\delta T_1 e^{i(kz-\omega t)} \quad \text{and} \quad \delta T_2 e^{i(kz-\omega t)}. \tag{4.110}$$

The non-vanishing components of the linearized perturbations of the individual hydrodynamic energy-momentum tensors then turn out to be:

$$\begin{aligned} \delta t^{00} &= \left(\frac{1}{a^2}\frac{\mathrm{d}\epsilon_1}{\mathrm{d}T_1}\delta T_1 - 2\frac{\epsilon_1}{a^3}\delta a\right) e^{i(kz-\omega t)}, \quad \delta t^{03} = \left(\frac{P_1}{a^2 b^2}\beta + \frac{\epsilon_1 + P_1}{a}\nu\right) e^{i(kz-\omega t)}, \\ \delta t^{11} = \delta t^{22} &= \left(\frac{1}{b^2}\frac{\mathrm{d}P_1}{\mathrm{d}T_1}\delta T_1 - 2\frac{P_1}{b^3}\delta b - \frac{P_1}{b^4}\chi + i\frac{2\eta_1}{3b^2}k\nu + i\frac{\eta_1}{ab^4}\omega\chi\right) e^{i(kz-\omega t)}, \\ \delta t^{33} &= \left(\frac{1}{b^2}\frac{\mathrm{d}P_1}{\mathrm{d}T_1}\delta T_1 - 2\frac{P_1}{b^3}\delta b + 2\frac{P_1}{b^4}\chi - i\frac{4\eta_1}{3b^2}k\nu - 2i\frac{\eta_1}{ab^4}\omega\chi\right) e^{i(kz-\omega t)}, \end{aligned} \tag{4.111}$$

and similarly

$$\begin{aligned} \delta \tilde{t}^{00} &= \left(\frac{1}{\tilde{a}^2}\frac{\mathrm{d}\epsilon_2}{\mathrm{d}T_2}\delta T_2 - 2\frac{\epsilon_2}{\tilde{a}^3}\delta \tilde{a}\right) e^{i(kz-\omega t)}, \quad \delta \tilde{t}^{03} = \left(\frac{P_2}{\tilde{a}^2 \tilde{b}^2}\tilde{\beta} + \frac{\epsilon_2 + P_2}{\tilde{a}}\tilde{\nu}\right) e^{i(kz-\omega t)}, \\ \delta \tilde{t}^{11} = \delta \tilde{t}^{22} &= \left(\frac{1}{\tilde{b}^2}\frac{\mathrm{d}P_2}{\mathrm{d}T_2}\delta T_2 - 2\frac{P_2}{\tilde{b}^3}\delta \tilde{b} - \frac{P_2}{\tilde{b}^4}\tilde{\chi} + i\frac{2\eta_2}{3\tilde{b}^2}k\tilde{\nu} + i\frac{\eta_2}{\tilde{a}\tilde{b}^4}\omega\tilde{\chi}\right) e^{i(kz-\omega t)}, \\ \delta \tilde{t}^{33} &= \left(\frac{1}{\tilde{b}^2}\frac{\mathrm{d}P_2}{\mathrm{d}T_2}\delta T_2 - 2\frac{P_2}{\tilde{b}^3}\delta \tilde{b} + 2\frac{P_2}{\tilde{b}^4}\chi - i\frac{4\eta_2}{3\tilde{b}^2}k\tilde{\nu} - 2i\frac{\eta_2}{\tilde{a}\tilde{b}^4}\omega\tilde{\chi}\right) e^{i(kz-\omega t)}. \end{aligned} \tag{4.112}$$

The linearized coupling equations take the form:

$$\begin{aligned} \delta g_{\mu\nu} &= \gamma\sqrt{-\tilde{g}}\left(\eta_{\mu\rho}\delta\tilde{t}^{\rho\sigma}\eta_{\sigma\nu} + \frac{1}{2}\eta_{\mu\rho}\tilde{t}^{(\mathrm{eq})\rho\sigma}\eta_{\sigma\nu}\tilde{g}^{\alpha\beta}\delta\tilde{g}_{\alpha\beta}\right) \\ &\quad +\gamma'\eta_{\mu\nu}\sqrt{-\tilde{g}}\left(\eta_{\rho\sigma}\delta\tilde{t}^{\rho\sigma} + \frac{1}{2}\eta_{\rho\sigma}\tilde{t}^{(\mathrm{eq})\rho\sigma}\tilde{g}^{\alpha\beta}\delta\tilde{g}_{\alpha\beta}\right), \\ \delta \tilde{g}_{\mu\nu} &= \gamma\sqrt{-g}\left(\eta_{\mu\rho}\delta t^{\rho\sigma}\eta_{\sigma\nu} + \frac{1}{2}\eta_{\mu\rho}t^{(\mathrm{eq})\rho\sigma}\eta_{\sigma\nu}g^{\alpha\beta}\delta g_{\alpha\beta}\right) \\ &\quad +\gamma'\eta_{\mu\nu}\sqrt{-g}\left(\eta_{\rho\sigma}\delta t^{\rho\sigma} + \frac{1}{2}\eta_{\rho\sigma}t^{(\mathrm{eq})\rho\sigma}g^{\alpha\beta}\delta g_{\alpha\beta}\right). \end{aligned} \tag{4.113}$$

The hydrodynamic equations of motion in the respective effective metrics take the form:

$$\begin{aligned} & ika\nu - i\omega\left(\frac{\delta s_1}{s_1} + 3\frac{\delta b}{b}\right) = 0, \\ & ik\tilde{a}\tilde{\nu} - i\omega\left(\frac{\delta s_2}{s_2} + 3\frac{\delta \tilde{b}}{\tilde{b}}\right) = 0, \\ & ik\left(\frac{\delta T_1}{T_1} + \frac{\delta a}{a}\right) - i\omega\left(\frac{\beta}{a^2} + \frac{\nu b^2}{a}\right) + \frac{4}{3}k^2\frac{\eta_1}{\epsilon_1 + P_1}\nu + 2\omega k\frac{\eta_1}{\epsilon_1 + P_1}\frac{\chi}{ab^2} = 0, \\ & ik\left(\frac{\delta T_2}{T_2} + \frac{\delta \tilde{a}}{\tilde{a}}\right) - i\omega\left(\frac{\tilde{\beta}}{\tilde{a}^2} + \frac{\tilde{\nu}\tilde{b}^2}{\tilde{a}}\right) + \frac{4}{3}k^2\frac{\eta_2}{\epsilon_2 + P_2}\tilde{\nu} + 2\omega k\frac{\eta_2}{\epsilon_2 + P_2}\frac{\tilde{\chi}}{\tilde{a}\tilde{b}^2} = 0. \end{aligned} \tag{4.114}$$

To find the eigenmodes, we first solve (4.113) for δa, $\delta\tilde{a}$, δb, $\delta\tilde{b}$, χ, $\tilde{\chi}$, β and $\tilde{\beta}$ in terms of the physical dynamical hydrodynamic variables δT_1, δT_2, ν and $\tilde{\nu}$. Subsituting in that solution into (4.114) leaves us with four equations for four variables, ν, $\tilde{\nu}$, δT_1 and δT_2. We can represent this, like in the previous discussion of the shear sector, via

$$Q_{AB}(\omega, k)\nu_B = 0, \tag{4.115}$$

where $\nu_A = (\nu, \tilde{\nu}, \delta T_1, \delta T_2)$ and Q_{AB} is a 4×4 matrix. The dispersion relations of the eigenmodes are obtained by requiring that the determinant of Q vanishes, just as in the shear sector.

First off, it is useful to examine the simplest case: two identical perfect fluids, i.e. when the subsystems have the same number of degrees of freedom $n_1 = n_2$ and vanishing shear viscosity, $\eta_1 = \eta_2 = 0$. Furthermore, the individual energy momentum tensors and effective metrics are identical. Then the eigenmodes can be obtained from

$$\begin{aligned} ik\, a\, \nu - i\omega\left(\frac{\delta s_1}{s_1} + 3\frac{\delta b}{b}\right) &= 0, \\ ik\left(\frac{\delta T_1}{T_1} + \frac{\delta a}{a}\right) - i\omega\left(\frac{\beta}{a^2} + \frac{\nu b^2}{a}\right) &= 0. \end{aligned} \tag{4.116}$$

Remember that the full thermal equilibrium solution is parametrized by the temperature $\mathcal{T}$. We can vary (4.4) to arrive at

$$\delta\mathcal{T} = T_1(\mathcal{T})\delta a + a(\mathcal{T})\delta T_1, \tag{4.117}$$

with $\delta a = \delta\tilde{a} = (\mathrm{d}a(\mathcal{T})/\mathrm{d}\mathcal{T})\delta\mathcal{T}$, $\delta b = \delta\tilde{b} = (\mathrm{d}b(\mathcal{T})/\mathrm{d}\mathcal{T})\delta\mathcal{T}$ and $\delta T_1 = \delta T_2 = (\mathrm{d}T_1(\mathcal{T})/\mathrm{d}\mathcal{T})\delta\mathcal{T}$.

We can now perturb the full energy momentum tensor by an infinitesimal velocity υ in the z-direction and an infinitesimal temperature fluctuation, such that the non-zero components of the energy momentum tensor are

$$T^{00} = \mathcal{E} + \frac{\mathrm{d}\mathcal{E}}{\mathrm{d}\mathcal{T}}\delta\mathcal{T}, \quad T^{11} = T^{22} = T^{33} = \mathcal{P} + \frac{\mathrm{d}\mathcal{P}}{\mathrm{d}\mathcal{T}}\delta\mathcal{T}, \quad T^{03} = (\mathcal{E} + \mathcal{P})\upsilon. \tag{4.118}$$

The conservation of the full energy-momentum tensor in flat space yields the linearized Euler equations:

$$ik\upsilon - i\omega\frac{\delta\mathcal{S}}{\mathcal{S}} = 0, \quad ik\frac{\delta\mathcal{T}}{\mathcal{T}} - i\omega\upsilon = 0. \tag{4.119}$$

The diagonal components of the fluctuations can always be mapped to a change in $\delta\mathcal{T}$ even if the systems are not identical. If we solve β and $\tilde{\beta}$ in terms of ν and $\tilde{\nu}$ using the off-diagonal 03-component of the coupling equations, and then compute the off-diagonal 03-component of the full energy-momentum tensor, we can always define the υ of the full system as an appropriate linear combination of ν and $\tilde{\nu}$ by demanding the form (4.118) of the full energy-momentum tensor.

We now focus on the off-diagonal component T^{03}. Specifically, we observe from (4.118) that

$$\delta T^{03} = \delta T^0{}_3 = (\mathcal{E} + \mathcal{P})\upsilon, \quad \delta T_0{}^3 = -(\mathcal{E} + \mathcal{P})\upsilon. \tag{4.120}$$

With our assumptions for the effective metric and the perfect fluid forms of the energy-momentum tensor, we find

$$\begin{aligned}
\delta t^{03} &= \delta\tilde{t}^{03} = \frac{P_1}{a^2 b^2}\beta + \frac{\epsilon_1 + P_1}{a}\nu, \\
\delta {t_0}^3 &= \delta {\tilde{t}_0}^{\,3} = -(\epsilon_1 + P_1)\nu a, \\
\delta {t^0}_3 &= \delta {\tilde{t}^0}_{\,3} = (\epsilon_1 + P_1)\left(\frac{b^2}{a}\nu + \frac{1}{a^2}\beta\right).
\end{aligned} \tag{4.121}$$

From (4.118), any consistent coupling equations should lead to

$$\delta {T_0}^3 = 2ab^3 \delta {t_0}^3, \quad \delta {T^0}_3 = 2ab^3 \delta {t^0}_3. \tag{4.122}$$

Furthermore thermodynamic identities for any consistent coupling ensure that $\mathcal{E}+\mathcal{P} = 2ab^3(\epsilon_1 + P_1)$. Therefore it follows from (4.120), (4.121) and (4.122) that any consistent coupling equation should imply

$$\frac{b^2}{a}\nu + \frac{1}{a^2}\beta = \nu a = \upsilon. \tag{4.123}$$

The coupling equations always ensure that conservation of the individual energy-momentum tensor in the individual effective metric leads to conservation of the full energy-momentum tensor in flat space.

We can show that the eigenmode of the full system corresponds to the thermodynamic sound of the full system. To do this, we need to show that the Euler equations of the full energy-momentum tensor in flat space will lead to the individual Euler equations being satisfied in the individual effective metrics. We will need identical systems with identical energy-momentum tensors living in identical effective metrics. Otherwise the number of conservation equations of the full system are outnumbered by the individual conservation equations. At the linearized level, we need to show that (4.119) implies (4.116).

We note that thermodynamic variation ensures that $\delta\mathcal{S}/\mathcal{S} = 2\delta s_1/s_1 + 3\delta b/b$ since $\mathcal{S} = 2s_1 b^3$ in the case of identical systems. Similarly, $\delta\mathcal{T}/\mathcal{T} = \delta T_1/T_1 + \delta a/a$ since $\mathcal{T} = T_1 a$. It is then easy to see that (4.119) implies (4.116) because of the two relations in (4.123) which follows from consistent coupling equations. We then conclude that for any consistent coupling between two identical systems with identical effective metric solutions at equilibrium, the thermodynamic sound will correspond to one of the eigenmodes at the leading order in the derivative expansion. In this mode, the velocity fields in the two identical systems are parallel to each other so that $\tilde{\nu} = \nu$.

Even for identical perfect fluid systems there is another eigenmode where $\delta T_1 \neq \delta T_2$ and $\nu \neq \tilde{\nu}$. In this mode, the velocity fields are anti-parallel to each other so that $\tilde{\nu} = -\nu$. Most importantly, the thermodynamic relation $\delta\mathcal{T} = \delta(T_1 a) = \delta(T_2\tilde{a})$ is not satisfied by the fluctuations. This mode does not travel at the speed of thermodynamic sound. When $n_1 \neq n_2$, it turns out that neither of the two eigenmodes does; in this case the thermodynamically defined speed of sound is in between the velocities of the eigenmodes.

When the two systems are identical and we consider the eigenmode which at leading order propagates at the speed of full system thermodynamic sound, we find that we cannot map the first-order (identical) hydrodynamic fluctuations of the individual systems to that of a hydrodynamic form for the full system. To see this, we may repeat the steps of the above argument with $\chi = \tilde{\chi} \neq 0$ and $\eta_1 = \eta_2 \neq 0$ and find that for generic η_1 the modified form of (4.123) does not imply that we can obtain (4.116) with first-order corrections from the first-order correction of (4.119) (linearized Navier-Stokes equation in flat space).

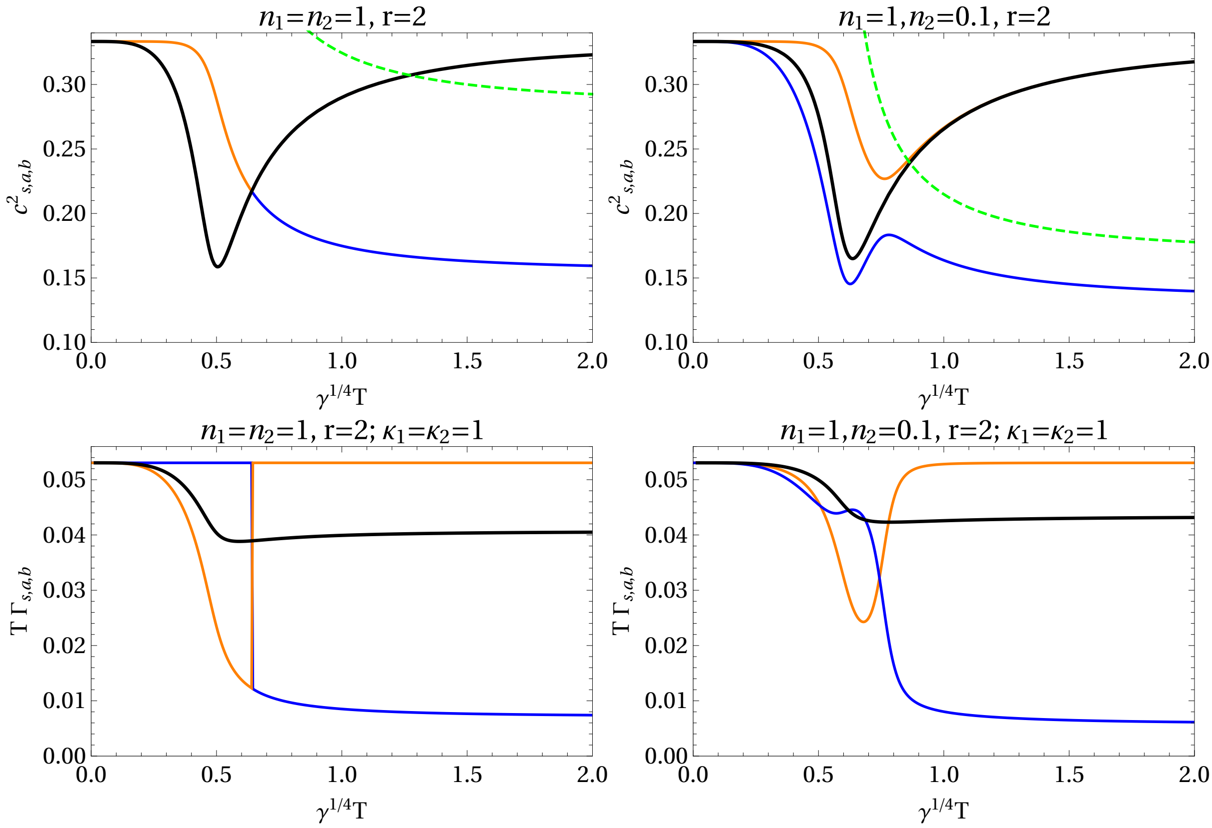

Figure 4.21: Sound modes and their attenuation coefficients for equal and unequal conformal systems, same $\kappa = 1$ (corresponding to $\eta_i/s_i = 1/4\pi$), with the slower mode a plotted in blue, and the faster mode b plotted in orange. The black line represents the thermodynamic speed of sound and associated attenuation coefficient from the Kubo formula. The green dashed line shows the light-cone velocities squared of the two subsystems (in the case of $n_2 = 1/10$ only $\tilde{v}^2$ is in plot region). In the case $n_1 = n_2$ the lines for $c^2_{a,b}$ meet and could be continued smoothly by switching the designation; however for any $n_1 \neq n_2$ we have $c_b > c_a$ at nonzero $\gamma^{1/4}\mathcal{T}$. The discontinuous behavior of the damping rates $\Gamma_{a,b}$ for $n_1 = n_2$ is in fact the limit of smooth curves as $n_1 \to n_2$ from different starting values.

The dispersion relations of the eigenmodes have the same characteristic sound-like form,

$$\omega_{(a,b)} = \pm c_{(a,b)} k - i\Gamma_{(a,b)} k^2 + \mathcal{O}(k^3). \tag{4.124}$$

The perturbative expansions of the speed of sound modes and their respective attenuation coefficients are given by

$$\begin{aligned}
c_a &= \frac{1}{\sqrt{3}}\Big(1 - 2(n_1+n_2)\gamma\mathcal{T}^4 - 48 n_1 n_2 \gamma^2 \mathcal{T}^8\Big) + \mathcal{O}(\gamma^3),\\
\Gamma_a &= \frac{\kappa_1 n_1 + \kappa_2 n_2}{6\pi\mathcal{T}(n_1+n_2)} - \frac{n_1 n_2(9\kappa_1 n_1 - \kappa_2 n_1 - \kappa_1 n_2 + 9\kappa_2 n_2)}{3\pi(n_1+n_2)^2}\gamma\mathcal{T}^3 + \mathcal{O}(\gamma^2),\\
c_b &= \frac{1}{\sqrt{3}}\Big(1 - 8 n_1 n_2 \gamma^2 \mathcal{T}^8\Big) + \mathcal{O}(\gamma^3),\\
\Gamma_b &= \frac{\kappa_2 n_1 + \kappa_1 n_2}{6\pi\mathcal{T}(n_1+n_2)} - \frac{(n_1-n_2)\left(2\kappa_2 n_1^2 + 7 n_1 n_2(\kappa_1-\kappa_2) - 2\kappa_1 n_2^2\right)}{3\pi(n_1+n_2)^2}\gamma\mathcal{T}^3 + \mathcal{O}(\gamma^2),
\end{aligned} \tag{4.125}$$

with the dependence on $r = -\gamma'/\gamma$ showing up only in the higher-order terms.

For equal partial pressures, $n_1 = n_2$, the dependence of the sound attenuation coefficients on κ_1 and κ_2 simplifies: both Γ_a and Γ_b are proportional to $(\kappa_1+\kappa_2)$ to all orders in $\gamma^{1/4}\mathcal{T}$. Moreover, the attenuation coefficient of the faster mode, Γ_b, (which coincides with the thermodynamically defined speed of sound (4.35)) becomes independent of the coupling $\gamma^{1/4}\mathcal{T}$.

Mode a has velocity and temperature fluctuation fields with perturbative expansions

$$\begin{aligned}
\tilde{\nu} &= \frac{n_1}{n_2}\left(1 + \frac{21}{2}(n_2-n_1)\gamma\mathcal{T}^4 + \mathcal{O}(\gamma^2,\gamma'^2,k)\right)\nu,\\
\delta T_1 &= \pm\frac{\mathcal{T}}{\sqrt{3}}\left(1 + 2n_2\gamma\mathcal{T}^4 + \mathcal{O}(\gamma^2,\gamma'^2,k)\right)\nu,\\
\delta T_2 &= \pm\frac{n_1}{n_2}\frac{\mathcal{T}}{\sqrt{3}}\left(1 + \frac{1}{2}\left(21n_2 - 17n_1\right)\gamma\mathcal{T}^4 + \mathcal{O}(\gamma^2,\gamma'^2,k)\right)\nu.
\end{aligned} \tag{4.126}$$

and mode b similarly has

$$\begin{aligned}
\tilde{\nu} &= -\left(1 - \frac{1}{2}(n_1-n_2)\gamma\mathcal{T}^4 + \mathcal{O}(\gamma^2,\gamma'^2,k)\right)\nu,\\
\delta T_1 &= \pm\frac{\mathcal{T}}{\sqrt{3}}\left(1 + 2n_2\gamma\mathcal{T}^4 + \mathcal{O}(\gamma^2,\gamma'^2,k)\right)\nu,\\
\delta T_2 &= \mp\frac{\mathcal{T}}{\sqrt{3}}\left(1 + \frac{1}{2}\left(n_2 + 3n_1\right)\gamma\mathcal{T}^4 + \mathcal{O}(\gamma^2,\gamma'^2,k)\right)\nu.
\end{aligned} \tag{4.127}$$

Above, the + sign refers to the case when the mode is propagating parallel to the momentum $\mathbf{k}$ and − sign refers to the case of opposite propagation. For equal partial pressures, $n_1 = n_2$, mode a and b have $\tilde{\nu} = \nu$ and $\tilde{\nu} = -\nu$, respectively, to all orders.

It is instructive to compare the attenuation coefficients of the two modes with the full system attenuation coefficient. The sound dispersion for a hydrodynamic system in flat space is given by

$$\omega = \pm c_s k - i\Gamma_s k^2 + \mathcal{O}(k^3), \tag{4.128}$$

where c_s is the speed of thermodynamic sound and $\Gamma_s = (2/3)(\eta/\mathcal{T}\mathcal{S})$ is the attenuation coefficient. The shear viscosity, η, for the system was computed in (4.106). Interestingly, none of the

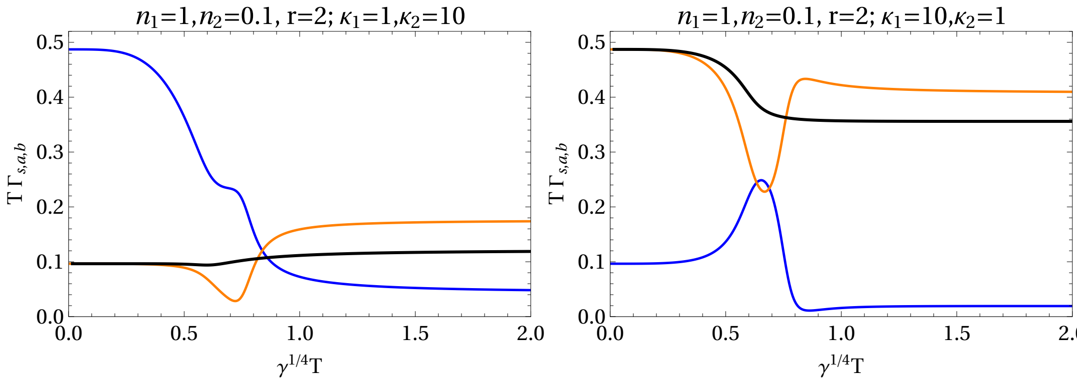

Figure 4.22: Attenuation coefficients $\Gamma_{a,b}$ of the sound eigenmodes (slower mode a in blue, faster mode b in orange) for unequal conformal systems with different κ. The black line gives the Kubo formula result for sound attenuation.

propagating modes attenuates in the expected hydrodynamic way, even when one mode travels at the speed of thermodynamic sound, as is the case for identical subsystems.

The nonperturbative results for the speeds and attenuations of the propagating modes in the sound channel have been plotted in Fig. 4.21 and 4.22, respectively. Two cases are considered, one where both fluids are strongly coupled and the other, where one is more weakly coupled than the other. Furthermore, the hydrodynamic sound attenuation Γ_s of the full system is included for comparison. We find that for equal partial pressures, $n_1 = n_2$, the value of $c_{a,b}$ coincide for two points: at the decoupling limit $\gamma^{1/4}\mathcal{T} = 0$ and one finite value of $\gamma^{1/4}\mathcal{T}$. For unequal partial pressures, $n_1 \neq n_2$, the crossing at the latter point is lifted, such that mode b is always faster than mode a for $\gamma^{1/4}\mathcal{T} > 0$. A cusp in $c_{a,b}$ develops in the limit $n_1 \to n_2$, while $\Gamma_{a,b}$ becomes discontinous. As we deduced previously from the perturbative series, for equal partial pressures, $\max(\Gamma_a, \Gamma_b)$ is a constant independent of $\gamma^{1/4}\mathcal{T}$ and the results for the two modes could all be connected smoothly.

Fig. 4.23 displays $\tilde{v}/v$ for the corresponding sound eigenmodes as well as the associated (adiabatic) fluctuations of the total entropy density $\mathcal{S}^{\mu=0}$. The discontinuities at $n_1 = n_2$ are spurious and only arise when taking the limit $n_1 \to n_2$ starting from $n_1 \neq n_2$.

In summary, our findings for the sound sector are:

1. The thermodynamic speed of sound of the full system, c_s, is always between the velocities of the two sound modes c_a and c_b, that is $c_a \leq c_s \leq c_b$, and coincides exactly with one of the modes for $n_1 = n_2$.

2. At high temperatures, c_s and c_b approach $1/\sqrt{3}$ due to emergent conformality.

3. At temperatures above the crossover from weak to strong inter-system coupling, the velocity of the faster mode (b) quickly approaches the thermodynamically defined speed of sound.

4. Near the crossover temperature, the velocity fields of the two modes change their phase with v (or $\tilde{v}$) vanishing at a certain value of $\gamma^{1/4}\mathcal{T}$ for mode a (or b). Mode a has out-of-phase oscillations for large $\gamma^{1/4}\mathcal{T}$ with decreasing total entropy fluctuations $\delta\mathcal{S}^{\mu=0}$ and speed slower than the thermodynamic speed of sound.

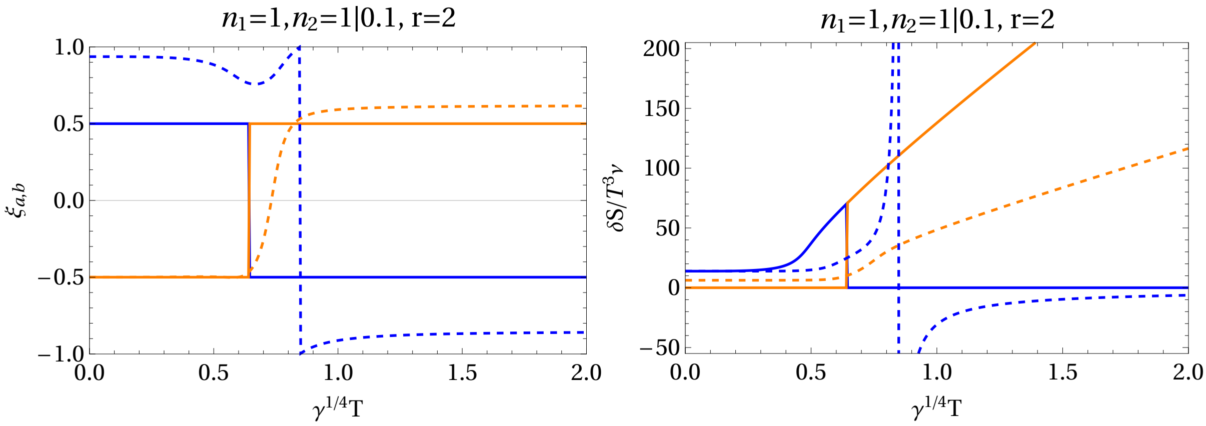

Figure 4.23: Left panel: the relation between the velocity amplitudes ν and $\tilde{\nu}$ of the sound eigenmodes displayed in Fig. 4.20 in the form $\xi \equiv \frac{2}{\pi}\arctan(\tilde{\nu}/\nu)$. Right panel: the corresponding fluctuation amplitude of the total entropy density, $\delta\mathcal{S} \equiv \delta\mathcal{S}^{\mu=0}$, divided by $\nu\mathcal{T}^3$. Mode a and b are given in blue and orange, respectively, with full and dashed lines representing $n_1 = n_2 = 1$ and $n_1 = 1, n_2 = 1/10$. The divergence of $\delta\mathcal{S}/(\mathcal{T}^3\nu)$ of mode a at one value of $\gamma^{1/4}\mathcal{T}$ is due to a zero of ν (corresponding to $|\xi_a| = 1$); here a velocity field is present only in subsystem 2.

5. While c_s and c_b can become larger than the effective light-cone speeds $v, \tilde{v}$, the velocity of the slower mode, c_a, remains smaller than $v, \tilde{v}$. This mode thus lies within both effective light cones.

6. The value of the attenuation coefficient obtained from the Kubo formula is between that of the sound modes for large $\gamma^{1/4}\mathcal{T}$.

7. While the dependence of the attenuation coefficients on $\gamma^{1/4}\mathcal{T}$ is in general complicated, at temperatures sufficiently above the crossover region the slower "non-acoustic" sound mode is always the more weakly damped one.

8. The coupling studied in our setup provides no pure damping modes, i.e. the imaginary part of the speed of sound vanishes as $k \to 0$. This reflects the fact, that this interaction is not sufficient to equilibrate the two subsystems, e.g. in a homogeneous configuration with subsystems at unequal temperatures.

4.4 Coupling a kinetic sector to a strongly coupled fluid

We now turn our attention to coupling a kinetic theory to a hydrodynamic sector in this section. We do this to obtain a qualitative understanding of a coupled system of weakly interacting and strongly interacting degrees of freedom. The system we have in mind is comprised of a subsystem $\mathfrak{S}_1$, a gas of massless particles (gluons) described by kinetic theory, and subsystem $\mathfrak{S}_2$, a strongly interacting holographic gauge theory described by dual gravitational perturbations of a black hole, which are coupled via the mutual effective metric coupling. Using the fluid/gravity correspondence [70], we may further simplify gravitational dynamics to that of a fluid with a low value of η/s if we are interested in the long time dynamics. Due to the appearance of spurious modes and associated acausalities we will need to embed first-order hydrodynamics in a more complete description, i.e. in an Israel-Stewart framework with an extremely small relaxation time. In the future we plan to do a more complete calculation by involving the relaxation dynamics of the strongly coupled sector as described holographically via quasi-normal mode perturbations of a black brane.

It is useful to revisit some of the discussion regarding kinetic theory in curved spacetime from Sec. 2.3. We will follow the discussion found in Refs. [89, 116]. Ignoring for simplicity effects of quantum statistics and thermal corrections, the thermal equilibrium of the weakly coupled and dilute kinetic sector is described by a Maxwell-Jüttner distribution

$$f_0(p^i) = n_0 e^{p^\mu u_\mu / T_1}, \tag{4.129}$$

where we have assumed that the distribution function is homogeneous and isotropic. Furthermore, we need to provide a mass-shell condition. We are interested in describing massless gluons, so we can determine p^0 via

$$p^\mu p^\nu g_{\mu\nu} = 0. \tag{4.130}$$

We now define

$$p \equiv \sqrt{p^{x2} + p^{y2} + p^{z2}}, \tag{4.131}$$

so that we can determine using (4.1) that

$$p^0 = p\frac{b}{a}. \tag{4.132}$$

Recalling from (4.2) that the four-velocity is $u_\mu = (-a, 0, 0, 0)$, leads us to

$$f_0(p^i) = n_0 e^{-pb/T_1}. \tag{4.133}$$

We are left to determine the normalization constant of the distribution function, n_0. Recall that the energy-momentum tensor corresponding to a quasi-particle distribution f is given by (2.51) with $p_0 = g_{0\mu} p^\mu$ satisfying the mass-shell condition, i.e. $p_0 = -a^2 p^0$. As before, $\sqrt{-g} = ab^3$. The equilibrium conformal energy-momentum tensor then takes our previously assumed form (4.2):

$$t^{\mu\nu} = \mathrm{diag}\left(\frac{3n_1 T_1^4}{a^2}, \frac{n_1 T_1^4}{b^2}, \frac{n_1 T_1^4}{b^2}, \frac{n_1 T_1^4}{b^2}\right), \tag{4.134}$$

where n_1 is our previously introduced (theory-dependent) parameter if we identify

$$n_0 = n_1 \pi^2. \tag{4.135}$$

Therefore, to make contact with the previous sections, we will set n_0 to $n_1 \pi^2$.

For convenience, we use spherical coordinates for the components of the momenta, so that

$$\begin{aligned} p^x &= p \sin\theta \cos\phi, \\ p^y &= p \sin\theta \sin\phi \\ p^z &= p \cos\theta. \end{aligned} \tag{4.136}$$

A linearized fluctuation of the quasi-particle distribution about equilibrium can be written as:

$$f(p, \theta, \phi, x^i, t) = n_1 \pi^2 e^{-pb/T_1} + \delta f(p, \theta, \phi, x^i, t). \tag{4.137}$$

For computational purposes, it is useful to split the linear term δf into two parts, one contribtuting to the dissipation and one not, each having a specific momentum $\mathbf{k}$ and a specific frequency ω component, according to

$$\delta f(p,\theta,\phi,x^i,t) = \left(\delta f^{(\mathrm{eq})}(p,\theta,\phi) + \Delta f(p,\theta,\phi)\right) e^{i(\mathbf{k}\cdot\mathbf{x}-\omega t)}. \tag{4.138}$$

The term $\delta f^{(eq)}$ can be defined uniquely such that it produces a perturbation $\delta t^{\mu\nu(\mathrm{eq})}$ in the energy-momentum tensor that is of a perfect fluid form. Only the term Δf will contribute to the dissipation. If $\delta g_{\mu\nu}$ is the self-consistent effective metric fluctuation in the kinetic theory, then in the relaxation time approximation δf obeys the linearized Boltzmann equation, also known as the Anderson-Wittig equation:

$$\left(\partial_t + \frac{p^i}{p^0}\partial_i\right)\delta f - \delta\Gamma^i_{\beta\gamma}\frac{p^\beta p^\gamma}{p^0}\frac{\partial}{\partial p^i} f_0 = -\frac{a}{\tau}\Delta f, \tag{4.139}$$

where $\delta\Gamma^\mu_{\alpha\beta}$ is the linearized Levi-Civita connection obtained from $\delta g_{\mu\nu}$. Note that p^0 also receives a corresponding linear contribution, such that the mass-shell condition is satisfied. Furthermore, in a conformal theory τ should be proportional to T_1^{-1} and we may parametrize

$$\tau(T_1) = \frac{5\kappa_1}{4\pi T_1} \tag{4.140}$$

where κ_1 is a dimensionless constant, which will be eventually identified with $4\pi\eta_1/s_1$ as before.

Furthermore, we will embed the strongly coupled fluid into an Israel-Stewart framework, where the relaxation time is set to

$$\tilde{\tau}(T_2) = \frac{5\lambda}{4\pi T_2}. \tag{4.141}$$

In order to isolate the strongly coupled fluid from the relaxation dynamics, we will take λ very small, such that $\tilde{\tau}$ is small. Unlike the kinetic sector where τ determines the shear viscosity (this can be seen via consistent reduction to hydrodynamics), note that $\tilde{\tau}$ is an independent parameter which only affects second-order hydrodynamics.

4.4.1 Branch cut in response functions of the kinetic sector

We can show that an infinite number of quasi-particle distribution fluctuations decouple from the strongly coupled sector in the sense that all perturbed observables will get contributions purely from the kinetic sector. For instance, it is easy to see that fluctuations of the form

$$\delta f = F(p)G(\theta,\phi)e^{-i\omega t + i\mathbf{k}\cdot\mathbf{x}}, \quad \text{with} \quad G(\theta,\phi) = H_1(\theta)\cos(n\phi) + H_2(\theta)\sin(n\phi) \quad \text{and} \quad n \geq 3 \tag{4.142}$$

have vanishing fluctuations of the energy-momentum tensor

$$\delta t^{\mu\nu} \propto \int \frac{\mathrm{d}^3 p}{p_0}\, p^\mu p^\nu \delta f(\mathbf{x},\mathbf{p},t) = 0. \tag{4.143}$$

Also, if all the perturbations in the strongly coupled fluid are set to zero, we can then self-consistently assume that the coupling equations yield

$$\delta g_{\mu\nu} = \delta\tilde{g}_{\mu\nu} = 0. \tag{4.144}$$

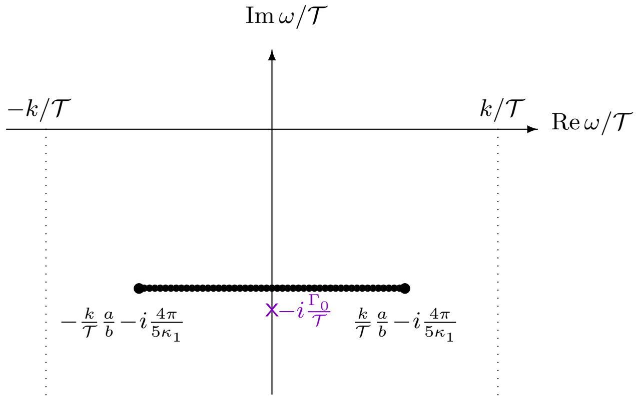

Figure 4.24: Analytic structure of the response function in the kinetic sector. The branch cut arising from (4.146) is given by the thick black line. The pole corresponding to the pure damping mode (4.166), which lies on the second Riemann sheet, is indicated by the cross in violet.

In this case we have $\delta f = \Delta f$ and the linearized Anderson-Wittig equation (4.139) reduces to

$$\left(\omega - \frac{a}{b}\mathbf{n}\cdot\mathbf{k} + i\frac{a}{\tau}\right)\delta f = 0, \tag{4.145}$$

where $n^i = p^i/p$ and τ is the relaxation time in the kinetic sector as defined in (4.140). Choosing without loss of generality $\mathbf{k}$ along the z-direction we obtain

$$\omega = \frac{a}{b}k\cos\theta - i\frac{a}{\tau(T_1)} = vk\cos\theta - i\frac{1}{\tau(\mathcal{T})}, \tag{4.146}$$

where we have used that $T_1 a = \mathcal{T}$ at equilibrium with $\mathcal{T}$ being the physical temperature of the full system. The above dispersion relation is summarized in Fig. 4.24. There is a branch cut in the response function that stretches in the lower half of the complex ω plane horizontally from $-(a/b)k - i/\tau(\mathcal{T})$ to $(a/b)k - i/\tau(\mathcal{T})$. Physically, the factor of $v = a/b$ is the effective equilibrium light-cone velocity, which reflects that the massless gluons propagate along this effective light cone. The imaginary part turns out to receive no correction when expressed in terms of the full system temperature $\mathcal{T}$.

4.4.2 Poles in response functions of the kinetic sector

We now consider quasi-particle distribution fluctuations which are dissipative. As in Sec. 4.3, we can split the propagating modes of the full theory into shear, sound, and tensor channels. Again, we will focus our attention particularly on the shear and sound channels – the tensor channel has no hydrodynamic mode. In order to characterize it properly, we would require to embed the strongly coupled fluid into gravity, which is beyond the scope of this thesis.

We find that some of the propagating modes in both the shear and sound channels are identical to the case of the conformal bi-hydrodynamics. This is not surprising, as both the kinetic and Israel-Stewart sectors can be consistently truncated to conformal hydrodynamics individually. In particular, we will see that with the parametrization (4.140) of the kinetic relaxation time, we get exactly the same results as before, when we identify κ_1 with $4\pi\eta_1/s_1$. Reproducing the results from bi-hydrodynamics provides a consistency check of our calculations.

In addition to the bi-hydrodynamic modes detailed in the previous section, there are two other non-hydrodynamic propagating modes in the full system in both the shear and sound channel. These contribute poles in the response function. We find that one of these modes is continuously connected to the damping in the kinetic sector as we switch off the effective metric coupling. This is particularly worthy of attention since in the case of the hydrodynamic sector, Israel-Stewart dynamics has been used simply as a tool for consistent embedding hydrodynamics and not for capturing actual relaxation dynamics. We will see that if the Israel-Stewart relaxation time is set to zero by taking $\lambda \to 0$ limit, the other damping mode has a smooth limit that captures the effective metric interactions of the kinetic sector with a strongly coupled fluid. Furthermore, if we take $\mathbf{k} \to 0$ limit, there is no way to distinguish the shear and sound channels owing to rotational symmetry of the equilibrium. Thus, we find that the damping coefficient of the full system will then be the same in both shear and sound channels. This provides a consistency check of our calculations.

Let us first focus on the shear channel. The effective metric fluctuations of the two sectors will be given by (4.81) and (4.82). In the kinetic sector, the local mass-shell condition (4.130) will imply that at the linearized level:

$$\begin{aligned} p^0(p,\theta,\phi,z,t) &= \frac{pb}{a} + \delta p^0(p,\theta,\phi,z,t), \\ \delta p^0(p,\theta,\phi,z,t) &= p\left(\frac{\beta}{a^2} + \frac{\gamma_{13}}{ab}\cos\theta\right)\sin\theta\cos\phi\, e^{i(kz-\omega t)}. \end{aligned} \tag{4.147}$$

Recall that the four velocity has a self-consistent fluctuation of $u^\mu = (1/a, \nu e^{i(kz-\omega t)}, 0, 0)$ and that there is no fluctuation in the temperature in the shear channel. Furthermore, we obtain:

$$p_\mu u^\mu = -pb + \frac{p}{b}(\nu b^3 - \gamma_{13}\cos\theta)\sin\theta\cos\phi\, e^{i(kz-\omega t)}. \tag{4.148}$$

The linearized fluctuation of the quasi-particle distribution function takes the form (4.138) with $\mathbf{k}$ in the z-direction and we find

$$\delta f^{(eq)}(p,\theta,\phi) = e^{-\frac{pb}{T_1}}\frac{p}{T_1 b}(\nu b^3 - \gamma_{13}\cos\theta)\sin\theta\cos\phi. \tag{4.149}$$

We compute $\delta f^{(eq)}$ by considering the fluctuation in $p_\mu u^\mu$ since the local equilibrium distribution by definition takes the form $n_1\pi^2 e^{-p_\mu u^\mu/T_1}$. Note that $\delta f^{(eq)}$ indeed reproduces the fluctuation in the energy-momentum tensor which takes a perfect fluid form.

The linearized Boltzmann equation (4.139) can then be explicitly solved to obtain:

$$\Delta f(p,\theta,\phi) = f_0\frac{p\sin\theta\cos\phi\,(-(\beta+\nu ab^2)b\omega + (k\nu a^2b^2 - a\gamma_{13}\omega)\cos\theta)}{T_1 ab(-\omega + k\frac{a}{b}\cos\theta - i\frac{a}{\tau})}. \tag{4.150}$$

In the kinetic sector, the energy-momentum tensor (2.51) assumes the linearized form

$$t^{\mu\nu} = \mathrm{diag}\left(\frac{\epsilon_1}{a^2}, \frac{P_1}{b^2}, \frac{P_1}{b^2}, \frac{P_1}{b^2}\right) + \delta t^{\mu\nu}, \quad \epsilon_1 = 3P_1 = 3n_1T_1^4, \tag{4.151}$$

with the non-vanishing components of $\delta t^{\mu\nu}$:

$$\delta t^{01} = -\frac{P_1\beta + (P_1+\epsilon_1)\nu ab^2}{a^2b^2}e^{i(kz-\omega t)}, \quad \delta t^{13} = \left(-\frac{P_1\gamma_{13}}{b^4} + \pi_{13}\right)e^{i(kz-\omega t)}, \tag{4.152}$$

where

$$\pi_{13} = \frac{1}{8\pi^3}\int_{-\infty}^{\infty} \mathrm{d}p \int_0^{\pi} \mathrm{d}\theta \int_0^{2\pi} \mathrm{d}\phi\; p^3 b^2 \cos\theta \sin^2\theta \cos\phi\; \Delta f(p,\theta,\phi). \tag{4.153}$$

Comparing (4.152) with (4.85), we see that the perfect fluid parts of the energy-momentum tensor perturbation match perfectly. The dissipative contribution in (4.152) originates from Δf and is given by π_{13}. Using the solution (4.150) for Δf in (4.153) we find that:

$$\begin{aligned}\pi_{13} \;=\; & \frac{2n_1 T_1^4}{k^5 a^5 b^2 \tau^4}\Big(\gamma_{13}\omega(ia+\tau\omega) + k(-i\nu a^2 b^2 + \beta\tau\omega)\Big) \\ & \Big(2k^3 a^3 \tau^3 + 3kab^2\tau(a - i\tau\omega)^2 \\ & + 3(iab + b\tau\omega)(-k^2 a^2 \tau^2 + (iab + b\tau\omega)^2)\mathrm{arctanh}\left(\frac{ka\tau}{iab+b\tau\omega}\right)\Big).\end{aligned} \tag{4.154}$$

In order to obtain the hydrodynamic limit, we need to expand the right hand side above for small τ, which yields

$$\pi_{13} = -i\frac{4n_1 T_1^4 \tau}{5ab^4}\Big(k\nu ab^2 - \gamma_{13}\omega\Big) + \mathcal{O}(\tau^2). \tag{4.155}$$

From the above expansion, it is clear that the expansion in τ is essentially the derivative expansion. Substituting the above form of π_{13} in (4.152) and comparing again with the hydrodynamic form (4.85), we find a perfect match, if we identify

$$\eta_1 = \frac{4n_1 T_1^4 \tau}{5}, \tag{4.156}$$

i.e. $\eta_1/s_1 = T_1\tau/5$ and $\kappa_1 = 4\pi\eta_1/s_1$ as we have claimed.

The energy-momentum conservation equation with $\delta t^{\mu\nu}$ given by (4.152) and the metric perturbation given by (4.82) amounts to:

$$\begin{aligned}\nabla_\mu t^{\mu\nu} = \partial_\mu \delta t^{\mu\nu} + \Gamma^\nu{}_{\mu\alpha}[\delta g_{\mu\nu}]t^{(0)\mu\alpha} + \Gamma^\alpha{}_{\mu\alpha}[\delta g_{\mu\nu}]t^{(0)\mu\nu} = 0 \\ \Rightarrow (\epsilon_1 + P_1)(\beta + \nu ab^2)\omega - ka^2b^2\pi_{13} = 0.\end{aligned} \tag{4.157}$$

It is straightforward to check that the above reduces to the standard hydrodynamic equation (4.87) when π_{13} is approximated by (4.155). We can regard (4.154) and (4.157) as dynamical equations for π_{13} and ν.

One can explicitly check that the conservation equation (4.157) is equivalent to the linearized version of the matching condition

$$u_\mu(t^{\mu\nu} - t^{\mu\nu\,(\mathrm{eq})}) = 0, \tag{4.158}$$

in which the projected energy-momentum tensor obtained from the full quasi-particle distribution f should agree with that obtained from $f^{(\mathrm{eq})}$. In fact, this matching condition is necessary to ensure energy-momentum conservation. At the level of linearized shear-sector fluctuation, the matching condition reduces to

$$\Delta t^{01} \equiv \frac{1}{8\pi^3}\int_{-\infty}^{\infty} \mathrm{d}p \int_0^{\pi} \mathrm{d}\theta \int_0^{2\pi} \mathrm{d}\phi\; \frac{p^3 b^3}{a} \sin^2\theta \cos\phi\; \Delta f(p,\theta,\phi) = 0. \tag{4.159}$$

Explicitly, we can check that if we use $\Delta t^{01} = 0$ with the on-shell form of Δf given by (4.150) and the equation of motion (4.154) for π_{13} to solve for the variables ν and π_{13}, we find that indeed the energy momentum tensor (4.157) is conserved.

Embedding the holographic conformal fluid (with $\epsilon_2 = 3P_2 = 3n_2T_2^4$ as in the previous subsection) in the Israel-Stewart framework we obtain:

$$\delta\tilde{t}^{01} = -\frac{P_2\tilde{\beta} + (P_2+\epsilon_2)(\tilde{\nu}ab)^2}{\tilde{a}^2\tilde{b}^2}e^{i(kz-\omega t)}, \quad \delta\tilde{t}^{13} = \left(-\frac{P_2\tilde{\gamma}_{13}}{\tilde{b}^4} + \tilde{\pi}_{13}\right)e^{i(kz-\omega t)}. \tag{4.160}$$

The linearized Israel-Stewart equation of motion of $\tilde{\pi}_{13}$ is:

$$(-i\tilde{b}\tilde{\tau}\omega + (\tilde{a}\tilde{b})^4)\tilde{\pi}_{13} - i\eta_2\tilde{\gamma}_{13}\omega - ik\eta_2\tilde{\nu}ab^2 = 0. \tag{4.161}$$

The conservation of energy-momentum tensor is similar to that of the kinetic sector in (4.157):

$$(\epsilon_2 + P_2)(\tilde{\beta} + \tilde{\nu}ab^2)\omega - k\tilde{a}^2\tilde{b}^2\tilde{\pi}_{13} = 0. \tag{4.162}$$

The equations (4.161) and (4.162) are the equations of motion for $\tilde{\pi}_{13}$ and $\tilde{\nu}$. Recall that the hydrodynamic limit is reproduced for small $\tilde{\tau}$.

We once again parametrize:

$$\eta_2 = \frac{n_2\kappa_2}{\pi}T_2^3. \tag{4.163}$$

Later, we will take the limit $\lambda \to 0$ in which $\tilde{\tau}$ (4.141) vanishes.

We now repeat the steps in the previous subsection. First, we use the coupling equations (4.90) to solve for β, $\tilde{\beta}$, γ_{13} and $\tilde{\gamma}_{13}$ in terms of the physical variables ν, $\tilde{\nu}$, π_{13} and $\tilde{\pi}_{13}$. Next, we substitute these solutions for β, $\tilde{\beta}$, γ_{13} and $\tilde{\gamma}_{13}$ in the dynamical equations, namely (4.154), (4.157), (4.161) and (4.162) to obtain the 4×4 matrix equations:

$$Q_{AB}(\omega,k)\Lambda_B = 0 \tag{4.164}$$

where $\Lambda_B = (\nu, \pi_{13}, \tilde{\nu}, \tilde{\pi}_{13})$. Finally, we obtain the eigenmodes $\omega(k)$ by solving $\det Q = 0$ at each k.

There are four propagating modes for each k as discussed earlier. Two of these exactly reproduce the bi-hydro shear-like eigenmodes obtained earlier with diffusion constants $\mathcal{D}_a$ and $\mathcal{D}_b$. This serves as a consistency check.

Additionally, there are two relaxation eigenmodes. One of these eigenmodes is related to the Israel-Stewart relaxation mode. Its damping constant becomes large for small λ and therefore can be decoupled. The corresponding propagating mode in this limit is localized mostly in the Israel-Stewart sector and involves the following combination of π_{13} and $\tilde{\pi}_{13}$ where

$$\pi_{13} = \left(\frac{4n_1}{5}\gamma\mathcal{T}^4 + \mathcal{O}(\gamma^2\mathcal{T}^8)\right)\tilde{\pi}_{13} \tag{4.165}$$

when $\gamma\mathcal{T}^4$ is small.

The damping constant of the other relaxation mode remains finite. It is of the form

$$\omega(k) = -i\left[\Gamma_0 + \mathcal{O}(k^2)\right] \tag{4.166}$$

with perturbative expansion in the limit $\lambda \to 0$ according to

$$\Gamma_0 = \frac{4\pi\mathcal{T}}{5\kappa_1} + \frac{16\pi n_1 n_2(5\kappa_1 - 4\kappa_2)}{125\kappa_1^2}\gamma^2\mathcal{T}^9 + \mathcal{O}(\gamma^3). \tag{4.167}$$

This is interesting because the Anderson-Witting kinetic theory does not have a non-hydrodynamic pole – the mutual metric coupling evidently causes a pole to be generated from the branch cut

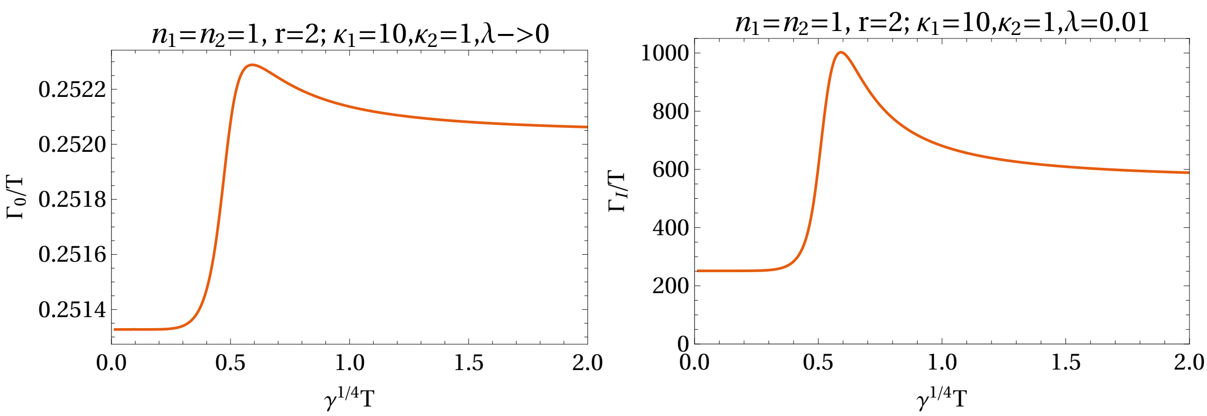

Figure 4.25: Pure damping modes (identical in shear sector and sound sector). Left panel: damping constant Γ_0 that remains finite when $\lambda \to 0$; right panel: damping constant Γ_I of the Israel-Stewart relaxational mode which is large for small λ (however, λ cannot be made arbitrarily small at large $\gamma^{1/4}\mathcal{T}$, see text).

discussed above (for $\gamma\mathcal{T}^4 \to 0$ it coincides with the cut). This pole is farther from the real axis than the cut when $\kappa_1 > \kappa_2$, i.e. when the kinetic sector is more weakly coupled than the second sector described by pure hydrodynamics. The corresponding propagating mode involves the following combination of π_{13} and $\tilde{\pi}_{13}$ where

$$\tilde{\pi}_{13} = \left(\frac{4n_2\kappa_2}{5\kappa_1} \gamma\mathcal{T}^4 + \mathcal{O}(\gamma^2\mathcal{T}^8) \right) \pi_{13}, \tag{4.168}$$

so that it is mostly localized in the kinetic sector as expected in the limit of small $\gamma\mathcal{T}^4$.

Interestingly, when $5\kappa_1 = 4\kappa_2$ all corrections to $\Gamma_0/\mathcal{T}$ vanish and we find that $\Gamma_0/\mathcal{T} = 4\pi/5\kappa_1$, as the perturbation series (4.167) indicates. However, in this case the $\lambda \to 0$ limit becomes sick because the other mode becomes unstable. This is consistent with the expectation that the non-kinetic sector should have a lower η/s as it is more strongly coupled.

Furthermore, the departure of $\Gamma_0/\mathcal{T}$ from its decoupling limit value $4\pi/5\kappa_1$ in the full calculation is found to be very small for any value of $\gamma^{1/4}\mathcal{T}$ (see the left panel of Fig. 4.25). The damping constant Γ_I of the Israel-Stewart relaxational mode is evaluated in the right panel which is indeed large for all $\gamma^{1/4}\mathcal{T}$ for the small value of λ chosen. However, it turns out that one cannot take the limit $\lambda \to 0$ for large $\gamma^{1/4}\mathcal{T}$, since Γ_I diverges at a certain value of $\gamma^{1/4}\mathcal{T}$ beyond which it turns negative, corresponding to an instability. One thus has to keep λ finite in order to decouple this mode.

Repeating the same calculation in the sound channel, we find that we indeed reproduce the bi-hydro sound sector modes and the same damping coefficient Γ_0.

A remarkable outcome from our calculations is that non-hydrodynamic observables turn out to receive mild or no non-perturbative corrections even when the hydrodynamic sector receives large qualitative and quantitative modifications.

Chapter 5

Time evolution of a toy semiholographic glasma

In the present chapter, we describe a toy model of glasma, semiholographically coupled to a black hole via a scalar operator. In Sec. 5.1, we will first describe the setup in general, discussing the details of coupling an arbitrary dimensional semiholographic scalar coupling between classical Yang-Mills and a black hole, before moving on in Sec. 5.1.1 and 5.1.2 to detail the specifics of the model that we consider. In order to simplify the simulation presented in this chapter, we will model the hard sector by a classical Yang-Mills theory in $2+1$ dimensions and the soft sector by a gravitational theory in $3+1$ dimensions (although the field theoretic dual in this case is unknown). We are confident that the qualitative behavior of the system will not change in a $3+1$ dimensional spacetime. In Sec. 5.3, we demonstrate that energy is indeed transferred from the hard sector to the soft sector via this coupling.

This chapter is based on [37].

5.1 Scalar coupling between YM and AdS

As mentioned above, we model the hard degrees of freedom by a classical Yang-Mills theory. This is in agreement with the CGC and glasma description of the early stages of the QGP [117, 118]. We extend the glasma picture by including soft degrees of freedom by including a holographic description. Practically speaking, we replace non-perturbative QCD by $\mathcal{N}=4$ super Yang-Mills theory, which at infinite coupling and a large number of colors allows for a dual description in terms of classical supergravity.

In this discussion, the number of spacetime dimensions d will be kept arbitrary, before we specify the dimension in the next section. The interaction between the hard and soft sectors is established by deforming each of the sectors with gauge independent single trace operators of the respective other.

The (coarse-grained) operators at our disposal in the effective description of the soft sector are the energy momentum tensor $\mathcal{T}^{\mu\nu}$, the glueball density operator $\mathcal{H}$, and the Pontryagin density $\mathcal{A}$, as discussed in [33]. In the present chapter, we will restrict ourselves to the coupling of the scalar operator $\mathcal{H}$ only. This is obtained from the generating functional, W, by varying with respect to the source, h, e.g.

$$\mathcal{H} = \frac{1}{\sqrt{-g}}\frac{\delta W[h]}{\delta h}, \tag{5.1}$$

where $g_{\mu\nu}$ is the metric of the spacetime. In this context, the background metric $g_{\mu\nu}$ serves as a computational device and will be set to the Minkowski metric $\eta_{\mu\nu}$ eventually. Note that a non-trivial choice for the source corresponds to a marginal deformation of the theory.

Starting from the classical Yang-Mills action, we can also easily deform the hard sector with a scalar operator by adding a source term

$$S_{\text{YM}} = -\frac{1}{4g_{\text{YM}}^2}\int \mathrm{d}^d x\sqrt{-g}\,(1+\chi(x))\,F^a_{\mu\nu}F^{a\mu\nu}, \tag{5.2}$$

with the Yang-Mills coupling constant g_{YM} and a is an $SU(N)$ color index running from 1 to N. The non-Abelian field strength in terms of the gauge field is given by $F_{\mu\nu} = \partial_\mu A_\nu - \partial_\nu A_\mu - i[A_\mu, A_\nu]$. Some observations are in order. First, we notice that this deformation amounts to locally rescaling the Yang-Mills coupling constant g_{YM}. Second, a calculation of the reponse analogous to (5.1) yields

$$\frac{1}{\sqrt{-g}}\frac{\delta S_{\text{YM}}}{\delta\chi} = -\frac{1}{4g_{\text{YM}}^2}F^a_{\mu\nu}F^{a\mu\nu}. \tag{5.3}$$

In the next step, as outlined in Chapter 3, we bring the two deformed sectors into contact by simply adding $S_{\text{YM}}[A_\mu,\chi]$ and $W[h]$ supplemented with an interaction term for the two scalar deformations

$$S = -\frac{1}{4g_{\text{YM}}^2}\int \mathrm{d}^d x\sqrt{-g}\,(1+\chi(x))\,F^a_{\mu\nu}F^{a\mu\nu} + W[h] - \frac{Q_s^d}{\beta}\int \mathrm{d}^d x\sqrt{-g}h\chi. \tag{5.4}$$

The saturation scale Q_s appears for dimensional reasons and is accompanied by a phenomenological dimensionless free parameter β, which allows for the tuning of the interaction between the two sectors.

Inspecting (5.4) immediately reveals that the two scalar fields, $\mathcal{H}$ and h, are non-dynamical, i.e. auxiliary fields. Computing their equations of motion yields

$$h = -\frac{\beta}{4Q_s^d g_{\text{YM}}^2}F^a_{\mu\nu}F^{a\mu\nu}, \qquad \chi = \frac{\beta}{Q_s^d}\mathcal{H}, \tag{5.5}$$

which indeed connects the deformations of each sector to gauge independent single trace operators of the respective other sector. After integrating out $\mathcal{H}$ and h the action becomes

$$S = -\frac{1}{4g_{\text{YM}}^2}\int \mathrm{d}^d x\sqrt{-g}F^a_{\mu\nu}F^{a\mu\nu} + W\left[-\frac{\beta}{4Q_s^d g_{\text{YM}}^2}F^a_{\mu\nu}F^{a\mu\nu}\right]. \tag{5.6}$$

This form of the action is discussed in general, including the tensor and pseudoscalar coupling channels in [33].

Let us now turn to the equations for the dynamical degrees of freedom: the gauge field A_μ and the expectation value $\mathcal{H}$. The equation of motion arising from the variation w.r.t. the gauge field reads

$$D_\mu\left[\left(1+\frac{\beta}{Q_s^d}\mathcal{H}\right)F^{a\mu\nu}\right] = 0, \tag{5.7}$$

where the gauge covariant derivative is $D_\mu = \nabla_\mu - iA^a_\mu T^a$ with ∇_μ denoting the Levi-Civita connection of the background metric $g_{\mu\nu}$.

For calculating $\mathcal{H}$ we employ the holographic dictionary, which maps the generating functional W to the $(d+1)$ dimensional classical on-shell supergravity action and operators to fields in the gravity theory satisfying asymptotically AdS boundary conditions. The relevant terms of the action for our purposes are given by the Einstein–Hilbert action with a cosmological constant coupled to a massless Klein-Gordon scalar field

$$S_{hol} = \frac{1}{2\kappa}\int \mathrm{d}^{d+1}x\sqrt{-G}\left(R - 2\Lambda - \frac{1}{2}(\nabla\phi)^2\right), \tag{5.8}$$

where $\kappa = 8\pi G$, the cosmological constant is $\Lambda = -\frac{(d-1)(d-2)}{2L^2}$ and we set the AdS radius $L = 1$. The bulk equations of motion arising from (5.8) are

$$\begin{aligned} G^{MN}\nabla_M\nabla_N\phi &= 0\,, \\ R_{MN} - \frac{1}{2}RG_{MN} - \Lambda G_{MN} &= \kappa(\nabla_M\phi\nabla_N\phi - \frac{1}{2}G_{MN}(\nabla\phi)^2)\,. \end{aligned} \tag{5.9}$$

In Fefferman-Graham coordinates, where $\rho = 0$ denotes the location of the conformal boundary of the (d+1) dimensional spacetime, the metric and the scalar field have the following asymptotic expansions [119]:

$$G_{\mu\nu} = \frac{1}{\rho}\left(g_{(0)\mu\nu} + \ldots + \rho^{d/2}g_{(d)\mu\nu} + \mathcal{O}(\rho^{d/2}\log(\rho))\right), \tag{5.10}$$

$$\phi = \phi_{(0)} + \ldots + \rho^{d/2}\phi_{(d)} + \mathcal{O}(\rho^{d/2}\log(\rho)), \tag{5.11}$$

from which we can read off the expectation values

$$\mathcal{T}_{\mu\nu} = \frac{d}{\kappa}g_{(d)\mu\nu} + X_{\mu\nu}, \tag{5.12}$$

$$\mathcal{H} = \frac{d}{\kappa}\phi_{(d)} + \psi_{(d)}, \tag{5.13}$$

where $X_{\mu\nu}$ and $\psi_{(d)}$ are local functionals of the boundary sources. The leading coefficient in the metric expansion is fixed by the background metric, i.e. $g_{(0)\mu\nu} = g_{\mu\nu}$. The non-normalizable mode of the scalar field $\phi_{(0)}$ is dual to the source in the generating functional W, which in our setup is related to the Lagrange density of the classical Yang-Mills sector

$$\phi_{(0)} = -\frac{\beta}{4Q_s^d g_{\mathrm{YM}}^2}F^a_{\mu\nu}F^{a\mu\nu}\,. \tag{5.14}$$

We conclude this section by briefly discussing the energy momentum tensor of our semiholographic model

$$T^{\mu\nu} = t^{\mu\nu}_{\mathrm{YM}} + \mathcal{T}^{\mu\nu} + t^{\mu\nu}_{\mathrm{int}} \tag{5.15}$$

$$= \frac{1}{g_{\mathrm{YM}}^2}\left(1 + \frac{\beta}{Q_s^d}\mathcal{H}\right)\left(F^{\mu\alpha}F^{\nu}{}_{\alpha} - \frac{1}{4}g^{\mu\nu}F_{\alpha\beta}F^{\alpha\beta}\right) + \mathcal{T}^{\mu\nu} - h\mathcal{H}g^{\mu\nu}\,. \tag{5.16}$$

Each of the three contributions is obtained by the variation of the corresponding term in (5.4) with respect to $g_{\mu\nu}$ and employing Eqs. (5.5). We will refer to $t^{\mu\nu}_{\mathrm{YM}}$ as the Yang-Mills energy momentum tensor, $\mathcal{T}^{\mu\nu}$ as the holographic energy momentum tensor (computed in (5.12)) and $t^{\mu\nu}_{\mathrm{int}}$ as the interaction energy momentum tensor. Note that this expression defines the interaction energy in a different way than in [33], where the terms in $t^{\mu\nu}_{\mathrm{YM}}$ proportional to $\mathcal{H}$ were assigned to the interaction energy momentum tensor. The assignment of the contributions to the different sectors is somewhat arbitrary. The advantage of the above form is that $t^{\mu\nu}_{\mathrm{int}}$ only consists of the deformation terms, which in our case are the two simplest gauge independent single trace scalar operators.

The conservation of the energy momentum tensor $\nabla_\mu T^{\mu\nu} = 0$ is implied by separate Ward identities in the respective sectors of our model

$$\nabla_\mu \mathcal{T}^{\mu\nu} = \mathcal{H}\partial^\nu h, \tag{5.17}$$

$$\nabla_\mu t^{\mu\nu}_{\text{YM}} = \frac{Q_s^d}{\beta} h \partial^\nu \left(1 + \frac{\beta}{Q_s^d}\mathcal{H}\right). \tag{5.18}$$

The sum of the terms on the right hand side is precisely $-\nabla_\mu t^{\mu\nu}_{\text{int}}$. Furthermore, we also want to mention the trace anomalies of the individual sectors, which read

$$g_{\mu\nu}\mathcal{T}^{\mu\nu} = (d-4)\mathcal{H}h + A, \tag{5.19}$$

$$g_{\mu\nu}t^{\mu\nu}_{\text{YM}} = (d-4)\left(1 + \frac{\beta}{Q_s^d}\mathcal{H}\right)\frac{Q_s^d}{\beta}h, \tag{5.20}$$

where A denotes the holographic conformal anomaly, which is a local functional of the boundary sources and vanishes for the case considered below. Note that in general even if both $\mathcal{T}^{\mu\nu}$ and $t^{\mu\nu}_{\text{YM}}$ are tracefree, eg. for $g_{\mu\nu} = \eta_{\mu\nu}$ and $d = 4$, the full system is not conformal due to the contribution $g_{\mu\nu}t^{\mu\nu}_{\text{int}} = -d\,\mathcal{H}h$. This is a similar situation as discussed in the bi-hydrodynamics case with the tensor coupling in Chapter 4, where the two conformal subsystems coupled semi-holographically led to a full system which was not conformal generally.

5.1.1 Classical Yang-Mills sector

For the numerics presented in the next section, we will work in a $d = 2+1$ dimensional spacetime with $g_{\mu\nu} = \eta_{\mu\nu}$ and restrict to isotropic homogeneous SU(2) color gauge fields in temporal gauge, $A_0^a = 0, A_0^3 = 0$ with $a = 1, 2$. To further simplify this toy model as far as possible, we make $t^{\mu\nu}_{\text{YM}}$ diagonal by assuming color-space locking, $A_i^a = \delta_i^a f(t)$ and $A_i^3 = 0$ with $i = 1, 2$. The single remaining degree of freedom $f(t)$ satisfies an equation for an anharmonic oscillator with time dependent damping obtained from (5.7)[1]

$$f''(t) + f(t)^3 = f'(t)\frac{\beta\mathcal{H}'}{1 + \frac{\beta}{Q_s^3}\mathcal{H}}. \tag{5.21}$$

The energy density and the pressure are

$$\varepsilon = \frac{1 + \frac{\beta}{Q_s^3}\mathcal{H}}{2g_{\text{YM}}^2}(2f'(t)^2 + f(t)^4), \quad p = \frac{1 + \frac{\beta}{Q_s^3}\mathcal{H}}{2g_{\text{YM}}^2}f(t)^4. \tag{5.22}$$

The source for the dilaton in terms of the YM fields is given by (5.5)

$$h = \frac{\beta}{2Q_s^3 g_{\text{YM}}^2}(2f'^2 - f^4). \tag{5.23}$$

5.1.2 Holographic sector

To be consistent with the YM sector we also impose homogeneity and isotropy in the spatial field theory directions of the bulk theory of the holographic sector. We make the following ansätze for the metric and the massless scalar field in in-going Eddington-Finkelstein coordinates

$$ds^2 = -A(r,v)dv^2 + 2dvdr + S^2(r,v)(dx_1^2 + dx_2^2), \quad \phi = \phi(r,v). \tag{5.24}$$

[1] Eq. (5.21) is an unforced damped nonlinear Duffing equation. The latter appears in many contexts and has been extensively studied [120, 121].

We fix the residual gauge freedom $r \to r + \xi(v)$ of the metric by setting $\xi = 0$. The equations of motion (5.9) then take the following form[2]

$$S'' = -\frac{\kappa}{4} S \left(\phi'\right)^2 , \tag{5.25}$$

$$\dot{S}' = \frac{3S}{2} - \frac{\dot{S}S'}{S} , \tag{5.26}$$

$$\dot{\phi}' = -\frac{\dot{S}\phi'}{S} - \frac{\dot{\phi}S'}{S} , \tag{5.27}$$

$$A'' = \frac{4\dot{S}S'}{S^2} - \kappa\dot{\phi}\phi' , \tag{5.28}$$

$$\ddot{S} = \frac{\dot{S}A'}{2} - \frac{\kappa\dot{\phi}^2 S}{4} , \tag{5.29}$$

where prime denotes radial derivatives $f' = \partial_r f$ and the dot-derivative is defined as $\dot{f} = \partial_v f - \frac{1}{2}A(r,v)\partial_r f$. Near the boundary, $r = \infty$, solutions to these equations can be expressed as power series in r

$$A(r,v) = r^2 \sum_{n=0}^{\infty} a_n(v) r^{-n} , \tag{5.30}$$

$$S(r,v) = r \sum_{n=0}^{\infty} s_n(v) r^{-n} , \tag{5.31}$$

$$\phi(r,v) = \kappa \sum_{n=0}^{\infty} \phi_n(v) r^{-n} . \tag{5.32}$$

Fixing the conformal boundary metric to Minkowski $ds_b^2 = r^2 \eta_{\mu\nu} dx^\mu dx^\nu$ determines the leading coefficients $a_0 = 1$ and $s_0 = 1$, and the gauge choice $\xi = 0$ determines the subleading coefficient $a_1 = 0$. Solving the equations order by order in r gives

$$A(r,v) = r^2 - \frac{3}{4}\phi_0'(v)^2 + a_3(v)\frac{1}{r} + \mathcal{O}(r^{-2}) , \tag{5.33}$$

$$S(r,v) = r - \frac{1}{8}\phi_0'(v)^2 \frac{1}{r} + \frac{1}{384}\left(\phi_0'(v)^4 - 48\phi_3(v)\phi_0'(v)\right)\frac{1}{r^3} + \mathcal{O}(r^{-4}) , \tag{5.34}$$

$$\phi(r,v) = \phi_0(v) + \phi_0'(v)\frac{1}{r} + \phi_3(v)\frac{1}{r^3} + \mathcal{O}(r^{-4}) , \tag{5.35}$$

where the normalizable modes $\phi_3(v)$ and $a_3(v)$ remain undetermined in this procedure and need to be extracted from the full bulk solution. Furthermore one obtains the relation

$$a_3'(v) = \frac{1}{8}\left(12\phi_3\phi_0'(v) - 3\phi_0'(v)^4 + 4\phi_0'''(v)\phi_0'(v)\right) . \tag{5.36}$$

In order to identify the expectation values of the energy momentum tensor and the scalar operator it is convenient to asymptotically transform the series solutions (5.33) and (5.35) to Fefferman-Graham coordinates (5.10). The relevant coefficients in the Fefferman-Graham expansion in terms of their Eddington-Finkelstein counterparts are given by

$$\phi_{(0)} = \phi_0, \quad \phi_{(3)} = \phi_3 + \frac{1}{3}\phi_0''' - \frac{1}{4}(\phi_0')^3, \quad g_{(3)ij} = \frac{1}{3}\mathrm{diag}(-2a_3, a_3, a_3) . \tag{5.37}$$

[2]It is interesting to note that these equations are equivalent to those of a homogeneous but anisotropic black brane without scalar matter.

The expectation values of the energy momentum tensor and the scalar operator are then given by

$$\mathcal{T}_{\mu\nu} = \frac{3}{\kappa} g_{(3)\mu\nu} = \frac{1}{\kappa}\mathrm{diag}(-2a_3, -a_3, -a_3)\,, \tag{5.38}$$

$$\langle \mathcal{O} \rangle \equiv \mathcal{H} = \frac{3}{\kappa}\phi_{(3)} = \frac{3}{\kappa}(\phi_3 + \frac{1}{3}\phi_0''' - \frac{1}{4}(\phi_0')^3)\,. \tag{5.39}$$

Evaluating the holographic Ward identity (5.17) reproduces the relation (5.36) we find from solving the near boundary expansion

$$({g_{(3)0}}^0)' = \phi_{(3)}\phi_{(0)}\,. \tag{5.40}$$

5.2 The iterative procedure

In this section we describe how we obtain solutions for given values for the couplings β and g_{YM} for the time evolution problem of the coupled system (5.21), (5.25)–(5.29), given initial energies in the Yang-Mills sector (ϵ_{YM}^{ini}) and the holographic sector (ϵ_{hol}^{ini}).

We proceed to solve the coupled system in an iterative manner, which is summarized in Fig. 5.1. We initialize the iterative loop with an initial guess for the gauge field, $f(t)$, which we get from solving the uncoupled YM equation (5.21) with $\beta = 0$:

$$f(t)'' + 2f(t)^3 = 0\,. \tag{5.41}$$

This is just the equation for an anharmonic oscillator, with solutions given in terms of the Jacobi elliptic function

$$f(t) = \pm\sqrt[4]{2C}\,\mathrm{sn}\left(\sqrt[4]{\frac{C}{2}}(t-t_0)\middle| -1\right)\,, \tag{5.42}$$

where the integration constant $C/g_{\mathrm{YM}}^2 = \epsilon_{YM}^{ini}$ can be identified via (5.22) with the initial energy in the YM-sector. Without loss of generality we set $t_0 = 0$, which corresponds to our initial time.

Using this initial guess (5.42) with a particular value for β, we compute the time dependent boundary source for the gravity system $\phi_{(0)}(t) = h(t)$ via (5.23). This serves as the input for the gravity system, which we can now evolve using the spectral method as in [122], using 20 Chebyshev grid points in the holographic direction and a 4^{th} order Adams-Bashforth time stepping algorithm with step size $\Delta t = 1/800$. In order to get a well defined initial value problem resulting in a stable time evolution, it is necessary to choose a computational domain in the bulk direction that contains the apparent horizon r_{ah}, defined by $\dot{S}(t,r)|_{r_{ah}} = 0$, on the initial slice.[3] Initial data for the gravity system are fixed by $a_3(t=0) = -\epsilon_{hol}^{ini}/2$ and a radial profile for the scalar field which evaluates to $\phi(r, t=0) = -\beta\epsilon_{YM}^{ini}$ for the initial guess (5.42) in combination with the Ward identy (5.40). To measure the accuracy of our numerical scheme we monitor in each time step the violation of the constraint equation (5.29) and the Ward identity (5.40) whose absolute values we demand to be smaller than 10^{-6}. From the solution of the gravity problem we extract, via (5.38) and (5.39), the time evolution of $\mathcal{T}_{\mu\nu}(t)$ and $\mathcal{H}(t)$ respectively.

[3] Note that other authors [58, 63, 123] employ the gauge function ξ to fix the apparent horizon to a constant value in the radial direction which is then used to bound the computational domain.

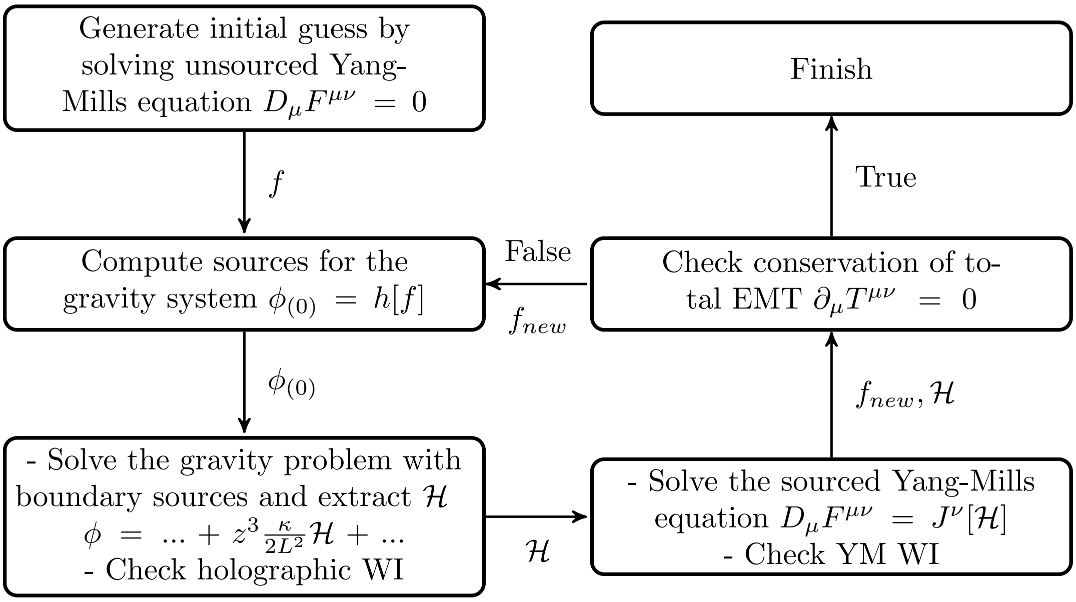

Figure 5.1: Flow chart of the iterative procedure explained in the main text.

We can now feed in $\mathcal{H}(t)$ into the Yang-Mills equation (5.21) and solve for the new $f(t)$ with the Mathematica routine NDSolve, with the same initial conditions as in the initial guess (5.42). This completes the first iteration.

To check how well the iterative procedure is working, we compute the total energy momentum tensor (5.16) with the new $f(t)$ and $\mathcal{H}(t)$ and check to see if it is conserved in time up to $\mathcal{O}(10^{-5})$ or better. If this is the case, we stop the iteration. If not, we proceed to iterate again.

We usually find that one iteration is not enough. At this point, we do not have an analytic guess for $f(t)$, which introduces numerical noise into the gravity system via the boundary source (5.23). This problem can be somewhat alleviated by implementing a low-pass filter on $f(t)$ before we feed it to the gravity code. We use the Mathematica routine LowpassFilter as our filtering tool and choose a cutoff frequency of 0.1 and filter kernel of length 1. In Appendix E we discuss the procedure in more detail.

5.3 Energy transfer from the hard to the soft sector

To obtain results, we set the Yang-Mills energy density to be $\epsilon_{\text{YM}}/Q_s^3 = 1$, the initial energy of the strongly coupled sector to be $\epsilon_{\text{hol}}/Q_s^3 = 0.004$ and the Yang-Mills coupling as $g_{\text{YM}}/\sqrt{Q_s} = 1$. As mentioned in the previous section, we stop the iterative procedure when we have a constant total energy of the system. The left panel in Fig. 5.2 shows the total energy density for each iteration for $\beta = 0.01$. Each iteration improves the total energy conservation. However, with each iteration the numerical errors in the solution of the respective sub-sectors accumulate, see Appendix E. We stop the procedure after four iterations in this case, since it provides the optimal trade off between obtaining sufficiently well-behaved total energy on the one hand and consistent sub-sectors on the other hand.

We plot the numerical solution for the gauge field degree of freedom, $f(t)$, in the right panel of Fig. 5.2 for three different values of β. We can already see that as time goes on, the solution

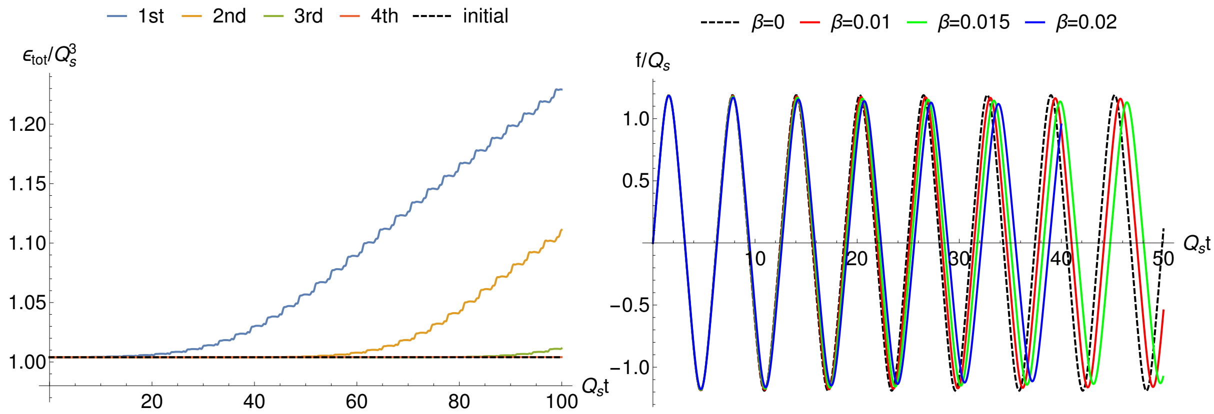

Figure 5.2: Left: Total energy for $\beta = 0.01$ as function of time for subsequent iterations. Right: The YM gauge field, $f(t)$.

decreases in amplitude and in frequency, indicating that the gauge field is losing energy. The stronger the coupling, β, the more rapidly the gauge field loses energy.

In top panel of Fig. 5.3, we see that indeed the energy is decreasing in the YM sector. In contrast to this, the holographic sector is gaining energy almost monotonically as seen in the middle panel of Fig. 5.3. We find that this behavior is independent of the sign of β. The interaction energy, dispayed in the bottom panel of Fig. 5.3, has an oscillatory behavior around zero, while decaying over time with decreasing frequency. The energy transfer is expected to continue until the YM sector is empty, i.e. when the source $h(t)$ vanishes.

Motivated by the CGC picture of heavy ion collisions, we chose the initial conditions such that the YM sector carries all of the energy initially in the form of highly overoccupied gluons at the saturation scale, while the holographic IR sector is initially empty and thus represented by pure AdS. However, due to numerical issues, we needed to start the simulation with a small regulator black hole in the gravitational bulk. To understand the role of this regulator, we plot in Fig. 5.4 the gain in the holographic energy for different initial conditions for fixed initial YM energy. Provided $\iota := \epsilon_{\text{hol}}^{\text{ini}}/\epsilon_{\text{YM}}^{\text{ini}} \ll 1$, we see that the results are fairly independent of the regulator and thus our choice $\iota = 0.004$ used for the plots is reasonable.

It is also worthwhile to discuss the role of entropy in our present setup. The hard sector consists only of a single dynamic degree of freedom, $f(t)$, which means that the associated entropy is zero. In the holographic sector, the situation is different. The area of the apparent horizon, shown in the left panel of Fig. 5.5, provides a commonly used proxy for entropy, which we use as estimate for the lower bound for the entropy in the combined system. We find that the entropy growth increases with increasing β, as can be seen in the right plot of Fig. 5.5. Furthermore, we numerically checked that the effective apparent horizon entropy is monotonically increasing with time in all our simulations.

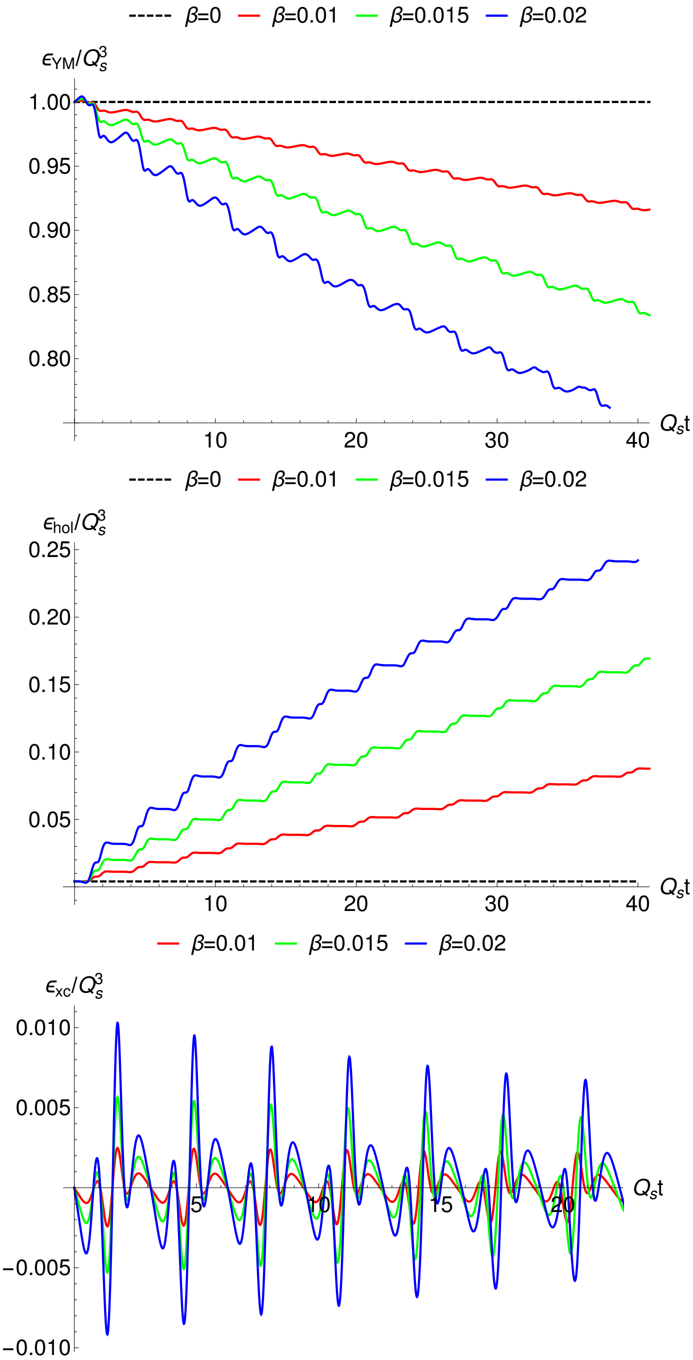

Figure 5.3: Upper: The energy density of the YM sector against time. Middle: The energy density of the holographic sector. Lower: The exchange energy as a function of time.

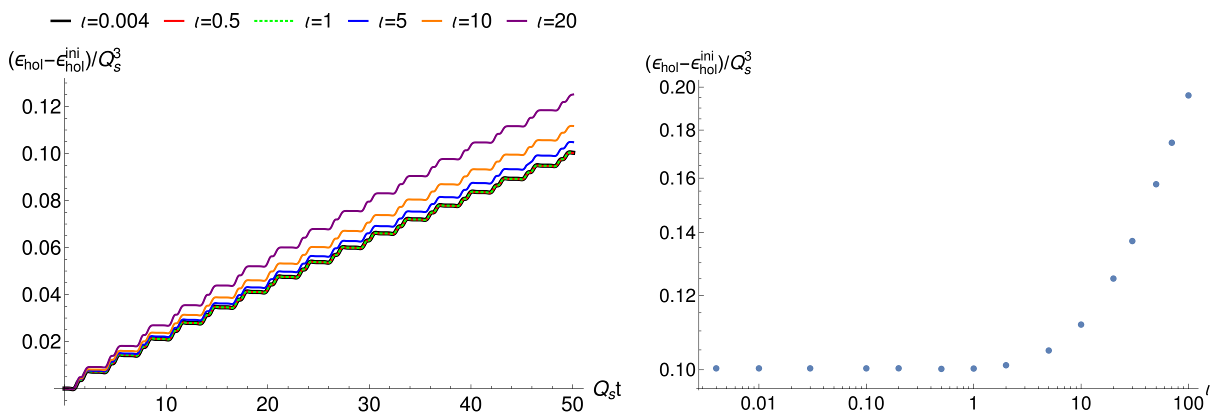

Figure 5.4: Left: The time evolution of the gain in ϵ_{hol} for different initial conditions $\epsilon_{\text{hol}}^{\text{ini}}$ with $\epsilon_{\text{YM}}^{\text{ini}}/Q_s^3 = 1$ and $\beta = 0.01$. The curves for $\iota \equiv \epsilon_{\text{hol}}^{\text{ini}}/\epsilon_{\text{YM}}^{\text{ini}} \leq 1$ lie on top of each other. Right: The gain in ϵ_{hol} at $Q_s t = 50$ as a function of ι.

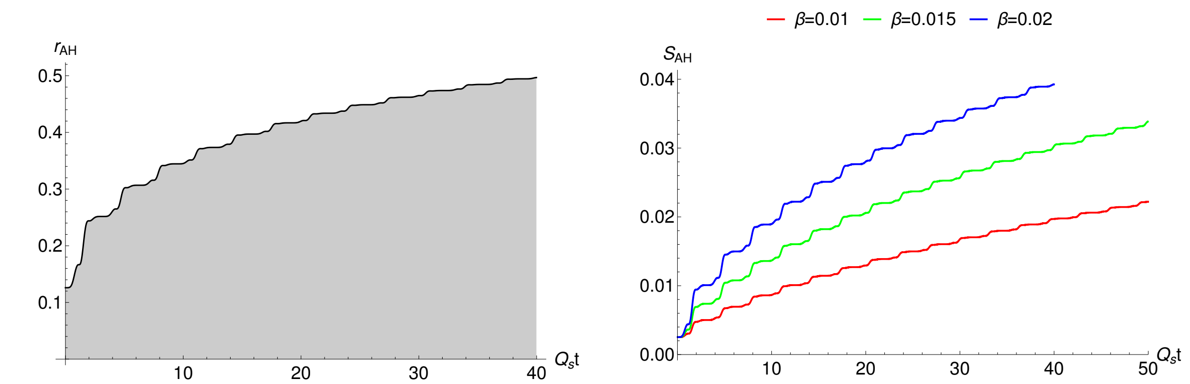

Figure 5.5: Left: Radial position of the apparent horizon for $\beta = 0.02$. The gray region indicates the interior of the black hole. Right: Entropy in the holographic sector computed from the corresponding areas of the apparent horizons.

Chapter 6

Semiholography in $NAdS_2$

In this chapter, we change gears and discuss a semiholographic model of impurities for low dimensional systems. As outlined in the Introduction, from the point of view of phenomenological applications, the semiholography approach gives us a flexible way to apply holography to various setups, where the UV-complete description is not relevant [16, 124]. It is from this perspective that we apply the semiholographic approach to study confined strongly interacting impurities.

In particular, the nearly-AdS_2 (or $NAdS_2$) holographic subsystem that we will consider [125–128] is a useful arena to explore fundamental questions. It can be used to probe the AdS/CFT correspondence, given that some possible dual systems, like the Sachdev-Ye-Kitaev (SYK) model, can also be solved in the large N limit [129, 130] (see also [131–133]). It can also pave the way for a better understanding of real-time holography, potentially leading to new insights on quantum many-body systems (especially those which are maximally chaotic) and on the black hole information loss paradox. The latter could be approached via a solvable toy model of real-time black hole evaporation. In order to accommodate these applications, $NAdS_2$ holography would need to be extended to include additional propagating modes, i.e. bulk fields, which we do here in the classical regime in real time.

In the model described in this chapter, the $NAdS_2$ holographic sector captures the dual infrared dynamics of many-body interactions localized at the origin, where the impurities are confined. The motion in space of an impurity can be thought of as a deformation of this $0+1-$dimensional $NAdS_2$ holographic theory with the time-dependent position of the impurity representing a self-consistent external source of an irrelevant operator with a dynamically generated expectation value. The displaced impurity follows simple Newtonian dynamics under the influence of the force generated by its coupling to the $NAdS_2$ – the dual irrelevant holographic operator now generates the tension of the confining force. Since the $NAdS_2$ holographic sector is an infrared conformal theory, it should be deformed only via an irrelevant operator. The semiholographic model probes the dynamics at intermediate energy scales phenomenologically, such that the total energy of the system is always conserved. We study the exact time-dependent solutions of the full system in this model.

The gravitational description for $NAdS_2$ holography is two-dimensional Jackiw-Teitelboim (JT) gravity with non-conformal matter [134–136]. A key feature of the JT model is that the metric is always locally AdS_2, due to the non-propagating dilaton field. Acting like a Lagrange multiplier, the dilaton's equation of motion enforces the Ricci scalar to be a constant, as it is not coupled to matter. Moreover, the dilaton's boundary condition generates non-trivial states in the dual theory even in the absence of matter, which can be characterized by timereparametrizations just like in the SYK model. It should be noted that since the dilaton is not coupled to matter, this form of JT gravity cannot be lifted to a higher dimensional setup, as we expect that from a higher dimensional compactification that the dilaton would couple to matter, see e.g. [137–141].

As a warm-up, we turn our attention first to the pure holographic setup and explore boundary quenches. Unsurprisingly, we find that the mass of the pre-existing black hole always increases. The situation is remarkably different in our semiholographic model, where we find that the pre-existing black hole is always completely depleted of its mass at long time. This behavior is the opposite of what we find in higher dimensional semiholographic setups in the presence of scalar mutual couplings, as was the case in Chapter 5. A similar phenomenon of disappearance of horizon in the bulk in nearly AdS_2 setups has been found in [142]. The explanation proposed for this result also works naturally in our case. Furthermore, at late time the solution does not approach the vacuum as far as the radial profile of the dilaton is concerned. At a fixed value of the mutual coupling, we find a non-equilibrium phase transition as we increase the initial velocity of the impurity.

To do this, we introduce in Sec. 6.1 Jackiw-Teitelboim (JT) gravity coupled to matter and its holographic interpretation. In Sec. 6.2, we describe the algorithm used to find explicit time-dependent solutions in JT gravity and study quenches. In Sec. 6.3, we detail the semiholographic model of impurities and study its solutions.

The bulk of this chapter is based on work discussed in [143].

6.1 $NAdS_2$

6.1.1 Bulk equations of motion

The simplest example of a non-trivial two-dimensional pure gravity is the Jackiw-Teitelboim model [134–136]. The general version of the action which is suitable for taking the large N type limit in the dual theory is

$$S = \frac{1}{16\pi G}\left[\int \mathrm{d}^2x\sqrt{-g}\Phi\left(R+\frac{2}{L^2}\right)+S_{\text{matter}}[g,\chi]\right]+\frac{1}{8\pi G}\int \mathrm{d}u\,\sqrt{-h}\,\Phi_{\mathrm{b}}K, \tag{6.1}$$

where G is Newton's constant, Φ is the dilaton field with boundary value Φ_b, χ are matter fields and the final term is the Gibbons-Hawking-York counterterm. Note that the u appearing in the final term is the *boundary time*, i.e. the time an observer on the boundary would measure.

We can learn a lot about this theory by considering the equations of motion. We see that the dilaton field Φ does *not* couple to matter, which means that if we vary the action w.r.t. Φ, we simply obtain

$$R+\frac{2}{L^2}=0. \tag{6.2}$$

In other words, the bulk metric, $g_{\mu\nu}$, is always *locally* pure AdS_2. Furthermore, variation w.r.t. the bulk metric leads us to

$$T^{\Phi}_{\mu\nu}+T_{\mu\nu}=0, \tag{6.3}$$

where

$$T^{\Phi}_{\mu\nu}\equiv\nabla_\mu\nabla_\nu\Phi-g_{\mu\nu}\nabla^2\Phi+\frac{1}{L^2}g_{\mu\nu}\Phi,\qquad\text{and}\qquad T_{\mu\nu}=-\frac{2}{\sqrt{-g}}\frac{\delta S_{\text{matter}}}{\delta g^{\mu\nu}}. \tag{6.4}$$

Note that the Bianchi identity is satisfied when $R=-2/l^2$. Therefore, the equation of motion (6.3) is indeed consistent in a locally AdS_2 background spacetime. We set the AdS radius $L=1$.

We have yet to specify the matter action. In fact, we will avoid doing so until Sec. 6.1.3 to keep the discussion general. In doing so, we will *not* assume that the matter sector is conformal, thus generalizing the results in [125, 128].

To proceed, we make use of the local conservation law:

$$\nabla_\mu T^{\mu\nu} = 0, \tag{6.5}$$

where the metric is locally AdS_2. We adopt Fefferman-Graham coordinates:

$$\mathrm{d}s^2 = \frac{1}{z^2}\left(-\mathrm{d}t^2 + \mathrm{d}z^2\right), \tag{6.6}$$

in which (6.5) reads

$$\partial_z T_{zt} = \partial_t T_{tt}, \quad \partial_z(zT_{zz}) = T_{tt} + z\,\partial_t T_{zt}. \tag{6.7}$$

The general form of $T_{\mu\nu}$ is

$$T_{zt}(z,t) = F_\epsilon(t) + \int_\epsilon^z \mathrm{d}z_1\ \partial_t T_{tt}(z_1,t), \tag{6.8}$$

$$\begin{aligned} T_{zz}(z,t) = {} & \frac{G_\epsilon(t)}{z} + \frac{z}{2}\partial_t F_\epsilon(t) + \frac{1}{z}\int_\epsilon^z \mathrm{d}z_1\ T_{tt}(z_1,t) \\ & + \frac{z}{2}\int_\epsilon^z \mathrm{d}z_1\ \partial_t^2 T_{tt}(z_1,t) - \frac{1}{2z}\int_\epsilon^z \mathrm{d}z_1\ \partial_t^2 T_{tt}(z_1,t) z_1^2, \end{aligned} \tag{6.9}$$

with

$$F_\epsilon(t) = T_{zt}(\epsilon,t), \tag{6.10}$$

$$G_\epsilon(t) = \epsilon T_{zz}(\epsilon,t) - \frac{\epsilon^2}{2}\partial_t T_{zt}(\epsilon,t), \tag{6.11}$$

where ϵ is an arbitrary radial cut-off, which we will eventually take to the *boundary* at $z = 0$. The boundary conditions for the bulk matter fields determine $F_\epsilon(t)$ and $G_\epsilon(t)$. Thus, the components of the energy momentum tensor are entirely determined in terms of T_{tt}.

Explicitly, the components of (6.3) are

$$\partial_z^2\Phi + \frac{\partial_z\Phi}{z} - \frac{\Phi}{z^2} = -T_{tt}, \tag{6.12}$$

$$\partial_z\partial_t\Phi + \frac{\partial_t\Phi}{z} = -T_{zt}, \tag{6.13}$$

$$\partial_t^2\Phi + \frac{\partial_z\Phi}{z} + \frac{\Phi}{z^2} = -T_{zz} \tag{6.14}$$

in the Fefferman-Graham coordinates. We see that (6.12) involves only radial derivatives, which determines the radial profile of Φ. The other two equations are simply time-dependent equations determining data at the cut-off $z = \epsilon$. The most general solution of (6.12) can be parameterized as

$$\Phi(z,t) = \frac{\alpha_\epsilon(t)}{z} + \beta_\epsilon(t)z - \frac{z}{2}\int_\epsilon^z \mathrm{d}z_1\ T_{tt}(z_1,t) + \frac{1}{2z}\int_\epsilon^z \mathrm{d}z_1\ T_{tt}(z_1,t)z_1^2. \tag{6.15}$$

Substituting the above into (6.13) and (6.14), and also utilizing (6.8) and (6.9) we obtain

$$2\partial_t\beta_\epsilon(t) + F_\epsilon(t) = 0, \tag{6.16}$$

$$\partial_t^2\alpha_\epsilon(t) + 2\beta_\epsilon(t) + G_\epsilon(t) = 0. \tag{6.17}$$

As claimed, these determine the two time-dependent functions in (6.15) and thus the data on the cut-off. Finally, with (6.10) and (6.11), we obtain the following useful form of these constraints:

$$\partial_t \beta_\epsilon(t) = -\frac{1}{2} T_{zt}(\epsilon, t), \tag{6.18}$$

$$\partial_t^3 \alpha_\epsilon(t) = T_{zt}(\epsilon, t) + \frac{\epsilon^2}{2} \partial_t^2 T_{zt}(\epsilon, t) - \epsilon\, \partial_t T_{zz}(\epsilon, t). \tag{6.19}$$

Note that (6.16) and (6.17) are equivalent to the above only if we choose appropriate integration constants in $\alpha_\epsilon(t)$. We can readily address this issue if we use the following integral forms for $\alpha_\epsilon(t)$ and $\beta_\epsilon(t)$:

$$\beta_\epsilon(t) = -C_\epsilon - \frac{1}{2} \int_{-\infty}^{t} \mathrm{d}t_1 T_{zt}(\epsilon, t_1), \tag{6.20}$$

$$\begin{aligned} \alpha_\epsilon(t) &= A_\epsilon + B_\epsilon t + C_\epsilon t^2 \\ &\quad + \int_{-\infty}^{t} \mathrm{d}t_1 \int_{-\infty}^{t_1} \mathrm{d}t_2 \int_{-\infty}^{t_2} \mathrm{d}t_3 \left[T_{zt}(\epsilon, t_3) - \epsilon\, \partial_t T_{zz}(\epsilon, t_3) + \frac{\epsilon^2}{2} \partial_t^2 T_{zt}(\epsilon, t_3) \right]. \end{aligned} \tag{6.21}$$

Above A_ϵ, B_ϵ and C_ϵ are arbitrary integration constants. These expressions together with (6.15) thus completely specify Φ in the presence of bulk matter.

6.1.2 Holographic interpretation

The holographic dictionary for the JT model has been established in [125–128] with holographic renormalization established in [144–146]. In general, it is necessary to establish a cut-off, such that the dual quantum theory lives on an appropriate slice, $z = \epsilon f(t)$, which should be determined self-consistently from the EOM. The dimensionful parameter ϵ is related to the UV cut-off of the dual theory and as such is an external parameter. Under certain circumstances when the matter sector satifies certain conditions, we can take the limit $\epsilon \to 0$ and the trajectory z coincides with the boundary at $z = 0$. In this happy situation, the dual quantum theory is UV complete.[1]

We first work in the latter case, when the limit $\epsilon \to 0$ can be taken. It is natural to impose that background metric for the dual quantum theory is $\mathrm{d}s^2 = -\mathrm{d}u^2$. Let us parametrize bulk coordinates via the boundary time $z(u)$ and $t(u)$, which we use to describe the cut-off trajectory. The holographic dictionary then implies that the induced metric on the cut-off should be

$$h_{tt}(z(u), t(u)) = -\frac{1}{\epsilon^2}. \tag{6.22}$$

To achieve this, we require that

$$z(u) = \epsilon t'(u) + \mathcal{O}(\epsilon^2), \tag{6.23}$$

where the prime denotes differentiation w.r.t. u. We can determine the function $t(u)$ by the boundary condition on Φ. The key to obtain $SL(2, R)$ symmetry in the IR is to impose the boundary condition where the value of Φ on the cut-off trajectory satisfies

$$\Phi_{\mathrm{b}}(u) = \Phi(z(u), t(u)) = \frac{\phi_r(u)}{\epsilon}, \tag{6.24}$$

[1] This statement is true strictly in the large N limit only where the classical gravity approximation is valid. In such cases however, the theory is not actually embeddable in a higher dimensional holographic theory as discussed before. Nevertheless, the presence of UV completion for a large range of irrelevant deformations should not surprise us because the dual quantum theory lives in $0 + 1$-D.

where $\phi_r(u)$ is an arbitrary function, which we will set to a constant and refer to it by $\overline{\phi}_r$ following [127].

We will see later that for well behaved matter sector where we can take the limit $\epsilon \to 0$, the most singular term in (6.15) is indeed z^{-1} and its coefficient is

$$\alpha_0(t) = \lim_{\epsilon \to 0} \alpha_\epsilon(t). \tag{6.25}$$

Then it follows from (6.15), (6.23) and (6.24) that

$$\alpha_\epsilon(t(u)) = \overline{\phi}_r t'(u) + \mathcal{O}(\epsilon^\gamma) \quad \text{with} \quad \gamma > 0, \quad \text{i.e.} \quad \alpha_0(t(u)) = \overline{\phi}_r t'(u). \tag{6.26}$$

As an example, the subleading power, γ, is $1/2$ in presence of a minimally coupled massive free bulk scalar field with $m^2 = 5/16$.

Clearly, the function $t(u)$, which reparameterizes the boundary time, captures the dynamics of gravity. It should be determined from the bulk equations of motion. To see this, we consider the on-shell action of the pure gravity sector. First, we compute the extrinsic curvature K of the cut-off trajectory $\{\gamma(u) : (z(u) = \epsilon t'(u), t(u))\}$. The result is

$$K = \frac{1 - \epsilon^2 \frac{t'''(u)}{t'(u)}}{\left(1 - \epsilon^2 \frac{t''(u)^2}{t'(u)^2}\right)^{\frac{3}{2}}} = 1 - Sch(t,u)\epsilon^2 + \mathcal{O}(\epsilon^4).$$

The on-shell action of the pure gravity sector is then

$$\begin{aligned} S^{\text{grav}}_{\text{on-shell}} &= \frac{1}{8\pi G} \int \mathrm{d}u \sqrt{-h}\ \Phi_{\mathrm{b}} K = \frac{1}{8\pi G} \int \mathrm{d}u \frac{1}{\epsilon} \frac{\overline{\phi}_r}{\epsilon} K \\ &= \frac{\overline{\phi}_r}{8\pi G} \int \mathrm{d}u \left(\frac{1}{\epsilon^2} + \text{other singular terms} - Sch(t,u) + \cdots \right), \end{aligned} \tag{6.27}$$

where

$$Sch(t,u) = \frac{t'''(u)}{t'(u)} - \frac{3}{2} \frac{t''(u)^2}{t'(u)^2} \tag{6.28}$$

is the Schwarzian derivative [147]. The higher order terms vanish in the limit $\epsilon \to 0$. The ε-divergent terms, such as the ϵ^{-2} and divergences arising from the matter sector, e.g. one proportional to $\epsilon^{-3/2}$ which occurs in the presence of a minimally coupled free bulk scalar field with $m^2 = 5/16$, can be subtracted away by appropriate local counterterms to render the limit $\epsilon \to 0$ finite [144, 145]. We emphasize that new singular terms at subleading orders in ϵ can appear in the presence of bulk matter. After adding the counterterms and taking the $\epsilon \to 0$ limit, we obtain

$$S^{\text{grav}}_{\text{on-shell}} = \frac{\overline{\phi}_r}{16\pi G} \int \mathrm{d}u \ (-2\, Sch(t,u)), \tag{6.29}$$

which gives part of the action for the variable $t(u)$ that determines the cut-off trajectory.

This equation for $t(u)$ can always be obtained from the renormalized on-shell action. However, equivalently assuming that the limit $\epsilon \to 0$ exists we will be able to also obtain it from the constraint (6.19) rather easily. This will be the topic of the next subsection.

6.1.3 Time-reparametrization at the boundary

We now work in the limit of $\epsilon \to 0$. We return to (6.26) and differentiate both sides three times w.r.t. t to find

$$\dddot{\alpha}_0 = \overline{\phi}_r \frac{(Sch(t(u),u))'}{t'(u)^2}, \tag{6.30}$$

where the dot and prime denote differentiation w.r.t. t and u, respectively. Cleary (6.19) now reads

$$\overline{\phi}_r \; (Sch(t(u),u))' = t'(u)^2 \lim_{\epsilon\to 0} \left[T_{zt}(\epsilon, t(u)) - \epsilon\, \partial_t T_{zz}(\epsilon, t(u))\right], \tag{6.31}$$

where we dropped the term proportional to ϵ^2. Thus, the existence of the limit on the RHS consititutes a necessary condition on the matter sector. We would then only need to worry about choosing the right integration constants, such that we have (6.20) and (6.21).

We now consider a simple example, which will be our workhorse for the rest of this chapter. We consider a minimally coupled massive free scalar field, χ, in the bulk with mass squared $m^2 = 5/16$. The dual operator in the quantum theory has $\Delta = \frac{1}{2}(1+\sqrt{1+4m^2}) = \frac{5}{4}$. As we will later describe, this example can be generalized in a straightforward manner to $3/2 > \Delta > 1$. Sourcing the bulk scalar then results in an irrelevant deformation in the dual quantum theory.

The Klein-Gordon equation for the scalar field

$$\partial_z^2\chi - \partial_t^2\chi - \frac{5}{16z^2}\chi = 0, \tag{6.32}$$

in the locally AdS_2 spacetime has a solution with the following asymptotic expansion

$$\chi(z,t) = J_p(t) z^{-\frac{1}{4}} + O_p(t) z^{\frac{5}{4}} + \ddot{J}_p(t) z^{\frac{7}{4}} + \mathcal{O}(z^{\frac{13}{4}}), \tag{6.33}$$

where J_p, the non-normalizable mode, will be interpreted as the source term in subsequent discussion, while O_p, the normalizable mode, will be viewed as the response. Although the Klein-Gordon equation can be solved exactly, we will focus only on its asymptotic expansion, specified entirely in terms of $J_p(t)$ and $O_p(t)$.

The components of the energy momentum tensor of this field are given by

$$\begin{aligned} T_{tt} &= \frac{1}{2}\left((\partial_t\chi)^2 + (\partial_z\chi)^2 + \frac{5}{16z^2}\chi^2\right), \\ T_{zt} &= \partial_t\chi\partial_z\chi, \\ T_{zz} &= \frac{1}{2}\left((\partial_t\chi)^2 + (\partial_z\chi)^2 - \frac{5}{16z^2}\chi^2\right). \end{aligned} \tag{6.34}$$

Using the asymptotic expansion (6.33), we can readily find that

$$\lim_{\epsilon\to 0}\left[T_{zt}(\epsilon,t) - \epsilon\,\partial_t T_{zz}(\epsilon,t)\right] = \frac{3}{2}\left(\frac{5}{4}O_p(t)\dot{J}_p(t) + \frac{1}{4}J_p(t)\dot{O}_p(t)\right). \tag{6.35}$$

Therefore, we satisfy the necessary condition for our holographic dictionary to make sense in the limit $\epsilon \to 0$.

We can now check that the formal solution of the dilaton field, given by (6.15), indeed yields the desired asymptotic behavior when $\epsilon \to 0$. Using the explicit form of the energy momentum tensor (6.34) with the asymptotic expansion (6.33), we find

$$\Phi(z,t) = \frac{\alpha_0(t)}{z} + \frac{J_p^2(t)}{4\sqrt{z}} + \lim_{\epsilon\to 0}\left(\beta_\epsilon(t) - \frac{J_p^2(t)}{16\epsilon^{\frac{3}{2}}}\right) z + \mathcal{O}(z^{\frac{3}{2}}) \tag{6.36}$$

where all the other subleading termshave finite $\epsilon \to 0$ limit. It might seem that we have a problem with the term proportional to z, but we can use (6.20) to obtain

$$\begin{aligned}\beta_\epsilon(t) &= -C_0 + \frac{1}{8\epsilon^{\frac{3}{2}}}\int_{-\infty}^{t} \mathrm{d}t_1 J_p(t_1)\dot{J}_p(t_1) \\ &\quad -\frac{1}{2}\int_{-\infty}^{t} \mathrm{d}t_1 \left(\frac{5}{4}O_p(t_1)\dot{J}_p(t_1) - \frac{1}{4}\dot{O}_p(t_1)J_p(t_1)\right) \\ &= -C_0 + \frac{J_p^2(t)}{16\epsilon^{\frac{3}{2}}} - \frac{1}{2}\int_{-\infty}^{t} \mathrm{d}t_1 \left(\frac{5}{4}O_p(t_1)\dot{J}_p(t_1) - \frac{1}{4}\dot{O}_p(t_1)J_p(t_1)\right)\end{aligned} \tag{6.37}$$

with $C_0 = \lim_{\epsilon\to 0} C_\epsilon$. Crucially, we have assumed above that

$$\lim_{t\to-\infty} J_p^2(t) = 0. \tag{6.38}$$

This is a vital assumption as it underpins the sensible asymptotic behavior that we want for Φ. Assembling the result using (6.20), (6.21), (6.35), (6.36) and (6.37), we find

$$\begin{aligned}\Phi(z,t) = \frac{1}{z}\Bigg(& A_0 + B_0 t + C_0 t^2 \\ &+ \frac{3}{2}\int_{-\infty}^{t}\mathrm{d}t_1\int_{-\infty}^{t_1}\mathrm{d}t_2\int_{-\infty}^{t_2}\mathrm{d}t_3\left[\frac{5}{4}O_p(t)\dot{J}_p(t) + \frac{1}{4}J_p(t)\dot{O}_p(t)\right]\Bigg) \\ &+ \frac{J_p^2(t)}{4\sqrt{z}} + z\left(-C_0 - \frac{1}{2}\int_{-\infty}^{t}\mathrm{d}t_1\left(\frac{5}{4}O_p(t_1)\dot{J}_p(t_1) - \frac{1}{4}\dot{O}_p(t_1)J_p(t_1)\right)\right) \\ &+ \mathcal{O}(z^{\frac{3}{2}}),\end{aligned} \tag{6.39}$$

where we assume (6.38).

Thus, we can conclude that if $J_p(t)$ vanishes sufficiently fast in the far past, then the asymptotic expansion of Φ has non-singular coefficients in the limit $\epsilon \to 0$. Furthermore, the relevant integrals are finite.

Eventually we determine $O_p(t)$ from $J_p(t)$ due to *regularity* which implements *causal response* in holography (see Sec. 2.2.3 for a discussion on response in hydrodynamics). Also due to the time-translation symmetry of AdS_2, if $J_p(t)$ is constant then so is $O_p(t)$. In this case, although Φ is modified as evident from (6.39), the $\epsilon \to 0$ limit is non-problematic.

Now that we know we are working with a finite theory, we can investigate the time-reparametrization equation (6.31) in the limit $\epsilon \to 0$, which in our example reduces to

$$(Sch(t(u),u))' = t'(u)^2\frac{3}{2\bar{\phi}_r}\left(\frac{5}{4}O_p(t(u))\dot{J}_p(t(u)) + \frac{1}{4}J_p(t(u))\dot{O}_p(t(u))\right). \tag{6.40}$$

The bulk regularity condition which we will study explicitly later implies that

$$O_p(t) = \int_{-\infty}^{t}\mathrm{d}t_1\, G_R(t-t_1)J_p(t_1), \tag{6.41}$$

where $G_R(t-t_1)$ is the retarded Green function.

We can now reparameterize our time to the boundary time, u, such that the source (perturbation), which couples to the dual operator with $\Delta = 5/4$ is actually

$$J(u) = t'(u)^{-\frac{1}{4}}J_p(t(u)) \tag{6.42}$$

and similarly the expectation value of the operator that is the measured response is

$$O(u) = t'(u)^{\frac{5}{4}} O_p(t(u)). \tag{6.43}$$

Therefore, the regularity condition implies in the boundary time that

$$O(u) = \int_{-\infty}^{u} \mathrm{d}u_1\, G_R(t(u) - t(u_1)) t'(u)^{\frac{5}{4}} t'(u_1)^{\frac{5}{4}} J(u_1). \tag{6.44}$$

Substituting (6.42) and (6.43) in (6.40), we obtain the time reparameterization equation

$$(Sch(t(u), u))' = \frac{3}{2\overline{\phi}_r} \left(\frac{5}{4} O(u) J'(u) + \frac{1}{4} J(u) O'(u) \right). \tag{6.45}$$

The above equation should be understood with $O(u)$ defined via (6.44). Thus the time-reparametrization equation is actually a fourth-order integro-differential equation. One of the main properties of the Schwarzian derivative is that it is invariant under a fractional linear transformation of $t(u)$

$$t(u) \to \frac{at(u) + b}{ct(u) + d}, \tag{6.46}$$

where $ad - bc = 1$. Note that this means that the transformation can be characterized by three parameters. The reparametrized retarded correlation function

$$G_R(t(u) - t(u_1)) t'(u)^{\frac{5}{4}} t'(u_1)^{\frac{5}{4}},$$

is also invariant under such a transformation, owing to the $SL(2, R)$ symmetry of the background AdS_2 geometry in which the Klein-Gordon equation is solved. Thus, we can conclude that the time-reparameterization equation (6.45) retains $SL(2, R)$ symmetry even in the presence of minimally coupled bulk matter.

This discussion can be generalized in a straightforward manner. It becomes clear that Δ has a limited range for the case of a minimally coupled free bulk scalar field. If we choose $\Delta \geq 3/2$, then the leading asymptotic behavior of Φ is more singular than z^{-1}. For example, the choice of $\Delta = 3/2$ corresponds to leading $z^{-1} \log z$ asymptotics of Φ. Then the on-shell action has a $\log \epsilon\, Sch(t, u)$ term, which cannot be subtracted by a local counterterm, similar to the case of a conformal anomaly. Thus, a holographic interpretation of a $\Delta \geq 3/2$ deformation makes sense only after imposing a UV cut-off in the dual theory.

Hence, if we consider a minimally coupled free bulk scalar field with $-1/4 < m^2 < 3/4$, i.e. corresponding to a deformation with $1/2 < \Delta < 3/2$, the general form of the time-reparametrization equation is

$$(Sch(t(u), u))' = C_\Delta \left(\Delta O(u) J'(u) + (\Delta - 1) J(u) O'(u) \right), \tag{6.47}$$

with

$$O(u) = \int_{-\infty}^{u} \mathrm{d}u_1\, G_R(t(u) - t(u_1)) t'(u)^{\Delta} t'(u_1)^{\Delta} J(u_1), \tag{6.48}$$

and $C_\Delta = (2\Delta - 1)/\overline{\phi}_r$, which can be set to unity by choosing $\overline{\phi}_r = 2\Delta - 1$. As before, the equation is symmetric under $SL(2, R)$ transformation of $t(u)$ due to the $SL(2, R)$ invariance of

$$G_R(t(u) - t(u_1)) t'(u)^{\Delta} t'(u_1)^{\Delta}.$$

Furthermore, Φ has an asymptotic expansion with non-singular coefficients in the limit $\epsilon \to 0$.

6.1.4 Useful coordinate transformations

As we saw from the equation of motion from the dilaton field (6.2), the metric is locally always AdS_2 in JT gravity. Gravity has no local bulk dynamics. Nevertheless, a diffeomorphism of the bulk coordinates which is non-trivial at the boundary has a physical effect as it produces a non-topological on-shell action. The time-reparametrization is described by the variable $t(u)$, which maps the physical (boundary) time u of the observer to the time coordinate t of Fefferman-Graham coordinates. However, due to the $SL(2,R)$ symmetry of the on-shell action, an $SL(2,R)$ transformation of $t(u)$ has no physical effect on observables, such as correlation functions. Thus, the physically distinct solutions of $t(u)$ are members of the *Diff*$/SL(2,R)$ coset.

In absence of matter, the time-reparametrization equation (6.47) implies that the Schwarzian derivative of $t(u)$ must be a constant, i.e.

$$Sch(t(u),u) = \pm\frac{2\pi^2}{\beta^2}, \tag{6.49}$$

with β a real parameter. This represents a third order differential equation for $t(u)$. We have two distinct solutions, depending on the sign of the constant.

For the *negative* sign of the Schwarzian derivative of $t(u)$, the solution is

$$t(u) = \tanh\left(\frac{\pi u}{\beta}\right), \tag{6.50}$$

up to a $SL(2,R)$ transformation. The three parameters of the $SL(2,R)$ transformation (6.46) along with β supply the necessary four integration constants of (6.47).

If the Schwarzian derivative of $t(u)$ is a *positive* constant, then the solution is

$$t(u) = \tan\left(\frac{\pi u}{\beta}\right), \tag{6.51}$$

up to a $SL(2,R)$ transformation. In this case, the solution is periodic with period β. A periodic Lorentzian time does not make sense, so we reject such solutions as unphysical.

However, if we were working in an Euclidean signature, we would accept the periodic solutions, as these can indeed be interpreted to be thermal solutions with temperature β^{-1}. Under Euclidean continuation where both $t \to it$ and $u \to iu$, the Schwarzian reverses sign. In this case, only positive constant values of the Schwarzian are physically acceptable. Futhermore, under $u \to iu$, the Lorentzian solution (6.50) goes to the Euclidean solution (6.51), such that indeed $t \to it$.

The bulk interpretation of the time reparameterization, $t(u)$, is that it is the boundary limit of a bulk diffeomorphism. It is important to note that the bulk diffeomorphism corresponding to a given $t(u)$ is not unique, since we need to *gauge fix.* To address this, it is convenient to go from Fefferman-Graham coordinates to ingoing Eddington-Finkelstein gauge in which the AdS_2 metric takes the form:

$$\mathrm{d}s^2 = -\frac{2}{r^2}\mathrm{d}r\mathrm{d}u - \left(\frac{1}{r^2} - M(u)\right)\mathrm{d}u^2, \tag{6.52}$$

where the boundary time u is also an ingoing null bulk coordinate. The function $M(u)$ parametrizes the residual gauge freedom, i.e. diffeomorphisms which preserve this gauge. To see this explicitly, we first choose $M(u) = 1$ and write the metric in this gauge as

$$\mathrm{d}s^2 = -\frac{2}{\rho^2}\mathrm{d}\rho\mathrm{d}\tau - \left(\frac{1}{\rho^2} - 1\right)\mathrm{d}\tau^2. \tag{6.53}$$

To get back to (6.52) with an arbitrary $M(u)$, we need to perform the (gauge-preserving) diffeomorphism

$$\tau = \tau(u), \qquad \rho = \frac{\tau'(u) r}{1 - \frac{\tau''(u)}{\tau'(u)} r}, \tag{6.54}$$

with

$$-2Sch(\tau(u), u) + \tau'(u)^2 = M(u). \tag{6.55}$$

Under such a diffeomorphism, the ingoing null coordinate (observer's boundary time) u maps to τ which is the ingoing null coordinate (boundary time) of a black hole with a fixed mass of $M = 1$. The map, $\tau(u)$, is determined by the dynamical mass $M(u)$. Furthermore, the radial coordinate, ρ, transforms by a time-dependent fractional linear transformation, whose parameters are determined by $\tau(u)$.

We now want to relate the Fefferman-Graham time t to the observer's time u. We can do this by first mapping t to τ and then mapping τ to u. To bring the bulk metric (6.6) to the ingoing Eddington-Finkelstein form (6.53) with $M(u) = 1$, we need to perform the diffeomorphism

$$\begin{aligned} t &= \frac{1}{2}\left(\tanh\left(\frac{\tau}{2} + \operatorname{arctanh}\rho\right) + \tanh\left(\frac{\tau}{2}\right)\right), \\ z &= \frac{1}{2}\left(\tanh\left(\frac{\tau}{2} + \operatorname{arctanh}\rho\right) - \tanh\left(\frac{\tau}{2}\right)\right). \end{aligned} \tag{6.56}$$

At the boundary $z = 0$, i.e. $\rho = 0$, we find that

$$t = \tanh\left(\frac{\tau}{2}\right), \tag{6.57}$$

which matches with the form (6.50) if we set $\beta = 2\pi$. In this case, as we see from (6.49),

$$Sch(t, \tau) = -\frac{1}{2}. \tag{6.58}$$

Next, we obtain the general ingoing Eddington-Finkelstein form of the metric (6.52) with an arbitrary $M(u)$ from the canonical Fefferman-Graham coordinates by simply substituting (6.54) into (6.56). Then at the boundary $z = 0$, i.e. $r = 0$, we find that

$$t(u) = \tanh\left(\frac{\tau(u)}{2}\right). \tag{6.59}$$

The composition law of the Schwarzian derivatives is given by

$$Sch((f \circ g)(u), u) = Sch(g(u), u) + g'(u)^2 Sch((f \circ g)(u), g(u)), \tag{6.60}$$

which we use along with (6.58) and (6.59) to find that

$$Sch := Sch(t(u), u) = Sch(\tau(u), u) - \frac{1}{2}\tau'(u)^2. \tag{6.61}$$

Comparing with (6.55), we obtain

$$Sch = -\frac{1}{2} M(u). \tag{6.62}$$

This relates the boundary variable $t(u)$ to the time-dependent black hole mass $M(u)$, and thus provides a bulk interpretation of $t(u)$. As such, we have derived this time-reparametization equation from the bulk gravitational constraints.

Another way to arrive at the equation of motion for $t(u)$ given by (6.47) is by working directly with the ADM mass, M_{ADM}, in terms of the Schwarzian of $t(u)$ [127]. The actual ADM mass of the black hole is [125, 127]

$$M_{\mathrm{ADM}}(u) = \frac{\bar{\phi}_r}{16\pi G}(-2\,Sch) = \frac{\bar{\phi}_r}{16\pi G}M(u). \tag{6.63}$$

Therefore,

$$-Sch(t(u),u) = \frac{8\pi G}{\bar{\phi}_r}M_{\mathrm{ADM}}(u). \tag{6.64}$$

The pure JT on-shell gravitational action (6.29) in the presence of a minimally coupled bulk scalar field is modified to

$$S^{\mathrm{grav}}_{\mathrm{on-shell}} = \frac{\bar{\phi}_r}{16\pi G}\int \mathrm{d}u\,(-2Sch(t(u),u)) + \frac{1}{16\pi G}\int \mathrm{d}u\, J(u)O(u). \tag{6.65}$$

Computing the EOM for t leads directly to (6.47).

6.2 Finding explicit time-dependent solutions

6.2.1 Conserved charges and Ward identities

In the case of pure JT gravity, the Noether charges corresponding to the $SL(2,R)$ symmetries have been discussed in [127]. The infinitesimal $SL(2,R)$ transformations are $t(u) \to t(u) + \epsilon\,\delta t(u)$, with $\delta t(u) = 1, t(u), t(u)^2$ generating translation, dilation and special conformal transformation, respectively, with corresponding conserved charges:

$$\begin{aligned} Q_0 &= \frac{t'''(u)}{t'(u)^2} - \frac{t''(u)^2}{t'(u)^3}, & (6.66)\\ Q_1 &= t(u)\left(\frac{t'''(u)}{t'(u)^2} - \frac{t''(u)^2}{t'(u)^3}\right) - \frac{t''(u)}{t'(u)}, & (6.67)\\ Q_2 &= t(u)^2\left(\frac{t'''(u)}{t'(u)^2} - \frac{t''(u)^2}{t'(u)^3}\right) - 2t(u)\left(\frac{t''(u)}{t'(u)} - \frac{t'(u)}{t(u)}\right). & (6.68)\end{aligned}$$

We can readily see that

$$Q_i'(u) = \frac{t(u)^i}{t'(u)}Sch', \tag{6.69}$$

for $i = 0, 1, 2$. Clearly, these charges are conserved on-shell in pure JT gravity, i.e. when $Sch(t(u),u)$ is a constant. Furthermore, the Casimir

$$Q_1^2 - Q_0 Q_2 = -2\,Sch, \tag{6.70}$$

is a constant in the absence of matter.

For later convenience, we define the Noether charges

$$Q = \frac{1}{2}(Q_0 - Q_2), \quad Q_\pm = \frac{1}{2}(Q_0 + Q_2 \pm 2Q_1). \tag{6.71}$$

Shifting to the variable $\tau(u)$, which is the boundary time of the $M(u) = 1$ black hole and is related to $t(u)$ via (6.59), we obtain the explicit forms

$$\begin{aligned} Q &= \frac{\tau'''(u)}{\tau'(u)^2} - \frac{\tau''(u)^2}{\tau'(u)^3} - \tau'(u), && (6.72)\\ Q_+ &= \left(\frac{\tau'''(u)}{\tau'(u)^2} - \frac{\tau''(u)^2}{\tau'(u)^3} - \frac{\tau''(u)}{\tau'(u)}\right) e^{\tau(u)}, && (6.73)\\ Q_- &= \left(\frac{\tau'''(u)}{\tau'(u)^2} - \frac{\tau''(u)^2}{\tau'(u)^3} + \frac{\tau''(u)}{\tau'(u)}\right) e^{-\tau(u)}, && (6.74)\end{aligned}$$

which satisfy

$$Q' = \frac{1}{\tau'(u)} Sch', \quad Q'_\pm = \frac{e^{\pm\tau(u)}}{\tau'(u)} Sch'. \tag{6.75}$$

Furthermore, the Casimir is

$$Q^2 - Q_+Q_- = -2\,Sch. \tag{6.76}$$

We can solve for the derivatives of τ at a given value of τ in terms of the Noether charges:

$$\begin{aligned} \tau' &= \frac{1}{2}\left(Q_-e^{\tau} + Q_+e^{-\tau} - 2Q\right), && (6.77)\\ \tau'' &= \frac{1}{4}\left(Q_-e^{\tau} - Q_+e^{-\tau}\right)\left(Q_-e^{\tau} + Q_+e^{-\tau} - 2Q\right), && (6.78)\\ \tau''' &= \frac{1}{4}\left(Q_-^2e^{2\tau} + Q_+^2e^{-2\tau} - Q\left(Q_-e^{\tau} + Q_+e^{-\tau}\right)\right)\left(Q_-e^{\tau} + Q_+e^{-\tau} - 2Q\right). && (6.79)\end{aligned}$$

This suggests a method to obtain $\tau(u)$ in the absence of matter. We initialize at a boundary time $u = u_{in}$ by specifying the value of $\tau(u_{in})$ and the three Noether charges, $Q_\pm$ and Q. From (6.75), it is clear that in the absence of matter, the Noether charges remain constant. At the initial instant we can then use (6.77) to obtain $\tau'(u_{in})$. Next, we update τ using a finite difference method, such as

$$\tau(u_{in} + \Delta u) = \tau(u_{in}) + \tau'(u_{in})\Delta u. \tag{6.80}$$

Thus, we can generate the complete numerical solution of $\tau(u)$.

Note that one can always set the Noether charges to the following constant values

$$Q = -\frac{2\pi}{\beta}, \quad Q_\pm = 0, \tag{6.81}$$

via an appropriate $SL(2,R)$ transformation. In this case, $Sch = -2\pi^2/\beta^2$ and

$$\tau(u) = \tau(u_{in}) + \frac{2\pi}{\beta}(u - u_{in}). \tag{6.82}$$

Furthermore, without changing the values of the charges given by (6.81), we can set initially

$$\tau(u_{in}) = \frac{2\pi}{\beta}u_{in},$$

and reproduce (6.50). When we choose the initial value of $\tau(u_{in})$, we are effectively rotating $t(u)$ in $SL(2,R)$. We can define an $SL(2,R)$ *frame* by the one parameter family of $SL(2,R)$

transformations that leaves a chosen set of Noether charges invariant. As such, the $SL(2,R)$ transformation is not physically observable, so we can derive all real-time properties of the thermal equilibrium state at temperature β^{-1} from the solution (6.50) linear in u.

For a constant value of $Sch = -2\pi^2/\beta^2$, we can parametrize all *real* values of $SL(2,R)$ charges as follows

$$Q = -\frac{2\pi}{\beta}\cosh\theta\cos\phi, \quad Q_- = \frac{2\pi}{\beta}(\sinh\theta\cos\phi + \sin\phi),$$
$$Q_+ = \frac{2\pi}{\beta}(\sinh\theta\cos\phi - \sin\phi). \tag{6.83}$$

The general solution corresponding to the above charges are:

$$\tau(u) = \frac{\beta}{\pi}\text{arctanh}\left(\frac{e^{\frac{\theta}{2}}\left(\cosh\frac{\eta}{2}\cos\frac{\phi}{2} + \sinh\frac{\eta}{2}\sin\frac{\phi}{2}\right)\tanh\left(\frac{\pi}{\beta}u\right) + e^{\frac{\theta}{2}}\left(\sinh\frac{\eta}{2}\cos\frac{\phi}{2} + \cosh\frac{\eta}{2}\sin\frac{\phi}{2}\right)}{e^{-\frac{\theta}{2}}\left(\sinh\frac{\eta}{2}\cos\frac{\phi}{2} - \cosh\frac{\eta}{2}\sin\frac{\phi}{2}\right)\tanh\left(\frac{\pi}{\beta}u\right) + e^{-\frac{\theta}{2}}\left(\cosh\frac{\eta}{2}\cos\frac{\phi}{2} - \sinh\frac{\eta}{2}\sin\frac{\phi}{2}\right)}\right). \tag{6.84}$$

The parameters θ, ϕ and η represent an $SL(2,R)$ transformation of $t(u)$ as should be clear from (6.50). However, it is explicit in (6.83) that only θ and ϕ along with β determine the Noether charges. The parameter η nevertheless sets the value of $\tau(u_{in})$ and is thus *not* a redundant variable. The above parametrization will be useful in characterising the dynamics in the presence of matter.

6.2.2 The algorithm

In this subsection, we detail the algorithm used to determine time-dependent solutions, namely $\tau(u)$ for a given source $J(u)$. We build on the discussion from the previous subsection, by first turning our attention to the modified Noether charges in the presence of matter. This is a straightforward computation, using the time reparameterization equation (6.47) and the conservation equations for the charges (6.75). Then, setting $C_\Delta = 1$ by choosing $\overline{\phi}_r$ appropriately, these modified Ward identities are

$$Q' = \tau'(u)\left(\Delta O_{th}(\tau(u))\frac{\mathrm{d}J_{th}(\tau(u))}{\mathrm{d}\tau(u)} + (\Delta-1)J_{th}(\tau(u))\frac{\mathrm{d}O_{th}(\tau(u))}{\mathrm{d}\tau(u)}\right), \tag{6.85}$$

$$Q'_+ = e^{\tau(u)}\tau'(u)\left(\Delta O_{th}(\tau(u))\frac{\mathrm{d}J_{th}(\tau(u))}{\mathrm{d}\tau(u)} + (\Delta-1)J_{th}(\tau(u))\frac{\mathrm{d}O_{th}(\tau(u))}{\mathrm{d}\tau(u)}\right), \tag{6.86}$$

$$Q'_- = e^{-\tau(u)}\tau'(u)\left(\Delta O_{th}(\tau(u))\frac{\mathrm{d}J_{th}(\tau(u))}{\mathrm{d}\tau(u)} + (\Delta-1)J_{th}(\tau(u))\frac{\mathrm{d}O_{th}(\tau(u))}{\mathrm{d}\tau(u)}\right), \tag{6.87}$$

where

$$J_{th}(\tau(u)) = J(u)\tau'(u)^{\Delta-1}, \tag{6.88}$$
$$O_{th}(\tau(u)) = O(u)\tau'(u)^{-\Delta}. \tag{6.89}$$

Note that the subscript th is meant to remind the reader that the relevant object is living in the thermal background (6.53). The integrated form of the Ward identities are

$$Q(u) - Q(u_{in}) = \int_{\tau(u_{in})}^{\tau(u)} \mathrm{d}\tau_1 \left(\Delta O_{th}(\tau_1)\frac{\mathrm{d}J_{th}(\tau_1)}{\mathrm{d}\tau_1} + (\Delta-1)J_{th}(\tau_1)\frac{\mathrm{d}O_{th}(\tau_1)}{\mathrm{d}\tau_1}\right), \tag{6.90}$$

$$Q_+(u) - Q_+(u_{in}) = \int_{\tau(u_{in})}^{\tau(u)} \mathrm{d}\tau_1\, e^{\tau_1} \left(\Delta O_{th}(\tau_1)\frac{\mathrm{d}J_{th}(\tau_1)}{\mathrm{d}\tau_1} + (\Delta-1)J_{th}(\tau_1)\frac{\mathrm{d}O_{th}(\tau_1)}{\mathrm{d}\tau_1}\right), \tag{6.91}$$

$$Q_-(u) - Q_-(u_{in}) = \int_{\tau(u_{in})}^{\tau(u)} \mathrm{d}\tau_1\, e^{-\tau_1} \left(\Delta O_{th}(\tau_1)\frac{\mathrm{d}J_{th}(\tau_1)}{\mathrm{d}\tau_1} + (\Delta-1)J_{th}(\tau_1)\frac{\mathrm{d}O_{th}(\tau_1)}{\mathrm{d}\tau_1}\right). \tag{6.92}$$

Furthermore, we can identify the Hamiltonian, $H(u)$, i.e. the Noether charge corresponding to the u-translation symmetry which is broken explicitly in the presence of $J(u)$, by rewriting the time-reparametrization equation (6.47) in the following form

$$\frac{\mathrm{d}H(u)}{\mathrm{d}u} = J'(u)O(u), \tag{6.93}$$

from which we can read off

$$\begin{aligned} H(u) &= Sch(t(u), u) - (\Delta - 1)J(u)O(u) \\ &= Sch(\tau(u), u) - \frac{1}{2}\tau'(u)^2 - (\Delta - 1)\tau'(u)J_{th}(\tau(u))O_{th}(\tau(u)). \end{aligned} \tag{6.94}$$

where in the last line we have used (6.61). In our algorithm, the Ward identity (6.93) will provide a consistency check and accuracy test for numerics.

As a final ingredient in our algorithm, we will need a method to obtain $O(u)$ self-consistently from $J(u)$. Of course, if we know $t(u)$ for $u < u_0$, then (6.48) tells us how to obtain $O(u)$. Unfortunately, the integral in (6.48) can only be defined via an appropriate analytic continuation for which it is necessary to first go to frequency space – this will be a cumbersome procedure for a non-trivial $t(u)$, which is not linear or a simple function of u.

We can circumvent this problem by exploiting the scalar source, $J_{th}(\tau(u))$, and the response, $O_{th}(\tau(u))$, defined in (6.88) and (6.89) living in the metric (6.53) with $M(u) = 1$ and with boundary time $\tau(u)$. In these coordinates, the form of the Klein-Gordon equation is

$$\partial_\rho(d_+\chi) + \frac{\Delta(\Delta - 1)}{2\rho^2}\chi = 0, \tag{6.95}$$

where

$$d_+ = \xi \cdot \nabla, \quad \text{with} \quad \xi^\rho = -\frac{1}{2}(1 - \rho^2),\ \xi^\tau = 1. \tag{6.96}$$

With an input of $J_{th}(\tau)$ obtained from (6.88) and initial conditions $\chi(\rho, \tau = 0)$, we can readily solve this equation via the method of characteristics to obtain $O_{th}(\tau)$. Then, we can extract $O(u)$ using (6.89).

To see how this works explicitly, we return to the specific case of $\Delta = 5/4$. It is useful to first define the finite term

$$\overline{d_+\chi} := d_+\chi - \frac{1}{8}J_{th}(\tau)\rho^{-\frac{5}{4}} - \frac{5}{8}\frac{\mathrm{d}J_{th}(\tau)}{\mathrm{d}\tau}\rho^{-\frac{1}{4}}, \tag{6.97}$$

because $\overline{d_+\chi}$ has a non-singular asymptotic expansion

$$\overline{d_+\chi} \approx -\frac{5}{8}O_{th}(\tau)\rho^{\frac{1}{4}}, \tag{6.98}$$

near the boundary $\rho = 0$. We note that

$$\partial_\tau\chi = \overline{d_+\chi} + \frac{1}{2}(1 - \rho^2)\partial_\rho\chi + \frac{1}{8}J_{th}(\tau)\rho^{-\frac{5}{4}} + \frac{5}{8}\frac{\mathrm{d}J_{th}(\tau)}{\mathrm{d}\tau}\rho^{-\frac{1}{4}}. \tag{6.99}$$

Furthermore, the equation of motion for $\overline{d_+\chi}$ is

$$\partial_\rho\overline{d_+\chi} + \frac{5}{32\rho^2}\left(\chi - J_{th}(\tau)\rho^{-\frac{1}{4}} - \frac{\mathrm{d}J_{th}(\tau)}{\mathrm{d}\tau}\rho^{\frac{3}{4}}\right) = 0. \tag{6.100}$$

so that

$$\overline{d_+\chi}(\rho,\tau) = -\int_o^\rho \mathrm{d}\rho_1 \, \frac{5}{32\rho_1^2}\left(\chi(\rho_1,\tau) - J_{th}(\tau)\rho_1^{-\frac{1}{4}} - \frac{\mathrm{d}J_{th}(\tau)}{\mathrm{d}\tau}\rho_1^{\frac{3}{4}}\right). \tag{6.101}$$

Note that the integral above on the right hand side is finite.

We can now compute $O(u)$ as follows. At an initial time τ_{in}, we have $\chi(\rho,\tau=\tau_{in})$ and $J_{th}(\tau)$ for all $\tau < \tau_{in}$. This means that we can use (6.101) to generate $\overline{d_+\chi}$. We can then compute $\partial_\tau\chi$ using (6.99), which enables us to propagate χ to the next time instant. Furthermore, we can extract $O_{th}(\tau)$ from (6.98) for all $\tau < \tau_0$, which means we can compute $O(u)$ from (6.89).

We are now ready to describe our algorithm for finding $\tau(u)$ for a given $J(u)$:

1. Given initial values of $\tau(u_{in})$ and the three $SL(2,R)$ charges, we can extract $\tau'(u_{in})$ using (6.77) and $\tau''(u_{in})$ using (6.78).

2. From $\tau'(u_{in})$ and known $J(u)$, we can extract $J_{th}(\tau(u_{in}))$ using (6.88) and then $\mathrm{d}J_{th}/\mathrm{d}\tau$ at $\tau(u_{in})$ since we also know $\tau''(u_{in})$.

3. Given an initial profile of χ (more on this later), J_{th} and $\mathrm{d}J_{th}/\mathrm{d}\tau$ at $\tau(u_{in})$ we extract the initial profile of $\overline{d_+\chi}$.

4. We then obtain $O_{th}(\tau)$ at $\tau(u_{in})$ using (6.98).

5. We can now update the three $SL(2,R)$ charges corresponding to the next time instant using (6.90), (6.91), (6.92).

6. We propagate τ to the next time instant using a finite difference scheme with $\tau'(u_{in})$. Furthermore, we propagate the radial profile of χ to the next time instant via $\partial_\tau\chi$ which can be extracted from known $\overline{d_+\chi}$ via (6.99).

7. We repeat all steps above at the next time instant.

Note that the bulk scalar field is evolving in a geometry (6.53), whose boundary time is $\tau(u)$ with a $M(u) = 1$ black hole. The integrated form of the Ward identity (6.93)

$$H(u) - H(u_{in}) = \int_{u_{in}}^u \mathrm{d}u_1 \, J'(u_1)O(u_1) \tag{6.102}$$

can be used to check the accuracy of the numerics, namely by extracting $O(u)$ from $O_{th}(\tau(u))$ using (6.89).

The source $J(u)$ has two physical effects: (i) the Hamiltonian H becomes time-dependent, and (ii) the $SL(2,R)$ frame varies since all Noether charges (6.72) are time-dependent. The latter point suggests that even if the system settles down in the far future with a constant value of the Hamiltonian, the $SL(2,R)$ frame will still be generically different from the initial one. The difference between initial and final $SL(2,R)$ frames can be detected via long-time correlations between far past and far future, although only the relative difference between the initial and final $SL(2,R)$ frames is physical.

We can keep track of the change in the $SL(2,R)$ frame of the pure AdS_2 boundary time by making use of (6.83). Since we know the three Noether charges and $\tau(u)$, we can obtain the instantaneous values of $\beta(u)$, $\theta(u)$ and $\phi(u)$, as well as $\eta(u)$. Note that we are not promoting β, θ, ϕ and η to time-dependent variables in (6.84).

An alternative algorithm: We could have followed a more direct route, without appealing to a conformal mapping of the source $J(u)$ to that of a state with a constant temperature. In this case, we could have used the bulk geometry (6.52) to update $M(u) = -2Sch = Q^2 - Q_+Q_-$ along with the $SL(2,R)$ charges. The Klein-Gordon equation would contain $M(u)$ (but not its derivative), which leads directly to $O(u)$ via the method of characteristics. However, it turns out that especially in the semiholographic case of Sec. 6.3, J_{th} and O_{th} give us useful insights.

6.2.3 Quenches in $NAdS_2$ holography

In this subsection, we will investigate quenches in $NAdS_2$ holography. It may be interesting to note that quantum quenches in the SYK model have been studied in [148,149], although here we studied different types of deformations.

We perturb a pre-existing thermal state by a decaying scalar source. In this case, the minimally coupled bulk scalar fields will vanish initially in absence of sources, otherwise they would be singular. Therefore, as initial conditions, we will choose for χ to vanish on the initial time surface – if chosen sufficiently far in the past, then it will be so in any bulk coordinate system. Furthermore, due to the presence of $SL(2,R)$ symmetry, we can always set initial temperature to be $1/(2\pi)$ (i.e. $\beta(u \to -\infty) = 2\pi$ and $M(u \to -\infty) = 1$ in the bulk). Additionally, by means of an appropriate time-independent $SL(2,R)$ transformation, we can choose $\tau(u \to -\infty) \approx u$. These conditions thus can be expressed as:

$$\tau(u_{\rm in}) = u_{\rm in}, \quad Q(u_{\rm in}) = -1, \quad Q_+(u_{\rm in}) = Q_-(u_{\rm in}) = 0. \tag{6.103}$$

Specifically, we will work with a Gaussian source, $J(u)$, plotted in Fig. 6.1a. The source $J(u)$ couples to an operator $O(u)$ with $\Delta = 5/4$, which is ploted in Fig. 6.1b. After conformal mapping to the state with constant temperature 2π, the source $J_{th}(\tau(u))$ and the response $O_{th}(\tau(u))$ are plotted in Fig. 6.1c and Fig. 6.1d, respectively. Clearly, there is little visible difference due to the conformal mapping.

The time-dependence of the black hole mass (remember that $H_{sch} = -M/2$) and the $SL(2,R)$ charges are shown in Fig. 6.2a and Fig. 6.2b, respectively. The final black hole mass is larger than the initial value, although the mass does not grow monotonically, as is in the case of high dimensional analogues. The final $SL(2,R)$ frame is different from the initial one. In principle, this $SL(2,R)$ rotation would be physically measurable. There would be some numerical difficulty, as it would require computing correlation functions $G(u,u')$ with very large separation $u-u'$ and with fixed $(u+u')/2$ when J is large. Thus, we explicitly find that the quench (pump) leads to formation of soft hair on the black hole represented by $SL(2,R)$ frame rotation.

From the $SL(2,R)$ charges, we can construct the derivatives of $\tau(u)$, shown in Fig. 6.3. Remarkably, τ always saturates to a constant value at late times, so that the map of the time of the physical state to that of the fixed temperature state has a finite endpoint. We observe that τ' is always positive (ensuring that the map to the time of the fixed temperature state is causal), whereas τ'' is always negative.

6.3 A semiholographic model for trapped impurities

Having properly motivated the holographic sector, we can now turn our attention to a $NAdS_2$ semiholographic model. The model aims to describe confined impurities, which are strongly interacting.

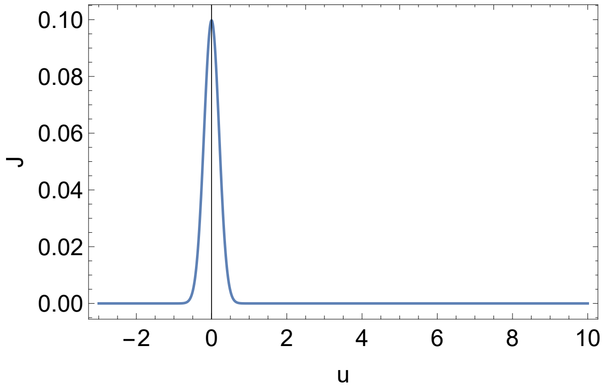

(a) Plot of $J(u)$.

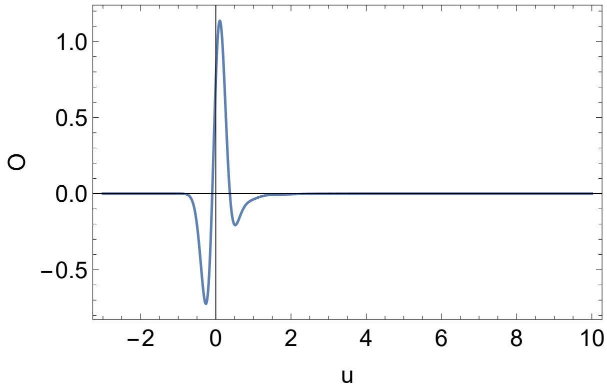

(b) Plot of $O(u)$.

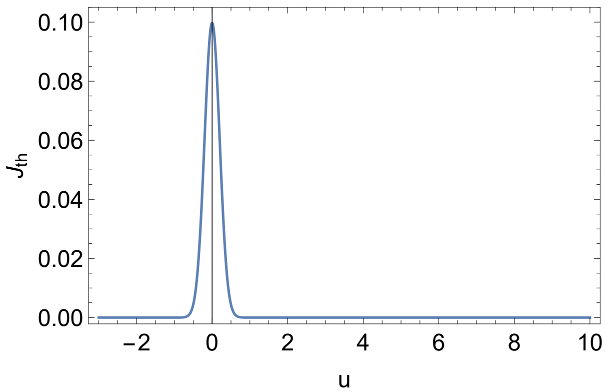

(c) Plot of $J_{th}(\tau(u))$.

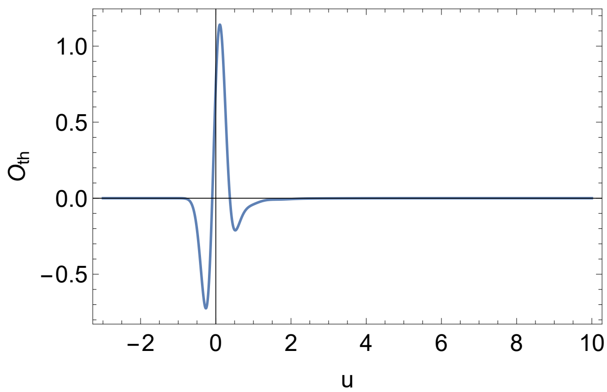

(d) Plot of $O_{th}((\tau(u))$.

Figure 6.1: Sources and responses: As expected, the responses die down at late time once the sources vanish.

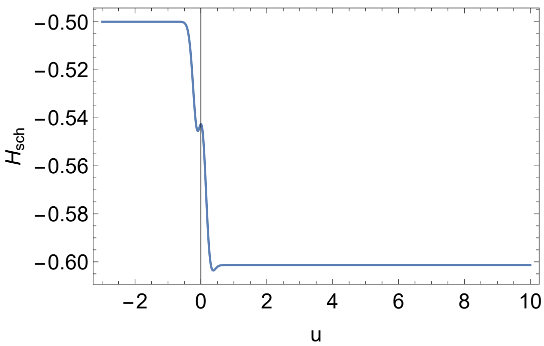

(a) Plot of $H_{Sch} = -1/2\, M(u)$: This plot is very similar to the case of quenches in higher dimensional holographic systems where $M(u)$ grows but not monotonically.

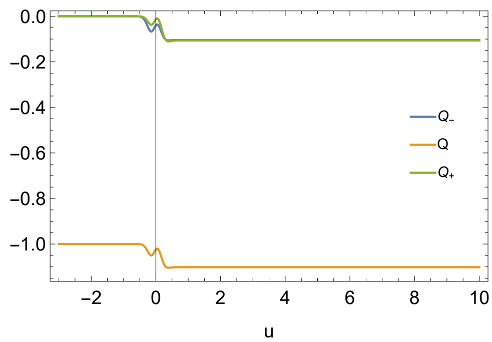

(b) Plot of the $SL(2,R)$ charges as a function of time: Note that the final $SL(2,R)$ frame is different since $Q^{\pm}$ are non-vanishing.

Figure 6.2: The time-dependence of the black hole mass and the $SL(2,R)$ charges.

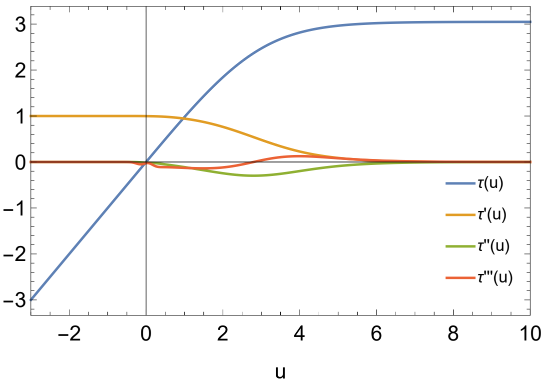

Figure 6.3: The plot of $\tau(u)$, which maps the time of the physical state to that of the fixed temperature state, and its derivatives. The generic result is that $\tau(u)$ saturates to a constant and its derivatives vanish.

The time-dependent position of an impurity, $\vec{X}(u)$, can be treated as an extra field in the effective $0+1$−D theory. When the orbital angular momentum vanishes, the motion is one-dimensional. Here we will restrict ourselves to this simple situation of one-dimensional motion of a single impurity. We will assume that the impurity follows Newtonian dynamics, subject to a confining potential from the holographic side.

The role of the strongly interacting $NAdS_2$ holographic sector in our model is to depict the dual IR dynamics of the localized mutual interactions of the impurities confined at the origin $X(u) = 0$. The motion in space of a displaced impurity can be thought of as sourcing a deformation of the $NAdS_2$ holographic theory. Then we can interpret $X(u)$ as a self-consistent external source to the $NAdS_2$. The center of the force, $X(u) = 0$, is the value of the source for which the deformation to the Schwarzian action vanishes.

Thus, the whole description is semiholographic, i.e. there is a holographic sector with a self-consistent dynamical source at the boundary and with a total conserved energy.

The effective string tension of the confining force is the self-consistent expectation value of an operator O in the $NAdS_2$ holographic theory. Therefore, the confining potential takes the form

$$V = \lambda O(u) X(u), \tag{6.104}$$

where λ is a dimensionful hard-soft coupling constant. We can then identify

$$J(u) = \lambda X(u), \tag{6.105}$$

i.e. that the position of the impurity is proportional the source $J(u)$ (non-normalizable mode) of the bulk scalar field χ dual to the operator $O(u)$. As before, we require that the holographic theory admits only irrelevant deformations about the Schwarzian action, while retaining $SL(2, R)$ invariance in the large N limit (classical gravity approximation). This implies that $O(u)$ must have scaling dimension Δ such that $1 < \Delta < 3/2$. The dual bulk field χ has mass $0 < m^2 < 3/4$ since $m^2 = \Delta(\Delta - 1)$ (recall that we set the AdS radius to unity) with asymptotic expansion

$$\chi(r, u) \approx \lambda X(u) r^{1-\Delta} + \cdots . \tag{6.106}$$

The boundary field $X(u)$ follows Newton's law in the potential (6.104):

$$m_i X''(u) = -\lambda O(u) \tag{6.107}$$

where m_i is the mass of the impurity. Its *kinetic energy* is

$$H_{kin} = \frac{1}{2} m_i X'(u)^2, \tag{6.108}$$

which satisfies

$$H'_{kin} = -\lambda O(u) X'(u). \tag{6.109}$$

The algorithm for determining $O(u)$ along with the time reparametrization $\tau(u)$ (equivalently, the mass $M(u)$ of the AdS_2 black hole) has been discussed Sec. 6.2. Assembling our previous results, we quote the equation of motion (6.93) for $\tau(u)$

$$\left(Sch(\tau(u), u) - \frac{1}{2}\tau'(u)^2 - \lambda(\Delta - 1) X(u) O(u) \right)' = \lambda O(u) X'(u). \tag{6.110}$$

As before, we can map the source to the AdS_2 black hole background (6.53) with $M(u) = 1$

$$X_{th}(\tau(u)) = X(u)\tau'(u)^{\Delta-1}, \tag{6.111}$$

solve the Klein-Gordon equation in that background to find $O_{th}(\tau(u))$ from which we can extract $O(u)$ using the relation:

$$O(u) = O_{th}(\tau(u))\tau'(u)^{\Delta}. \tag{6.112}$$

The equations (6.107) and (6.110) completely specify the semiholographic dynamics.

In fact, we are considering a similar semiholographic system as in Chapter 5, see (5.6), since we have a scalar coupling. We can write the action of the full system

$$S[X, t] = \frac{1}{16\pi G} \int \mathrm{d}u \frac{1}{2} m_i X'^2 - S^{\text{grav}}_{\text{on-shell}}[J(u) = \lambda X(u)], \tag{6.113}$$

where S^{grav} is given by (6.65). This action should be viewed as a functional of the impurity position, $X(u)$, and the time reparameterization function, $t(u)$.

Varying the action w.r.t. $X(u)$, using

$$16\pi G \frac{\delta S_{grav}}{\delta X(u)} = 16\pi G \frac{\delta S^{\text{grav}}_{\text{on-shell}}}{\delta J(u)} \frac{\delta J(u)}{\delta X(u)} = \lambda O(u),$$

we recover (6.107). On the other hand, extremizing $S^{\text{grav}}_{\text{on-shell}}$ w.r.t. $t(u)$ yields (6.110).

We note that adding (6.109) to (6.110) yields a total conserved energy, H_{tot},

$$H'_{tot} = 0, \tag{6.114}$$

which is explicitly given by

$$\begin{aligned} H_{tot} &= H_{kin} + Sch(\tau(u), u) - \frac{1}{2}\tau'(u)^2 - \lambda(\Delta - 1) X(u) O(u), \\ &= H_{kin} - \frac{1}{2} M(u) - \lambda(\Delta - 1) X(u) O(u), \\ &= H_{kin} + H_{sch} + H_{int}. \end{aligned} \tag{6.115}$$

In the second line, we have used (6.62) relating $M(u)$ and $\tau(u)$. In the third line we define the various contributions to the total energy, H_{tot}, into (i) the kinetic energy of the particle H_{kin} as defined in (6.108), (ii) the black hole mass term $H_{sch} = -1/2\, M(u)$ and (iii) the hard-soft interaction energy $H_{int} = -\lambda(\Delta - 1)X$. We readily see that the terms other than H_{kin} can be interpreted as a self-consistent effective potential:

$$V_{eff} = -\frac{1}{2}M(u) - \lambda(\Delta - 1)X(u)O(u). \tag{6.116}$$

It might seem a bit unusual that the impurity and the on-shell gravitational action have a relative sign between them in (6.113), but such a relative sign is expected in the context of effective JT gravities (see Appendix A of [150] for a simple example of this in the case of a central force problem).

Furthermore, we should point out that, in order to have the right dimensions, we would need to write $M(u)c_{IR}^2$ in (6.115), where c_{IR} is the effective velocity for causal propagation in the infrared sector. We set $c_{IR} = 1$.

We set our initial conditions by considering the equilibrium. This is when $X(u) = 0$, where the confining force vanishes. In this case, the bulk is thermal at the ambient medium temperature, i.e. $M(u)$ is a constant. The bulk scalar vanishes as does $O(u)$.

To usher in time-dependence, we introduce a kick, generated by an external force $F(u)$. This can be thought of originating from a fluctuation in the medium where the impurities are living. We will assume that the impulse has the form of a delta function, i.e.

$$F(u) = m_i v_0 \delta(u - u_0). \tag{6.117}$$

The equation for $X(u)$ given by (6.107) should be replaced by

$$m_i X''(u) = F(u) - \lambda O(u). \tag{6.118}$$

Thus, the full system exists in the equilibrium configuration for times before the impulse is imparted, $u < u_0$. At $u = u_0$, the system is kicked by $F(u)$, which imparts a finite velocity $X'(u_0) = v_0$ for the impurity, which means the total energy is not conserved at this time instant. Immediately following the impulse $u > u_0$, the total energy will be conserved. We will set $m_i = 1$ for convenience and the initial temperature to $\beta^{-1} = 1/(2\pi)$ by using scaling symmetry as before. Thus, the time-evolution will be determined by the parameters v_0 and the hard-soft coupling λ.

The algorithm detailed in Sec. 6.2.2 will be slightly modified in this case. Unlike in the previous case, where the source was fixed initially to be Gaussian, here we have to update the source $X(u)$ dynamically according to (6.118). Thus, we update the value of $X(u)$ via a finite difference method after the sixth step of the algorithm.

As for parameters, we freely choose our initial $SL(2, R)$ frame and thus choose them according to (6.103). We will set the scaling dimension Δ of O to be 5/4. We will also assume that $v_0 > 0$ because we want to investigate how far the impurity can be pushed from the center of the confining force.

It should be noted that the sign of λ is not relevant in our model. Since the source of the bulk scalar is $J(u) = \lambda X(u)$, it follows that the response $O(u)$ will also be proportional to λ. Thus, we see that the interaction term $\lambda X(u)O(u)$ and the confining force $\lambda O(u)$ in (6.107) are even in λ.

6.3.1 Non-equilibrium phase transitions

In this subsection, we will numerically explore the semiholographic model described in the previous section, by varying the initial velocity v_0 and the hard-soft coupling λ.

The behavior of the system for any value of v_0 and λ *at early times* is that the mass of the hole $M(u)$ increases (i.e. H_{sch} decreases), while the interaction energy H_{int} is positive. Due to total energy conservation, it is clear that the particle kinetic energy H_{kin} increases initially, i.e. the impurity accelerates.

At late times, we find the unintuitive result that the mass of the black hole $M(u)$ *always* goes to zero, with the remaining energy going to either the particle kinetic energy, H_{kin}, or to the interaction energy, H_{int}.

Moreover, the late time behavior of the impurity is that it *always* decelerates, eventually reaching a terminal velocity, v_f. When the energy goes to the kinetic energy, the final kinetic energy of the impurity is less than its initial velocity v_i. Energy conservation implies that

$$\frac{1}{2}m_i v_i^2 - \frac{1}{2}M_o = \frac{1}{2}m_i v_f^2, \tag{6.119}$$

where m_i is the mass of the impurity (particle) and M_0 is the initial black hole mass. The interaction term is absent, as we start in equilibrium with the impurity at the center $X = 0$. The above relation determines v_f. In the other case, when the energy at late times goes entirely to the interaction energy, H_{int}, the particle comes to a full stop as its kinetic energy vanishes.

We can determine which of these outcomes is fated for the impurity, by noting that the interaction energy at late times is *always* negative. The two cases then boil down to the interaction energy going to zero from below or saturating to a negative constant. The first outcome is possible if and only if the total energy is positive since the kinetic energy is always positive. In the other case, the total energy has to be negative. Since the initial interaction energy is zero as noted above, H_{tot} is simply given by

$$H_{tot} = \frac{1}{2}m_i v_0^2 - \frac{1}{2}M_0 \tag{6.120}$$

as the sum of initial values of the kinetic energy and H_{sch}. The final outcomes can be summarized for

$$v_0 > \sqrt{\frac{M_0}{m_i}}, \quad H_{kin} \text{ has non-zero energy at late times,} \tag{6.121}$$

$$v_0 < \sqrt{\frac{M_0}{m_i}}, \quad H_{int} \text{ has non-zero energy at late times.} \tag{6.122}$$

In the marginal case when $v_0 = \sqrt{M_0/m_i}$, i.e. the total energy is zero $H_{tot} = 0$, both H_{int} and H_{kin} vanish at late time along with H_{sch}.

Another phase transition can be revealed when considering the bulk solution. The phase transition depends on whether the mass of the black hole $M(u)$ always stays positive throughout the time evolution, or whether it oscillates between being positive and negative as it goes to zero. The first case occurs for

$$v_0 > v_c(\lambda) > \sqrt{\frac{M_0}{m_i}}, \tag{6.123}$$

where the energy ends up entirely in the impurity sector. We will refer to this as phase I behavior. For $v_0 < v_c(\lambda)$, we can have either the impurity comes to a full stop or reaches a terminal velocity, depending on which condition of (6.121) or (6.122) is satisfied. We will refer to this phase as phase II. The critical velocity $v_c(\lambda)$ separating the two phases is a monotonically increasing function of λ.

The remarkable result of our semiholographic setup is that the final black hole mass always vanishes for late times. This is in stark contrast to the pure holographic case considered in the previous section and at odds with a higher dimensional picture. This is similar to the observation of a disappearing horizon in [142], where the work was being done by the black hole rather than on it (see also [151]). The semiholographic model has a similar interpretation due to total energy conservation: the black hole does work on the impurity, as well as contributing to the confining potential. Furthermore, it is worthwhile to point out that in semiholography, the late time dynamics are controlled by the hybrid collective modes, as was discussed in Chapter 4, and not by the quasi-normal modes of the individual subsystems. Thus, the long term behavior of a semiholographic system can be very different from that of a purely holographic system.

However, in higher dimensions, a similar simulation shows that if the boundary fields do not have many degrees of freedom and only scalar hard-soft couplings are present as in our case, the black hole sucks up all the energy, depleting the boundary sources [37]. The case of JT gravity is then peculiar. We also note that it cannot be embedded in a higher dimensional setup as the dilaton does not couple to matter directly.

An illustrative example of phase I behavior

Here we will study the case of $v_0 = 2.0$ for $\lambda = 0.4$ as an example of phase I behavior, i.e. behavior found in (6.123). The black hole mass is always positive definite as it approaches zero for late time. H_{sch} is negative definite and it goes to zero from below. We plot the energies in Fig. 6.4a. In this example, one can observe that H_{sch} and H_{int} both vanish at long time, while H_{kin} stabilizes to a constant value.

In Fig. 6.4b, we plot the time-dependence of the $SL(2,R)$ charges, which diverge at long time, although the Casimir goes to zero, which is not surprising as the Casimir is proportional to the black hole mass.

In Fig. 6.5a, we plot the sources in both geometries, $X(u)$ and $X_{th}(\tau(u))$. We plot the responses in $O(u)$ in Fig. 6.5b and $O_{th}(\tau(u))$ in Fig. 6.5c. We find that the source $X(u)$ reaches a terminal velocity at late times, while the response $O(u)$ suprisingly vanishes faster than $X(u)$ grows, such that H_{int} also vanishes. Interestingly, the source and the response in the thermal background, $X_{th}(\tau(u))$ and $O_{th}(\tau(u))$, respectively, do not behave at all like their counterparts in the other geometry. This is what we would have expected from the discussion of the pumped states in Sec. 6.2.3. Instead, we find that neither decays at late time, but H_{int} is proportional to $\tau'(u)X_{th}O_{th}$, which goes to zero, since $\tau'(u)$ decays rapidly. Finally, $O(u)$ stays positive from some intermediate timescale to late times, such that the force on the impurity is indeed confining in the long run.

Our solution raises an interesting question: as the black hole evaporates classically, can we recover the information of the initial conditions from the asymptotic late time behavior? As Fig. 6.4b makes clear, all of the $SL(2,R)$ charges diverge at late time while their Casimir vanishes. Intriguingly, we can fit the late time behavior to an exponential proportional to e^{au} extremely well (with an adjusted R square $= 0.99$), which means that all the $SL(2,R)$ charges grow exponentially with the same exponent a. Since the Casimir vanishes at late times, we can conclude that the exponent a is $SL(2,R)$ invariant and an observable. Remember that the initial conditions are labelled by two parameters: (i) the velocity v_0 and (ii) the initial mass of the black hole. The total conserved energy determines v_f, the terminal velocity of the impurity. We can then expect that the initial conditions can be recovered completely from the exponent a, as well as v_f. Fig. 6.6, where we have plotted a against v_0 for a fixed unit initial mass of the black hole, supports this point of view, as a grows monotonically as a function of v_0. This

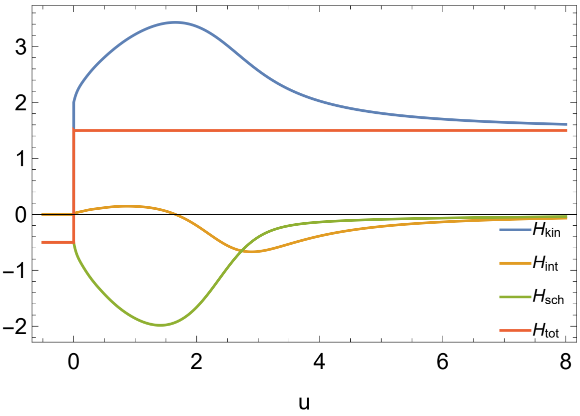

(a) Plot of energies as function of time: Note that the total energy $H_{tot} = H_{kin} + H_{int} + H_{sch}$ is conserved after the initial impulse and is finally transferred to H_{kin}, the particle kinetic energy. The mass of the black hole $M = -2H_{sch}$ remains positive and decays to zero eventually.

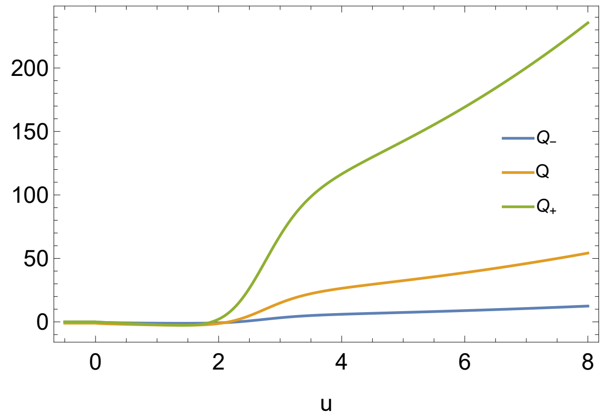

(b) Plot of the $SL(2,R)$ charges as a function of time in phase I. Although all of them diverge at late time, their Casimir (and thus the black hole mass) vanishes.

Figure 6.4: The plots for energies and $SL(2,R)$ charges for $v_0 = 2.0$ and $\lambda = 0.4$

merits more investigation.

Illustrative examples of phase II behavior

The second phase appears for $v_0 < v_c(\lambda)$. We first set $v_0 = 0.9$ and $\lambda = 0.4$. In this case, the mass of the black hole becomes negative after finite time (i.e. H_{sch} becomes positive) before vanishing at long time as shown in Fig. 6.7a. As we will discuss below, a naked singularity forms exactly when the mass vanishes and it should imply a burst of soft bulk radiation. However, unlike phase I, the kinetic energy of the impurity goes to zero at late time, meaning that the impurity comes to a full stop after travelling a finite distance, with the remaining energy ending up in H_{int}, the self-consistent confining potential energy. The $SL(2,R)$ charges decrease and seem to saturate to a finite value, unlike in the first phase, as shown in Fig. 6.7b.

Clearly, Fig. 6.8a shows that $X(u)$ and $X_{th}(u)$ saturate to a finite value. Similarly, in Fig. 6.8b we can see that $O(u)$ saturates to a non-zero value at long time, so that indeed $H_{int} = -(\lambda/4)XO$ becomes a constant at long time. In the thermal geometry, $O_{th}(\tau(u))$ diverges (see Fig. 6.8c), but τ' decays faster, which leaves $H_{int} = -(\lambda/4)\tau' X_{th} O_{th}$ going to a constant. Note that $O(u)$ is positive at long time and the final value of confining potential energy is negative as claimed before.

We now turn our attention to the case of $\sqrt{M_0/m_i} < v_0 < v_c(\lambda)$. Let us study what happens with $\lambda = 0.5$. When $v_0 = 1.1$, the impurity retains a terminal velocity because we choose $\sqrt{M_0/m_i} = 1.0$, but H_{sch} crosses zero *twice* before finally vanishing from below as illustrated in Fig. 6.9 (see the inset plot). In other words, for a finite time period there is a naked singularity, but before and after this period, the black hole mass is positive and the singularity is hidden by the horizon. As mentioned above, the development of a naked singularity could again indicate that the particle should disintegrate into softer fragments if we incorporate quantum effects in the bulk as suggested in [152].

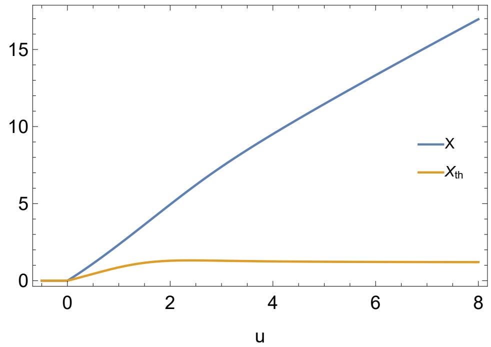

(a) Plot of $X(u)$ and $X_{th}(\tau(u))$ as functions of time. Note $X(u)$ eventually reaches linear growth regime implying that the particle reaches a terminal velocity. $X_{th}(\tau(u))$, the source conformally mapped to a black hole of unit mass, saturates to a constant.

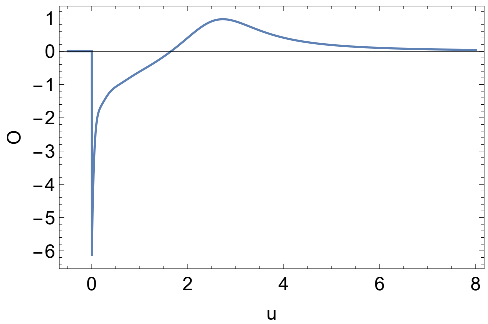

(b) Plot of $O(u)$ as a function of time. The eventual rapid decay of $O(u)$ ensures that $H_{int} \propto X(u)O(u)$ vanishes at long time.

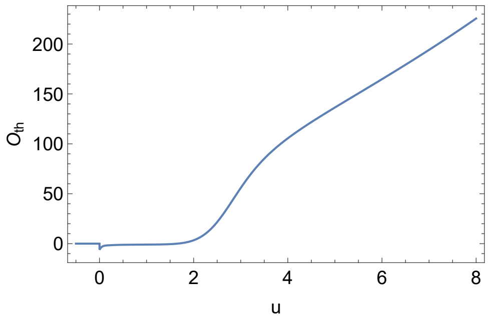

(c) Plot of $O_{th}(\tau(u))$: Note as $X_{th}(\tau(u))$ saturates, $O_{th}(\tau(u))$ grows with time. However, the rapid decay of τ' ensures that $H_{int} \propto \tau'(u)X_{th}(\tau(u))O_{th}(\tau(u))$ also decays in this frame.

Figure 6.5: The plots of sources and responses for $v_0 = 2$ and $\lambda = 0.4$.

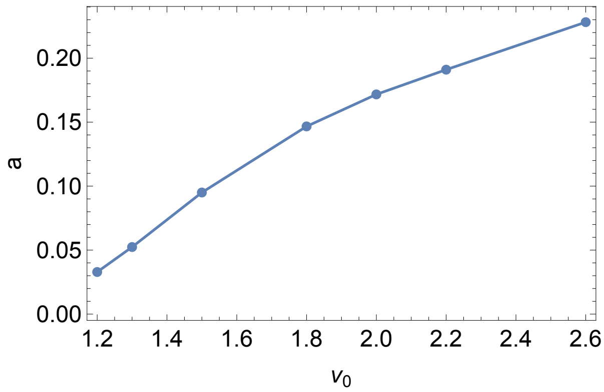

Figure 6.6: a, the exponent for late-time growth of $SL(2,R)$ charges as a function of v_0 for $\lambda = 0.4$ and fixed unit initial mass of the black hole. Note that a grows monotonically with v_0.

Our results suggest that for $\sqrt{M_i/m_0} < v_0 < v_c(\lambda)$, corresponding to the energy ending up in the kinetic sector, the mass $M(u)$ crosses zero an even number of times before finally vanishing from above. The case of $v_0 = 1.1$ is illustrated further in Fig. 6.10. For $v_0 < \sqrt{M_i/m_0}$, our results are consistent with odd number of zero crossings of $M(u)$ before its final disappearance. Interestingly, the case of $v_0 = \sqrt{M_i/m_0}$, where H_{int}, H_{kin} and $M(u)$ all disappear finally corresponds to a single zero crossing of $M(u)$. However, we warn the reader that since the amplitude of the oscillation of $M(u)$ drops dramatically, it is not easy to numerically verify definitively the number of zero crossings. This would require refined numerics, taking into account higher precision and also longer time simulations.

This phase transition merits further detailed study. In particular, we know that the order parameter of this transition is simply the inverse of the crossing time, which is the smallest value u^* when $M(u^*) = 0$. Since $M(u)$ never crosses the origin and is positive definite at any finite value of u for $v_0 > v_c(\lambda)$, the order parameter vanishes in phase I. In phase II, the order parameter is finite leading to the formation of a naked singularity at $u = u^*$ as discussed above. However, in order to study the phase transition carefully, we need to simulate the full system for very long time for v_0 close to v_c which is currently a significant numerical challenge. We leave this for the future.

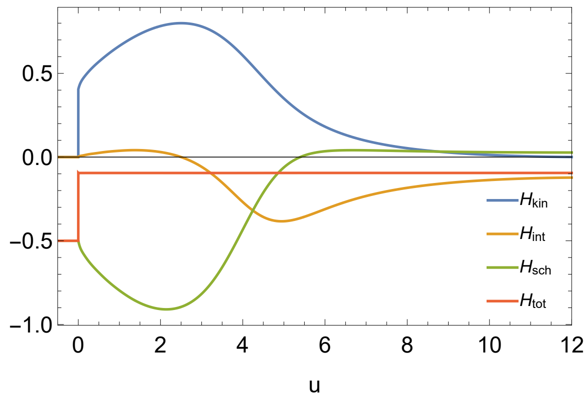

(a) Plot of energies as function of time: Note that the total energy H_{tot} is conserved after initial kick and is finally transferred to H_{int}, the confining potential energy. The mass of the black hole $M = -2H_{sch}$ becomes negative after finite time and then eventually vanishes at long time.

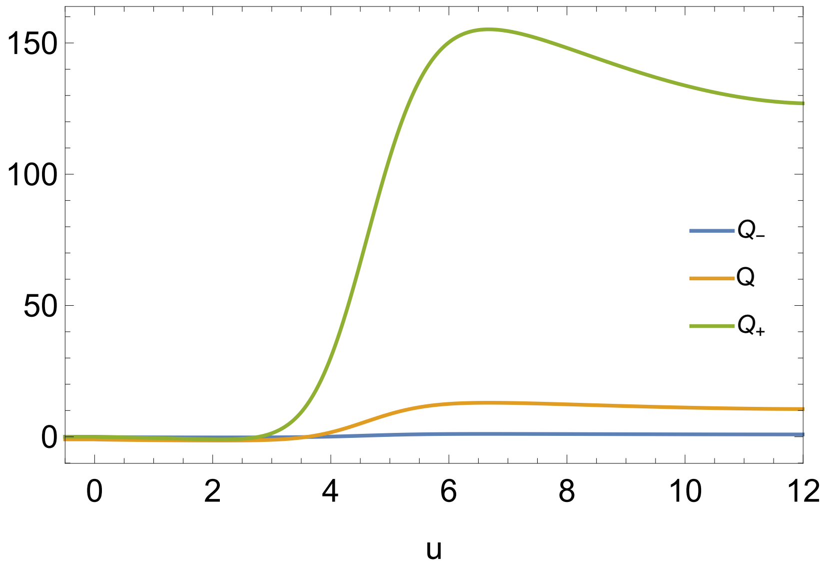

(b) Plot of $SL(2,R)$ charges as a function of time. Note that they saturate to finite values.

Figure 6.7: The plots for energies and $SL(2,R)$ charges for $v_0 = 0.9$ and $\lambda = 0.4$.

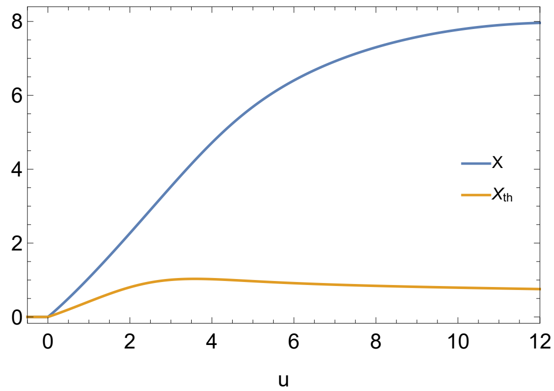

(a) Plot of $X(u)$ and $X_{th}(\tau(u))$: Both of them saturate to constant values at late time. The particle stops at a finite distance from the origin.

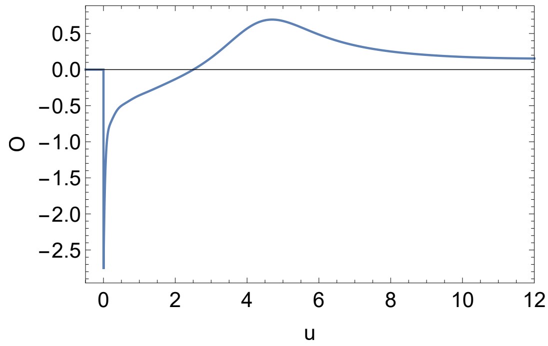

(b) Plot of $O(u)$: $O(u)$ saturates to a constant value at late time so that $H_{int} \propto X(u)O(u)$ also saturates to a constant.

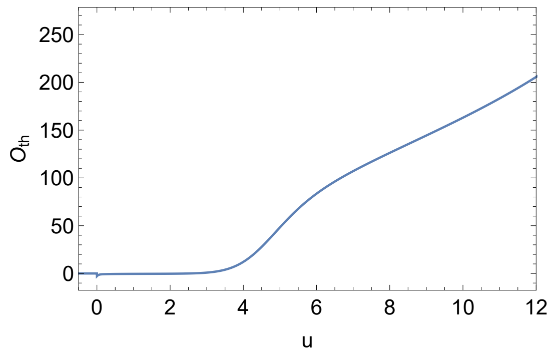

(c) Plot of $O_{th}(\tau(u))$: Note $O_{th}(\tau(u))$ diverges at late time since $X_{th}(\tau(u))$ saturates to a constant value. However, $H_{int} \propto \tau'(u)X_{th}(\tau(u))O_{th}(\tau(u))$ also saturates to a constant in this frame because the decay of τ' compensates for the growth of $O_{th}(\tau(u))$.

Figure 6.8: The plots of sources and responses for $v_0 = 1.4$ and $\lambda = 0.4$.

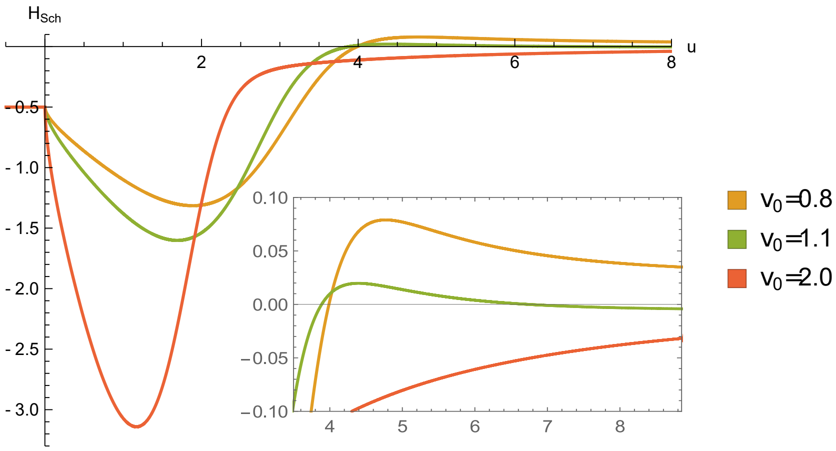

Figure 6.9: Different phases for $\lambda = 0.5$ as can be seen from the behavior of $M(u) = -2H_{sch}(u)$ for various choices of initial velocities. The inset plot shows that multiple crossings of zero is possible for $M(u)$ when the total conserved energy is positive.

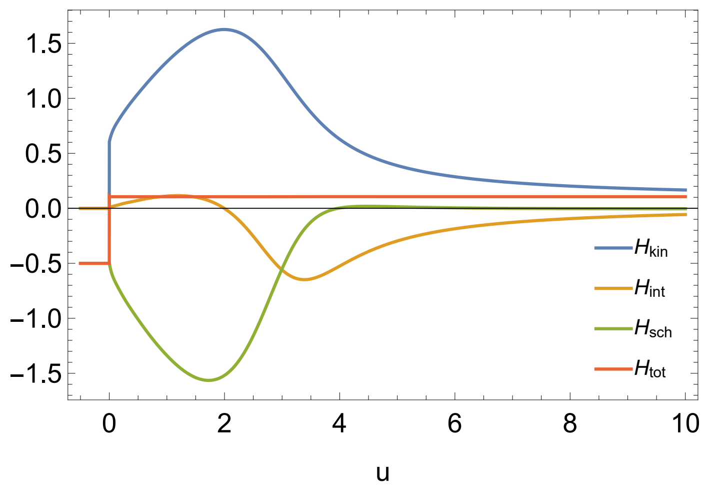

Figure 6.10: The four energies in the case of $v_0 = 1.1$ and $\lambda = 0.5$. The double crossing of H_{sch} about zero is hard to discern here, so one can refer to the inset plot in Fig. 6.9. The final transfer of energy goes to the kinetic energy of the particle.

Chapter 7

Closing remarks

7.1 Summary

In this thesis I studied semiholographic models with the ultimate goal to understand thermalization in nonabelian gauge theories. After reviewing in Chapter 2 the relevant theoretical background of holography, hydrodynamics and kinetic theory, I described the semiholographic framework in Chapter 3. I first motivated the phenomenological construction of semiholography in Sec. 3.1. Semiholography only needs an effective description in order to provide self-consistent couplings between two sectors. Although requiring only effective descriptions is the main advantage of semiholography for phenomenology, I discussed in Sec. 3.2 the more general case of semiholography in the case the microscopic detail is known, i.e. when there is an action principle. I then described two simple examples of the scalar and metric coupling in Sec. 3.3 and 3.4, respectively, to demonstrate how semiholography works.

Having set the stage, in Chapter 4, I discussed a phenomenological model of semiholography near equilibrium. In Sec. 4.1, I described the metric coupling between two perfect fluids in a flat Minkowski background, where the effective metric tensors encode the interactions. My collaborators and I found that the metric coupling induces a change in the light cones of each subsystem. Moreover, we found that there is a first or second order phase transition (otherwise an analytic crossover) in this model depending on the coupling parameters. In Sec. 4.2, I studied fluids in a Bjorken expanding background and found novel behavior of the coupled systems. I then turned the discussion back to Minkowski space, where we investigated viscous corrections to the perfect fluids in Sec. 4.3. In the shear channel, we found that the shear diffusion constant would decrease in each subsystem with increasing coupling, while the overall shear viscosity assumed an intermediate value between the two modes. In the sound channel, we found that one of the two modes would always have a speed close to the thermodynamic speed of sound, whereas the other was slower. In Sec. 4.4, one of sectors was described by a kinetic sector. We found that the non-hydrodynamic relaxation modes changed little or not at all due to the effective metric coupling.

Then in Chapter 5, I discussed a toy glasma model, which demonstrated for the first time energy transfer from the hard Yang Mills UV sector to the soft IR gravity theory. This was accomplished via a self-consistent numerical AdS/CFT simulation with a backreacted dynamical boundary source. Although this model was formulated in $2+1$ dimensions for simplicity, the same results should hold qualitatively in $3+1$ dimensions.

In the final example in Chapter 6, we investigated a semiholographic model describing the motion of a trapped impurity, where an impurity following Newtonian dynamics was coupled to the strongly coupled dual of $NAdS_2$, describing the self-consistent confining potential. We found that there were two distinct phases, depending on the initial velocity of the impurity. Remarkably, the black hole would always lose its mass to the dynamical boundary source or the interaction energy.

7.2 Outlook

There are plenty of possible applications and extensions of the ideas presented in this thesis. Here is a nonexhaustive list:

Fluctuations in semiholography. It would be useful to include fluctuations in semiholography. They very well may be crucial for full thermalization, but are beyond the large N limit. Furthermore, in Chapter 5, although the strongly coupled sector was inherently in a quantum regime, fluctuations did not couple to the glasma. Thus, the model can be improved from a more conceptual point of view by implementing couplings to quantum fluctuations.

Viscous corrections to Bjorken flow. In Chapter 4.2, we have only considered the invsicid case for a semiholographically coupled Bjorken fluid. Of course, if we would like to make the story more closely related to the situation in QGP, we would need to add viscous effects to see if isotropization can occur.

Attractors for conformal fluids. In the context of Bjorken flow, we can also take a look at attractor solutions in models like [82] to study off-equilibrium attractors as in [153]. It would be interesting to, say, couple two fluids and understand the late-time behaviors, such as if the full system would go to a hydrodynamic attractor as well. One of the sectors could be replaced by a kinetic-like sector, possibly providing an avenue to study the interplay of non-hydrodynamic modes with hydrodynamic attractors.

Making the toy glasma model more realistic. We can make the discussion in Chapter 5 more realistic by incorporating anisotropies in $3+1$ dimensions. This would require work on two fronts. First, we have to improve the numerical stability of our solution procedure, particularly solving the Yang-Mills equation without introducing too much numerical noise. Second, we would want to relax the symmetry assumptions, incorporating anisotropies and spatial inhomogeneities. This would mean that the spin-2 coupling channel would be opened allowing to use the full semiholographic description as detailed in [33, 36].

Improving the $NAdS_2$ model. A simple way to extend the discussion in Chapter 6 is to experiment with the form of the impurity. We can generalize its Newtonian dynamics to the relativistic case. Furthermore, we can make the impurities massive, as well as self-interacting, and investigate the effect of multiple impurities.

Recovering initial information in $NAdS_2$. As the semiholographic $NAdS_2$ represented a simple example of an evaporating black hole, it can work as a laboratory to study the sensitivity of the final state to initial conditions. In particular, it will be interesting to explore to what extent the soft hairs, i.e. the $SL(2,R)$ charges, can preserve information about the initial conditions.

$NAdS_2$ **chain models**. We can further expand our discussion in Chapter 6 by considering a chain or lattice of $NAdS_2$ holographic systems. The neighboring sites would be coupled by the the local $SL(2, R)$ charges. This can be used to explore many interesting questions at the interface of quantum information and many-body dynamics. For instance, as we have mentioned previously, in the semiholographic model we are already able to recover the complete information of the initial conditions from the final state, involving the evaporating black hole. We could investigate the existence of possible bounds on the response of the final state to initial conditions. Finally, we can use this model to study chaotic behavior in a far from equilibrium state.

Semiholography in other contexts. Semiholography is quite a flexible framework, allowing one to couple in principle any classical field theory to a strongly coupled dual. For instance, it would be interesting to couple a kinetic theory to a holographic theory to study how the quasinormal mode spectrum can influence analytic structure in kinetic theory.

7.3 Conclusions

In conclusion, semiholography is an interesting framework to explore the possible interplay between strongly and weakly coupled subsystems, by coupling a field theory to a theory dual to a gravitational one in a self-consistent manner. The features of the theory are as rich as they are diverse: phase transitions, irreversible energy transfer and even something akin to black hole evaporation in $NAdS_2$, to name a few. Although the specific examples considered in this thesis were motivated by understanding the QGP and other strongly coupled nonabelian plasmas, the framework is robust enough to work in other contexts, such as condensed matter systems and cosmology.

Appendix A

Derivation of the semiholographic action

Here we calculate the full action of the semiholographic model with democratic couplings, which recovers the full stress tensor given by (3.49). We make the following ansatz for the form of the full Lagrangian

$$\sqrt{-g^{(B)}}\mathcal{L}_{full} = \sqrt{-g}\mathcal{L}[g_{\mu\nu}] + \sqrt{-\tilde{g}}\tilde{\mathcal{L}}[\tilde{g}_{\mu\nu}] + \sqrt{-g^{(B)}}\mathcal{L}_{int} \tag{A.1}$$

with the idea that as $\gamma, \gamma' \to 0$, $\mathcal{L}_{int} \to 0$ and the subsystems decouple. We find that

$$\mathcal{L}_{int} = \frac{1}{2}\frac{\sqrt{-g}\sqrt{-\tilde{g}}}{\sqrt{-g^{(B)}}\sqrt{-g^{(B)}}}\left(\gamma t \cdot \tilde{t} + \gamma' t^{\rho\sigma} g^{(B)}_{\rho\sigma} \tilde{t}^{\gamma\delta} g^{(B)}_{\gamma\delta}\right) \tag{A.2}$$

It is worthwhile to point out that the derivation does not depend on the variation of the stress tensor with respect to the effective metric, i.e. the only information that we need from each subsystem is that the variation of the subsystem Lagrangian w.r.t. the effective metric is the subsystem stress tensor.

The derivation of this result proceeds as follows. We consider the full energy-momentum tensor:

$$\begin{aligned}
T^{\mu}{}_{\beta}\sqrt{-g^{(B)}} &= -2g^{(B)}_{\alpha\beta}\frac{\partial\left(\sqrt{-g^{(B)}}\mathcal{L}_{full}\right)}{\partial g^{(B)}_{\alpha\mu}}, \\
&= -2g^{(B)}_{\alpha\beta}\Big[\frac{\partial(\sqrt{-g}\mathcal{L})}{\partial g^{(B)}_{\alpha\mu}} + \frac{\partial(\sqrt{-\tilde{g}}\tilde{\mathcal{L}})}{\partial g^{(B)}_{\alpha\mu}} + \frac{\partial(\sqrt{-g^{(B)}}\mathcal{L}_{int})}{\partial g^{(B)}_{\alpha\mu}}\Big], \\
&= -2g^{(B)}_{\alpha\beta}\Big[\frac{\partial(\sqrt{-g}\mathcal{L})}{\partial g_{\rho\sigma}}\frac{\partial g_{\rho\sigma}}{\partial g^{(B)}_{\alpha\mu}} + \frac{\partial(\sqrt{-\tilde{g}}\tilde{\mathcal{L}})}{\partial \tilde{g}_{\rho\sigma}}\frac{\partial \tilde{g}_{\rho\sigma}}{\partial g^{(B)}_{\alpha\mu}} + \frac{\partial(\sqrt{-g^{(B)}}\mathcal{L}_{int})}{\partial g^{(B)}_{\alpha\mu}}\Big], \\
&= g^{(B)}_{\alpha\beta}\Big[\sqrt{-g}t^{\rho\sigma}\frac{\partial g_{\rho\sigma}}{\partial g^{(B)}_{\alpha\mu}} + \sqrt{-\tilde{g}}\tilde{t}^{\rho\sigma}\frac{\partial \tilde{g}_{\rho\sigma}}{\partial g^{(B)}_{\alpha\mu}} - 2\frac{\partial(\sqrt{-g^{(B)}}\mathcal{L}_{int})}{\partial g^{(B)}_{\alpha\mu}}\Big].
\end{aligned} \tag{A.3}$$

Now we make use of the coupling equations

$$g_{\mu\nu} = g^{(B)}_{\mu\nu} + \gamma \frac{\sqrt{-\tilde{g}}}{\sqrt{-g^{(B)}}} g^{(B)}_{\mu\gamma} \tilde{t}^{\gamma\delta} g^{(B)}_{\delta\nu} + \gamma' \frac{\sqrt{-\tilde{g}}}{\sqrt{-g^{(B)}}} g^{(B)}_{\mu\nu} \tilde{t}^{\gamma\delta} g^{(B)}_{\gamma\delta}$$

$$\tilde{g}_{\mu\nu} = g^{(B)}_{\mu\nu} + \gamma \frac{\sqrt{-g}}{\sqrt{-g^{(B)}}} g^{(B)}_{\mu\gamma} t^{\gamma\delta} g^{(B)}_{\delta\nu} + \gamma' \frac{\sqrt{-g}}{\sqrt{-g^{(B)}}} g^{(B)}_{\mu\nu} t^{\gamma\delta} g^{(B)}_{\gamma\delta} \tag{A.4}$$

We then have

$$\begin{aligned} T^{\mu}{}_{\beta}\sqrt{-g^{(B)}} = g^{(B)}_{\alpha\beta}\Big[&\Big(\sqrt{-g}t^{\rho\sigma} + \sqrt{-\tilde{g}}\tilde{t}^{\rho\sigma}\Big)\delta^{(\alpha}_{\rho}\delta^{\mu)}_{\sigma} \\ &+ \gamma\sqrt{-g}t^{\rho\sigma}\frac{\partial}{\partial g^{(B)}_{\alpha\mu}}\Big(\frac{\sqrt{-\tilde{g}}}{\sqrt{-g^{(B)}}} g^{(B)}_{\rho\gamma}\tilde{t}^{\gamma\delta}g^{(B)}_{\delta\sigma}\Big) \\ &+ \gamma\sqrt{-\tilde{g}}\tilde{t}^{\rho\sigma}\frac{\partial}{\partial g^{(B)}_{\alpha\mu}}\Big(\frac{\sqrt{-g}}{\sqrt{-g^{(B)}}} g^{(B)}_{\rho\gamma}t^{\gamma\delta}g^{(B)}_{\delta\sigma}\Big) \\ &+ \gamma'\sqrt{-g}t^{\rho\sigma}\frac{\partial}{\partial g^{(B)}_{\alpha\mu}}\Big(\frac{\sqrt{-\tilde{g}}}{\sqrt{-g^{(B)}}} g^{(B)}_{\rho\sigma}\tilde{t}^{\gamma\delta}g^{(B)}_{\gamma\delta}\Big) \\ &+ \gamma'\sqrt{-\tilde{g}}\tilde{t}^{\rho\sigma}\frac{\partial}{\partial g^{(B)}_{\alpha\mu}}\Big(\frac{\sqrt{-g}}{\sqrt{-g^{(B)}}} g^{(B)}_{\rho\sigma}t^{\gamma\delta}g^{(B)}_{\gamma\delta}\Big) - 2\frac{\partial(\sqrt{-g^{(B)}}\mathcal{L}_{int})}{\partial g^{(B)}_{\alpha\mu}}\Big] \end{aligned} \tag{A.5}$$

We can rewrite the second line as

$$\begin{aligned} \gamma\sqrt{-g}t^{\rho\sigma}\frac{\partial}{\partial g^{(B)}_{\alpha\mu}}\Big(\frac{\sqrt{-\tilde{g}}}{\sqrt{-g^{(B)}}} g^{(B)}_{\rho\gamma}\tilde{t}^{\gamma\delta}g^{(B)}_{\delta\sigma}\Big) &= \gamma\frac{\partial}{\partial g^{(B)}_{\alpha\mu}}\Big(\sqrt{-g}t^{\rho\sigma}\frac{\sqrt{-\tilde{g}}}{\sqrt{-g^{(B)}}} g^{(B)}_{\rho\gamma}\tilde{t}^{\gamma\delta}g^{(B)}_{\delta\sigma}\Big) \\ &- \gamma\frac{\sqrt{-\tilde{g}}}{\sqrt{-g^{(B)}}} g^{(B)}_{\rho\gamma}\tilde{t}^{\gamma\delta}g^{(B)}_{\delta\sigma}\frac{\partial}{\partial g^{(B)}_{\alpha\mu}}\Big(\sqrt{-g}t^{\rho\sigma}\Big), \end{aligned} \tag{A.6}$$

and the third line as

$$\begin{aligned} \gamma\sqrt{-\tilde{g}}\tilde{t}^{\rho\sigma}\frac{\partial}{\partial g^{(B)}_{\alpha\mu}}\Big(\frac{\sqrt{-g}}{\sqrt{-g^{(B)}}} g^{(B)}_{\rho\gamma}t^{\gamma\delta}g^{(B)}_{\delta\sigma}\Big) &= \gamma\frac{\sqrt{-\tilde{g}}}{\sqrt{-g^{(B)}}} g^{(B)}_{\rho\gamma}\tilde{t}^{\rho\sigma}g^{(B)}_{\delta\sigma}\frac{\partial}{\partial g^{(B)}_{\alpha\mu}}\Big(\sqrt{-g}t^{\gamma\delta}\Big) \\ &+ \gamma\frac{\sqrt{-\tilde{g}}}{\sqrt{-g^{(B)}}}\sqrt{-g}\tilde{t}^{\rho\sigma}t^{\gamma\delta}\frac{\partial}{\partial g^{(B)}_{\alpha\mu}}\Big(g^{(B)}_{\delta\sigma}g^{(B)}_{\rho\gamma}\Big) \\ &+ \gamma\sqrt{-g}\sqrt{-\tilde{g}}\tilde{t}^{\rho\sigma}g^{(B)}_{\rho\gamma}t^{\gamma\delta}g^{(B)}_{\delta\sigma}\frac{\partial}{\partial g^{(B)}_{\alpha\mu}}\frac{1}{\sqrt{-g^{(B)}}}. \end{aligned} \tag{A.7}$$

Similarly to the terms proportional to γ, we can rewrite the fourth line and fifth lines as

$$\begin{aligned} \gamma'\sqrt{-g}t^{\rho\sigma}\frac{\partial}{\partial g^{(B)}_{\alpha\mu}}\Big(\frac{\sqrt{-\tilde{g}}}{\sqrt{-g^{(B)}}} g^{(B)}_{\rho\sigma}\tilde{t}^{\gamma\delta}g^{(B)}_{\gamma\delta}\Big) &= +\gamma'\frac{\partial}{\partial g^{(B)}_{\alpha\mu}}\Big(\sqrt{-g}t^{\rho\sigma}\frac{\sqrt{-\tilde{g}}}{\sqrt{-g^{(B)}}} g^{(B)}_{\rho\sigma}\tilde{t}^{\gamma\delta}g^{(B)}_{\gamma\delta}\Big) \\ &- \gamma'\frac{\sqrt{-\tilde{g}}}{\sqrt{-g^{(B)}}} g^{(B)}_{\rho\sigma}\tilde{t}^{\gamma\delta}g^{(B)}_{\gamma\delta}\frac{\partial}{\partial g^{(B)}_{\alpha\mu}}\Big(\sqrt{-g}t^{\rho\sigma}\Big), \end{aligned} \tag{A.8}$$

and

$$\gamma'\sqrt{-\tilde g}\tilde t^{\rho\sigma}\frac{\partial}{\partial g^{(B)}_{\alpha\mu}}\Big(\frac{\sqrt{-g}}{\sqrt{-g^{(B)}}}g^{(B)}_{\rho\sigma}t^{\gamma\delta}g^{(B)}_{\gamma\delta}\Big)=\gamma'\frac{\sqrt{-\tilde g}}{\sqrt{-g^{(B)}}}\tilde t^{\rho\sigma}g^{(B)}_{\rho\sigma}g^{(B)}_{\gamma\delta}\frac{\partial}{\partial g^{(B)}_{\alpha\mu}}\Big(\sqrt{-g}t^{\gamma\delta}\Big)$$
$$+\gamma'\frac{\sqrt{-g}\sqrt{-\tilde g}}{\sqrt{-g^{(B)}}}\tilde t^{\rho\sigma}t^{\gamma\delta}\frac{\partial}{\partial g^{(B)}_{\alpha\mu}}\Big(g^{(B)}_{\rho\sigma}g^{(B)}_{\gamma\delta}\Big)$$
$$+\gamma'\sqrt{-\tilde g}\sqrt{-g}\tilde t^{\rho\sigma}g^{(B)}_{\rho\sigma}t^{\gamma\delta}g^{(B)}_{\gamma\delta}\frac{\partial}{\partial g^{(B)}_{\alpha\mu}}\Big(\frac{1}{\sqrt{-g^{(B)}}}\Big).$$

Finally, recall that

$$\frac{\partial}{\partial g^{(B)}_{\alpha\mu}}\frac{1}{\sqrt{-g^{(B)}}}=-\frac{1}{2\sqrt{-g^{(B)}}}g^{(B)\alpha\mu}. \tag{A.9}$$

Putting it all together

$$T^\mu{}_\beta\sqrt{-g^{(B)}}=g^{(B)}_{\alpha\beta}\Big[\Big(\sqrt{-g}t^{\rho\sigma}+\sqrt{-\tilde g}\tilde t^{\rho\sigma}\Big)\delta^{(\alpha}_\rho\delta^{\mu)}_\sigma$$
$$+\gamma\frac{\sqrt{-\tilde g}\sqrt{-g}}{\sqrt{-g^{(B)}}}\tilde t^{\rho\sigma}t^{\gamma\delta}\frac{\partial}{\partial g^{(B)}_{\alpha\mu}}\Big(g^{(B)}_{\delta\sigma}g^{(B)}_{\rho\gamma}\Big)+\gamma'\frac{\sqrt{-g}\sqrt{-\tilde g}}{\sqrt{-g^{(B)}}}\tilde t^{\rho\sigma}t^{\gamma\delta}\frac{\partial}{\partial g^{(B)}_{\alpha\mu}}\Big(g^{(B)}_{\rho\sigma}g^{(B)}_{\gamma\delta}\Big)$$
$$-\gamma g^{(B)\alpha\mu}\frac{\sqrt{-g}\sqrt{-\tilde g}}{2\sqrt{-g^{(B)}}}t\cdot\tilde t-\gamma' g^{(B)\alpha\mu}\frac{\sqrt{-g}\sqrt{-\tilde g}}{2\sqrt{-g^{(B)}}}g^{(B)}_{\rho\sigma}\tilde t^{\rho\sigma}t^{\gamma\delta}g^{(B)}_{\gamma\delta}$$
$$+\frac{\partial}{\partial g^{(B)}_{\alpha\mu}}\Big[-2\sqrt{-g^{(B)}}\mathcal{L}_{int}+\frac{\sqrt{-g}\sqrt{-\tilde g}}{\sqrt{-g^{(B)}}}(\gamma t\cdot\tilde t+\gamma' t^{\rho\sigma}g^{(B)}_{\rho\sigma}\tilde t^{\gamma\delta}g^{(B)}_{\gamma\delta})\Big] \tag{A.10}$$
$$+\gamma'\frac{\sqrt{-\tilde g}}{\sqrt{-g^{(B)}}}g^{(B)}_{\rho\sigma}\tilde t^{\gamma\delta}g^{(B)}_{\gamma\delta}\frac{\partial}{\partial g^{(B)}_{\alpha\mu}}\Big(\sqrt{-g}t^{\rho\sigma}\Big)-\gamma'\frac{\sqrt{-\tilde g}}{\sqrt{-g^{(B)}}}\tilde t^{\rho\sigma}g^{(B)}_{\rho\sigma}g^{(B)}_{\gamma\delta}\frac{\partial}{\partial g^{(B)}_{\alpha\mu}}\Big(\sqrt{-g}t^{\gamma\delta}\Big) \tag{A.11}$$
$$+\gamma\frac{\sqrt{-\tilde g}}{\sqrt{-g^{(B)}}}g^{(B)}_{\rho\gamma}\tilde t^{\gamma\delta}g^{(B)}_{\delta\sigma}\frac{\partial}{\partial g^{(B)}_{\alpha\mu}}\Big(\sqrt{-g}t^{\rho\sigma}\Big)-\gamma\frac{\sqrt{-\tilde g}}{\sqrt{-g^{(B)}}}g^{(B)}_{\rho\gamma}\tilde t^{\rho\sigma}g^{(B)}_{\delta\sigma}\frac{\partial}{\partial g^{(B)}_{\alpha\mu}}\Big(\sqrt{-g}t^{\gamma\delta}\Big)\Big]. \tag{A.12}$$

We see that the last two lines vanish. The line above that vanishes as well, if we identify

$$\mathcal{L}_{int}=\frac{1}{2}\frac{\sqrt{-g}\sqrt{-\tilde g}}{\sqrt{-g^{(B)}}\sqrt{-g^{(B)}}}\Big(\gamma t\cdot\tilde t+\gamma' t^{\rho\sigma}g^{(B)}_{\rho\sigma}\tilde t^{\gamma\delta}g^{(B)}_{\gamma\delta}\Big). \tag{A.13}$$

The terms that are left are nothing more than the stress tensor. This becomes clear after further manipulation.

$$T^\mu{}_\beta\sqrt{-g^{(B)}}=g^{(B)}_{\alpha\beta}\Big[\Big(\sqrt{-g}t^{\rho\sigma}+\sqrt{-\tilde g}\tilde t^{\rho\sigma}\Big)\delta^{(\alpha}_\rho\delta^{\mu)}_\sigma$$
$$+\gamma\frac{\sqrt{-\tilde g}\sqrt{-g}}{\sqrt{-g^{(B)}}}\tilde t^{\rho\sigma}t^{\gamma\delta}\frac{\partial}{\partial g^{(B)}_{\alpha\mu}}\Big(g^{(B)}_{\delta\sigma}g^{(B)}_{\rho\gamma}\Big)-\frac{\gamma}{2}g^{(B)\alpha\mu}\frac{\sqrt{-g}\sqrt{-\tilde g}}{\sqrt{-g^{(B)}}}t\cdot\tilde t$$
$$+\gamma'\frac{\sqrt{-g}\sqrt{-\tilde g}}{\sqrt{-g^{(B)}}}\tilde t^{\rho\sigma}t^{\gamma\delta}\frac{\partial}{\partial g^{(B)}_{\alpha\mu}}\Big(g^{(B)}_{\rho\sigma}g^{(B)}_{\gamma\delta}\Big)-\frac{\gamma'}{2}g^{(B)\alpha\mu}\frac{\sqrt{-g}\sqrt{-\tilde g}}{\sqrt{-g^{(B)}}}g^{(B)}_{\rho\sigma}t^{\gamma\delta}g^{(B)}_{\gamma\delta}\tilde t^{\rho\sigma}\Big] \tag{A.14}$$

We expand the first line of the above

$$g^{(B)}_{\alpha\beta}\left(\sqrt{-g}t^{\rho\sigma}+\sqrt{-\tilde{g}}\tilde{t}^{\rho\sigma}\right)\delta^{(\alpha}_{\rho}\delta^{\mu)}_{\sigma}=\frac{1}{2}\sqrt{-g}\left(t^{\mu\sigma}g^{(B)}_{\beta\sigma}+t^{\sigma\mu}g^{(B)}_{\beta\sigma}\right)+\frac{1}{2}\sqrt{-\tilde{g}}\left(\tilde{t}^{\mu\sigma}g^{(B)}_{\beta\sigma}+\tilde{t}^{\sigma\mu}g^{(B)}_{\beta\sigma}\right) \tag{A.15}$$

Using the coupling equations, we have

$$\begin{aligned}
&\frac{1}{2}\sqrt{-g}\left(t^{\mu\sigma}g^{(B)}_{\beta\sigma}+t^{\sigma\mu}g^{(B)}_{\beta\sigma}\right)+\frac{1}{2}\sqrt{-\tilde{g}}\left(\tilde{t}^{\mu\sigma}g^{(B)}_{\beta\sigma}+\tilde{t}^{\sigma\mu}g^{(B)}_{\beta\sigma}\right)\\
&=\frac{\sqrt{-g}}{2}\left({t^{\mu}}_{\beta}+{t_{\beta}}^{\mu}\right)+\frac{\sqrt{-\tilde{g}}}{2}\left({\tilde{t}^{\mu}}_{\beta}+{\tilde{t}_{\beta}}^{\mu}\right)\\
&-\gamma\frac{\sqrt{-g}\sqrt{-\tilde{g}}}{\sqrt{-g^{(B)}}}\left(g^{(B)}_{\beta\gamma}\tilde{t}^{\gamma\delta}g^{(B)}_{\delta\sigma}t^{\mu\sigma}+g^{(B)}_{\sigma\gamma}\tilde{t}^{\gamma\delta}g^{(B)}_{\delta\beta}t^{\mu\sigma}\right)\\
&-\gamma'\frac{\sqrt{-g}\sqrt{-\tilde{g}}}{\sqrt{-g^{(B)}}}\left(t^{\mu\sigma}g^{(B)}_{\beta\sigma}\tilde{t}^{\gamma\delta}g^{(B)}_{\gamma\delta}+\tilde{t}^{\mu\sigma}g^{(B)}_{\beta\sigma}t^{\gamma\delta}g^{(B)}_{\gamma\delta}\right)\\
&=\frac{\sqrt{-g}}{2}\left({t^{\mu}}_{\beta}+{t_{\beta}}^{\mu}\right)+\frac{\sqrt{-\tilde{g}}}{2}\left({\tilde{t}^{\mu}}_{\beta}+{\tilde{t}_{\beta}}^{\mu}\right)\\
&-\gamma g^{(B)}_{\mu\alpha}\frac{\sqrt{-\tilde{g}}\sqrt{-g}}{\sqrt{-g^{(B)}}}\tilde{t}^{\rho\sigma}t^{\gamma\delta}\frac{\partial}{\partial g^{(B)}_{\alpha\mu}}\left(g^{(B)}_{\delta\sigma}g^{(B)}_{\rho\gamma}\right)\\
&-\gamma' g^{(B)}_{\mu\alpha}\frac{\sqrt{-\tilde{g}}\sqrt{-g}}{\sqrt{-g^{(B)}}}\tilde{t}^{\rho\sigma}t^{\gamma\delta}\frac{\partial}{\partial g^{(B)}_{\alpha\mu}}\left(g^{(B)}_{\rho\sigma}g^{(B)}_{\delta\gamma}\right)
\end{aligned} \tag{A.16}$$

Thus, we have

$$\begin{aligned}
{T^{\mu}}_{\beta}\sqrt{-g^{(B)}}&=g^{(B)}_{\alpha\beta}\left(\sqrt{-g}t^{\rho\sigma}+\sqrt{-\tilde{g}}\tilde{t}^{\rho\sigma}\right)\delta^{(\alpha}_{\rho}\delta^{\mu)}_{\sigma}\\
&+\gamma g^{(B)}_{\mu\alpha}\frac{\sqrt{-\tilde{g}}\sqrt{-g}}{\sqrt{-g^{(B)}}}\tilde{t}^{\rho\sigma}t^{\gamma\delta}\frac{\partial}{\partial g^{(B)}_{\alpha\mu}}\left(g^{(B)}_{\delta\sigma}g^{(B)}_{\rho\gamma}\right)-\frac{\gamma}{2}\delta^{\mu}_{\nu}\frac{\sqrt{-g}\sqrt{-\tilde{g}}}{\sqrt{-g^{(B)}}}t\cdot\tilde{t}\\
&+\gamma' g^{(B)}_{\mu\alpha}\frac{\sqrt{-\tilde{g}}\sqrt{-g}}{\sqrt{-g^{(B)}}}\tilde{t}^{\rho\sigma}t^{\gamma\delta}\frac{\partial}{\partial g^{(B)}_{\alpha\mu}}\left(g^{(B)}_{\rho\sigma}g^{(B)}_{\delta\gamma}\right)-\frac{\gamma'}{2}\delta^{\mu}_{\nu}\frac{\sqrt{-g}\sqrt{-\tilde{g}}}{\sqrt{-g^{(B)}}}g^{(B)}_{\rho\sigma}t^{\gamma\delta}g^{(B)}_{\gamma\delta}\tilde{t}^{\rho\sigma}]\\
&=\frac{\sqrt{-g}}{2}\left({t^{\mu}}_{\beta}+{t_{\beta}}^{\mu}\right)+\frac{\sqrt{-\tilde{g}}}{2}\left({\tilde{t}^{\mu}}_{\beta}+{\tilde{t}_{\beta}}^{\mu}\right)\\
&-\frac{\gamma}{2}\delta^{\mu}_{\beta}\frac{\sqrt{-g}\sqrt{-\tilde{g}}}{\sqrt{-g^{(B)}}}t\cdot\tilde{t}-\frac{\gamma'}{2}\delta^{\mu}_{\beta}\frac{\sqrt{-g}\sqrt{-\tilde{g}}}{2\sqrt{-g^{(B)}}}\tilde{t}^{\rho\sigma}g^{(B)}_{\rho\sigma}t^{\gamma\delta}g^{(B)}_{\gamma\delta}
\end{aligned} \tag{A.17}$$

which is indeed the full stress tensor.

A.1 Rewriting the interaction term

Temporarily setting $\gamma' \to 0$, it is also interesting to note that we can rewrite the interaction term via the coupling equations. First observe that using the coupling equations

$$\begin{aligned}(g_{\mu\nu} - g^{(B)}_{\mu\nu})g^{(B)\mu\alpha}(\tilde{g}_{\alpha\beta} - g^{(B)}_{\alpha\beta})g^{(B)\nu\beta} &= g^{(B)\mu\alpha}g^{(B)\nu\beta}\gamma\frac{\sqrt{-\tilde{g}}}{\sqrt{-g^{(B)}}}g^{(B)}_{\mu\gamma}\tilde{t}^{\gamma\delta}g^{(B)}_{\delta\nu}\gamma\frac{\sqrt{-g}}{\sqrt{-g^{(B)}}}g^{(B)}_{\alpha\gamma}t^{\gamma\delta}g^{(B)}_{\delta\beta}\\ &= \frac{\sqrt{-\tilde{g}}}{\sqrt{-g^{(B)}}}\frac{\sqrt{-\tilde{g}}}{\sqrt{-g^{(B)}}}\gamma^2 t\cdot\tilde{t}. \end{aligned} \tag{A.18}$$

We can write the action as

$$\begin{aligned}S_{full}[\phi,\tilde{\phi},g_{\mu\nu},\tilde{g}_{\mu\nu},g^{(B)}_{\mu\nu}] = \int \mathrm{d}^D x\Big[\sqrt{-g}\mathcal{L}[\phi,g_{\mu\nu}] + \sqrt{-\tilde{g}}\tilde{\mathcal{L}}[\tilde{\phi},\tilde{g}_{\mu\nu}]\\ + \frac{1}{2\gamma}\sqrt{-g^{(B)}}(g_{\mu\nu} - g^{(B)}_{\mu\nu})g^{(B)\mu\alpha}(\tilde{g}_{\alpha\beta} - g^{(B)}_{\alpha\beta})g^{(B)\nu\beta}\Big]. \end{aligned} \tag{A.19}$$

Then the equations of motion for the matter fields are the standard Euler-Lagrange equations. The variation of the above action w.r.t. $g^{\mu\nu}$ yields

$$\begin{aligned}0 &= -\frac{1}{2}t_{\mu\nu}\sqrt{-g} + \frac{1}{2\gamma}\sqrt{-g^{(B)}}(\tilde{g}_{\mu\nu} - g^{(B)}_{\mu\nu})\\ \to \tilde{g}_{\mu\nu} &= g^{(B)}_{\mu\nu} + \gamma t_{\mu\nu}\frac{\sqrt{-g}}{\sqrt{-g^{(B)}}}, \end{aligned} \tag{A.20}$$

where we used the shorthand

$$t_{\mu\nu} \equiv g^{(B)}_{\mu\gamma}t^{\gamma\delta}g^{(B)}_{\delta\nu}. \tag{A.21}$$

This is nothing more than the coupling equation, which we can view as a constraint equation on the form of the two effective metrics.

A.1.1 Adding the trace term

We will still need to incorporate the trace term. First we take the trace of a coupling equation with respect to the background metric

$$\begin{aligned}\tilde{g}_{\mu\nu} &= g^{(B)}_{\mu\nu} + \frac{\sqrt{-g}}{\sqrt{-g^{(B)}}}(\gamma t_{\mu\nu} + \gamma' g^{(B)}_{\mu\nu} t\cdot g^{(B)}),\\ \to \frac{\sqrt{-g}}{\sqrt{-g^{(B)}}}t\cdot g^{(B)} &= \frac{\tilde{g}\cdot g^{(B)} - D}{\gamma + \gamma' D}, \end{aligned} \tag{A.22}$$

where $D = g^{(\mathrm{B})}_{\mu\nu}g^{(\mathrm{B})\mu\nu}$ is the spacetime dimension. This means that we can reinterpret the coupling equations

$$\begin{aligned}\tilde{g}_{\mu\nu} &= g^{(B)}_{\mu\nu}(1 + \gamma'\frac{\tilde{g}\cdot g^{(B)} - D}{\gamma + \gamma' D}) + \frac{\sqrt{-g}}{\sqrt{-g^{(B)}}}\gamma t_{\mu\nu}\\ \Rightarrow \frac{\sqrt{-g}}{\sqrt{-g^{(B)}}}\gamma t_{\mu\nu} &= \tilde{g}_{\mu\nu} - g^{(B)}_{\mu\nu}(1 + \gamma'\frac{\tilde{g}\cdot g^{(B)} - D}{\gamma + \gamma' D}). \end{aligned}$$

So if we improve our interaction term by this factor

$$\frac{1}{\gamma}\sqrt{-g^{(B)}}\Big((g - g^{(B)}(1+\gamma'\frac{g\cdot g^{(B)}-D}{\gamma+\gamma' D}))\cdot(\tilde{g} - g^{(B)}(1+\gamma'\frac{\tilde{g}\cdot g^{(B)}-D}{\gamma+\gamma' D})) + extra\Big), \quad \text{(A.23)}$$

(where we now aim to determine the form of the *extra* terms), then the variation of the full action w.r.t. $g_{\mu\nu}$ is

$$0 = -t_{\mu\nu}\sqrt{-g} + \frac{1}{\gamma}\sqrt{-g^{(B)}}\Big(\tilde{g}_{\mu\nu} - g^{(B)}_{\mu\nu}(1+\gamma'\frac{\tilde{g}\cdot g^{(B)}-D}{\gamma+\gamma' D})$$
$$-\gamma' g^{(B)}_{\mu\nu}(\frac{g^{(B)}\cdot(\tilde{g}-g^{(B)}(1+\gamma'\frac{\tilde{g}\cdot g^{(B)}-D}{\gamma+\gamma' D}))}{\gamma+\gamma' D}) + \frac{\delta extra}{\delta g_{\mu\nu}}\Big)$$

$$\Rightarrow \tilde{g}_{\mu\nu} = g^{(B)}_{\mu\nu} + \gamma t_{\mu\nu}\frac{\sqrt{-g}}{\sqrt{-g^{(B)}}} + \gamma' g^{(B)}_{\mu\nu}\Big(\frac{\tilde{g}\cdot g^{(B)}-D}{\gamma+\gamma' D} + \frac{g^{(B)}\cdot\tilde{g} - D(1+\gamma'\frac{\tilde{g}\cdot g^{(B)}-D}{\gamma+\gamma' D})}{\gamma+\gamma' D}\Big) - \frac{\delta extra}{\delta g_{\mu\nu}}$$

$$\tilde{g}_{\mu\nu} = g^{(B)}_{\mu\nu} + \gamma t_{\mu\nu}\frac{\sqrt{-g}}{\sqrt{-g^{(B)}}} + \frac{\gamma' g^{(B)}_{\mu\nu}(\tilde{g}\cdot g^{(B)}-D)}{\gamma+\gamma' D}(1+\frac{\gamma}{\gamma+\gamma' D}) - \frac{\delta extra}{\delta g_{\mu\nu}} \quad \text{(A.24)}$$

So we see that if we add a term like

$$\frac{\gamma\gamma'(g\cdot g^{(B)}-D)(\tilde{g}\cdot g^{(B)}-D)}{(\gamma+\gamma' D)^2} \quad \text{(A.25)}$$

to the action, then we have exactly the right coupling rules. Note that (A.25) is nothing more than the term proportional to γ' in (A.13)

$$\frac{\gamma'(g\cdot g^{(B)}-D)(\tilde{g}\cdot g^{(B)}-D)}{(\gamma+\gamma' D)^2} = \gamma'\frac{\sqrt{-g}}{\sqrt{-g^{(B)}}}\frac{\sqrt{-\tilde{g}}}{\sqrt{-g^{(B)}}}t\cdot g^{(B)}\tilde{t}\cdot g^{(B)} \quad \text{(A.26)}$$

The full action now reads

$$S_{full}[\phi,\tilde{\phi},g_{\mu\nu},\tilde{g}_{\mu\nu},g^{(B)}_{\mu\nu}] = \int \mathrm{d}^D x\Big[\sqrt{-g}\mathcal{L}[\phi,g_{\mu\nu}] + \sqrt{-\tilde{g}}\tilde{\mathcal{L}}[\tilde{\phi},\tilde{g}_{\mu\nu}]$$
$$+\frac{1}{2\gamma}\sqrt{-g^{(B)}}\Big(g - g^{(B)}(1+\gamma'\frac{g\cdot g^{(B)}-D}{\gamma+\gamma' D})\Big)\cdot\Big(\tilde{g} - g^{(B)}(1+\gamma'\frac{\tilde{g}\cdot g^{(B)}-D}{\gamma+\gamma' D})\Big)$$
$$+\frac{\gamma'}{2}\sqrt{-g^{(B)}}\frac{(g\cdot g^{(B)}-D)(\tilde{g}\cdot g^{(B)}-D)}{(\gamma+\gamma' D)^2}\Big], \quad \text{(A.27)}$$

which can be further simplified to

$$S_{full}[\phi,\tilde{\phi},g_{\mu\nu},\tilde{g}_{\mu\nu},g^{(B)}_{\mu\nu}] = \int \mathrm{d}^D x\Big[\sqrt{-g}\mathcal{L}[\phi,g_{\mu\nu}] + \sqrt{-\tilde{g}}\tilde{\mathcal{L}}[\tilde{\phi},\tilde{g}_{\mu\nu}]$$
$$+\frac{1}{2\gamma}\sqrt{-g^{(B)}}\Big(g-g^{(B)}\Big)\cdot\Big(\tilde{g}-g^{(B)}\Big)$$
$$-\frac{\gamma'}{2\gamma}\sqrt{-g^{(B)}}\frac{(g\cdot g^{(B)}-D)(\tilde{g}\cdot g^{(B)}-D)}{\gamma+\gamma' D}\Big], \quad \text{(A.28)}$$

where the contractions are to be taken w.r.t. the background metric $g^{(B)\mu\nu}$.

Now the story is complete: the variation of this action w.r.t. the matter fields yields the usual EOMs. The variation w.r.t. the effective metrics now gives the complete coupling rules. These can be thought of as auxiliary fields since their EOMs are just algebraic equations. Finally, the variation w.r.t. the background metric yields the full theory stress tensor.

A.1.2 A check on the Ward identities

It is straightforward to see that the Ward identity for each system holds. We treat $g_{\mu\nu}$, $\tilde{g}_{\mu\nu}$ and $g^{(B)}_{\mu\nu}$ as fundamental fields and consider the variation of the on-shell action

$$\delta S_{full} = \int \mathrm{d}^4x \Big[\frac{\delta\sqrt{-g}\mathcal{L}[g_{\mu\nu}]}{\delta g_{\mu\nu}}\delta_X g_{\mu\nu} + \frac{\delta\sqrt{-\tilde{g}}\tilde{\mathcal{L}}[\tilde{g}_{\mu\nu}]}{\delta\tilde{g}_{\mu\nu}}\delta_X\tilde{g}_{\mu\nu} + \delta(interactions) \tag{A.29}$$

Consider the infinitesimal spacetime translation

$$x^\mu \to x^\mu + \varepsilon^\mu, \tag{A.30}$$

under which the metrics transform as

$$\delta_\varepsilon g_{\mu\nu} = \nabla_\mu\varepsilon_\nu + \nabla_\nu\varepsilon_\mu, \tag{A.31}$$
$$\delta_\varepsilon\tilde{g}_{\mu\nu} = \tilde{\nabla}_\mu\varepsilon_\nu + \tilde{\nabla}_\nu\varepsilon_\mu. \tag{A.32}$$
$$\delta_\varepsilon g^{(B)}_{\mu\nu} = \nabla^{(B)}_\mu\varepsilon_\nu + \nabla^{(B)}_\nu\varepsilon_\mu. \tag{A.33}$$

Note that considering the variation with $g^{(B)}_{\mu\nu}$ means we arrive at the Ward identity for the complete system. Now we focus on just the variation with respect to $g_{\mu\nu}$. Then, using that

$$\sqrt{-g}t^{\mu\nu} = -2\frac{\delta\sqrt{-g}\mathcal{L}[g_{\mu\nu}]}{\delta g_{\mu\nu}} \tag{A.34}$$

and after partial integration

$$\begin{aligned}
0 = \delta S_{full} &= \int \mathrm{d}^4x\Big[\frac{1}{2}\varepsilon_{(\nu}\nabla_{\mu)}t^{\mu\nu}\sqrt{-g} + \frac{1}{2\gamma}\varepsilon_{(\nu}\nabla_{\mu)}\Big[\sqrt{-g^{(B)}}\Big\{\Big(\tilde{g} - g^{(B)}(1+\gamma'\frac{\tilde{g}\cdot g^{(B)}-D}{\gamma+\gamma' D})\Big)^{\mu\nu} \\
&- \frac{\gamma'}{\gamma+\gamma' D}g^{(B)\mu\nu}g^{(B)}\cdot\Big(\tilde{g} - g^{(B)}(1+\gamma'\frac{\tilde{g}\cdot g^{(B)}-D}{\gamma+\gamma' D})\Big) + \frac{\gamma'\gamma g^{(B)\mu\nu}(\tilde{g}\cdot g^{(B)}-D)}{(\gamma+\gamma' D)^2}\Big\}\Big] \\
&= \int \mathrm{d}^4x\Big[\frac{1}{2}\varepsilon_{(\nu}\nabla_{\mu)}t^{\mu\nu}\sqrt{-g} + \frac{1}{2\gamma}\varepsilon_{(\nu}\nabla_{\mu)}\Big[\sqrt{-g^{(B)}}\Big\{\Big(\tilde{g} - g^{(B)}(1+\gamma'\frac{\tilde{g}\cdot g^{(B)}-D}{\gamma+\gamma' D})\Big)^{\mu\nu} \\
&- \frac{\gamma'}{\gamma+\gamma' D}g^{(B)\mu\nu}(\tilde{g}\cdot g^{(B)}-D)g^{(B)}\cdot\Big(1 - \frac{\gamma' D}{\gamma+\gamma' D} - \frac{\gamma}{\gamma+\gamma' D}\Big)\Big\}\Big] \\
&= \int \mathrm{d}^4x\Big[\frac{1}{2}\varepsilon_{(\nu}\nabla_{\mu)}t^{\mu\nu}\sqrt{-g} + \frac{1}{2\gamma}\varepsilon_{(\nu}\nabla_{\mu)}\Big[\sqrt{-g^{(B)}}\Big(\tilde{g} - g^{(B)}(1+\gamma'\frac{\tilde{g}\cdot g^{(B)}-D}{\gamma+\gamma' D})\Big)^{\mu\nu}\Big].
\end{aligned} \tag{A.35}$$

Then using the coupling equation, we have that

$$\frac{1}{\gamma}\nabla_\mu\Big[\sqrt{-g^{(B)}}\Big(\tilde{g} - g^{(B)}(1+\gamma'\frac{\tilde{g}\cdot g^{(B)}-D}{\gamma+\gamma' D})\Big)^{\mu\nu}\Big] = \nabla_\mu t^{\mu\nu}\sqrt{-g}, \tag{A.36}$$

i.e.

$$0 = \delta S_{full} \propto \int \mathrm{d}^4x\varepsilon_{(\nu}\nabla_{\mu)}t^{\mu\nu}\sqrt{-g}. \tag{A.37}$$

Thus the WI are satisfied for the individual subsystems.

Appendix B

Semiholographic perfect fluids in arbitrary dimensions

Here we generalize the previous discussion in Sec. 4.1 of two perflect fluids in 3+1 dimensions to $d+1$ dimensions. As usual, we choose the background metric to be flat $g^{(B)}_{\mu\nu} = \eta_{\mu\nu}$. We assume homogeneity and isotropy, so that the metric will be diagonal and of the form

$$g_{00} = -a^2, \quad g_{ii} = b^2, \quad \tilde{g}_{00} = -\tilde{a}^2 \quad \text{and} \quad \tilde{g}_{ii} = \tilde{b}^2. \tag{B.1}$$

The energy momentum tensors of the two perfect fluids are

$$T^{00} = \frac{\varepsilon}{a^2}, \quad T^{ii} = \frac{P}{b^2}, \quad \tilde{T}^{00} = \frac{\tilde{\varepsilon}}{\tilde{a}^2} \quad \text{and} \quad \tilde{T}^{ii} = \frac{\tilde{P}}{\tilde{b}^2}. \tag{B.2}$$

The coupling equations are

$$\begin{aligned} g_{\mu\nu} &= \eta_{\mu\nu} + \gamma \tilde{T}_{\mu\nu}\sqrt{\tilde{g}} + \gamma' \eta_{\mu\nu}\tilde{T}_{\alpha\beta}\eta^{\alpha\beta}\sqrt{\tilde{g}}, \\ \tilde{g}_{\mu\nu} &= \eta_{\mu\nu} + \gamma T_{\mu\nu}\sqrt{g} + \gamma' \eta_{\mu\nu}T_{\alpha\beta}\eta^{\alpha\beta}\sqrt{g}. \end{aligned} \tag{B.3}$$

Explicitly, this reads

$$1 - a^2 = \tilde{a}\tilde{b}^d\Big[\gamma\frac{\tilde{\varepsilon}}{\tilde{a}^2} - \gamma'\Big(\frac{d\tilde{P}}{\tilde{b}^2} - \frac{\tilde{\varepsilon}}{\tilde{a}^2}\Big)\Big], \tag{B.4}$$

$$b^2 - 1 = \tilde{a}\tilde{b}^d\Big[\gamma\frac{\tilde{P}}{\tilde{b}^2} + \gamma'\Big(\frac{d\tilde{P}}{\tilde{b}^2} - \frac{\tilde{\varepsilon}}{\tilde{a}^2}\Big)\Big], \tag{B.5}$$

$$1 - \tilde{a}^2 = ab^d\Big[\gamma\frac{\varepsilon}{a^2} - \gamma'\Big(\frac{dP}{b^2} - \frac{\varepsilon}{a^2}\Big)\Big], \tag{B.6}$$

$$\tilde{b}^2 - 1 = ab^d\Big[\gamma\frac{P}{b^2} + \gamma'\Big(\frac{dP}{b^2} - \frac{\varepsilon}{a^2}\Big)\Big] \tag{B.7}$$

Clearly, there is no time dependence in these equations. As such, these equations represent a set of algebraic equations. After specifying an equation of state for both $P(\varepsilon)$ and $\tilde{P}(\tilde{\varepsilon})$, (B.4)-(B.7) represents a closed set of equations.

Note that we require $\gamma > 0$ to ensure that the light cones are within the light cone defined by the Minkowski metric, i.e. $1 > \frac{a}{b} \Rightarrow b > a$. This can be seen by adding the first two equations and, equivalently, the last two:

$$b^2 - a^2 = \gamma\Big[\frac{\tilde{P}}{\tilde{b}^2} - \frac{\tilde{\varepsilon}}{\tilde{a}^2}\Big]\tilde{a}\tilde{b}^d > 0, \tag{B.8}$$

$$\tilde{b}^2 - \tilde{a}^2 = \gamma\Big[\frac{P}{b^2} - \frac{\varepsilon}{a^2}\Big]ab^d > 0. \tag{B.9}$$

To make contact with Sec. 4.1, we choose for both sectors to be conformal, such that their equation of state is

$$\varepsilon = dP = dn_1 T_1^{d+1}, \quad \text{and} \quad \tilde{\varepsilon} = d\tilde{P} = dn_2 T_2^{d+1}. \tag{B.10}$$

Furthermore, we assume that the system is in thermal equilibrium, such that the physical, system temperature, $\mathcal{T}$, is related to the effective temperatures, T_1 and T_2, via

$$\mathcal{T} = \sqrt{-g_{00}}T_1 = aT_1, \tag{B.11}$$
$$\mathcal{T} = \sqrt{-\tilde{g}_{00}}T_2 = \tilde{a}T_2. \tag{B.12}$$

We now make a change of variables to include light-cone velocities, namely $v = \frac{a}{b}$ and $\tilde{v} = \frac{\tilde{a}}{\tilde{b}}$. This is a useful choice as the light-cone velocity is bounded between $1 > v > 0$, $1 > \tilde{v} > 0$. This leads to the following equations

$$\frac{dn_1 \mathcal{T}^{d+1}(\gamma + \gamma'(1-v^2))}{v^{2+d}b^2} + \tilde{v}^2\tilde{b}^2 = 1, \tag{B.13}$$
$$\frac{n_1 \mathcal{T}^{d+1}(d\gamma'(1-v^2) - \gamma)}{v^3 b^2} + \tilde{b}^2 = 1, \tag{B.14}$$
$$\frac{dn_2 \mathcal{T}^{d+1}(\gamma + \gamma'(1-\tilde{v}^2))}{\tilde{v}^{2+d}\tilde{b}^2} + v^2 b^2 = 1, \tag{B.15}$$
$$\frac{n_2 \mathcal{T}^{d+1}(d\gamma'(1-\tilde{v}^2) - \gamma)}{\tilde{v}^{2+d}\tilde{b}^2} + b^2 = 1, \tag{B.16}$$

Introducing the dimensionless ratio

$$r = -\frac{\gamma'}{\gamma}, \tag{B.17}$$

and eliminating b^2 and $\tilde{b}^2$, leads us to

$$\gamma n_1 \mathcal{T}^{d+1} = \frac{v^{d+2}(1-\tilde{v}^2)(d+v^2)}{[d + v^2\tilde{v}^2 - dr(v^2-1)(\tilde{v}^2-1)]^2}, \tag{B.18}$$
$$\gamma n_2 \mathcal{T}^{d+1} = \frac{\tilde{v}^{d+2}(1-v^2)(d+\tilde{v}^2)}{[d + v^2\tilde{v}^2 - dr(v^2-1)(\tilde{v}^2-1)]^2}. \tag{B.19}$$

Since the light cone velocities are bounded by causality to the range $1 > v, \tilde{v} > 0$, we see that solutions with arbitrary temperatures are only possible when the denominator on the right hand side of the above equations is zero. This provides a condition on the range of r:

$$r = \frac{d + v^2\tilde{v}^2}{d(v^2-1)(\tilde{v}^2-1)} \tag{B.20}$$

Clearly, we require that $r > 1$ for arbitrary dimensions.

B.1 Phase transition in arbitrary dimensions for $\frac{n_2}{n_1} = 1$

We now consider phase transitions in arbitrary dimensions for equal subsystems, i.e. when $v = \tilde{v}$ and $b = \tilde{b}$. Note that a phase transition corresponds to $v(\mathcal{T})$ being a multivalued function of $\mathcal{T}$. This can be seen in Fig. B.1, where we plotted for the value of r where the second-order

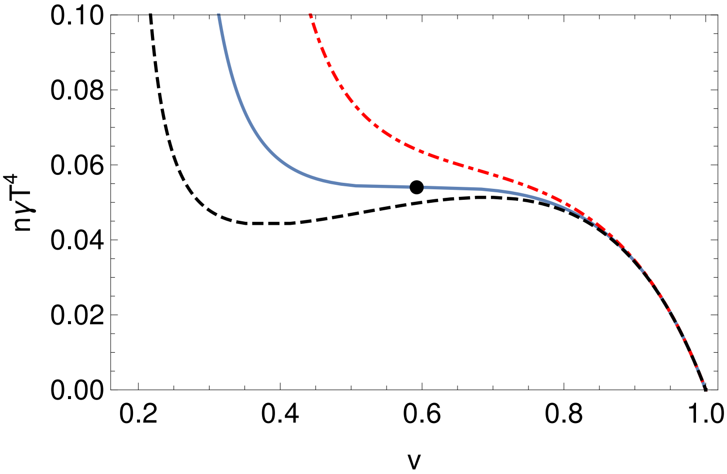

Figure B.1: The relation between $\gamma\mathcal{T}^4$ and $v = a/b$ (for $n_1 = n_2$) at the critical value $r = r_c$ (full line) with the critical point indicated by a black dot on top of it in $3+1$ dimensions. The dotted and dashed lines correspond to a crossover situation with $r = 1.1r_c$ and a first-order phase transition with $r = 0.95r_c$, respectively.

phase transition occurs, as well as one value in the crossover and another in the first-order regime. Note that in this plot only the part connected to $v = 1$ (corresponding to $\gamma\mathcal{T}^4 = 0$) is physically realised; increasing $\gamma\mathcal{T}^4$ from zero to infinity lowers v to a finite limiting value (in $3+1$ dimensions, given in (4.37)).

Hence, if we are interested in determining the onset of a phase transition, we are interested in the critical points of $T(v)$. We begin by considering (B.18) for identical systems:

$$\gamma n_1 \mathcal{T}^{d+1} = \frac{v^{d+2}(1-v^2)(d+v^2)}{[d+v^2v^2 - dr(v^2-1)(v^2-1)]^2}. \tag{B.21}$$

Below r_*, r will have multiple zeros, which correspond to the minima/maxima of $T(v)$. Above r_*, there are no zeros. It is not difficult to conclude that the zero of (**??**) will coincide with the minimum/maximum of r in the range $0 < v < 1$. So, we are interested when r has one minimum in the range $0 < v < 1$. It turns out that there is exactly one such value. We can find the critical points by taking the derivative of the above w.r.t. v:

$$\frac{d}{dv}\left(\gamma n_1 \mathcal{T}^{d+1}\right) = 0. \tag{B.22}$$

This then produces an equation linear in r, which we can then solve for

$$r = \frac{d^3(v^2-1) + d^2(v^6+3v^2-2) + d(v^6-5v^4+12v^2-4)v^2 - 2(v^2-2)v^6}{d(v^2-1)^2(d^2(v^2-1) + d(v^4-5v^2-2) - 2v^2(v^2+2))} \tag{B.23}$$

The maxima of $r(v)$ determines the critical value r_c, as this determines the critical behavior of $\mathcal{T}$. This means that we need to solve

$$\begin{aligned} 0 &= \frac{dr}{dv}, \\ \Rightarrow 0 &= d^5(v^2-1)^2 + 3d^4(v^2-1)^2v^2 + d^3(3v^8-6v^6-13v^4+8v^2-4) \\ &\quad + d^2(v^8-2v^6-23v^4-12)v^2 - 12d(v^4+2)v^4 - 4(v^4-2v^2+4)v^6 \end{aligned} \tag{B.24}$$

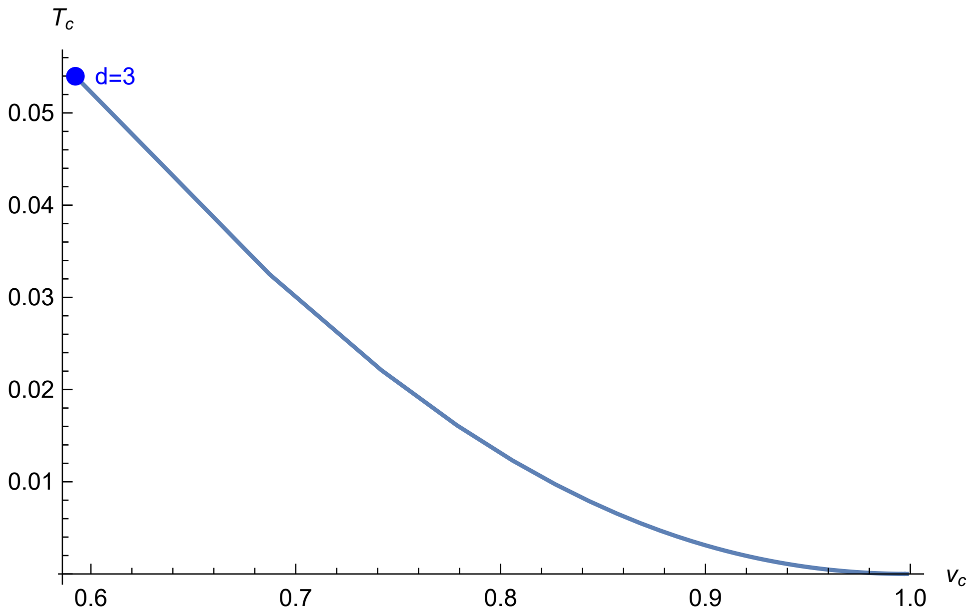

Figure B.2: The critical temperature as a function of the critical velocity. The blue point represents the $d = 3$ critical point. Note that the $d \to \infty$ limit is represented in the lower right hand corner, $T_c \to 0$ as $v \to 1$.

in the range $1 > v > 0$. This determines the critical velocity v_c, which is then used to determine r_c and the critical temperature T_c.

If one considers $d = 1, 2$, it becomes clear that the above equation has no solution for physical values of the light-cone velocity, i.e. $1 > v > 0$. This leads us to conclude that for identical conformal subsystems, there are no phase transitions in $d = 1, 2$. The $d = 3$ case is the lowest dimension of a phase transition, which was discussed in [36] and Sec. 4 and will be the subject of the next subsection. It is worthwhile to mention some observations on higher dimensions. As $d \to \infty$, we have that $r_c \to \infty$, $T_c \to 0$ and $v_c \to 1$. This behavior is monotonic as can be seen in Fig. B.2.

B.1.1 The critical value in $3 + 1$ dimensions

In this subsection we compute the associated critical values in $3 + 1$ dimensions for equal subsystems. We begin by considering (B.24) when $d = 3$, which reads

$$0 = 5v^{10} + 35v^8 - 142v^6 - 666v^4 - 135v^2 + 135, \tag{B.25}$$

which is a quintic in v^2. There is only one solution in the range $1 > v^2 > 0$, which can be given in closed form

$$v_c^2\Big|_{n_1=n_2} = \frac{1}{5}\left(2\sqrt{85 + 10\sqrt{15}} - 5 - 4\sqrt{15}\right) \approx 0.35097. \tag{B.26}$$

We can plug this critical value of the light-cone velocity into (B.23) to find the critical value of r:

$$r_c\Big|_{n_1=n_2} = \frac{1}{540}\left(195 + 43\sqrt{15} + \sqrt{30\left(4082 - 557\sqrt{15}\right)}\right) \approx 1.114509. \tag{B.27}$$

This leads to a critical value of the temperature in (B.21) to be $n\gamma T_c^4 \approx 0.0539768$.

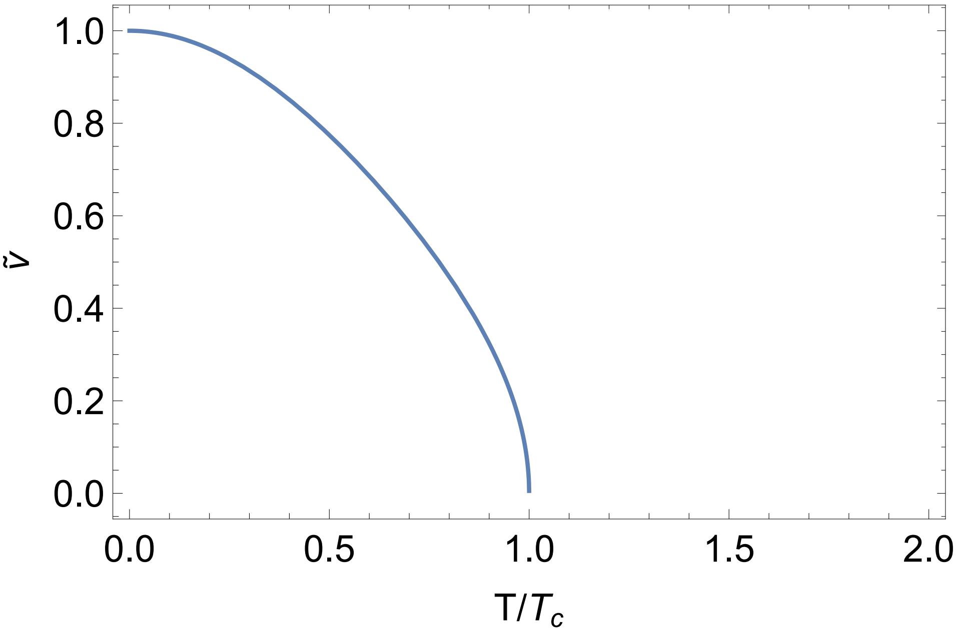

Figure B.3: The effective light-cone velocity of the vacuum subsystem as a function of temperature.

B.2 Vacuum solution

A curious observation can be made when we examine the consequences of setting the number of degrees of freedom in one subsystem to zero, i.e. the vacuum state, whereas the other system is non-vacuum. We can set $\tilde{T}_{\mu\nu} = 0$, but $T_{\mu\nu} \neq 0$, and consider the coupling equations (B.3):

$$g_{\mu\nu} = \eta_{\mu\nu}, \tag{B.28}$$

$$\tilde{g}_{\mu\nu} = \eta_{\mu\nu} + \gamma T_{\mu\nu}\sqrt{g} + \gamma' \eta_{\mu\nu} T_{\alpha\beta}\eta^{\alpha\beta}\sqrt{g}. \tag{B.29}$$

Clearly, the matter sees the physical background metric $\eta_{\mu\nu}$, i.e. the light-cone velocity $v = 1$. What about the other, empty sector? For conformal matter, the coupling equations imply that the light-cone velocity of the empty sector is

$$\tilde{v} = \frac{\sqrt{1 - d\gamma P}}{\sqrt{1 + \gamma P}} \tag{B.30}$$

where d is the spatial dimension. Note that the light-cone velocity is physical for a limited range of pressures. To illustrate the point, let's consider an arbitrary dimension, where the pressure can be parameterized by $n_1 T^{d+1}$. This means that there is a critical temperature where the light-cone velocity drops to zero, given by

$$T_c = (n_1\gamma)^{-\frac{1}{d+1}} \tag{B.31}$$

This extreme case can be understood by re-examining Fig. 4.6. In the case $n_2 \to 0$, $v \to 1$ for all $\gamma^{1/4}\mathcal{T}$ (the blue line), while the other line $\tilde{v}$ will behave like in Fig. B.3.

Appendix C

Low and high temperature behavior of perfect fluids

This appendix centers on discussing the low and high temperature regime for conformal perfect fluid subsystems in the case $r = -\gamma'/\gamma > 1$ in $3+1$ dimensions, such that solutions exist for all values of the physical temperature $\mathcal{T}$. Moreover, we show the emergence of conformality in the limit of large $\gamma\mathcal{T}^4$.

For small $\gamma\mathcal{T}^4$, a power series expansion of the solutions to the set of equations (4.29) can be easily obtained and we find that the leading terms of the metric coefficients are

$$\begin{aligned}
a^2 &= 1 - 3n_2\gamma\mathcal{T}^4 + (12r-27)n_1n_2(\gamma\mathcal{T}^4)^2 + O\left((\gamma\mathcal{T}^4)^3\right), \\
\tilde{a}^2 &= 1 - 3n_1\gamma\mathcal{T}^4 + (12r-27)n_1n_2(\gamma\mathcal{T}^4)^2 + O\left((\gamma\mathcal{T}^4)^3\right), \\
b^2 &= 1 + n_2\gamma\mathcal{T}^4 + (12r+5)n_1n_2(\gamma\mathcal{T}^4)^2 + O\left((\gamma\mathcal{T}^4)^3\right), \\
\tilde{b}^2 &= 1 + n_1\gamma\mathcal{T}^4 + (12r+5)n_1n_2(\gamma\mathcal{T}^4)^2 + O\left((\gamma\mathcal{T}^4)^3\right),
\end{aligned} \tag{C.1}$$

while the effective light-cone velocities can be expanded as:

$$\begin{aligned}
v = \frac{a}{b} &= 1 - 2n_2\gamma\mathcal{T}^4 - 16n_1n_2(\gamma\mathcal{T}^4)^2 + O\left((\gamma\mathcal{T}^4)^3\right), \\
\tilde{v} = \frac{\tilde{a}}{\tilde{b}} &= 1 - 2n_1\gamma\mathcal{T}^4 - 16n_1n_2(\gamma\mathcal{T}^4)^2 + O\left((\gamma\mathcal{T}^4)^3\right).
\end{aligned} \tag{C.2}$$

Note that r first shows up at third order.

As discussed in Section 4.1.4, the light-cone velocities asymptote to finite values v_∞, $\tilde{v}_\infty$ for large $\gamma\mathcal{T}^4$, provided $r > 1$. These values are obtained by solving the sixth-order algebraic equations (4.38), which reduces to a quadratic equation with solution (4.37) when $n_1 = n_2$.

The full, nonperturbative equation determining the light-cone velocities as a function of $\gamma\mathcal{T}^4$ is given by (4.31) and (4.32) which were obtained by solving first the quadratic equations for b^2 and $\tilde{b}^2$ that are implied by (4.29). Using (4.31) and (4.32) in the relations for b^2 and $\tilde{b}^2$ one finds

$$\begin{aligned}
a^4 &\equiv b^4v^4 = \frac{3+\tilde{v}^2}{v(1-\tilde{v}^2)}n_1\gamma\mathcal{T}^4, \\
\tilde{a}^4 &\equiv \tilde{b}^4\tilde{v}^4 = \frac{3+v^2}{\tilde{v}(1-v^2)}n_2\gamma\mathcal{T}^4.
\end{aligned} \tag{C.3}$$

Moreover, one can derive the simple identity

$$\frac{\tilde{b}^2}{b^2} = \frac{3+v^2}{3+\tilde{v}^2}. \tag{C.4}$$

At small $\gamma\mathcal{T}^4$, all metric coefficients as well as v and $\tilde{v}$ tend to unity, with $1-v^2$ and $1-\tilde{v}^2$ proportional to $\gamma\mathcal{T}^4$. As one can check easily, (C.3) confirms the first-order coefficients in (C.2).

At large $\gamma\mathcal{T}^4$, where v and $\tilde{v}$ approach nonvanishing values v_∞ and $\tilde{v}_\infty$ below unity, (C.3) implies that the metric coefficients $a, \tilde{a}, b, \tilde{b}$ grow linearly with physical temperature $\mathcal{T}$. Since the effective temperatures of the subsystems are given by $T_1 = \mathcal{T}/a$ and $T_2 = \mathcal{T}/\tilde{a}$, this means that they saturate at finite values proportional to $\gamma^{-1/4}$,

$$\gamma\mathcal{T}^4 \to \infty \;\Rightarrow\quad T_1 \to \left(\frac{3+\tilde{v}_\infty^2}{v_\infty(1-\tilde{v}_\infty^2)} n_1\gamma\right)^{-1/4}, \quad T_2 \to \left(\frac{3+v_\infty^2}{\tilde{v}_\infty(1-v_\infty^2)} n_2\gamma\right)^{-1/4}. \tag{C.5}$$

This behavior of the metric coefficients, together with saturation of t^μ_ν and $\tilde{t}^\mu_\nu$, implies that at large $\mathcal{T}$ the coupling rules (3.17) become

$$\begin{aligned} g_{\mu\nu} &\approx \gamma\, g_{\mu\rho}\tilde{t}^{\rho\sigma}g_{\sigma\nu}\frac{\sqrt{-\tilde{g}}}{\sqrt{-g}} + \gamma'\, g_{\rho\sigma}\tilde{t}^{\rho\sigma}g_{\mu\nu}\frac{\sqrt{-\tilde{g}}}{\sqrt{-g}}, \\ \tilde{g}_{\mu\nu} &\approx \gamma\, g_{\mu\rho}t^{\rho\sigma}g_{\sigma\nu}\frac{\sqrt{-g}}{\sqrt{-g}} + \gamma'\, g_{\rho\sigma}t^{\rho\sigma}g_{\mu\nu}\frac{\sqrt{-g}}{\sqrt{-g}}. \end{aligned} \tag{C.6}$$

Hence, for conformal subsystems

$$t^{\mu\nu}\left(\gamma\, g_{\mu\rho}\tilde{t}^{\rho\sigma}g_{\sigma\nu}\frac{\sqrt{-\tilde{g}}}{\sqrt{-g}} + \gamma'\, g_{\rho\sigma}\tilde{t}^{\rho\sigma}g_{\mu\nu}\frac{\sqrt{-\tilde{g}}}{\sqrt{-g}}\right) \approx t^{\mu\nu}g_{\mu\nu} = 0, \tag{C.7}$$

or, equivalently,

$$\tilde{t}^{\mu\nu}\left(\gamma\, g_{\mu\rho}t^{\rho\sigma}g_{\sigma\nu}\frac{\sqrt{-g}}{\sqrt{-g}} + \gamma'\, g_{\rho\sigma}t^{\rho\sigma}g_{\mu\nu}\frac{\sqrt{-g}}{\sqrt{-g}}\right) \approx \tilde{t}^{\mu\nu}g_{\mu\nu} = 0, \tag{C.8}$$

so that the pure trace terms in the full energy-momentum tensor $T^\mu{}_\nu$ proportional to $\delta^\mu{}_\nu$ become small compared $\mathcal{T}^4$, $\Delta K/\mathcal{T}^4 \approx 0$. Hence, at large $\mathcal{T}$,

$$T^\mu{}_\mu/\mathcal{T}^4 \approx (t^\mu{}_\mu\sqrt{-g} + \tilde{t}^\mu{}_\mu\sqrt{-\tilde{g}})/\mathcal{T}^4 = 0. \tag{C.9}$$

From the full solution we in fact find that $T^\mu{}_\mu/\mathcal{T}^4 \sim \gamma^{-1/2}\mathcal{T}^{-2}$.

Appendix D

The critical exponent of the second-order phase transition

In this appendix, we derive the value of the critical exponent α in the specific heat of the full system,

$$\mathcal{C}_V = \mathcal{T}\partial\mathcal{S}/\partial\mathcal{T} \sim |\mathcal{T} - \mathcal{T}_c|^{-\alpha} \tag{D.1}$$

when $\mathcal{T} \to \mathcal{T}_c$, for the case of two conformal subsystems (4.25) where $\mathcal{S}$ is given by (4.27). The full entropy can be computed in $d+1$ dimensions, where we find

$$\mathcal{S} = (d+1)\mathcal{T}^d\Big(n_1 v^{-d} + n_2\tilde{v}^{-d}\Big). \tag{D.2}$$

The critical exponent α in the specific heat (D.1) can be inferred from the simple relationship (D.2) between entropy and effective light-cone velocities. In the vicinity of the critical point we have for equal subsystems $n = n_1 = n_2$,

$$|\mathcal{S} - \mathcal{S}_c| \sim 2d(d+1)n\mathcal{T}_c^d v_c^{-d-1}|v - v_c|. \tag{D.3}$$

As we have seen, the critical point is determined by the simultaneous vanishing of the first and second derivatives of $\mathcal{T}^4$ as given by (B.21) with respect to v. Hence,

$$|\mathcal{T}^{d+1} - \mathcal{T}_c^{d+1}| \sim (d+1)\mathcal{T}_c^d|\mathcal{T} - \mathcal{T}_c| \sim |v - v_c|^d \tag{D.4}$$

up to some constant prefactor, and thus

$$|\mathcal{S} - \mathcal{S}_c| \sim |\mathcal{T} - \mathcal{T}_c|^{1/d}, \quad \mathcal{C}_V \sim |\mathcal{T} - \mathcal{T}_c|^{-1+1/d}. \tag{D.5}$$

Recall from the discussion in Appendix B for equal subsystems in $d = 1, 2$, there is no phase transition. Thus, this result is valid for $d \geq 3$. We see that $\alpha \to 1$ when $d \to \infty$.

In the main text, we are concerned with a $3+1$ dimensional system, so we have

$$\mathcal{C}_V \sim |\mathcal{T} - \mathcal{T}_c|^{-2/3}, \tag{D.6}$$

i.e. $\alpha = 2/3$.

In the case of two conformal systems with $n_1 \neq n_2$, the critical exponent α is independent of n_2/n_1 and only the values of r_c and $\mathcal{T}_c$ change. One then has to solve the two equations (4.31) and (4.32) numerically, which gives functions $v = v(\mathcal{T})$ and $\tilde{v} = \tilde{v}(\mathcal{T})$. For sufficiently large values of r, both functions are single-valued; phase transitions occur when these functions develop infinite tangents. Combining (4.31) and (4.32), one finds that

$$\frac{n_2}{n_1} = \frac{\tilde{v}^5(1-v^2)(3+v^2)}{v^5(1-\tilde{v}^2)(3+\tilde{v}^2)} \equiv \rho(v,\tilde{v}) = const. \tag{D.7}$$

Because

$$0 = \frac{\partial \rho}{\partial v}\frac{dv}{d\mathcal{T}} + \frac{\partial \rho}{\partial \tilde{v}}\frac{d\tilde{v}}{d\mathcal{T}}, \tag{D.8}$$

the zeros of $d\mathcal{T}/dv$ and $d\mathcal{T}/d\tilde{v}$ have to occur simultaneously in general. A critical endpoint with second-order phase transition appears when two zeros of $d\mathcal{T}/dv$ (or $d\mathcal{T}/d\tilde{v}$) merge as $r \to r_c$ from below, such that also $d^2\mathcal{T}/dv^2$ vanishes and a saddle point (in one dimension) arises. In principle, such a saddle point could have the next two higher derivatives vanish, too, which would change the critical exponent α to $-4/5$. However, with the one additional free parameter n_2/n_1 there is not enough freedom for a corresponding fine-tuning.

Appendix E

Numerical accuracy of the toy glasma iterative procedure

In this appendix we use an illustrative example, to demonstrate the numerical feasibility of our iterative procedure, outlined in Chapter 5. We set our couplings to $\beta = 0.2$ and $g_{\mathrm{YM}}/\sqrt{Q_s} = 0.5$, while the initial conditions are $\epsilon_{YM}^{ini}/Q_s^3 = 0.1$ and $\epsilon_{hol}^{ini}/Q_s^3 = 1/250$.

In Fig. E.1, we plot the violation of the total energy conservation $\Delta\epsilon_{tot}(t) = \epsilon_{tot}^{ini} - \epsilon_{tot}(t)$. This is defined as difference between the total energy at $t_0 = 0$, namely $\epsilon_{tot}^{ini} = \epsilon_{YM}^{ini} + \epsilon_{hol}^{ini}$, and the total energy during the time evolution $\epsilon_{tot}(t) = \epsilon_{YM}(t) + \epsilon_{hol}(t) + \epsilon_{xc}(t)$. We find that our numerical scheme reaches $\Delta\epsilon_{tot}(t)/Q_s^3 \approx \mathcal{O}(10^{-5})$ (or smaller) after four iterations.

A characteristic feature of our numerical method is that more iterations make the long time behavior better behaved, as can be seen in the plot of the Yang-Mills energy in four subsequent iterations, see the right panel of Fig. E.1. This behavior is induced by the way we choose our initial guess, which typically is more accurate at earlier times. At later times, when already a significant amount of energy has been transferred, the ansatz and the true solution can have very different amplitude and phase, thus requiring multiple iterations to improve upon the initial guess.

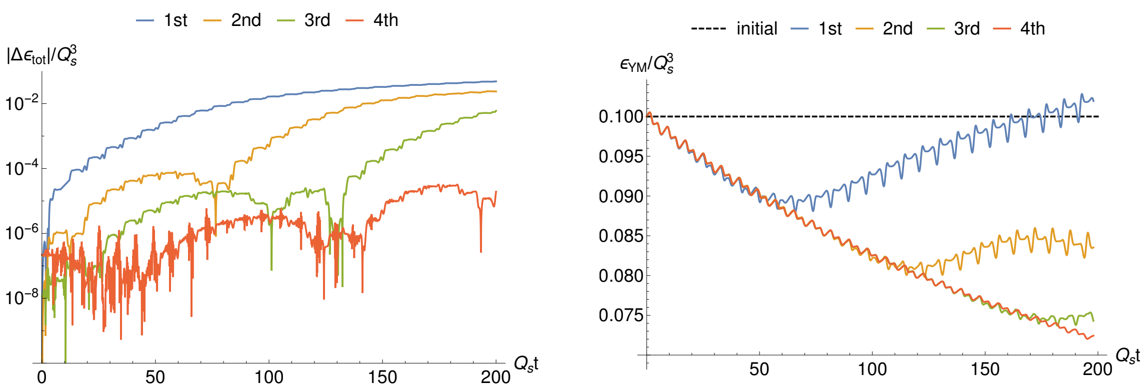

Figure E.1: Left: Violation of the total energy conservation ($\Delta\epsilon_{tot}(t) = (\epsilon_{YM}^{ini} + \epsilon_{hol}^{ini}) - (\epsilon_{YM}(t) + \epsilon_{hol}(t)) + \epsilon_{xc}(t)$) as function of time in four subsequent iterations for parameters described in this appendix. Right: Time evolution of the energy in the Yang-Mills sector for the same parameters in four subsequent iterations.

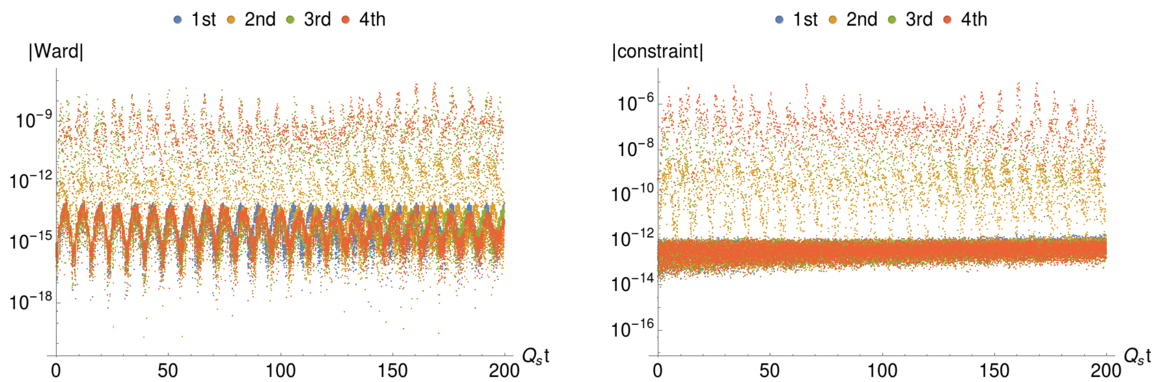

Figure E.2: Left: Violation of the holographic Ward identity. Right: Constraint in the Einstein equations.

During each iteration, we monitor the Ward identity (5.17) and the constraint (5.29). We can see that in the left plot of Fig. E.2, the Ward identity is fulfilled to an accuracy better than 10^{-12} during most time steps. In the current example, there are a small number of times steps for which the accuracy decreases systematically with each iteration, but we find that this always remains below 10^{-7}. In right plot of Fig. E.2, we see that a similar picture holds for the constraint in the gravity simulation. During most time steps for subsequent iterations, the absolute value of the maximum violation in the bulk direction of the constraint (5.29) remains smaller than 10^{-12}, while for a handful of time steps the error grows with the number of iterations. This numerical noise can be traced back to numerical errors introduced when solving the classical Yang-Mills equation (5.21). In particular (5.39) shows that derivative of higher order enter the calculation of $\mathcal{H}$, which then in turn complicate the solution of the classical Yang-Mills equation and make the filtering procedure necessary in the first place.

Appendix F

Abbreviations

3+1D	3+1 dimensions / dimensional
AdS/CFT	Anti-de Sitter/Conformal Field Theory
BGK	Bhatnagar-Gross-Krook
EOM	equation(s) of motion
IR	infrared
JT	Jackiw-Teitelboim
LHC	Large Hadron Collider
LHS	left hand side
$NAdS_2$	nearly-Anti-de Sitter in $1+1$ dimensions
QCD	quantum chromodynamics
QGP	quark-gluon plasma
RHIC	Relativistic Heavy Ion Collider
RHS	right hand side
RTA	relaxed time approximation
SU	special unitary
UV	ultraviolet
w.r.t.	with respect to
YM	Yang-Mills

Bibliography

[1] U. Heinz and R. Snellings, *Collective flow and viscosity in relativistic heavy-ion collisions*, *Ann. Rev. Nucl. Part. Sci.* **63** (2013) 123–151, [1301.2826].

[2] J. C. Collins and M. J. Perry, *Superdense matter: Neutrons or asymptotically free quarks?*, *Phys. Rev. Lett.* **34** (May, 1975) 1353–1356.

[3] E. Shuryak, *Physics of Strongly coupled Quark-Gluon Plasma*, *Prog. Part. Nucl. Phys.* **62** (2009) 48–101, [0807.3033].

[4] S. Cremonini, *The Shear Viscosity to Entropy Ratio: A Status Report*, *Mod. Phys. Lett.* **B25** (2011) 1867–1888, [1108.0677].

[5] P. Romatschke and U. Romatschke, *Viscosity Information from Relativistic Nuclear Collisions: How Perfect is the Fluid Observed at RHIC?*, *Phys. Rev. Lett.* **99** (2007) 172301, [0706.1522].

[6] P. Kovtun, D. T. Son and A. O. Starinets, *Viscosity in strongly interacting quantum field theories from black hole physics*, *Phys. Rev. Lett.* **94** (2005) 111601, [hep-th/0405231].

[7] N. Iqbal and H. Liu, *Universality of the hydrodynamic limit in AdS/CFT and the membrane paradigm*, *Phys. Rev.* **D79** (2009) 025023, [0809.3808].

[8] S. C. Huot, S. Jeon and G. D. Moore, *Shear viscosity in weakly coupled $N = 4$ super Yang-Mills theory compared to QCD*, *Phys. Rev. Lett.* **98** (2007) 172303, [hep-ph/0608062].

[9] E. Iancu, *QCD in heavy ion collisions*, in *Proceedings, 2011 European School of High-Energy Physics (ESHEP 2011): Cheile Gradistei, Romania, September 7-20, 2011*, pp. 197–266, 2014, 1205.0579, DOI.

[10] A. Kurkela, A. Mazeliauskas, J.-F. Paquet, S. Schlichting and D. Teaney, *Matching the Nonequilibrium Initial Stage of Heavy Ion Collisions to Hydrodynamics with QCD Kinetic Theory*, *Phys. Rev. Lett.* **122** (2019) 122302, [1805.01604].

[11] A. Kurkela, A. Mazeliauskas, J.-F. Paquet, S. Schlichting and D. Teaney, *Effective kinetic description of event-by-event pre-equilibrium dynamics in high-energy heavy-ion collisions*, *Phys. Rev.* **C99** (2019) 034910, [1805.00961].

[12] J. Casalderrey-Solana, D. C. Gulhan, J. G. Milhano, D. Pablos and K. Rajagopal, *A Hybrid Strong/Weak Coupling Approach to Jet Quenching*, *JHEP* **10** (2014) 019, [1405.3864].

[13] J. Casalderrey-Solana, D. C. Gulhan, J. G. Milhano, D. Pablos and K. Rajagopal, *Predictions for Boson-Jet Observables and Fragmentation Function Ratios from a Hybrid Strong/Weak Coupling Model for Jet Quenching*, *JHEP* **03** (2016) 053, [1508.00815].

[14] J. Casalderrey-Solana, D. Gulhan, G. Milhano, D. Pablos and K. Rajagopal, *Angular Structure of Jet Quenching Within a Hybrid Strong/Weak Coupling Model*, *JHEP* **03** (2017) 135, [1609.05842].

[15] Z. Hulcher, D. Pablos and K. Rajagopal, *Resolution Effects in the Hybrid Strong/Weak Coupling Model*, *JHEP* **03** (2018) 010, [1707.05245].

[16] T. Faulkner and J. Polchinski, *Semi-Holographic Fermi Liquids*, *JHEP* **06** (2011) 012, [1001.5049].

[17] S.-S. Lee, *A Non-Fermi Liquid from a Charged Black Hole: A Critical Fermi Ball*, *Phys. Rev.* **D79** (2009) 086006, [0809.3402].

[18] H. Liu, J. McGreevy and D. Vegh, *Non-Fermi liquids from holography*, *Phys. Rev.* **D83** (2011) 065029, [0903.2477].

[19] M. Cubrovic, J. Zaanen and K. Schalm, *String Theory, Quantum Phase Transitions and the Emergent Fermi-Liquid*, *Science* **325** (2009) 439–444, [0904.1993].

[20] T. Faulkner, H. Liu, J. McGreevy and D. Vegh, *Emergent quantum criticality, Fermi surfaces, and AdS(2)*, *Phys. Rev.* **D83** (2011) 125002, [0907.2694].

[21] T. Senthil, *Critical fermi surfaces and non-fermi liquid metals*, *Phys. Rev. B* **78** (Jul, 2008) 035103.

[22] T. Senthil, *Theory of a continuous mott transition in two dimensions*, *Phys. Rev. B* **78** (Jul, 2008) 045109.

[23] S. A. Hartnoll, *Lectures on holographic methods for condensed matter physics*, *Class. Quant. Grav.* **26** (2009) 224002, [0903.3246].

[24] C. P. Herzog, *Lectures on Holographic Superfluidity and Superconductivity*, *J. Phys.* **A42** (2009) 343001, [0904.1975].

[25] J. McGreevy, *Holographic duality with a view toward many-body physics*, *Adv. High Energy Phys.* **2010** (2010) 723105, [0909.0518].

[26] A. Mukhopadhyay and G. Policastro, *Phenomenological Characterization of Semiholographic Non-Fermi Liquids*, *Phys. Rev. Lett.* **111** (2013) 221602, [1306.3941].

[27] B. Doucot, C. Ecker, A. Mukhopadhyay and G. Policastro, *Density response and collective modes of semiholographic non-Fermi liquids*, *Phys. Rev.* **D96** (2017) 106011, [1706.04975].

[28] U. Gursoy, E. Plauschinn, H. Stoof and S. Vandoren, *Holography and ARPES Sum-Rules*, *JHEP* **05** (2012) 018, [1112.5074].

[29] U. Gursoy, V. Jacobs, E. Plauschinn, H. Stoof and S. Vandoren, *Holographic models for undoped Weyl semimetals*, *JHEP* **04** (2013) 127, [1209.2593].

[30] V. P. J. Jacobs, S. Grubinskas and H. T. C. Stoof, *Towards a field-theory interpretation of bottom-up holography*, *JHEP* **04** (2015) 033, [1411.4051].

[31] V. P. J. Jacobs, P. Betzios, U. Gursoy and H. T. C. Stoof, *Electromagnetic response of interacting Weyl semimetals*, *Phys. Rev.* **B93** (2016) 195104, [1512.04883].

[32] E. Iancu and A. Mukhopadhyay, *A semi-holographic model for heavy-ion collisions*, *JHEP* **06** (2015) 003, [1410.6448].

[33] A. Mukhopadhyay, F. Preis, A. Rebhan and S. A. Stricker, *Semi-Holography for Heavy Ion Collisions: Self-Consistency and First Numerical Tests*, *JHEP* **05** (2016) 141, [1512.06445].

[34] A. Mukhopadhyay and F. Preis, *Semiholography for heavy ion collisions*, *EPJ Web Conf.* **137** (2017) 07015, [1612.00140].

[35] S. Banerjee, N. Gaddam and A. Mukhopadhyay, *Illustrated study of the semiholographic nonperturbative framework*, *Phys. Rev.* **D95** (2017) 066017, [1701.01229].

[36] A. Kurkela, A. Mukhopadhyay, F. Preis, A. Rebhan and A. Soloviev, *Hybrid Fluid Models from Mutual Effective Metric Couplings*, *JHEP* **08** (2018) 054, [1805.05213].

[37] C. Ecker, A. Mukhopadhyay, F. Preis, A. Rebhan and A. Soloviev, *Time evolution of a toy semiholographic glasma*, *JHEP* **08** (2018) 074, [1806.01850].

[38] S. M. Carroll, *Spacetime and geometry: An introduction to general relativity.* 2004.

[39] S. Weinberg, *Gravitation and Cosmology.* John Wiley and Sons, New York, 1972.

[40] M. E. Peskin and D. V. Schroeder, *An Introduction to quantum field theory.* Addison-Wesley, Reading, USA, 1995.

[41] M. Srednicki, *Quantum field theory.* Cambridge University Press, 2007.

[42] E. D'Hoker and D. Z. Freedman, *Supersymmetric gauge theories and the AdS / CFT correspondence*, in *Strings, Branes and Extra Dimensions: TASI 2001: Proceedings*, pp. 3–158, 2002, hep-th/0201253.

[43] O. Aharony, S. S. Gubser, J. M. Maldacena, H. Ooguri and Y. Oz, *Large N field theories, string theory and gravity*, *Phys. Rept.* **323** (2000) 183–386, [hep-th/9905111].

[44] G. T. Horowitz and J. Polchinski, *Gauge/gravity duality*, gr-qc/0602037.

[45] A. V. Ramallo, *Introduction to the AdS/CFT correspondence*, *Springer Proc. Phys.* **161** (2015) 411–474, [1310.4319].

[46] V. E. Hubeny, *The AdS/CFT Correspondence*, *Class. Quant. Grav.* **32** (2015) 124010, [1501.00007].

[47] J. Casalderrey-Solana, H. Liu, D. Mateos, K. Rajagopal and U. A. Wiedemann, *Gauge/string Duality, hot QCD and heavy ion collisions.* Cambridge University Press, 2014.

[48] M. Ammon and J. Erdmenger, *Gauge-gravity duality.* Cambridge University Press, 2015.

[49] H. Nastase, *Introduction to the AdS/CFT correspondence.* Cambridge University Press, 2015.

[50] G. 't Hooft, *Dimensional reduction in quantum gravity*, *Conf. Proc.* **C930308** (1993) 284–296, [gr-qc/9310026].

[51] L. Susskind, *The World as a hologram*, *J. Math. Phys.* **36** (1995) 6377–6396, [hep-th/9409089].

[52] J. D. Bekenstein, *Black holes and entropy*, *Phys. Rev. D* **7** (Apr, 1973) 2333–2346.

[53] S. Hawking, *Particle creation by black holes*, *Commun.Math. Phys.* **43** (1975) 199–220.

[54] J. M. Maldacena, *The Large N limit of superconformal field theories and supergravity*, *Int. J. Theor. Phys.* **38** (1999) 1113–1133, [hep-th/9711200].

[55] D. Tong, *String Theory*, 0908.0333.

[56] D. Z. Freedman, S. D. Mathur, A. Matusis and L. Rastelli, *Correlation functions in the CFT(d) / AdS(d+1) correspondence*, *Nucl. Phys.* **B546** (1999) 96–118, [hep-th/9804058].

[57] E. Witten, *Anti-de Sitter space and holography*, *Adv. Theor. Math. Phys.* **2** (1998) 253–291, [hep-th/9802150].

[58] J. Casalderrey-Solana, M. P. Heller, D. Mateos and W. van der Schee, *From full stopping to transparency in a holographic model of heavy ion collisions*, *Phys. Rev. Lett.* **111** (2013) 181601, [1305.4919].

[59] A. Ipp and D. Müller, *Broken boost invariance in the Glasma via finite nuclei thickness*, *Phys. Lett.* **B771** (2017) 74–79, [1703.00017].

[60] G. Policastro, D. T. Son and A. O. Starinets, *From AdS / CFT correspondence to hydrodynamics*, *JHEP* **09** (2002) 043, [hep-th/0205052].

[61] G. Policastro, D. T. Son and A. O. Starinets, *From AdS / CFT correspondence to hydrodynamics. 2. Sound waves*, *JHEP* **12** (2002) 054, [hep-th/0210220].

[62] P. M. Chesler and L. G. Yaffe, *Horizon formation and far-from-equilibrium isotropization in supersymmetric Yang-Mills plasma*, *Phys. Rev. Lett.* **102** (2009) 211601, [0812.2053].

[63] P. M. Chesler and L. G. Yaffe, *Holography and colliding gravitational shock waves in asymptotically AdS_5 spacetime*, *Phys. Rev. Lett.* **106** (2011) 021601, [1011.3562].

[64] M. P. Heller, R. A. Janik and P. Witaszczyk, *The characteristics of thermalization of boost-invariant plasma from holography*, *Phys. Rev. Lett.* **108** (2012) 201602, [1103.3452].

[65] W. van der Schee, *Holographic thermalization with radial flow*, *Phys. Rev.* **D87** (2013) 061901, [1211.2218].

[66] M. Attems, J. Casalderrey-Solana, D. Mateos, D. Santos-Oliván, C. F. Sopuerta, M. Triana et al., *Paths to equilibrium in non-conformal collisions*, *JHEP* **06** (2017) 154, [1703.09681].

[67] W. Busza, K. Rajagopal and W. van der Schee, *Heavy Ion Collisions: The Big Picture, and the Big Questions*, *Ann. Rev. Nucl. Part. Sci.* **68** (2018) 339–376, [1802.04801].

[68] G. Policastro, D. T. Son and A. O. Starinets, *The Shear viscosity of strongly coupled N=4 supersymmetric Yang-Mills plasma*, *Phys. Rev. Lett.* **87** (2001) 081601, [hep-th/0104066].

[69] R. A. Lacey, N. N. Ajitanand, J. M. Alexander, P. Chung, W. G. Holzmann, M. Issah et al., *Has the QCD Critical Point been Signaled by Observations at RHIC?*, *Phys. Rev. Lett.* **98** (2007) 092301, [nucl-ex/0609025].

[70] M. Rangamani, *Gravity and Hydrodynamics: Lectures on the fluid-gravity correspondence*, *Class. Quant. Grav.* **26** (2009) 224003, [0905.4352].

[71] L. D. Landau and E. M. Lifshitz, *Fluid Mechanics*. Elsevier Science, 1987.

[72] N. Andersson and G. L. Comer, *Relativistic fluid dynamics: Physics for many different scales*, *Living Rev. Rel.* **10** (2007) 1, [gr-qc/0605010].

[73] P. Romatschke and U. Romatschke, *Relativistic Fluid Dynamics In and Out of Equilibrium – Ten Years of Progress in Theory and Numerical Simulations of Nuclear Collisions*, 1712.05815.

[74] PHENIX collaboration, K. Adcox et al., *Formation of dense partonic matter in relativistic nucleus-nucleus collisions at RHIC: Experimental evaluation by the PHENIX collaboration*, *Nucl. Phys.* **A757** (2005) 184–283, [nucl-ex/0410003].

[75] BRAHMS collaboration, I. Arsene et al., *Quark gluon plasma and color glass condensate at RHIC? The Perspective from the BRAHMS experiment*, *Nucl. Phys.* **A757** (2005) 1–27, [nucl-ex/0410020].

[76] B. B. Back et al., *The PHOBOS perspective on discoveries at RHIC*, *Nucl. Phys.* **A757** (2005) 28–101, [nucl-ex/0410022].

[77] STAR collaboration, J. Adams et al., *Experimental and theoretical challenges in the search for the quark gluon plasma: The STAR Collaboration's critical assessment of the evidence from RHIC collisions*, *Nucl. Phys.* **A757** (2005) 102–183, [nucl-ex/0501009].

[78] B. Schenke, S. Jeon and C. Gale, *Elliptic and triangular flow in event-by-event (3+1)D viscous hydrodynamics*, *Phys. Rev. Lett.* **106** (2011) 042301, [1009.3244].

[79] J.-P. Blaizot and J.-Y. Ollitrault, *Hydrodynamics of Quark - Gluon Plasmas*, *Adv. Ser. Direct. High Energy Phys.* **6** (1990) 393–470.

[80] P. F. Kolb and U. W. Heinz, *Hydrodynamic description of ultrarelativistic heavy ion collisions*, nucl-th/0305084.

[81] C. Eckart, *The thermodynamics of irreversible processes. iii. relativistic theory of the simple fluid*, *Phys. Rev.* **58** (Nov, 1940) 919–924.

[82] R. Baier, P. Romatschke, D. T. Son, A. O. Starinets and M. A. Stephanov, *Relativistic viscous hydrodynamics, conformal invariance, and holography*, *JHEP* **04** (2008) 100, [0712.2451].

[83] P. Romatschke, *New Developments in Relativistic Viscous Hydrodynamics*, *Int. J. Mod. Phys.* **E19** (2010) 1–53, [0902.3663].

[84] I. Muller, *Zum Paradoxon der Warmeleitungstheorie*, *Z. Phys.* **198** (1967) 329–344.

[85] W. Israel, *Nonstationary irreversible thermodynamics: A Causal relativistic theory*, *Annals Phys.* **100** (1976) 310–331.

[86] W. Israel and J. M. Stewart, *Transient relativistic thermodynamics and kinetic theory*, *Annals Phys.* **118** (1979) 341–372.

[87] M. S. Green, *Markoff Random Processes and the Statistical Mechanics of Time-Dependent Phenomena. II. Irreversible Processes in Fluids*, *The Journal of Chemical Physics* **22** (Mar, 1954) 398–413.

[88] R. Kubo, *Statistical mechanical theory of irreversible processes.1. General theory and simple applications in magnetic and conduction problems*, *J. Phys. Soc. Jap.* **12** (1957) 570–586.

[89] P. Romatschke, *Retarded correlators in kinetic theory: branch cuts, poles and hydrodynamic onset transitions*, *Eur. Phys. J.* **C76** (2016) 352, [1512.02641].

[90] D. T. Son and A. O. Starinets, *Viscosity, Black Holes, and Quantum Field Theory*, *Ann. Rev. Nucl. Part. Sci.* **57** (2007) 95–118, [0704.0240].

[91] S. S. Gubser, S. S. Pufu and F. D. Rocha, *Bulk viscosity of strongly coupled plasmas with holographic duals*, *JHEP* **08** (2008) 085, [0806.0407].

[92] D. S. Gorbunov and V. A. Rubakov, *Introduction to the theory of the early universe.* World Scientific, 2014.

[93] D. Tong, *Lectures on kinetic theory*, 2012.

[94] E. M. Lifshitz and L. P. Pitaevskii, *Physical kinetics.* Elsevier Butterworth Heinemann, Amsterdam Boston, 2008.

[95] C. Cercignani and G. M. Kremer, *The Relativistic Boltzmann Equation: Theory and Applications.* Birkhäuser Basel.

[96] S. Mrowczynski, B. Schenke and M. Strickland, *Color instabilities in the quark–gluon plasma*, *Phys. Rept.* **682** (2017) 1–97, [1603.08946].

[97] F. Debbasch and W. van Leeuwen, *General relativistic boltzmann equation, i: Covariant treatment*, *Physica A: Statistical Mechanics and its Applications* **388** (2009) 1079–1104.

[98] F. Debbasch and W. van Leeuwen, *General relativistic boltzmann equation, ii: Manifestly covariant treatment*, *Physica A: Statistical Mechanics and its Applications* **388** (2009) 1818–1834.

[99] H. Andreasson, *The Einstein-Vlasov System/Kinetic Theory*, *Living Rev. Rel.* **14** (2011) 4, [1106.1367].

[100] F. Jüttner, *Das Maxwellsche Gesetz der Geschwindigkeitsverteilung in der Relativtheorie*, *Annalen der Physik* **339** (1911) 856–882.

[101] S. R. De Groot, *Relativistic Kinetic Theory. Principles and Applications.* 1980.

[102] J. Yvon, *La théorie statistique des fluides et l'équation d'état*, *Actual. Sci. & Indust.* ***203*** (1935) .

[103] N. N. Bogoliubov, *Kinetic Equations*, *Journal of Experimental and Theoretical Physics* **16** (1946) 691–702.

[104] J. G. Kirkwood, *The Statistical Mechanical Theory of Transport Processes I. General Theory*, *The Journal of Chemical Physics* **14** (1946) .

[105] M. Born and H. S. Green, *A general kinetic theory of liquids i. the molecular distribution functions*, *Proceedings of the Royal Society of London. Series A. Mathematical and Physical Sciences* **188** (1946) 10–18.

[106] J. C. Maxwell, *On the dynamical theory of gases*, *Philosophical Transactions of the Royal Society of London* **157** (1867) 49–88.

[107] P. L. Bhatnagar, E. P. Gross and M. Krook, *A model for collision processes in gases. i. small amplitude processes in charged and neutral one-component systems*, *Phys. Rev.* **94** (May, 1954) 511–525.

[108] G. Colonna, *Boltzmann and vlasov equations in plasma physics*, in *Plasma Modeling*, 2053-2563, pp. 1–1 to 1–23. IOP Publishing, 2016. DOI.

[109] G. Boyd, J. Engels, F. Karsch, E. Laermann, C. Legeland, M. Lutgemeier et al., *Thermodynamics of SU(3) lattice gauge theory*, *Nucl. Phys.* **B469** (1996) 419–444, [`hep-lat/9602007`].

[110] S. Borsányi, G. Endrődi, Z. Fodor, A. Jakovác, S. D. Katz, S. Krieg et al., *The QCD equation of state with dynamical quarks*, *JHEP* **11** (2010) 077, [`1007.2580`].

[111] R. Guida and J. Zinn-Justin, *Critical exponents of the N vector model*, *J. Phys.* **A31** (1998) 8103–8121, [`cond-mat/9803240`].

[112] R. D. Pisarski and V. V. Skokov, *Gross-Witten-Wadia transition in a matrix model of deconfinement*, *Phys. Rev.* **D86** (2012) 081701, [`1206.1329`].

[113] I. G. Enting, *Critical exponents for the four-state potts model*, *Journal of Physics A: Mathematical and General* **8** (apr, 1975) L35–L38.

[114] R. J. Baxter, *Exactly solved models in statistical mechanics.* Dover Publications, 2007.

[115] J. D. Bjorken, *Highly Relativistic Nucleus-Nucleus Collisions: The Central Rapidity Region*, *Phys. Rev.* **D27** (1983) 140–151.

[116] A. Kurkela and U. A. Wiedemann, *Analytic structure of nonhydrodynamic modes in kinetic theory*, `1712.04376`.

[117] F. Gelis, E. Iancu, J. Jalilian-Marian and R. Venugopalan, *The Color Glass Condensate*, *Ann. Rev. Nucl. Part. Sci.* **60** (2010) 463–489, [`1002.0333`].

[118] T. Lappi and L. McLerran, *Some features of the glasma*, *Nucl. Phys.* **A772** (2006) 200–212, [`hep-ph/0602189`].

[119] S. de Haro, S. N. Solodukhin and K. Skenderis, *Holographic reconstruction of space-time and renormalization in the AdS / CFT correspondence*, *Commun. Math. Phys.* **217** (2001) 595–622, [hep-th/0002230].

[120] G. Duffing, *Erzwungene Schwingungen bei veranderlicher Eigenfrequenz und ihre technische Bedeutung*, *Sammlung Vieweg* **41-42** (1918) .

[121] S. Bravo Yuste and J. Diaz Bejarano, *Construction of approximate analytical solutions to a new class of non-linear oscillator equations*, *Journal of Sound and Vibration* **110** (1986) 347 – 350.

[122] P. M. Chesler and L. G. Yaffe, *Numerical solution of gravitational dynamics in asymptotically anti-de Sitter spacetimes*, *JHEP* **07** (2014) 086, [1309.1439].

[123] M. Attems, J. Casalderrey-Solana, D. Mateos, D. Santos-Oliván, C. F. Sopuerta, M. Triana et al., *Holographic Collisions in Non-conformal Theories*, *JHEP* **01** (2017) 026, [1604.06439].

[124] T. Faulkner, H. Liu and M. Rangamani, *Integrating out geometry: Holographic Wilsonian RG and the membrane paradigm*, *JHEP* **08** (2011) 051, [1010.4036].

[125] A. Almheiri and J. Polchinski, *Models of AdS_2 backreaction and holography*, *JHEP* **11** (2015) 014, [1402.6334].

[126] K. Jensen, *Chaos in AdS_2 Holography*, *Phys. Rev. Lett.* **117** (2016) 111601, [1605.06098].

[127] J. Maldacena, D. Stanford and Z. Yang, *Conformal symmetry and its breaking in two dimensional Nearly Anti-de-Sitter space*, *PTEP* **2016** (2016) 12C104, [1606.01857].

[128] J. Engelsöy, T. G. Mertens and H. Verlinde, *An investigation of AdS_2 backreaction and holography*, *JHEP* **07** (2016) 139, [1606.03438].

[129] S. Sachdev and J. Ye, *Gapless spin fluid ground state in a random, quantum Heisenberg magnet*, *Phys. Rev. Lett.* **70** (1993) 3339, [cond-mat/9212030].

[130] A. Kitaev and S. J. Suh, *The soft mode in the Sachdev-Ye-Kitaev model and its gravity dual*, *JHEP* **05** (2018) 183, [1711.08467].

[131] D. J. Gross and V. Rosenhaus, *A Generalization of Sachdev-Ye-Kitaev*, *JHEP* **02** (2017) 093, [1610.01569].

[132] E. Witten, *An SYK-Like Model Without Disorder*, 1610.09758.

[133] I. R. Klebanov and G. Tarnopolsky, *Uncolored random tensors, melon diagrams, and the Sachdev-Ye-Kitaev models*, *Phys. Rev.* **D95** (2017) 046004, [1611.08915].

[134] C. Teitelboim, *Gravitation and Hamiltonian Structure in Two Space-Time Dimensions*, *Phys. Lett.* **126B** (1983) 41–45.

[135] R. Jackiw, *Lower Dimensional Gravity*, *Nucl. Phys.* **B252** (1985) 343–356.

[136] J. D. Brown, *LOWER DIMENSIONAL GRAVITY*. 1988.

[137] T. G. Mertens, *The Schwarzian theory — origins*, *JHEP* **05** (2018) 036, [1801.09605].

[138] A. Gaikwad, L. K. Joshi, G. Mandal and S. R. Wadia, *Holographic dual to charged SYK from 3D Gravity and Chern-Simons*, 1802.07746.

[139] P. Nayak, A. Shukla, R. M. Soni, S. P. Trivedi and V. Vishal, *On the Dynamics of Near-Extremal Black Holes*, *JHEP* **09** (2018) 048, [1802.09547].

[140] F. Larsen, *A nAttractor Mechanism for $nAdS_2/nCFT_1$ Holography*, 1806.06330.

[141] S. R. Das, A. Jevicki and K. Suzuki, *Three Dimensional View of the SYK/AdS Duality*, *JHEP* **09** (2017) 017, [1704.07208].

[142] I. Kourkoulou and J. Maldacena, *Pure states in the SYK model and nearly-AdS_2 gravity*, 1707.02325.

[143] L. K. Joshi, A. Mukhopadhyay and A. Soloviev, *Time-dependent $NAdS_2$ holography with applications*, 1901.08877.

[144] M. Cvetivc and I. Papadimitriou, *AdS_2 holographic dictionary*, *JHEP* **12** (2016) 008, [1608.07018].

[145] H. A. González, D. Grumiller and J. Salzer, *Towards a bulk description of higher spin SYK*, *JHEP* **05** (2018) 083, [1802.01562].

[146] D. Grumiller and R. McNees, *Thermodynamics of black holes in two (and higher) dimensions*, *JHEP* **04** (2007) 074, [hep-th/0703230].

[147] V. Ovsienko and S. Tabachnikov, *What is the schwarzian derivative*, *Notices of the AMS* **56** (2009) 34–36.

[148] A. Eberlein, V. Kasper, S. Sachdev and J. Steinberg, *Quantum quench of the Sachdev-Ye-Kitaev Model*, *Phys. Rev.* **B96** (2017) 205123, [1706.07803].

[149] R. Bhattacharya, D. P. Jatkar and N. Sorokhaibam, *Quantum Quenches and Thermalization in SYK models*, 1811.06006.

[150] A. R. Brown, H. Gharibyan, H. W. Lin, L. Susskind, L. Thorlacius and Y. Zhao, *Complexity of Jackiw-Teitelboim gravity*, *Phys. Rev.* **D99** (2019) 046016, [1810.08741].

[151] A. Dhar, A. Gaikwad, L. K. Joshi, G. Mandal and S. R. Wadia, *Gravitational collapse in SYK models and Choptuik-like phenomenon*, 1812.03979.

[152] C. Vaz and L. Witten, *Quantum naked singularities in 2-D dilaton gravity*, *Nucl. Phys.* **B487** (1997) 409–441, [hep-th/9604064].

[153] M. P. Heller and M. Spalinski, *Hydrodynamics Beyond the Gradient Expansion: Resurgence and Resummation*, *Phys. Rev. Lett.* **115** (2015) 072501, [1503.07514].